Carlos Macías Gállego

Aerogeles de carbono y compuestos funcionales híbridos con propiedades adecuadas para electrodos en desionización capacitiva

Tesis doctoral

Directores

Pedro Lavela Cabello

Profesor Titular del Dpto de Química Inorgánica de la Universidad de Córdoba

Mª Concepción Ovín Ania

Científico Titular del Instituto Nacional del Carbón del Consejo Superior de Investigaciones Científicas (CSIC)

DEPARTAMENTO DE QUÍMICA INORGÁNICA E INGENIERÍA QUÍMICA

UNIVERSIDAD DE CÓRDOBA

2016

TITULO: *Aerogeles de carbono y compuestos funcionales híbridos con propiedades adecuadas para electrodos en desionización capacitiva*

AUTOR: *Carlos Macías Gállego*

Campus de Rabanales
Ctra. Nacional IV, Km. 396 A
14071 Córdoba

www.uco.es/publicaciones
publicaciones@uco.es

TÍTULO DE LA TESIS: "Aerogeles de carbono y compuestos funcionales híbridos con propiedades adecuadas para electrodos en desionización capacitiva"

DOCTORANDO/A: Carlos Macías Gállego

INFORME RAZONADO DEL/DE LOS DIRECTOR/ES DE LA TESIS

D. Pedro Lavela Cabello, Profesor Titular, miembro del Departamento de Química Inorgánica e Ingeniería Química de la Universidad de Córdoba, y Dña. Concepción Ovín Ania, Científico Titular del Consejo Superior de Investigaciones Científicas en el Instituto Nacional del Carbón, informan que la Tesis Doctoral presentada por Carlos Macías Gállego:

"Aerogeles de carbono y compuestos funcionales híbridos con propiedades adecuadas para electrodos en desionización capacitiva"

se ha realizado, dentro del Programa de Doctorado con Mención hacia la Excelencia de Química Fina en el laboratorio de Química Inorgánica de la Universidad de Córdoba en colaboración con la empresa Nanoquimia, S.A. y el Instituto Nacional del Carbón. El trabajo experimental fue soportado económicamente por el Ministerio de Ciencia e Innovación, en el ámbito de los proyectos INNPACTO IPT-2011-1450-310000 (ADECAR) y CTM2014/56770-R. La presente memoria reúne, a juicio de sus directores, los requisitos exigidos, incluyendo los artículos publicados en revistas científicas con índice de calidad relativo y en los cuales el doctorando es primer autor. Los directores de la Tesis informan que tanto la dedicación como los conocimientos adquiridos por el doctorando en el campo objeto de su trabajo han sido adecuados. Asimismo, realzamos su capacidad investigadora, incluyendo diseño y realización de experimentos, discusión de resultados y extracción de conclusiones.

Por todo ello, se autoriza la presentación de la tesis doctoral.

Córdoba, 1 de Septiembre de 2016

Firma del/de los director/es

Fdo.: Dr. Pedro Lavela Cabello Fdo.: Dra. Mª Concepción Ovín Ania

Informe del Journal Citation Report

Los artículos que se exponen en la presente memoria han sido publicados en revistas cuya información de impacto según el Journal Citation Reports de ISI web of Knowledge del último año están recogidos en la siguiente tabla:

Capítulo	Revista	Indice de impacto	Categoría	Nº de revistas en la categoría	Ranking en la categoría	Cuartil en la categoría
2.1	*Journal of Solid State Chemistry*	2.265	Chemistry, inorganic & Nuclear	46	17	Q2
			Chemistry, Physical	144	72	Q2
3.4	*ACS Sustainable Chemistry & Engineering*	5.267	Chemistry Multidisciplinary	163	26	Q1
			Green & Sustainable Science & Technology	29	4	Q1
			Engineering, Chemical	135	9	Q1
3.1/3.2	*Carbon*	6.160	Materials Science, Multidisciplinary	136	22	Q1
			Chemistry, Physical	251	24	Q1
2.2	*Journal of Applied Electrochemistry*	2.223	Electrochemistry	28	11	Q2

Aerogeles de carbono y compuestos funcionales híbridos con propiedades adecuadas para electrodos en desionización capacitiva

Memoria presentada por **CARLOS MACÍAS GÁLLEGO** para optar al grado de **DOCTOR** por la **UNIVERSIDAD DE CORDOBA**

Fdo.: Carlos Macías Gállego

VºBº de los directores de la tesis

Fdo.: Pedro Lavela Cabello

Profesor Titular del Dpto. de Química Inorgánica de la Universidad de Córdoba

Fdo.: Mª Concepción Ovín Ania

Científico Titular del Instituto Nacional del Carbón del Consejo Superior de Investigaciones Científicas (CSIC)

Agradecimientos

Quiero expresar mi más sincero agradecimiento a todas las personas e instituciones que han hecho posible la elaboración de la presente tesis doctoral.

Primeramente quiero mostrar mi agradecimiento a mi Director principal el Profesor Pedro Lavela por confiar en mi para la realización del presente trabajo, por su tiempo y dedicación, por su rapidez y diligencia en la revisión de mi trabajo, por su paciencia y sobre todo por el conocimiento que me ha transmitido, no solo sobre el tema de esta tesis sino sobre el oficio de Investigador Científico.

Igualmente quiero dar las gracias a mi codirectora la Dra. Concepción Ania, por aceptar la codirección de este trabajo aportando sus inestimables conocimientos sobre materiales de carbono, por el conocimiento que me ha aportado sobre el trato con las editoriales científicas, por los enfoques novedosos que ha aportado a este trabajo y por todo el tiempo dedicado tanto a la caracterización de materiales como a la revisión de todas las publicaciones aquí presentadas y del resto de los apartadosde esta tesis.

Quiero dar las gracias también al Director del grupo de Química y electroquímica de materiales inorgánicos, el Profesor Jose Luis Tirado, por su revisión y aportaciones a todas las publicaciones presentadas en esta tesis.

También quiero dar las gracias muy especialmente a la Dra. Gloria Rasines Calonge porque sin ella no habría sido posible la realización de este trabajo. Tu también has sido y eres mi gran apoyo Gloria.

No quiero olvidarme de todas las personas del Departamento de Química Inorgánica e Ingeniería Química y del personal del SCAI que han colaborado en este trabajo de forma directa o indirecta, especialmente a la Dra. Mª del Carmen Zafra, cuyas caracterizaciones electroquímicas de materiales han sido indispensables.

Tampoco quiero olvidarme de mi viejo amigo (y lo de viejo no va con segundas) el Dr. J.B. Parra del INCAR, que ha sido mi principal maestro en lo que a materiales porosos se refiere y que lleva inculcándome fascinación por ellos desde hace casi veinte años. Gracias de todo corazón por estar siempre ahí a la hora de resolver cualquier duda y por darme el privilegio de aprender de uno de los Grandes en este campo de forma tan desinteresada.

Quiero también agradecer a mi amiga la Profesora Mª Dolores Calzada todos sus consejos y todas las atenciones que ha tenido conmigo durante todo este tiempo que he pasado en la UCO y al Profesor Francisco Vicente del Departamento de Química Física de la UV por las estancias realizadas en su Departamento durante esta tesis y por su invitación a la XXXIV Reunión de Grupo de Electroquímica RSEQ.

Finalmente, quiero expresar mi más sincero agradecimiento al Instituto IMDEA Energía, al Dr. Jesús Palma y al Profesor Marc Anderson por invitar a mi empresa Nanoquimia, a participar en el proyecto ADECAR (IPT-2011-1450-310000) bajo el cual se ha llevado a cabo el presente trabajo, y al Ministerio de Economía y Competitividad por su apoyo financiero. Sin ellos esta tesis no se habría realizado.

A mi hijo Carlos.

Espero que este trabajo te sirva de inspiración algún día para la profesión que has decidido emprender.

“La ciencia de hoy en día es la tecnología del mañana”

Edward Teller

ÍNDICE

Capítulo 1

Introducción

1. INTRODUCCIÓN

1.1. HISTORIA DE LA DESIONIZACIÓN CAPACITIVA COMO SOLUCIÓN EN DESMINERALIZACIÓN DE AGUA

La disponibilidad de agua potable en cantidad suficiente para la creciente población mundial, es uno de los principales retos sociales, económicos y tecnológicos del siglo 21. El agua potable, siendo una necesidad vital y un derecho humano reconocido por Naciones Unidas, no está disponible para uno de cada siete habitantes del planeta y es un recurso en constante retroceso debido en gran parte a la eutrofización de embalses y lagos, a la sobreexplotación de acuíferos y a la infiltración de sales en los mismos, dando lugar a aguas salobres no aptas para el consumo humano. A día de hoy, el volumen de agua salobre en el planeta es superior al de agua potable, por lo que es lógico pensar en aquella como la principal fuente de suministro si se somete a un tratamiento de desalinización mediante una tecnología adecuada. Desde hace algunas décadas, se vienen desarrollando y aplicando varias de estas tecnologías entre las que podemos destacar la destilación, la ósmosis inversa y la electrodiálisis como las más extendidas y contrastadas. Sin embargo estas tecnologías tienen un elevado consumo de energía y en el caso de las dos últimas, la generación de salmuera residual es elevada. Por este motivo, es un reto importante el conseguir poner a punto una tecnología que tenga un consumo energético moderado o bajo y produzca una cantidad mínima de residuo.

La desionización capacitiva (siglas en inglés, CDI) es una técnica electroquímica para la eliminación de sales disueltas en agua que se basa en la adsorción del exceso de iones en una doble capa eléctrica (siglas en inglés, EDL) sobre la superficie de un electrodo (Figura 1). Consiste en la aplicación de un campo eléctrico entre dos electrodos separados por una disolución de las especies iónicas que se quieren eliminar. Ello provoca la migración de aniones y cationes hacia su correspondiente contralectrodo para compensar el exceso de carga generado en los mismos por el campo eléctrico. Cuando el electrodo tiene una elevada superficie la cantidad de sal adsorbida en la EDL puede ser significativa lo que convierte a la CDI en una técnica factible para la desalación de aguas. En este caso el sistema compuesto por ánodo, cátodo y medio salino, se comporta como un condensador electroquímico. Por esta razón, cuanto más carga sean capaces de acumular los electrodos a un voltaje dado, es decir cuanto mayor

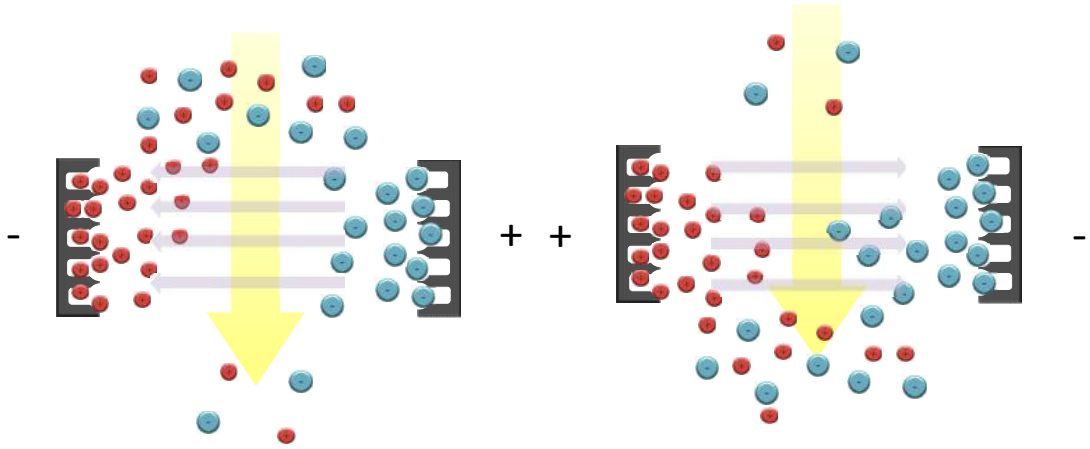

CDI no ha pasado de pequeñas unidades piloto y de demostración a ser una tecnología madura. Por entonces se pensaba que los materiales solo podían adsorber iones cuando tenían grupos superficiales que podían oxidarse o reducirse formando entonces un enlace iónico con el contraión correspondiente. Esta suposición clasificaba los materiales de electrodo en un principio como anión o catión selectivos y centró la atención en dilucidar qué factores determinaban que un material fuera de uno u otro grupo. En 1966, Evans y col. [2] proponen un mecanismo que implica la formación de iones hidroxilo en el cátodo mediante reacciones farádicas. Con ello se crearía un entorno básico necesario para la disociación de grupos ácidos débiles que serían los responsables de la adsorción de iones. En 1967, Murphy y Caudle [3] proponen el primer modelo teórico de electroadsorción de sal en continuo por un mecanismo capacitivo y otro estudio de Arnold y col. de 1961 [4] se centra en la modificación de las propiedades superficiales de los carbones después de tratamientos químicos y su influencia en la eficacia en desionización. En 1968, Reid y col. [5] ensamblan la primera unidad de desmineralización y la operan en modo continuo durante un periodo largo de tiempo sin una pérdida significativa en eficacia en la adsorción de sal. Además demostraron con esta unidad que también se podían eliminar de forma efectiva iones calcio, magnesio, sulfato, nitrato y fosfato.

A principios de los 70, Johnson y col. [6] proponen que el mecanismo de adsorción de iones es el de doble capa eléctrica y se introduce el concepto de operación de celda en ciclos asimétricos de adsorción y desorción. Comprobaron que en estas condiciones de ciclo asimétrico o modulando el potencial de la celda durante la fase de adsorción, se podía optimizar la eficacia del sistema sin revertir la polaridad. En el mismo estudio se demostró que las reacciones farádicas que se producían entre la disolución electrolítica y la pared del electrodo producían la degradación progresiva del mismo. Mediante un simple análisis de costes se demuestra por primera vez que la CDI solo es factible si se emplean electrodos dimensionalmente estables. En un estudio posterior de Johnson y Newman [7] concluyen que la eficacia de adsorción dependía de la capacidad de la EDL, de la superficie del electrodo y del voltaje aplicado. En otro estudio de finales de los 70 efectuado por Soffer y Oren [8], se concluye que los poros entre 0,5 y 3 nm se humectan y contribuyen a la adsorción de iones. Durante los 80 parece disminuir el interés en la investigación en desionización capacitiva, pero a partir de los 90 se renuevan los esfuerzos científicos. A partir de esas fechas, los estudios se centran sobre

todo en producir materiales adecuados para los electrodos de CDI. Entre los materiales más destacados durante esta década, están los aerogeles de carbono sintetizados por primera vez por Farmer y Pekala en 1996 [9, 10]. Su estructura monolítica, elevada superficie específica y la posibilidad de controlar el tamaño de poro variando las condiciones de síntesis, lo convierten en uno de los mejores candidatos para esta tecnología. Se han llevado a cabo varios estudios relevantes con estos materiales aplicándolos a aniones como nitrato y fluoruro [11] y cationes como Cr^{+3} y Hg^{+2} [12, 13]. Las siguientes dos décadas son fructíferas en el desarrollo de materiales para electrodos. Siempre tomándose como base diferentes materiales de carbono como son los aerogeles de carbono, las fibras y telas de carbono activadas, los nanotubos de carbono (CNT), el grafeno y óxido de grafeno reducido (RGO), el carbón ordenado mesoporoso (OMC) y el carbón activado (CA), durante las décadas de 2000 y 2010 se llevan a cabo diversas investigaciones aplicando a la CDI los anteriores materiales bien puros o bien funcionalizados y/o compuestos híbridos con óxidos metálicos, sílices o polímeros.

Con respecto a los aerogeles y(CAG) xerogeles de carbono (XGC), podemos destacar la aplicación de aerogeles con gel de sílice [14, 15], carbón activado [15], negro de carbono (siglas en inglés CB) [16], óxidos metálicos [17] y xerogeles con fibras de carbono [18].

En 2001 se aplica por vez primera la tela de carbono activada para la adsorción de diversas sales de sodio y azufre [19] y en 2003, Ryoo y col. funcionalizan las telas de carbón activado con TiO_2 para aplicación en CDI [20].

Otro material relevante en las aplicaciones de desionización capacitiva son los nanotubos de carbono, pudiendo señalar la aplicación de composites con nanofibras de carbono por primera vez en 2006 [21, 22]. A partir de aquí, se pueden destacar los trabajos con materiales basados en nanotubos de carbono como la aplicación de esponjas de CNT como electrodos por Wang [23] y de materiales de CNT compuesto con quitosano [24], ácido poliacrílico [25], OMC [26], MnO_2-PSS [27], polianilina [28], RGO [29] y zeolita [30]. Asimismo, se ha demostrado la eficacia de la funcionalización con grupos amino, sulfato y carboxilo [31].

El grafeno (GF) es otro material interesante de extensa aplicación en CDI. La primera referencia se debe a Li y col. en 2010 [32]. A partir de aquí cabe destacar los

trabajos en 2012 de Zhuo y col. con composites RGO-GF-CA [33] y de Zhang con composites GF-OMC y GF-CNT [34, 35]. Recientemente, se ha propuesto el empleo de esponjas de grafeno [36]y grafeno funcionalizado con nanopartículas de TiO_2 [37].

Paralelamente, entre 2000 y 2010 se fueron desarrollando diferentes tecnologías y aplicaciones de la CDI distintas a la eliminación de sal del agua. En 2001 Conway emplea tela de carbono activada de 2500 $m^2\ g^{-1}$ para la electroadsorción de sales como sulfuros, sulfatos, tiocianatos o xantato, o bien compuestos orgánicos como la anilina y su sal catiónica [19]. En 2002, Andelman patenta una importante mejora en la tecnología de CDI consistente en el recubrimiento de los electrodos con membranas ión selectivas (MCDI) lo que mejora notablemente la eficiencia de carga debido a que se imposibilita en transporte de co-iones a los electrodos [38]. En 2004, Madaria y col. aplican la desionización capacitiva con electrodos de aerogeles de carbono a la eliminación de iones Hg^{2+} del agua optimizando el proceso mediante superficie de respuesta y llegando a obtener valores de eliminación del 96.3% [12]. En 2005, Welgemoed lleva a cabo el primer estudio piloto escalable aportando costes de explotación y de inversión para una instalación industrial de CDI [39]. En 2008, Dermentzis y col. combinan el concepto de electro-deionización con el de electrodiálisis empleando electrodos de gafito poroso que actúan como membranas huecas en cuyo interior se acumulan aniones y cationes que forman una fase de concentrado [40]. El sistema puede operar en continuo obteniendo eficacias de eliminación de sal del 90%. En el mismo año, Xu y col. llevan a cabo un estudio de selectividad de la CDI de iones en agua salobre con electrodos de aerogeles de carbono encontrando el siguiente orden de selectividad iónica I>Br>Ca>alcalinidad>Mg>Na>Cl [41]. Noked y col. en 2009 estudiaron la relación entre el tamaño iónico y la distribución del tamaño de poro del electrodo encontrando que un tamaño de poro próximo al del ión da elevadas capacidades pero cinéticas lentas por lo que concluyen que la distribución óptima corresponde una mezcla jerárquica de mesoporos y microporos, siendo el aerogel de carbono activado el que más se adaptaba a estas características [42].

En el área de las aplicaciones, en 2010 Kim y col aplican MCDI a la eliminación de sales en agua contaminada con octano para simular una contaminación con aceite, encontrando que la eficacia de eliminación de sal decrecía con la concentración de octano pero se mantenían eficacias del 70% estables en el tiempo con eficiencias de carga superiores al 90% [43]. En 2010 Anderson y col llevan a cabo un estudio

comparativo de las diferentes tecnologías de desalación encontrando que la CDI es competitiva desde el punto de vista energético solo si se puede recuperar la energía de la fase de regeneración de los electrodos [44]. En el mismo año, Jae-Hun lleva a cabo un estudio de las reacciones farádicas en los electrodos en función del voltaje aplicado a la celda concluyendo que estas reacciones son importantes a partir de 1 V [45]. En 2011 Arar aplica la CDI a la eliminación de Cu [46] y Zhang lleva a cabo una aplicación real de CDI para aguas residuales reales de la industria del acero [47]. Un importante nuevo concepto aparece en 2012 con el trabajo de Forrestal y Xu donde se combina el concepto de CDI con el de pila de combustible microbiana (MFC) para dar lugar a la celda de desalación microbiana (MDC) en donde se aprovecha la energía obtenida de la oxidación microbiana de compuestos orgánicos disueltos en agua para alimentar una celda de CDI y obtuvieron eficacias de desalación del 70% para una concentración de 10 g/l de NaCl [48]. En el mismo año, Suss y col introducen otro concepto novedoso, los electrodos de flujo a través, en los que la solución pasa en flujo perpendicular a través de ánodo y cátodo porosos dando velocidades de captación de NaCl de hasta 1 mg/g.min, en torno a 4 veces más que en la CDI clásica [49]. En relación con la estabilidad de los electrodos de carbón poroso, Chen y col llevaron a cabo en 2013 un minucioso estudio sobre la evolución de tales electrodos en el tiempo, encontrando que la superficie específica disminuye mientras que el tamaño de los poros aumenta y se forman grupos funcionales, sobre todo carboxilos, en la superficie del carbón [50]. Otro interesante estudio sobre la optimización de las condiciones de operación de una CDI llevado a cabo en el mismo año por Demirer y col, demuestra que no se pueden optimizar simultáneamente las condiciones para la eficacia energética, la eficacia de desalación y la velocidad de desalación, requiriendo el punto óptimo de cada una de estas variables unas condiciones de operación específicas diferentes [51]. En 2013 se prueba un nuevo concepto por parte de Jeon y col consistente en combinar la electrodiálisis con la CDI empleando una suspensión de CA en polvo en las cámaras anódica y catódica de la celda, de modo que se comportaba como un electrodo líquido, dando lugar a la CDI en flujo (FCDI) [52].

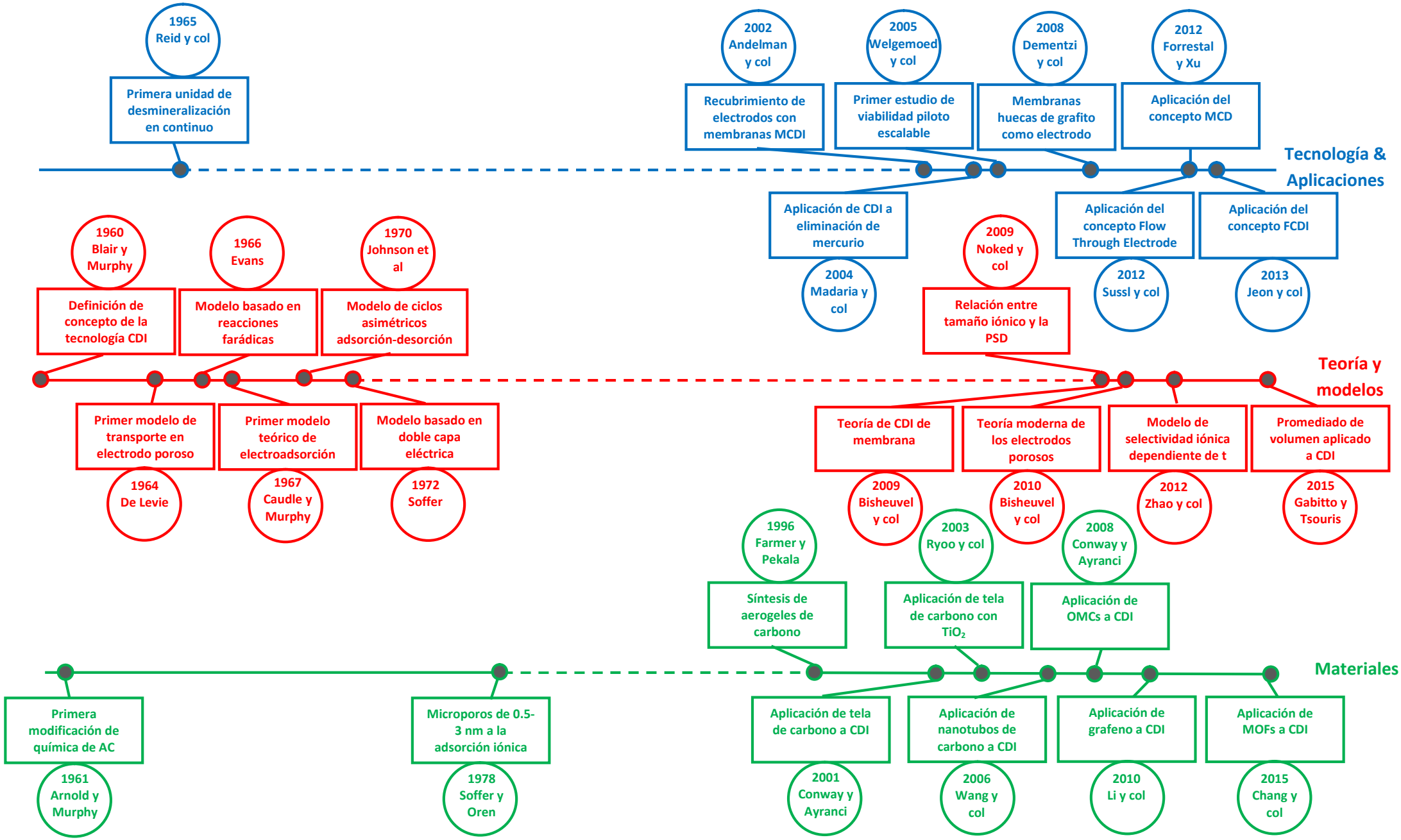

Figura 2. Hitos históricos de la investigación científica en CDI actualizado a 2016

Esta tecnología parece vencer la mayoría de las limitaciones de la CDI convencional obteniendo eficacias de desalación del 95% en soluciones de NaCl de 32,1 gL^{-1}. En la misma línea tecnológica, Hatzell y col eliminan la necesidad de membranas de la celda de FCDI [53] y Porada y col introducen una mejora que aprovecha la energía almacenada en los gradientes salinos [54].

Como puede apreciarse, durante los más de 50 años que se lleva investigando la CDI, se han probado diversas combinaciones de materiales y dispositivos lográndose configuraciones de la tecnología cada vez más eficientes (Figura 2). Entre ellas, la tecnología FCDI parece ser la más prometedora hasta el momento y los primeros resultados indican que puede competir con la ósmosis inversa tanto desde el punto de vista energético como del de la eficacia en desalación, incluso para concentraciones salinas del orden del agua marina.

1.2. COMPORTAMIENTO DE DIFERENTES MATERIALES EN CDI

En este apartado se hace un repaso exhaustivo de las propiedades físico-químicas relevantes para que un material sea apto para su empleo como electrodo en procesos de CDI y del comportamiento de los diferentes materiales que se han aplicado hasta el momento en esta técnica.

1.2.1. Propiedades de un material aplicable en CDI

A día de hoy no existe una respuesta a cuál es el mejor material de electrodo para CDI ya que entre otras cosas la eficacia del proceso depende de la interacción entre los materiales de electrodo, la ingeniería y diseño del sistema y el tipo y concentración de iones que se quieren eliminar. En este sentido, para evaluar la eficacia de un material, se deben definir unas condiciones estándar que sean representativas del problema a tratar y que deben incluir factores como el tipo de celda, el procesado del material para la conformación de los electrodos, el modo y condiciones de operación y el tipo de ión o iones que se quieren eliminar. Además es necesario definir también qué conjunto de

propiedades y variables marcan la bondad de un material para esta aplicación y el rango de valores que estas deben tener para cada caso concreto.

En 2008, Oren [55] hace una revisión de las características que definirían al material ideal para CDI y que se podrían resumir en la siguiente lista:

- **Elevada superficie accesible a los iones que se quiere eliminar**.- Cuanto mayor sea la superficie accesible, mayor será la cantidad de iones que se pueden adsorber y por tanto alojar en el material. Un material de elevada superficie no es necesariamente un buen material si su superficie activa está formada por poros de tamaño del orden del radio iónico de las especies que se quiere eliminar.
- **Elevada movilidad iónica en la red porosa.-** Esto requiere una red porosa interconectada y lo suficientemente amplia con respecto al tamaño iónico de las especies a electroadsorber, necesaria para una rápida cinética y una baja resistencia iónica lo que a su vez repercute sobre la eficiencia de carga.
- **Elevada estabilidad química en el rango de pH y potenciales al que opera la CDI.-** Esto es importante para una elevada vida útil de los electrodos.
- **Elevada mojabilidad.-** Esto asegura también un buen transporte iónico por toda la red y elimina las resistencias debidas al transporte del solvente.
- **Elevada movilidad electrónica.-** Necesaria para una buena eficiencia energética del proceso.
- **Bajo coste y producción escalable.-** Necesario para las aplicaciones a gran escala.
- **Versatilidad de fabricación.-** Tiene que permitir fabricarse en diferentes conformaciones (láminas, monolitos, honeycombs etc.)
- **Abundancia y renovabilidad.-** Esto garantiza no solo una baja huella de carbono sino la sostenibilidad del material.
- **Elevada inercia biológica.-** Esto evita la formación de biopelículas que comprometerían seriamente la eficacia del material.
- **Baja resistencia de contacto con el colector de corriente.-** Esto evita altas caídas de potencial en el electrodo que comprometen energéticamente el proceso.

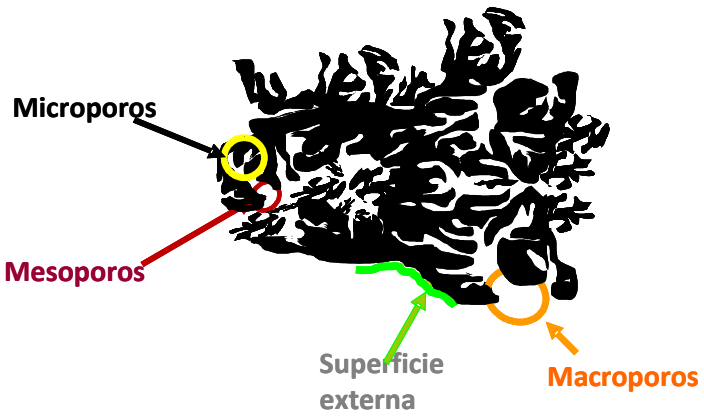
Microporos
Mesoporos
Superficie
externa
Macroporos

matemáticos a datos experimentales de adsorción de algún fluido a diferentes presiones. Así, aunque los límites de esta clasificación de poros son, en cierta manera arbitrarios, están relacionados con el análisis de las isoterma de adsorción/desorción de nitrógeno a -196 ºC. Se diferencia entre llenado primario de poros del recubrimiento superficial que ocurre en la superficie externa y en las paredes de macroporos abiertos. A menudo es útil distinguir entre microporos estrechos o ultramicroporos a aquellos de anchura < 0,7 nm, y microporos anchos o supermicroporos para tamaños mayores de que 0,7 nm, cuyo llenado se produce por adsorción cooperativa (llenado secundario) a presiones relativas más altas.

Los poros también se pueden clasificar en función de su geometría. Las geometrías más comúnmente empleadas, que se suelen aplicar los modelos empleados para el cálculo de dimensiones de poro a partir de isotermas de adsorción de gases, son la geometría cilíndrica y la geometría en rendija. También se definen otras como geometría de poro corrugada, de cuello de botella o globular, algunas de las cuales se muestran en la Figura 4. Si atendemos a la accesibilidad a un fluido externo a la red interna de poros, podemos clasificar estos como *cerrados*, es decir, sin acceso al exterior y por tanto inactivos al flujo de fluidos o *abiertos* que son aquellos que tienen comunicación con la superficie externa.

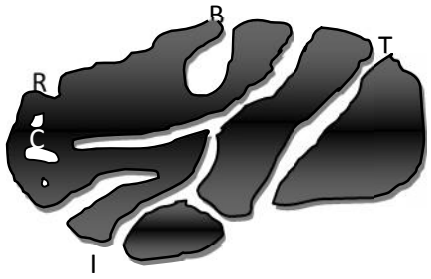

Figura 4.-Sección trasversal de un entramado poroso con varios tipos de poros: cerrados (C), globulares (B), trasversales (T), interconectados (I), adyacentes con cierta rugosidad (R).

Además de las propiedades anteriores de los poros, la tortuosidad de la red porosa es otra importante característica que raramente se menciona en los trabajos sobre CDI (no así en aquellos relacionados con teoría de transporte en medios porosos) y que influye

decisivamente en la cinética de transporte en una red porosa [57]. Se puede definir como la relación entre la longitud entre dos puntos unidos por una línea recta y la longitud definida por un canal de transporte que une los dos puntos (Figura 5).

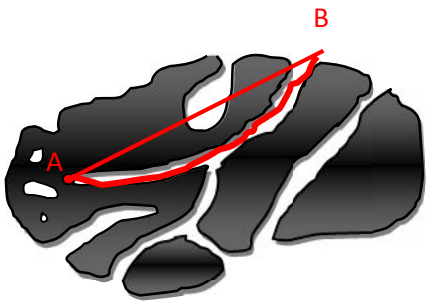

Figura 5.- Representación del factor de tortuosidad de la red de poros.

Como se ha mencionado más arriba, la superficie accesible a los iones y la movilidad iónica en el interior del material están íntimamente ligadas a las propiedades nanotexturales, concretamente a la superficie específica del material, a la distribución del tamaño de poros (PSD) y a la tortuosidad. Las dos primeras tienen que ver con la superficie accesible para la adsorción que determina en gran medida la capacidad de electroadsorción (CEA) en el equilibrio y la segunda y tercera, determinan la cinética del proceso de electroadsorción de forma que cuanto mayor sea el tamaño de los poros y menor sea la tortuosidad, más rápido será el transporte iónico y más rápido será el proceso. Sin embargo, un mayor tamaño de poros está reñido con una elevada superficie específica, por lo que a la hora de diseñar un material optimizado para CDI siempre hay que buscar una solución de compromiso entre superficie específica y tamaño de poro.

1.2.1.2. Química superficial

La electroadsorción de iones es de naturaleza electrostática, lo que implica la existencia de regiones en la superficie del material con densidades de carga contrarias a la del ión en cuestión. Esto es lo que ocurre en los materiales de carbono con hibridación sp^2, donde existe un conjunto de electrones π deslocalizados que se pueden mover en una banda de conducción por acción de un campo eléctrico, creando una densidad de carga negativa o positiva en la superficie del material de forma generalizada, haciendo de toda su superficie un lugar adecuado para la adsorción

mediante interacciones dispersivas tipo Van der Waals [58]. Esto es lo que se conoce como adsorción física o fisisorción. Pero además pueden existir sitios específicos formados por heteroátomos distintos del carbono que pueden generar otro tipo de interacciones con los iones como enlaces iónicos o covalentes, dando lugar a la adsorción química o quimisorción [59]. En el caso de materiales de carbono, los heteroátomos más frecuentes son B, N, S, P y fundamentalmente el oxígeno. Estos heteroátomos suelen estar ya en el material de partida, aunque pueden incorporarse mediante tratamientos post-síntesis (e.g., oxidación, dopado con azufre o nitrógeno, o funcionalización con óxidos metálicos) [60] [61]. La presencia de heteroátomos da lugar a grupos funcionales capaces de alterar la CEA del material de electrodo [62] ya que la adsorción en este tipo de sitios puede ser más estable que la adsorción física, y crear uniones irreversibles que provoquen que la eficacia del material decrezca con el uso del mismo. Este tipo de sitios puede generar también lo que se conoce como efectos pseudocapacitivos o pseudofarádicos, en los que ocurre una transferencia de carga desde el ión adsorbido al heteroátomo o viceversa pero sin que esa carga se transfiera a la matriz del material y sin que se produzca una oxidación o reducción efectivas del heteroátomo (o del ión). En este caso se genera una corriente farádica sin adsorción iónica asociada al transporte electrónico por lo que estos procesos tienden a disminuir la eficiencia de carga en una CDI como se explicó en la sección 1.1. En otros casos, la modificación mediante tratamientos específicos puede mejorar la CEA del material como es el caso del dopado con N o la funcionalización con óxidos metálicos [60] [61]. Estas modificaciones no solo aumentan la cantidad de sitios donde se genera una acumulación de portadores de carga (electrones o vacantes) sino que suelen mejorar la mojabilidad del material, disminuyendo su resistencia al transporte iónico, y su conductividad eléctrica.

1.2.1.3. Conductividad eléctrica

Se entiende por conductividad eléctrica de un material, la facilidad que tiene este para transportar sus portadores de carga en su seno bajo la acción de un campo eléctrico. Esta propiedad depende directamente de la concentración de portadores de carga y de la movilidad de los mismos, lo que comúnmente se denomina carga libre de un material.

Como se ha comentado anteriormente, para que se produzca la electroadsorción hemos visto que es necesaria la creación de un campo eléctrico entre dos electrodos.

Esto crea una asimetría de carga entre ambos electrodos generada por los portadores de carga del material (electrones o vacantes) que a su vez provoca la migración de aniones y cationes para compensarla y restablecer el equilibrio. Si forzamos externamente a que este campo se mantenga constante a pesar de los iones adsorbidos en los electrodos, se generará una corriente eléctrica entre ambos electrodos que trata de mantener el campo en un valor constante compensando el efecto neutralizador de los iones adsorbidos. En un proceso capacitivo ideal, esta corriente se irá atenuando hasta disiparse cuando ya no puedan adsorberse más iones de la solución al potencial aplicado.

Además de sus características texturales, la CEA de un material también depende de la cantidad de portadores de carga que pueden acumular y esto depende principalmente de su conductividad eléctrica. La conductividad eléctrica está relacionada con la existencia de niveles de energía atómicos que permiten la movilidad de electrones libremente por toda la red del material. En el caso de los conductores metálicos, esta movilidad se debe a la presencia de orbitales d y en el caso de los materiales de carbono a la de orbitales híbridos sp^2 que alojan electrones π deslocalizados que se pueden mover libremente por toda la red.

En el caso de los materiales de carbono porosos como el carbón activado, la conductividad también está relacionada con la cantidad de caminos disponibles para el transporte de carga, al tratarse de materiales discontinuos. Esto implica que, en general, cuanto más poroso es un material menor es su continuidad, menor el número de caminos de transporte y menor su conductividad, es decir, se produce una situación de conflicto entre dos parámetros importantes del proceso de electroadsorción en la que hay que llegar a una solución de compromiso. En este caso, el dopado con nitrógeno o la funcionalización con nanopartículas metálicas suele mejorar la conductividad del material proporcionando portadores de carga libre extra y más caminos de transporte.

En la bibliografía consultada para llevar a cabo esta memoria, se ha podido comprobar que el conjunto de condiciones empleadas para poner a prueba un material difiere de un trabajo a otro, por lo que es difícil hacer una comparación homogénea entre ellos. En las tablas 1 y 2 aparece un resumen de los materiales que se han ensayado a lo largo de la historia de esta tecnología, donde se puede comparar de un vistazo el comportamiento de los diferentes materiales tanto en medidas de CDI como de voltametría cíclica y de las condiciones en las que se han llevado a cabo los ensayos.

1.2.2. Electrodos basados en Carbón Activado

El carbón activado (CA) es uno de los materiales de electrodo más comúnmente utilizado en procesos de CDI ya que cumple muchas de las características idóneas requeridas para esta aplicación: posee elevada superficie (800-2000 m^2/g) y amplia distribución de tamaños de poro (anchura < 100 nm), posee por lo general una estructura porosa interconectada, tiene una buena conductividad eléctrica, se puede conformar empleando ligantes, es barato (0,5-2 €/kg), abundante, puede proceder de fuentes renovables y su composición química es fácilmente modificable para obtener materiales más hidrófilos y estables químicamente.

Los primeros estudios sobre CDI realizados entre principios de la década de 1960 y finales de los 70, se llevaron a cabo empleando carbón activado, grafito, y mezclas de negro de carbono o charcoal con grafito. Estas mezclas en polvo se depositaban sobre un soporte fibroso inerte el cual se presionaba sobre un colector de corriente metálico para conformar el electrodo. En la actualidad, y dado que se trata de un material barato y abundante, se ha seguido investigando sobre las posibilidades de este material llevando a cabo diferentes modificaciones químicas que mejoren su eficacia en CDI. Así mismo se ha empleado como material de referencia para comparar la propiedades de nuevos materiales de electrodo que han ido surgiendo, por lo que actualmente se dispone de una interesante colección de datos sobre el comportamiento en CDI de electrodos basados en CA. En las Tablas 1 y 2 se recoge un resumen de los trabajos encontrados en la bibliografía sobre el empleo de diferentes materiales de carbono como electrodo, tanto en CDI como en voltametría cíclica (CV) o descarga galvanostática (GD) en diferentes condiciones. En el caso de los carbones activados, se puede observar en la Tabla 1 que las capacidades de adsorción en CDI varían entre 0,28 y 20,91 mg/g. Esta enorme disparidad de resultados se debe en gran parte a las características de los materiales empleados en el electrodo, pero también a las diferentes condiciones experimentales, ya que existe una dependencia clara de la capacidad de electroadsorción con el voltaje aplicado a la celda y con la concentración inicial de electrólito.

En la mayoría de los casos se emplea NaCl como electrólito y se trabaja bien en celda tipo "Stack" (SK) en modo circuito cerrado (CC) o bien con celda tipo batch (BC) en modo batch (B) siendo estos dos modos equivalentes desde el punto de vista termodinámico, dado que en ambos casos la misma disolución salina está en contacto

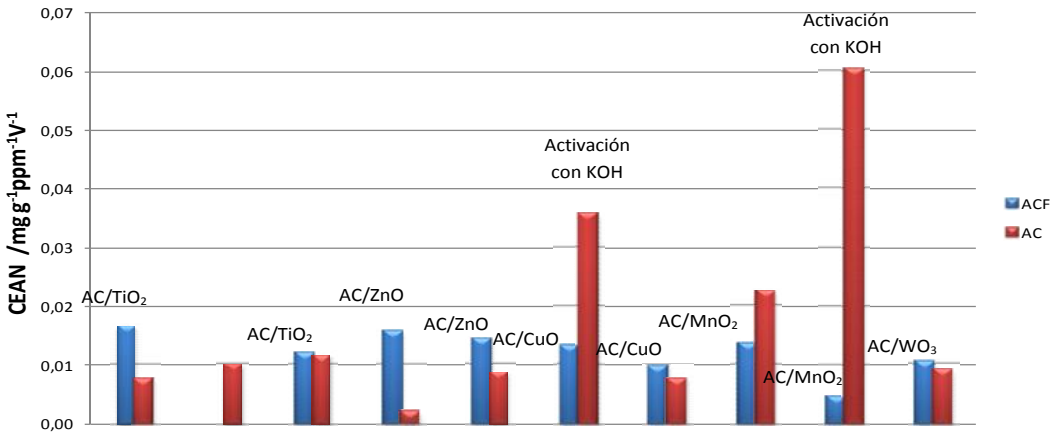
0,07
0,06
0,05
0,04
0,03
0,02
0,01
0,00
CEAN /mg g-1ppm-1V-1
AC/TiO2
AC/TiO2
AC/ZnO
AC/ZnO
AC/CuO
Activación con KOH
AC/CuO
AC/MnO2
AC/MnO2
Activación con KOH
AC/WO3
ACF
AC

voltaje de 1V y con una concentración inicial de electrólito de 0,5 mM. Sin embargo no se dan datos de eficiencia de carga para estos dos CAs.

Para tratar de discernir a qué se deben las variabilidades observadas en la CEAN de los diferentes electrodos, se ha estudiado la correlación entre este valor y las propiedades texturales (superficie específica y volúmenes de poro) de los carbones activados empleados en la fabricación de los electrodos. La Figura 7 refleja la relación entre la CEAN y la superficie y el volumen de microporos respectivamente. Se puede observar una fuerte correlación entre la CEAN y estos dos parámetros texturales, sin embargo, las correlaciones con la superficie y volumen de mesoporos (no mostradas) son menos claras. Los datos mostrados corresponden a medidas realizadas en condiciones de equilibrio y otra característica importante requerida para una aplicación comercial de CDI es una cinética rápida. La duración del ciclo de adsorción es indicativo de la cinética del material, si bien este parámetro está muy influenciado, al igual que en el caso de la CEA, por la concentración inicial de sal y por el voltaje aplicado a la celda. Para tener en cuenta ambos efectos se ha calculado, a partir de los resultados de la literatura, una velocidad media de adsorción dividiendo la CEAN por el tiempo del ciclo de adsorción para cada material referenciado. La relación entre este parámetro y la superficie y volumen de microporos aparece en las Figuras 7c y 7d. En ellas se puede observar nuevamente una clara correlación entre estos dos parámetros y el valor de la velocidad media de adsorción para los CA estudiados y que sorprende especialmente por proceder cada punto del gráfico de datos de trabajos diferentes. Nuevamente, la correlación con el volumen de mesoporos o fracción de los mismos no parece tan clara. A la vista de estos resultados se puede concluir que en el caso de los CA la superficie y volumen de microporos parecen ser el factor determinante tanto en la adsorción de iones como de la cinética del material.

En la literatura también se recogen datos de CA funcionalizados incorporando diversos heteroátomos (i.e., oxígeno, nitrógeno) o nanopartículas metálicas, puesto que la además de las propiedades texturales, la composición química es otro factor importante del que depende la CEA de un material de electrodo. En la Figura 6 se han representado las CEAN de los diferentes CA funcionalizados y como puede observarse, en general se mejoran ligeramente los valores en comparación con los CA de partida, si bien las capacidades son todavía relativamente bajas. Entre los mejores resultados destacan los obtenidos con CA funcionalizado con hexamina y TiO_2 [60], y con

nanopartículas deZnO [66]. No existen datos suficientes sobre textura de dichos materiales, por lo que no se puede establecer una relación entre sus CEAN y sus parámetros texturales; no obstante se puede concluir que la funcionalización con óxidos metálicos en muchos casos mejora la CEAN del CA. A modo de ejemplo, CA funcionalizados con TiO_2 exhiben CEAN entre 6,2 veces [60] y 49,8% [67] mayor que la del CA sin tratar. Esto se atribuye por un lado a una mayor generación de electrones en el cátodo y de vacantes en el ánodo bajo la acción de un campo eléctrico en los carbones funcionalizados y por otro a una mejor mojabilidad del electrodo, lo que favorece los procesos de transporte hasta los sitios de adsorción y la cantidad de estos disponibles.

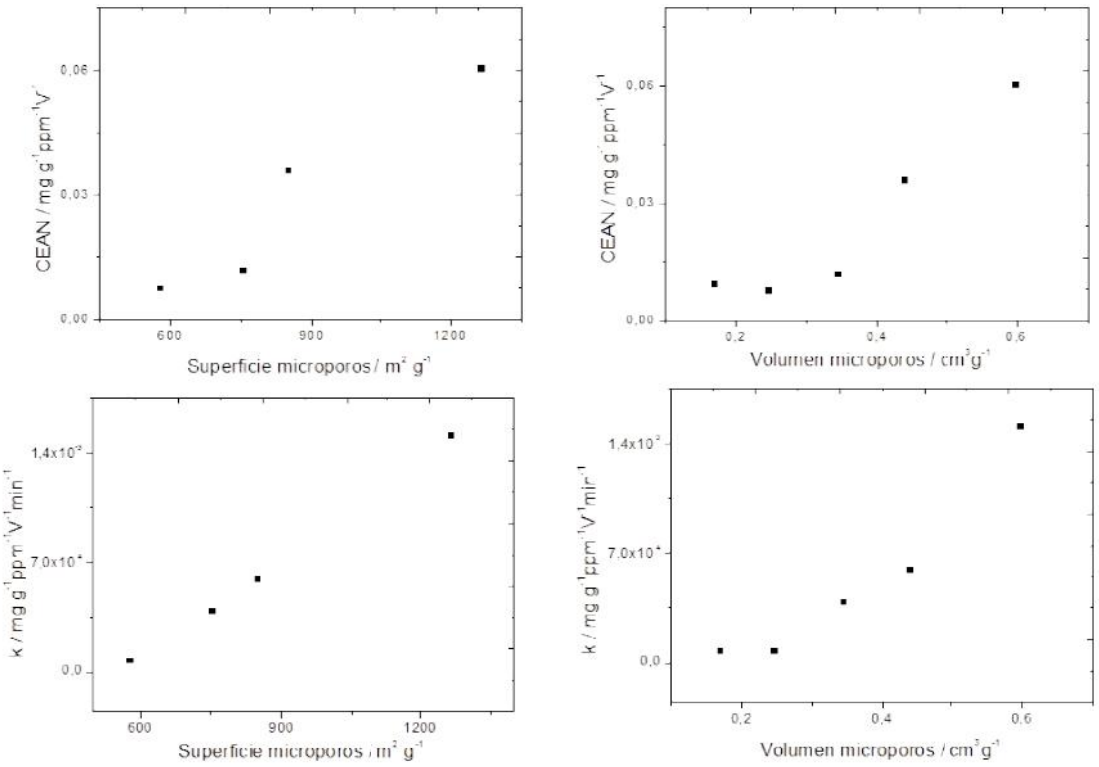

Figura 7. Relación entre parámetros texturales y propiedades electroquímicas en carbones activados.

A modo de resumen, si bien el carbón activado es un buen material de electrodo de acuerdo con los requisitos propuestos por Oren et al [55], presenta ciertas limitaciones como es su conformado en diferentes geometrías. Esto requiere el empleo de sustancias ligantes que confieran plasticidad a los electrodos y que son generalmente no conductores y no porosos, restando capacidad al CA y confiriendo una baja resistencia al efecto erosivo del agua, comprometiendo la estabilidad del conformado. .

REF	MATERIAL	CONFORMACION ELECTRODO	CELDA	M H	MEQ	V/I	ELEC	C.E (mg/l)	SADS (mg/g)	TADS (min)	E.Q	EST
[9]	CAG/PCP	Pegado a Ti colector con cola conductora	SK	CC	PS	1.2	NaCl	588	3.4	28	-	
[9]	CAG/PCP	Pegado a Ti colector con cola conductora	SK	CC	PS	1.2	$NaNO_3$	588	8.0	35	-	
[9]	CAG/PCP	Pegado a Ti colector con cola conductora	SK	CA	PS	1.2	NaCl	588	3.4	120	-	
[68]	CAG	Pegado a Ti colector con cola conductora	SK	CC	PS	1.2	FNa	42	2.7	180	-	
[68]	CAG	Pegado a Ti colector con cola conductora	SK	CC	PS	1.2	FNa	100	4.9	180	-	
[68]	CAG	Pegado a Ti colector con cola conductora	SK	CC	PS	1.2	NaCl	58.45	1.4	180	-	
[68]	CAG	Pegado a Ti colector con cola conductora	SK	CC	PS	1.2	NaCl	140.28	4.5	180	-	
[68]	CAG	Pegado a Ti colector con cola conductora	SK	CC	PS	1.2	$NaNO_3$	80.75	3.4	180	-	
[68]	CAG	Pegado a Ti colector con cola conductora	SK	CC	PS	1.2	$NaNO_3$	153	5.0	180	-	
[20]	ACC/TiO_2	Colector de acero y contacto por presión	BC	B	PS	1.0	NaCl	5.84	1.8	300	-	-
[69]	CAG/SG	Pasta de AGC/SG +binder extendida sobre colector	-	CC	PS	0.9	NaCl	1000	-	4	-	>100
[70]	CAG	Monolitos circulares+carbon glue+colector Ti	SK	CC	PS	1.5	NaCl	50	2.8	300	-	
[70]	CAG	Monolitos circulares+carbon glue+colector Ti	SK	CC	PS	1.5	NaCl	500	7.0	300	-	
[63]	CA GR	Carbón activo granular separado de la solución por membrana	SK	B	PS	2.0	NaCl	627	?	20	-	
[63]	CA GR+KOH	Carbón activo granular separado de la solución por membrana	SK	B	PS	2.0	NaCl	627	?	20	-	
[63]	CA GR	Carbón activo granular separado de la solución por membrana	SK	B	PS	2.0	NaCl	627	?	20	-	
[71]	CA	CA P+PTFE+CB prensado sobre colector de grafito	BC	CC	PS	0.8	NaCl	46.76	0.28	100	-	
[71]	OMC	OMC P+PTFE+CB prensado sobre colector de grafito	BC	CC	PS	0.8	NaCl	46.76	0.60	100	-	
[71]	OMC-S	OMC P+PTFE+CB prensado sobre colector de grafito	BC	CC	PS	0.8	NaCl	46.76	0.93	100	-	
[71]	OMC-N	OMC P+PTFE+CB prensado sobre colector de grafito	BC	CC	PS	0.8	NaCl	46.76	0.54	100	-	
[72]	SiO_2NP/$MgAl_2O_3$	Composite de SiO_2NPs y $MgAl_2O_3$ infiltradas en CCE (Porvair)	BC3E	B	PS-RE	-1.5	Cl_2Ca	40	0.034	20	-	
[72]	SiO_2NP/$MgAl_2O_3$	Composite de SiO_2NPs y $MgAl_2O_3$ infiltradas en CCE (Porvair)	BC3E	B	PS-RE	-1.5	Cl_2Mg	17	0.017	20	-	
[72]	SiO_2NP/$MgAl_2O_3$	Composite de SiO_2NPs y $MgAl_2O_3$ infiltradas en CCE (Porvair)	BC3E	B	PS-RE	-1.5	CO_3Ca	35	0.030	20	-	
[72]	SiO_2NP/$MgAl_2O_3$	Composite de SiO_2NPs y $MgAl_2O_3$ infiltradas en CCE (Porvair)	BC3E	B	PS-RE	-1.5	CO_3Mg	17	0.015	20	-	
[60]	CA/TiO_2	CA/TiO_2+RESINA+HEXAMINA sobre papel de grafito	BC	B	PS	1.2	NaCl	500	9.97	200	-	
[60]	CA	CA +RESINA+HEXAMINA sobre papel de grafito	BC	B	PS	1.2	NaCl	500	6.11	200	-	
[60]	CNTs	CNTs+RESINA+HEXAMINA sobre papel de grafito	BC	B	PS	1.2	NaCl	500	11.46	300	-	
[60]	ACFs	ACFs +presión sobre papel de grafito	BC	B	PS	1.2	NaCl	500	8.12	50	-	
[73]	RGO/RF	RGO/RF+PTFE+colector grafito	SK	B	PS	2.0	NaCl	65	3.23	30	-	
[73]	RGO	RGO+PTFE+colector grafito	SK	B	PS	2.0	NaCl	65	1.80	30	-	
[73]	CA	CA+PTFE+colector grafito	SK	B	PS	2.0	NaCl	65	1.51	30	-	
[74]	CNTs	CNTs+$Al(NO_3)_3$+colector de papel de grafito por EPD	SK	CC	PS	1.2	NaCl	32	0.97	90	-	
[25]	CNTs	CNTs+PAA+colector de papel de grafito por EPD	SK	CC	PS	1.2	NaCl	32	2.43	60	-	
[27]	MnO_2/PSS/CNTs	MnO_2/PSS/CNTs+GR+PTFE+colector de papel de grafito+IEM	SK	CC	PS	1.2	NaCl	128	4.7	25	-	

[27]	MnO_2/CNTs	MnO_2/CNTs+GR+PTFE+colector de papel de grafito+IEM	SK	CC	PS	1.2	NaCl	128	3.31	100	-	
[75]	CXG-SiO_2	CXG-SiO_2 MON+colector Ti	SK	CC	PS	1.2	NaCl	234	4.5	30	86%	8
[31]	CNTs/SO_3	CNTs/SiO_3+GR+PTFE+colector papel grafito	SK	CC	PS	1.2	NaCl	32	1.42	50	-	
[31]	CNTs/NH_3	CNTs/NH_3+GR+PTFE+colector papel grafito	SK	CC	PS	1.2	NaCl	32	1.39	30	-	
[31]	CNTs/COO^-	CNTs/COO^-+GR+PTFE+colector papel grafito	SK	CC	PS	1.2	NaCl	32	0.96	75	-	
[37]	GAG	GAG/Etanol+Ni foam como colector	SK	CC	PS	1.2	NaCl	500	10	7.5	73%	
[37]	GAG/TiO_2	GAG/TiO_2/Etanol+Ni foam como colector	SK	CC	PS	1.2	NaCl	500	15.8	4.1	65%	
[37]	CA	CA/DMF+PTFE+CB+Ni foam como colector	SK	CC	PS	1.2	NaCl	500	1.25	12.5	40%	
[37]	CA/ TiO_2	CA/ TiO_2/DMF+PTFE+CB+Ni foam como colector	SK	CC	PS	1.2	NaCl	500	2.5	14	-	
[76]	CA+NO_3H	CA/DMAC+PVDF sobre colector de lámina de grafito	SK	CC	PS	2.0	NaCl					
[61]	ACC-ZnO NR	ACC-ZnO NR/colector de grafito	SK	CA	PS	1.6	NaCl	1000	8.1	4	80%	
[61]	ACC	ACC-ZnO NR/colector de grafito	SK	CA	PS	1.6	NaCl	1000	5.4	4	57%	
[77]	GO/RFmsphere	GO/RF+CB+PTFE+colector Ni foam	SK	CC	PS	1.6	NaCl	800	27.76	30	81%	
[77]	CA	CA+CB+PTFE+colector Ni foam	SK	CC	PS	1.6	NaCl	800	11.3	>30	45%	
[64]	CA/KOH	CA/KOH+PVDF+DMAc	SK	CC	PS	1.0	NaCl	585	20.91	60		
[78]	GO/CNTs	GO/CNTs+CB+PVA sobre papel grafito	SK	CC	PS	1.2	NaCl	500	18.7	30	55%	
[78]	NGS	NGS+CB+PVA sobre papel grafito	SK	CC	PS	1.2	NaCl	500	21.0	40	60%	
[78]	GS	GS+CB+PVA sobre papel grafito	SK	CC	PS	1.2	NaCl	500	14.6	40	49%	
[79]	MnO_2/CF	MnO_2/CF por electrodeposición/TD=1000s (ánodo solo de CF)	SK	B	PS	0.8	$Cu(NO_3)_2$	6	140	600		
[67]	CA/TiO_2	CA/TiO_2/ DMAC+PVDF +GR sobre lámina de grafito	BC3E	B	PS	1.6	NaCl	200				
[80]	ACF-NO_3H	ACF-NO_3H/COLECTOR como cátodo/ ACF como ánodo	SK	CA	PS	1.2	NaCl	672	12.8		74%	
[81]	PPyC/CNT	PPyC/CNT+PVDF+GR+papel de grafito	SK	CC	PS	1.4	NaCl	640	11.3			
[82]	PCSs	PCSs+PVA+CB sobre colector de grafito	SK	CC	PS	1.6	NaCl	500	5.81		40%	
[83]	NPCSs	NPCSs+PVA+CB sobre colector de grafito	SK	CC	PS	1.6	NaCl	500	13.71		49%	
[66]	+CA/ZnONPs	CA/ZnONPs+PTFE sobre colector de Ti	SK	CC	PS	1.2	NaCl	500	7.2		59%	
[66]	-CA/ZnONPs	CA/ZnONPs+PTFE sobre colector de Ti	SK	CC	PS	1.2	NaCl	500	9.4	25	80%	
[66]	+CA/CuONPs	CA/ZnONPs+PTFE sobre colector de Ti	SK	CC	PS	1.2	NaCl	500	8.7		74%	
[66]	- CA/CuONPs	CA/ZnONPs+PTFE sobre colector de Ti	SK	CC	PS	1.2	NaCl	500	7.9		77%	
[66]	+CA/MnO_2NPs	CA/ZnONPs+PTFE sobre colector de Ti	SK	CC	PS	1.2	NaCl	500	5.9		38%	
[66]	-CA/ MnO_2NPs	CA/ZnONPs+PTFE sobre colector de Ti	SK	CC	PS	1.2	NaCl	500	8.2		71%	
[66]	+CA/WO_3NPs	CA/ZnONPs+PTFE sobre colector de Ti	SK	CC	PS	1.2	NaCl	500	2.7		13%	
[66]	-CA/ WO_3NPs	CA/ZnONPs+PTFE sobre colector de Ti	SK	CC	PS	1.2	NaCl	500	6.4		45%	
[66]	CA/CA	CA/CA+PTFE sobre colector de Ti	SK	CC	PS	1.2	NaCl	500	4.5		40%	
[84]	TEGO/KOH	TEGO/KOH+PTFE+CFP	SK	CC	PS	2	NaCl	74	11.9	22		
[84]	TEGO/KOH	TEGO/KOH+PTFE+CFP	SK	CC	PS	1.2	NaCl	74	4	17		
[84]	CA	CA+PTFE+CFP	SK	CC	PS	1.2	NaCl	74	2			

[65]	CA/KOH	CA/KOH+PVDF/DMAc en forma de monolito	SK	CC	PS	1.2	NaCl	29	2.1	40	
[85]	RGO/TiO_2Nr	RGO/TiO_2+ PVDF/DMAc sobre papel grafito	SK	CA	PS	1.2	NaCl	568	16	0.41	69%
[86]	OMC-H_2O_2	OMC-H_2O_2+ PVDF/DMAc en forma de monolito	SK	CC	PS	1.2	NaCl	500	6	30	50%
[87]	CNT/ACNF	CNT/ACNF sobre papel de grafito	SK	CC	PS	1.2	NaCl	500	6.4	20	25%
[88]	MOF	MOF+BINDER?	SK	CC	PS	1.2	NaCl	500	9.4	175	
[88]	CA	CA+BINDER?	SK	CC	PS	1.2	NaCl	500	5.5	125	
[89]	CNTs/CHS	CNTs/CHS+AAc sobre colector de Ti	SK	CC	PS	1.2	NaCl	58	10.7	20	
[90]	MWCNTs	MWCNT/PR+UROTROPINA sobre colector de grafito	SK	CA	PS	1	NaCl	790	-	15	
[91]	CAG act	CAG monolith/Ti collector	SK	B	PS	1,2	NaCl	5850	11,7	150	
[91]	CAG	CAG monolith/Ti collector	SK	B	PS	1,2	NaCl	5850	7,31	150	
[17]	CAG/MnAct	CAG-Mn monolith/Ti collector	SK	B	PS	0,9	NaCl	5850	6,43	130	
[17]	CAG/FeAct	CAG-Fe monolith/Ti collector	SK	B	PS	0,9	NaCl	1460	4,09	100	
[92]	CXG 355	CXGX/colector Ti	SK	B	PS	1,2	NaCl	1460	2,63	130	
[92]	CXG 480	CXGX/colector Ti	SK	B	PS	0,9	NaCl	1460	2,34	150	
[92]	CXG 500	CXGX/colector Ti	SK	B	PS	0,9	NaCl	1460	2,16	125	
[93]	CAG4-CB	CAG monolith/Ti collector	SK	B	PS	0,9	NaCl	1460	4	120	
[94]	CAG-MRF0	CAG monolith/Ti collector	SK	B	PS	0,9	NaCl	1460	3	120	
[94]	CAG-MRF1	CAG monolith/Ti collector	SK	B	PS	0,9	NaCl	1460	1	120	

Tabla 1.- Resultados de diferentes materiales en CDI. C.E. conformación de electrodo, CELDA: tipo de celda (swagelock SW o stack SK, batch cell BC); M H: modo hidráulico (B batch, CC circuito cerrado, CA circuito abierto); M EQ modo electroquímico (PS potenciostático, PS-RE potenciostático vs referencia y GS galvanostático), V/I voltaje intensidad; ELEC electrólito; C.E. concentración electrólito; SADS sal adsorbida; TADS tiempo de 9 adsorción; EQ eficiencia de carga y EST estabilidad en nº de ciclos para pérdida del 10% de actividad.

REF	**MATERIAL**	**CONFORMACION ELECTRODO**	**CELDA**	**M H**	**M EQ**	**ELEC**	**C.E**	**VV**	**J**	**v**	**CAPA**	**EST**
							(mol/l)	**(volt)**	**(mA/g)**	**(mV/s)**	**F/g**	
[95]	CAG/PCP	CAG/PCP+colector de Ni	SW	B	VC	SO_4H_2	1	0/0.8			95	
[95]	CAG/Ru/PCP	CAG/Ru /PCP+colector de Ni	SW	B	VC	SO_4H_2	1	0/0.8			268	
[96]	CAG	Monolito en contacto con colector de Ti por presión	BC	B	VC	FNa	0.01	-	-	1	30	
[97]	CAG	Monolito en contacto con colector de grafito por presión	SW	B	VC	SO_4H_2	1	-	-	1	220.4	-
[98]	G-Si	Monolito de resina de resorcinol con partículas de Si carbonizada, etched y grafitizada. grafito macroporoso			VC	FNa	0.01			1	25	
[99]	CA+CB	Casting sobre colector con termoplástico como binder	BC3E	B	VC	NaCl	0.5	.4/+0.6			45	
[100]	CA	PAC+PVDF+CB	SW3E	B	VC	SO_4H_2	1	0/1		5	150	
[100]	CA-U	PAC+PVDF+CB	SW3E	B	VC	SO_4H_2	1	0/1		5	200	
[100]	CA-M	PAC+PVDF+CB	SW3E	B	VC	SO_4H_2	1	0/1		5	330	

[100]	CA-UO	PAC+PVDF+CB	SW3E	B	VC	SO_4H_2	1	0/1		5	200
[100]	CA-MO	PAC+PVDF+CB	SW3E	B	VC	SO_4H_2	1	0/1		5	190
[100]	CA	PAC+PVDF+CB	SW3E	B	DG	SO_4H_2	1	0/1	50		253
[100]	CA-U	PAC+PVDF+CB	SW3E	B	DG	SO_4H_2	1	0/1	50		260
[100]	CA-M	PAC+PVDF+CB	SW3E	B	DG	SO_4H_2	1	0/1	50		330
[100]	CA-UO	PAC+PVDF+CB	SW3E	B	DG	SO_4H_2	1	0/1	50		246
[100]	CA-MO	PAC+PVDF+CB	SW3E	B	DG	SO_4H_2	1	0/1	50		235
[71]	CA	CA P+PTFE+CB prensado sobre colector de grafito	BC3E	B	VC	NaCl	0.1	-0.2/0.8		1	108
[71]	OMC-W	OMC P+PTFE+CB prensado sobre colector de grafito	BC3E	B	VC	NaCl	0.1	-0.2/0.8		1	140
[71]	OMC-S	OMC P+PTFE+CB prensado sobre colector de grafito	BC3E	B	VC	NaCl	0.1	-0.2/0.8		1	192
[71]	OMC-N	OMC P+PTFE+CB prensado sobre colector de grafito	BC3E	B	VC	NaCl	0.1	-0.2/0.8		1	174
[101]	CA	ACP+PVDF sobre colector de grafito	BC3E	B	VC	ClK	0.5	-0.5/0.5		5	79.4
[102]	CA	ACP+PVA sobre colector de grafito	BC3E	B	VC	ClK	0.5	-0.5/0.5		5	99.8
[103]	CAG -Mn	AGCP+PTFE+CB en 2 propanol+ colector de malla inox	BC3E	B	VC	KOH	6	-1/0		10	108
[103]	CAG-Mn mon.	AGCP+PTFE+CB en 2 propanol+colector de malla inox	BC3E	B	VC	KOH	6	-1/0		10	92
[104]	CA+MCCB	ACP+MCCP+binder termoplástico sobre colector de grafito	BC3E	B	VC	NaCl	0.5	-.4/+0.6		5	45
[104]	CAG	CAGP+binder termoplástico sobre colector de grafito	BC3E	B	VC	NaCl	0.5	-.4/+0.6		5	30
[104]	ACC	ACC+binder termoplástico sobre colector de grafito	BC3E	B	VC	NaCl	0.5	-.4/+0.6		5	31,6
[73]	RGO/RF	RGO/RF+PTFE+colector grafito	BC3E	B	VC	NaCl	1	-1/0		10	135
[73]	RGO	RGO+PTFE+colector grafito	BC3E	B	VC	NaCl	1	-1/0		10	112
[73]	CA	CA+PTFE+colector grafito	BC3E	B	VC	NaCl	1	-1/0		10	85
[105]	CAG	CAGP+PVDF+ colector de titanio	SW3E	B	VC	NaCl	0.17	-0.5/0.5		1	75
[74]	CNTs	CNTs+$Al(NO_3)_3$+colector de papel de grafito por EPD	BC3E	B	VC	ClK	1	-0.6/0.6		5	109.15
[25]	CNTs	CNTs+PAA+colector de papel de grafito por EPD	BC3E	B	VC	ClK	1	-0.6/0.6		5	59.9
[27]	MnO_2/PSS/CNTs	MnO_2/PSS/CNTs+GR+PTFE+colector de papel de grafito	BC3E	B	VC	NaCl	1	-.4/+0.6		10	78
[106]	CdD/Co Nps	CdD/Co Nps+Nafion+isoprop sobre GC como colector	BC3E	B	VC	NaCl	0.1	-.4/+0.6		10	206.1
[106]	RGO	RGO+Nafion+isoprop sobre GC como colector	BC3E	B	VC	NaCl	0.1	-.4/+0.6		10	205.5
[106]	CA	CA+Nafion+isoprop sobre GC como colector	BC3E	B	VC	NaCl	0.1	-.4/+0.6		10	120
[31]	CNTs/SO_3	CNTs/SO_3+GR+PTFE+colector papel grafito	BC3E	B	VC	NaCl	1	-.4/+0.6		10	140
[31]	CNTs/NH_3	CNTs/NH_3+GR+PTFE+colector papel grafito	BC3E	B	VC	NaCl	1	-.4/+0.6		10	110
[31]	CNTs/COO^-	CNTs/COO^-+GR+PTFE+colector papel grafito	BC3E	B	VC	NaCl	1	-.4/+0.6		10	100
[107]	VACNTs	VACNTs+colector de fibra de C pegado con resina de Si	BC2E	B	VC	NaCl	1	0/1		100	6.1 mF
[37]	GAG	GAG +nafion+colector de glassy carbon	BC3E	B	VC	NaCl	0.1	0/0.8		5	58.5
[37]	GAG/TiO_2	GAG/TiO_2+nafion+colector de glassy carbon	BC3E	B	VC	NaCl	0.1	0/0.8		5	142.6
[76]	CA	CA/DMAC+PVDF sobre colector de lámina de grafito	BC3E	B	VC	ClK	0.5	-0.5/0.5		2	53.5
[76]	CA+NO_3H	CA/DMAC+PVDF sobre colector de lámina de grafito	BC3E	B	VC	ClK	0.5	-0.5/0.5		2	73.13

[108]	THK-CA	THK-CA/PVDF sobre esponja de Ni como colector	BC3E	B	VC	KOH	6.0	-1/0	10	256
[108]	THNa-CA	THNa-CA/PVDF sobre esponja de Ni como colector	BC3E	B	VC	KOH	6.0	-1/0	10	84
[77]	GO/RFmsphere	GO/RF+CB+PTFE+colector Ni foam	BC3E	B	VC	KOH	5.3	-0.8/0.2	10	290
[77]	RFmsphere	RFMS+CB+PTFE+colector Ni foam	BC3E	B	VC	KOH	5.3	-0.8/0.2	10	72.7
[64]	CA-KOH	CA+PVDF+DMAc	BC3E	B	VC	NaCl	1	-.4/+0.6	10	175
[78]	GO/CNTs	GO/CNTs+CB+PVA sobre papel grafito	BC3E	B	VC	NaCl	1	-0.2/0.8	10	200
[78]	NGS	NGS+CB+PVA sobre papel grafito	BC3E	B	VC	NaCl	1	-0.2/0.8	5	286.86
[78]	GS	GS+CB+PVA sobre papel grafito	BC3E	B	VC	NaCl	1	-0.2/0.8	5	204.66
[79]	MnO_2/CF	MnO_2/CF por electrodeposición/TD=1000s	BC3E	B	VC	SO_4Na	1	0/1.0	5	387
[67]	CA/TiO_2	CA/TiO_2/ DMAC+PVDF +GR sobre lámina de grafito	BC3E	B	VC	NaCl	0.1	-1/1	5	135
[67]	CA	CA/DMAC+PVDF +GR sobre lámina de grafito	BC3E	B	VC	NaCl	0.1	-1/1	5	116
[109]	CA resid cafe		?	?	?	?	?	?	10	220
[82]	PCSs	PCSs+PVA+CB sobre colector de grafito	BC3E	B	VC	NaCl	1	-0.5/0.4	10	48
[83]	NPCSs	NPCSs+PVA+CB sobre colector de grafito	BC3E	B	VC	NaCl	1	-0.5/0.4	1	290
[66]	CA/ZnONPs	CA/ZnONPs+PTFE sobre colector de Ti	BC3E	B	VC	NaCl	1	-0.2/0.3	2	66
[66]	CA	CA +PTFE sobre colector de Ti	BC3E	B	VC	NaCl	1	-0.2/0.3	2	49.4
[84]	TEGO/KOH	TEGO/KOH+PTFE+CFP	SK	CC	VC	NaCl	1.2	0/2	2	20.1
[65]	CA/KOH	CA/KOH+ PVDF/DMAc en forma de monolito	BC3E	B	VC	NaCl	1	-0.4/0.6	10	66
[85]	RGO/TiO_2Nr	RGO/TiO_2+ PVDF/DMAc sobre papel grafito	BC3E	B	VC	NaCl	1	-0.4/0.6	10	450
[86]	OMC-H_2O_2	OMC-H_2O_2+ PVDF/DMAc en forma de monolito	BC3E	B	VC	NaCl	0.009	-0.4/0.8	5	99
[88]	MOF	MOF+ligante sin especificar	BC3E	B	VC	NaCl	0.5	-1.2/1.2	50	108
[88]	CA	CA+ ligante sin especificar	BC3E	B	VC	NaCl	0.5	-1.2/1.2	50	48
[89]	CNTs/CHS	CNTs/CHS+AAc sobre colector de Ti	BC3E	B	VC	NaCl	1	-0.4/0.6	20	38

Tabla 2.- Capacitancias de diferentes materiales. C.E. conformación de electrodo, CELDA: tipo de celda (swagelock SW o stack SK, batch cell 3 electrodos BC3E); MH: modo hidráulico (B batch, CC circuito cerrado, CA circuito abierto); M EQ: modo electroquímico (PS potenciostático y GS galvanostático); ELEC: electrólito; CON. EL: concentración electrólito; VV: ventana de voltaje; J: densidad gravimétrica de corriente ; v: velocidad de barrido; CAPA: capacitancia y EST: estabilidad en nº de ciclos para pérdida del 10% de actividad.

En cuanto a la estabilidad química del electrodo, es decir el número de ciclos de adsorción-desorción manteniendo su CEA, son pocos los datos que aparecen en la literatura, y en estos, apenas se estudia la estabilidad más allá de 12 ciclos [66].

A menudo en la literatura se evalúa la capacitancia electroquímica de un determinado material como un buen indicador de su comportamiento en CDI. La técnica comúnmente empleada para determinar este parámetro es la voltametría cíclica lo que dificulta los estudios comparativos, dada la variabilidad de parámetros de operación de estos ensayos (tipo y concentración de electrólito, ventana de potencial aplicada, electrodo de referencia, velocidad de barrido, del tipo de celda, etc.), No obstante se pueden establecer ciertas comparativas, Por ejemplo, Seredych y col. estudian el comportamiento electroquímica de CA modificados con melamina o con urea, empleando H_2SO_4 1 M como electrólito en una celda de tres electrodos y una ventana de potencial de 1V [100]. En estas condiciones, el CA tratado con melamina sin oxidación previa presenta un valor de capacitancia de 330 F g^{-1}, casi 3 veces superior al CA sin tratar, y que los autores atribuyen a la presencia del N aportado por la melamina. Otro ejemplo lo constituye los CA funcionalizados con óxidos metálicos [67] [66], o con tratamiento de oxidación [76], cuya capacitancia mejora con respecto a la del material no modificado.

1.2.3. Electrodos basados en fibras de carbono activadas

Las fibras de carbono activadas (ACF), se preparan por pirólisis seguida de activación química o física de fibras poliméricas estabilizadas térmicamente. Son pocos los trabajos realizados hasta el momento sobre CDI basada en ACFs. En [60] se comparan las ACF con CA y un material mixto CA/TiO_2), Si bien en este trabajo el CA/TiO_2 es el material que más sal elimina (44,9% de eliminación frente al 13,8% de las ACF), cuando la capacidad de eliminación se normaliza frente a la masa del material de electrodo, la concentración inicial de electrolito y el voltaje, se obtienen valores de CEAN muy similares para ambos materiales (0,017 y 0,014 mg $g^{-1}ppm^{-1}V^{-1}$, respectivamente). Por el contrario, la cinética del proceso es un orden de magnitud superior en el caso de las ACF ($2{,}71{,}10^{-4}$ frente a $8{,}308{,}10^{-5}$ mg $g^{-1}ppm^{-1}V^{-1}s^{-1}$).

También se han probado las ACF con tratamientos de oxidación con HNO_3 para mejorar su química superficial [80]. En este caso se obtuvo una CEA bastante similar a las anteriores de 0,0159 mg $g^{-1}ppm^{-1}V^{-1}$ aunque en este caso no se dan datos sobre la cinética del proceso. La eficiencia de carga estaba en torno al 74%.

En otro trabajo se funcionalizan las ACF con MnO_2 y se emplean para la eliminación de iones cobre en disolución de $Cu(NO_3)_2$ de 6 ppm obteniéndose una CEAN de 29,17 mg $g^{-1}ppm^{-1}V^{-1}$,valor sensiblemente más alto que los vistos hasta el momento. En este trabajo también se mide la capacitancia por voltametría cíclica en $NaSO_4$ 1M obteniéndose un valor de 387 F g^{-1}. Estos elevados valores de CEAN y capacitancia se deben por un lado al tipo de electrólito empleado y por otro al efecto pseudocapacitivo del MnO_2.

Finalmente, en [87] se sintetiza un composite de nanofibras activadas (ACNF) con CNT para eliminar NaCl, y obteniéndose una CEAN de 0,011 mg $g^{-1}ppm^{-1}V^{-1}$ y una cinética de $5,3,10^{-4}$ mg $g^{-1}ppm^{-1}V^{-1}s^{-1}$en línea con los valores del resto de los materiales, Sin embargo la eficiencia de carga para este material fue tan solo del 25%.

1.2.4. Electrodos basados en carbones mesoporosos ordenados

Los carbones ordenados mesoporosos (OMC), consisten en una estructura carbonosa altamente ordenada y uniforme procedente de la polimerización y carbonización de determinados precursores orgánicos en presencia de un molde o template, generalmente de carácter silíceo que se elimina después de la carbonización dejando una estructura porosa ordenada. El OMC se aplicó por vez primera a electrodos de CDI en 2008 [71], pero son pocas las publicaciones sobre este material en CDI. Entre los trabajos más representativos de OMCs aplicados a CDI tenemos [71] donde preparan OMCs empleando como molde ortosilicato de tetraetilo (TEOS) junto con $Ni\ SO_4 \cdot 6H_2O$ (OMC-S) o $Ni(NO_3)_2 \cdot 6H_2O$ (OMC-N) o TEOS solo (OMC-W). Para estos materiales se obtienen CEAs de 0,025, 0,0144 y 0,016 mg $g^{-1}ppm^{-1}V^{-1}$ con unas cinéticas de $2,49 \cdot 10^{-4}$, $1,44 \cdot 10^{-4}$ y $1,60 \cdot 10^{-4}$ mg $g^{-1}ppm^{-1}V^{-1}s^{-1}$ respectivamente. Se observa que tanto la CEA como la constante cinética del OMC-S son superiores a los de sus homólogos y a los valores típicos de materiales de carbono revisados hasta el momento. Esto se achaca a que el OMC-S aunque tiene un área superficial específica similar a la de OMC-N

(ambas mayores que OMC-W), el diámetro de los poros es mayor (3,7 nm frente a 3,3 nm). En las medidas de voltametría se obtuvieron valores de 192 (OMC-S), 174 (OMC-N) y 140 (OMC-W) F g^{-1}, lo que sigue más o menos la tendencia de los valores de CEAN.

En otro trabajo llevado a cabo en 2015 [86] se preparan seis OMC cambiando las condiciones de síntesis, obteniéndose materiales con superficies específicas entre 709-732 m^2 g^{-1} y 1400-1481 m^2 g^{-1}. Las CEAN del primer grupo son 0,007 y 0,003 mientras que en el segundo grupo van de 0,010 a 0,015 mg $g^{-1}ppm^{-1}V^{-1}$, observándose una clara correlación entre la superficie específica BET y la capacidad de electroadsorción en todas las muestras sintetizadas. Por otra parte, se obtienen mayores capacitancias medidas por voltametría cíclica en las muestras con mayores áreas superficiales, con eficiencias de carga rondando el 50% en todos los casos.

1.2.5. Electrodos basados en grafeno

El grafeno, aislado por vez primera por Andre Geim y Konstantin Novoselev en 2005, consiste, idealmente, en una lámina bidimensional de átomos de carbono con hibridación sp^2 que le confiere una elevada conductividad eléctrica y con una superficie teórica de 2630 m^2/g. El grafeno real, por su tendencia a agregarse, consta generalmente de 3-5 capas en los mejores casos y aparece formando pliegues intrincados que conforman poros tipo rendija en su seno. Todas estas propiedades hacen que sea un candidato a priori adecuado como material de electrodo para CDI.

El grafeno se aplicó por vez primera en CDI en 2009 [32], obteniéndose valores de capacidad de electroadsorción bastante elevados. Entre los trabajos más representativos cabe destacar el realizado por Li et al [32], que sintetizan copos de grafeno por exfoliación química y reducción con hidrazina. La CEAN obtenida de los electrodos de este material fue de 0,027 mg $g^{-1}ppm^{-1}V^{-1}$, del orden del doble de los materiales estudiados hasta el momento, con una constante cinética normalizada de $3{,}37 \cdot 10^{-2}$ mg $g^{-1}ppm^{-1}V^{-1}s^{-1}$, también de las más elevadas obtenidas hasta la fecha con otros materiales. En 2012, Wang y col [73] sintetizan un composite de RGO con resorcinol-formaldehido (RGO/RF) extendido sobre un colector de grafito consiguiendo CEAN de 0,025 mg $g^{-1}ppm^{-1}V^{-1}$ frente a 0,014 del RGO sin RF. Las constantes cinéticas

normalizadas fueron en este caso de $8{,}28 \cdot 10^{-4}$ y de $4{,}62 \cdot 10^{-4}$ mg g^{-1} ppm^{-1} V^{-1} s^{-1} respectivamente. Con estos materiales obtuvieron capacitancias por VC de 135 Fg^{-1} en NaCl 1M. En la misma línea Liu y col [77] sintetizaron microesferas de RF envueltas en GO depositadas sobre colectores de espuma de Ni donde conseguían, dependiendo de la cantidad de GO añadida, superficies de 94 a 1128 m^2/g. Con este último, conseguían CEAs en torno a 0,021-0,023 $mg(g.ppm.V)^{-1}$ dependiendo del voltaje aplicado y unas eficiencias de carga entre 78% y el 81%. Las cinéticas linearizadas de este material mostraron resultados en línea con el anterior.

Xu y col sintetizan esponjas híbridas de GO y CNT consiguiendo CEAN de hasta 0,035 mg $g^{-1}ppm^{-1}V^{-1}$y eficiencias de carga del 60% por la adición de los CNT [78]. También describen cinéticas muy elevadas para estos materiales, de hasta $9 \cdot 10^{-4}$ mg $g^{-1}ppm^{-1}V^{-1}s^{-1}$. En este caso las superficies específicas no son elevadas (valores de 345 y 493 m^2 g^{-1}), sin embargo tanto el diámetro de poros de en torno a 12 nm junto con la elevada conductividad eléctrica del material (ca. 1,1 S cm^{-1}) parecen ser factores clave para el elevado rendimiento de estos materiales. Li y col preparan GO activado con KOH obteniendo un valor de CEAN de 0,08 mg $g^{-1}ppm^{-1}V^{-1}$, el más elevado registrado hasta el momento [84]. La cinética de adsorción de $3{,}22 \cdot 10^{-3}$ mg $g^{-1}ppm^{-1}V^{-1}s^{-1}$ también es de las más elevadas. La capacitancia de 20 Fg^{-1} no se corresponde con los elevados valores de CEAN, hecho que puede ser debido a la baja concentración de electrólito (1,5 mM) empleada en los ensayos de voltametría cíclica.

En el apartado de materiales híbridos basados en grafeno, cabe destacar [85] donde se sintetiza un composite de RGO con nanorods (NR) de TiO_2. En este caso la CEAN y la eficiencia de carga son de 0,044 mg $g^{-1}ppm^{-1}V^{-}$ y 69% respectivamente, valores que están más o menos en línea con otros trabajos sobre estos materiales. Sin embargo, tanto la capacitancia como la cinética de adsorción se disparan considerablemente con valores de 443 Fg^{-1} a 10 mV/s en NaCl 1M, y $1{,}07 \cdot 10^{-1}$ mg $g^{-1}ppm^{-1}V^{-1}s^{-1}$. Este trabajo también aporta datos de estabilidad de los electrodos durante 25 ciclos de carga-descarga.

1.2.6. Electrodos basados en nanotubos de carbono (CNT)

Los CNT corresponden a la forma unidimensional de los alótropos de carbono y fueron aislados por vez primera por Iijima en 1991, aunque las primeras imágenes de

microscopia de transmisión fueron captadas por Radushkevich y Lukanovich en 1952 [110]. Se caracterizan, al igual que el grafeno por tener su área de adsorción expuesta al exterior, lo que es conveniente para la cinética de electroadsorción, y por tener una baja superficie específica. Su aplicación a CDI data de 2005 cuando se sintetizan por vez primera electrodos basados en nanotubos de carbono multipared MWCNT [90]. En este trabajo se preparan MWCNT mediante descomposición de metano sobre un catalizador de aerogel de óxido de niquel-sílice, los someten a oxidación y conforman electrodos con resina fenólica y urotropina. Las superficies de los materiales preparados varían de 50 a 128 m^2g^{-1} y el volumen de poros de 0,07 a 0,400 cm^3/g, sin embargo en este trabajo no aportan ningún dato sobre capacitancia o CEA.

Posteriormente se han llevado a cabo diversos trabajos sobre CDI empleando electrodos conformados con CNT, CNT funcionalizados y electrodos compuestos con otros materiales. En todos ellos, los valores de CEA son en general más elevados que los de otros materiales de carbono (a excepción del grafeno). Las CEAN que se obtienen en la mayoría de los trabajos consultados oscilan entre 0,020 y 0,037 mg $g^{-1}ppm^{-1}V^{-1}$, con cinéticas que van de $2\cdot10^{-3}$ a $3\cdot10^{-4}$ mg $g^{-1}ppm^{-1}V^{-}s^{-1}$. Esto incluye tanto electrodos fabricados con CNT mezclados con diferentes ligantes, como materiales compuestos mediante la adición de TiO_2 [60], ácido poliacrílico [25], MnO_2 y sulfonato sódico de poliestireno [27], con grafeno [78], con polipirrol [81], con CNF [87] o CNT funcionalizados con grupos amino y carboxilo [31] o depositados sobre el colector mediante electroforesis en presencia de $Al(NO_3)_3$ [74].

Entre todos los estudios revisados, llama especialmente la atención el comportamiento electroadsortivo de un electrodo compuesto de CNT y chitosano (CHS) montado sobre colector de Ti, por ser con diferencia el que mayor CEAN (valor de 0,15 mg $g^{-1}ppm^{-1}V^{-1}$) [89], casi el doble de lo obtenido con el mejor material a base de grafeno. También es de los materiales basados en CNT el que mejor cinética de adsorción presenta, con un valor de $8\cdot10^{-3}$ mg $g^{-1}ppm^{-1}V^{-1}s^{-1}$. Teniendo en cuenta la superficie específica de estos materiales (oscila entre 192 y 651 m^2 g^{-1}), que es sensiblemente menor que la de OMC o CA, los resultados de CEAN apuntan a que la conductividad eléctrica del material es un parámetro crucial para obtener capacidades de electroadsorción de iones elevadas. Al tener una elevada conductividad, la densidad superficial de cargas (electrones o vacantes) es más elevada que en otros materiales, lo que permite albergar mayor concentración de iones en la EDL por unidad de superficie,

compensando sobradamente la menor superficie específica que presentan estos materiales.

1.2.7. Electrodos basados en Aerogeles de Carbono

Posteriormente en 1995, y después de un periodo largo de 17 años en que no se llevó a cabo ninguna investigación sobre CDI, Farmer y Pekala fabrican electrodos a base de aerogel de carbono y los aplican a CDI [9]. En estas investigaciones, la conformación del electrodo para CDI se hacía infiltrando la solución de los precursores de los aerogeles en papel de carbón poroso (PCP), gelificando todo el conjunto entre dos placas selladas y siguiendo todo el proceso de intercambio, secado y pirólisis con la pieza del electrodo completa. En estos trabajos obtuvieron CEAN entre 0,005 y 0,020 mg $g^{-1}ppm^{-1}V^{-1}$para NaCl con unas cinéticas entre $1{,}1\cdot10^{-4}$ y $1{,}7\cdot10^{-4}$ mg $g^{-1}ppm^{-}1V^{-1}$ s^{-1}. También evaluaron la capacidad de estos materiales para la eliminación de iones nitrato y fluoruro, obteniendo valores de CEAN sensiblemente mayores para estas sales. Por ejemplo, para $NaNO_3$ obtuvieron valores entre 0,0113 y 0,0350 mg $g^{-1}ppm^{-1}V^{-1}$con cinéticas entre 1,5 y $3\cdot10^{-4}$ mg $g^{-1}ppm^{-1}V^{-1}s^{-1}$ para el aerogel infiltrado o directamente pegado a colector de Ti, respectivamente.

Además de estos primeros trabajos, cabe destacar el trabajo de Ying y col [68] sobre un composite de electrodo con aerogeles de carbono comerciales sobre un colector de Ti obtieniendo CEAN 0,02-0,026 mg $g^{-1}ppm^{-1}V^{-1}$ y cinéticas entre 1,1 y $1{,}5\cdot10^{-4}$ mg $g^{-1}ppm^{-1}V^{-1}s^{-1}$. Jung y col consiguen el mayor de valor de capacidad de electroadsorción publicado para un aerogel de carbono, de 0,037 mg $g^{-1}ppm^{-1}V^{-1}$, con monolitos activados en aire a 450 ºC (22 mm de diámetro x 0,44 mm de espesor) soportados sobre un colector de Ti [63]. En este material la cinética era del mismo orden que en los anteriores, en torno $1{,}2\cdot10^{-4}$ mg $g^{-1}ppm^{-1}V^{-1}s^{-1}$. Otros trabajos empleando electrodos monolíticos no presentan capacidades tan elevadas, probablemente debido a los mayores espesores de los electrodos (superiores a 1mm), que producen una elevada resistencia óhmica. Por ejemplo Zafra y col obtienen valores de CEAN de 0,001 y 0,002 en monolitos de aerogeles de carbono de grosor superior a 1 mm [91], y valores alrededor de 0,0030 para aerogeles de carbono funcionalizados con nanopartículas de manganeso o hierro [17]. Esta influencia negativa del espesor también se observa en las cinéticas de adsorción obteniéndose valores en el entorno de 10^{-5} mg $g^{-1}ppm^{-1}V^{-1}s^{-1}$ en

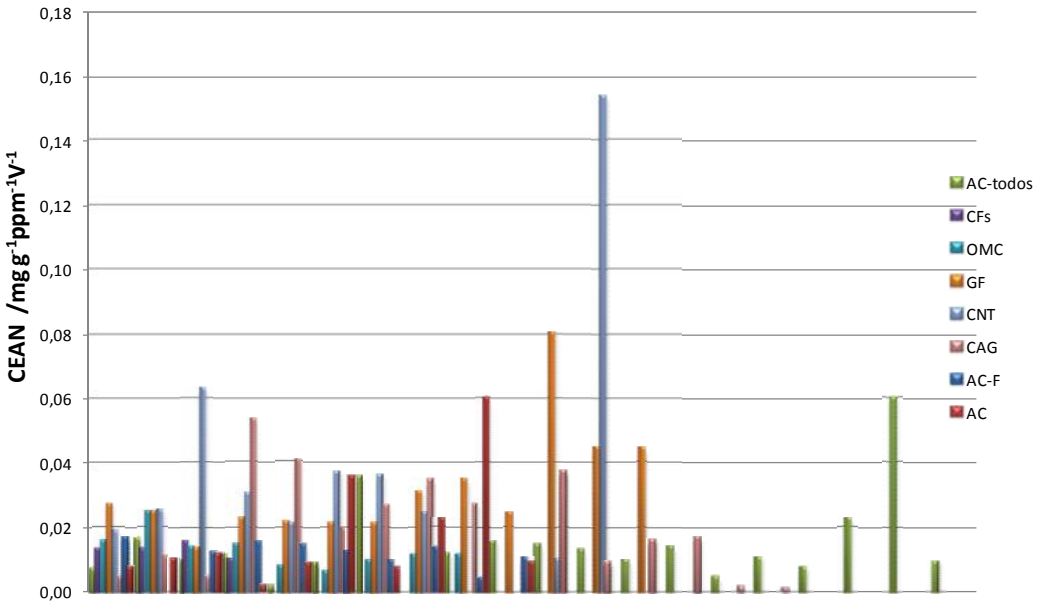
0,18
0,16
0,14
0,12
0,10
0,08
0,06
0,04
0,02
0,00
CEAN /mg g-1ppm-1V-1
AC-todos
CFs
OMC
GF
CNT
CAG
AC-F
AC

1.3. AEROGELES DE CARBONO

El motivo principal de este trabajo es ver cómo se comporta la capacidad de electroadsorción en relación con las propiedades texturales del material y en función de esta relación, ver si es posible conseguir un material optimizado para CDI basado en CAG.

1.3.1. Estructura y propiedades de los aerogeles de carbono

Los geles de carbono se pueden definir como una estructura porosa integrada por partículas nanométricas de tamaño variable y que están agrupadas en clusters ramificados también de tamaño variable. El diámetro de las partículas depende de ciertos factores de síntesis que se explican más abajo y oscila entre 3 y 100 nm.

Según se aprecia en la Figura 9, los espacios vacíos entre los clusters de nanopartículas, conforman la estructura de macroporos mientras que los espacios intersticiales entre las nanopartículas de gel conforman la red de mesoporos. Los microporos los conforman los espacios que quedan entre los pliegues de las láminas grafénicas agrupadas que constituyen las nanopartículas [111, 112] . El tamaño y grado de agregación de las nanopartículas se pueden en cierta medida definir controlando las condiciones de síntesis del gel, por lo que las propiedades texturales también vendrán definidas por estas condiciones [113, 114]. Son estas propiedades texturales las que confieren las propiedades físicas de los aerogeles de carbono como las conductividades térmica y eléctrica, la densidad o la capacidad eléctrica.

Con respecto a las propiedades texturales, los aerogeles de carbono presentan una superficie específica entre 500 y 750 $m^2\ g^{-1}$ para aerogeles pirolizados hasta más de 3000 $m^2\ g^{-1}$ para aerogeles activados [115, 116], con volúmenes de poro que van de 0,1 a cerca de 2 $cm^3\ g^{-1}$ para los aerogeles más activados. En cuanto al tamaño de poro, podemos encontrar distribuciones unimodales muy centradas en un tamaño concreto que puede ir de los 3 a los 15 nm o, más frecuentemente, distribuciones bimodales que se mueven en los mismos rangos [117]. En el rango de los macroporos, se pueden encontrar tamaños de los 60 a más de 100 nm dependiendo este parámetro fuertemente del procedimiento de secado del gel [118].

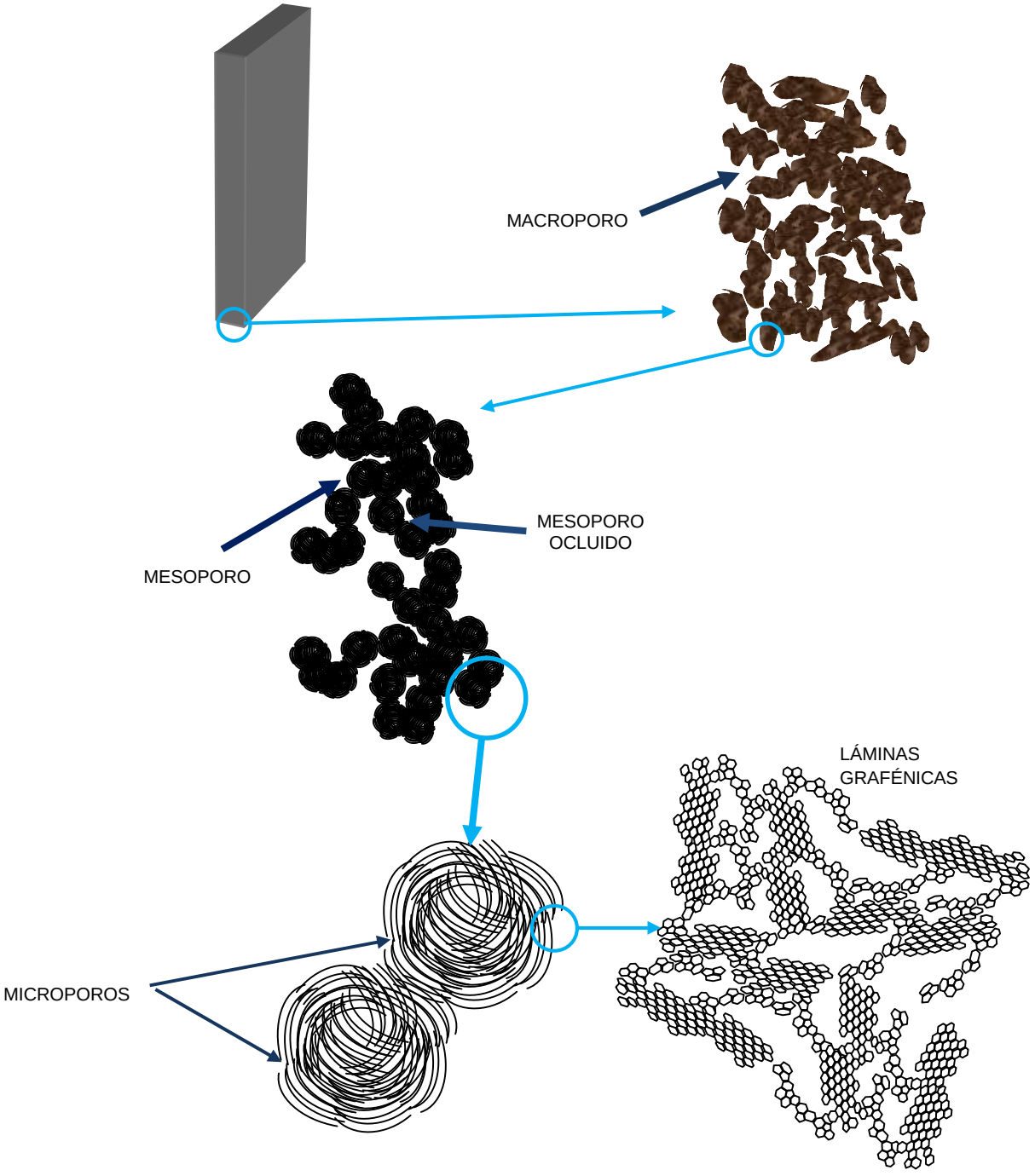
MACROPORO
MESOPORO
MESOPORO
OCLUIDO
LÁMINAS
GRAFÉNICAS
MICROPOROS

Otra propiedad interesante de los aerogeles de carbono es la capacidad electroquímica específica. Esta propiedad depende principalmente de características internas del material como la superficie específica y el volumen de poros y de la conductividad eléctrica del material [120, 121], aunque se ve altamente influenciada por factores externos como el tipo y la concentración de electrólito fundamentalmente. El valor de esta propiedad suele mostrar una elevada correlación con la capacidad de electroadsorción iónica en CDI cuando las medidas se hacen con el mismo tipo de electrólito.

Además de los aerogeles puros, ya se vio en la sección 1.2., que el empleo de aditivos funcionales en la formulación tiene una gran influencia en las propiedades texturales y conductoras del material mejorando en ciertos casos sus propiedades electroquímicas [93, 122, 123].

Como se mencionó en la sección 1.2.6., el interés de los CAG como material de electrodo para CDI radica en la posibilidad de controlar su textura y propiedades manejando los parámetros de síntesis como la naturaleza y concentración de los precursores, las condiciones de polimerización y curado de los hidrogeles, las condiciones de secado y las condiciones de pirólisis y/o activación de los aerogeles resultantes y en la influencia que tienen estos parámetros texturales en la eficacia electroadsortiva del material.

1.3.2. Síntesis de los aerogeles de carbono e influencia de los diferentes parámetros

Para obtener aerogeles de carbono se parte de un hidrogel orgánico que se obtiene por policondensación de un precursor aromático hidroxilado y un agente de entrecruzamiento. Entre los primeros se pueden emplear compuestos fenólicos como el fenol, catecol o hidroquinona siendo el más frecuente resorcinol ya que posee una buena solubilidad en agua y una elevada reactividad. Como agente de entrecruzamiento se empela un aldehído siendo el más común el formaldehido [115]. Entre los medios de polimerización más comunes se encuentran la acetona, el etanol o el agua, siendo este último el más frecuente. Las reacciones de policondensación son endotérmicas por lo que se hace necesario el uso de un catalizador, el cual puede ser ácido o básico, teniendo este factor una gran influencia en la nanoestructura final del gel [115]. En los geles de

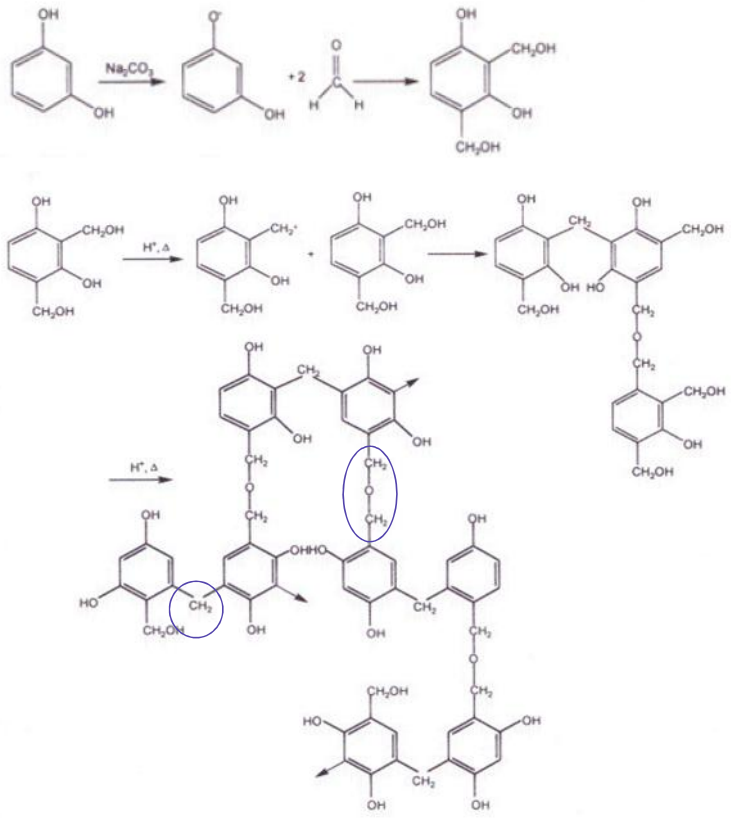
OH
Na2CO3
O-
+ 2
O
C
H
H
CH2OH
H+, Δ
CH2-
HO
CH2
O
OH

hidroximetilo que proporciona un nuevo punto de crecimiento. Según van progresando estas reacciones, van dando paso a la formación de clusters para las siguientes reacciones de condensación.

Esta etapa se lleva a cabo por incubación en estufa a temperaturas moderadas (60-70 ºC) durante 5 días, si bien en un trabajo reciente se han obtenido geles porosos con buen desarrollo micro-mesoporoso en 4 horas a temperaturas de 85-90 ºC demostrándose a su vez que la temperatura de la gelificación y el proceso de curado, afectan principalmente a la formación de la estructura mesoporosa, mientras que la microporosidad depende de la composición del precursor de mezcla [124]. Además del calentamiento convencional mediante estufa, la gelificación y curado se puede inducir por la aplicación de microondas obteniéndose materiales con porosidades similares [125].

En esta etapa queda definida la nanoestructura básica del material. Inicialmente, las reacciones de condensación forman clusters cuyo tamaño y grado de entrecruzamiento depende principalmente de la relación precursor/catalizador y de las concentraciones de precursor y agente de entrecruzamiento respectivamente pudiendo variar su tamaño entre 3 y 100 nm. Una vez formados, los clusters tienden a agregarse por interacciones electrostáticas inicialmente y covalentes posteriormente, dando lugar a estructuras altamente ramificadas que se preservarán en el aerogel carbonizado [115]. Cuando la relación precursor/catalizador es alta, tienden a formarse clusters de tamaño mayor lo que da lugar a geles meso-macro porosos de tipo coloidal y cuando esta relación llega a valores inferiores a 50, el tamaño de los clusters disminuye tanto que se hacen indistinguibles dando lugar a un gel polimérico microporoso con algo de mesoporosidad [119]. Las relaciones habituales de trabajo son entre 50 y 500 y se emplea normalmente un catalizador alcalino. La concentración de precursores por su parte, incide directamente sobre la densidad del gel y su macroporosidad [112]. A menor concentración, los geles son menos densos y más macro-mesoporosos y a mayores concentraciones predomina la microporosidad. Hay que decir que por debajo de una concentración crítica no se produce la gelificación.

El pH de la disolución inicial de precursores es una variable relacionada con la concentración de catalizador y tiene una influencia directa en las propiedades texturales. El rango de trabajo habitual está entre 6 y 7. A pH mayor de 7,5 se suprime la meso y la macroporosidad y la microporosidad disminuye mucho por los que se obtienen materiales de escasa funcionalidad. Para pH ácidos (inferior a 5,4) se suprime la mesoporosidad obteniéndose geles micro y macroporosos.

El disolvente empleado en la mezcla inicial tiene también una gran incidencia ya que influye en la cinética del proceso de polimerización lo que a su vez influye en la estructura y tamaño de las nanopartículas de gel y sus agrupamientos. En general, los disolventes orgánicos producen cinéticas más lentas que el agua [126].

- **Intercambio de disolvente.-** Cuando la etapa de gelificación se hace en medio acuoso, se hace necesario su sustitución por algún disolvente orgánico que tenga menor tensión superficial que el agua ya que con ello se evitará el colapso de la estructura porosa del gel por la evaporación del disolvente durante el secado, sea cual sea el método que se emplee en esta etapa. El proceso de intercambio se realiza con un disolvente orgánico como metanol, acetona o t-butanol, dependiendo del tipo de secado que se vaya a hacer.

- **Secado.-** Una vez intercambiado el disolvente, el gel resultante se puede secar por diversos procedimientos que se pueden englobar en tres tipos:

  - *Secado subcrítico*, en el que las condiciones de secado están por debajo de la presión y temperatura críticas del medio, normalmente aire, donde se produce el secado. Los geles obtenidos por este método se denominan “xerogeles” y requieren de un disolvente de muy baja tensión superficial para evitar el colapso de la estructura microporosa. La aplicación de microondas en este tipo de secado es especialmente conveniente ya que ahorra un tiempo y energía considerables y preserva la estructura microporosa [127].

  - *Secado por congelación* en el que las condiciones de secado están por debajo de la temperatura de fusión del disolvente el cual se elimina directamente por sublimación a vacío. Los geles obtenidos mediante este

tipo de secado se denominan “criogeles”. Al no haber fase líquida en este proceso, no se producen tensiones capilares en el interior de la estructura y el encogimiento es muy leve manteniendo la mesoporosidad. Para este secado conviene emplear un disolvente orgánico como el terbutanol con apenas variaciones en el cambio a estado sólido.

- *Secado supercrítico* en el que las condiciones del medio de secado, generalmente CO_2 se mantienen por encima de su temperatura y presión críticas. Los geles obtenidos con este tipo de secado se denominan “aerogeles”. En este procedimiento, primeramente se realiza un intercambio del disolvente del gel con CO_2 líquido en un reactor adecuado a tal efecto y a continuación se lleva a condiciones supercríticas directamente desde el estado líquido y seguidamente se pasa a fase gas desde el estado supercrítico para eliminar todo el CO_2 del gel. De este modo se evita la formación de fases líquidas que puedan dar lugar a tensiones capilares y se mantiene la estructura original del gel. Las condiciones empleadas son 45 ºC y 11MPa. Durante esta etapa puede darse una ligera pérdida de volumen si el gel húmedo conserva algunos pequeños nódulos inferiores a 20 nm o ultramicroporos [118].

- **Pirólisis**.- Una vez que se ha secado el gel, se procede a su carbonización que se realiza en atmósfera inerte empleando gases como el Ar, He o más comúnmente N_2, y aplicando un rango de temperaturas entre 600 y 1000 ºC. Durante esta etapa se eliminan por reacciones de pirólisis el carbono más inestable, el hidrógeno y gran parte del oxígeno del gel inicial, reorganizándose el carbono en láminas más o menos grafitizadas que constituyen la superficie de adsorción. Dependiendo de la temperatura de pirólisis, la pérdida de peso en este proceso puede rondar el 50%. Los cambios químicos producidos durante la carbonización, inducen ciertos cambios texturales en el material como es el incremento del volumen de mesoporos y microporos y en consecuencia el área superficial pero es preciso controlar la velocidad de calentamiento para impedir una formación brusca de los gases de pirólisis lo que podría comprometer la integridad del material. A temperaturas superiores a 600 ºC se produce una

disminución de la superficie específica y del volumen de poros en comparación con el aerogel orgánico.

La pirólisis también incide directamente sobre las propiedades conductoras del material ya que a temperaturas inferiores a 700 ºC el material pirolizado presenta muy baja conductividad eléctrica y a partir de 750 ºC esta se incrementa enormemente. Esto se debe a un aumento de la aromatización del material con la temperatura de pirólisis.

- **Activación.-** Esta etapa consiste en la eliminación del carbono más reactivo del material pirolizado mediante reacciones de gasificación con agentes oxidantes como agua, CO_2 o bases fuertes como KOH. La temperatura de este proceso debe ser igual o superior a la de pirólisis ya que esta última es a la que se ha estabilizado el carbono por lo que no reaccionaría con los agentes oxidantes. Mediante las reacciones de gasificación, se eliminan las regiones menos ordenadas desarrollándose la microporosidad y en muchas ocasiones desplazando el rango de mesoporos hacia tamaños mayores. Esto da como resultado un aumento en el volumen total de poros y en la superficie específica. El grado de activación depende de la temperatura y del tiempo y valores excesivos de estos dos parámetros pueden llevar a pérdida de superficie por exceso de quemado y a materiales demasiado débiles y pulverulentos.

1.4. HIPÓTESIS, OBJETIVOS Y PLAN DE TRABAJO

Hipótesis

La eficacia de un material de electrodo para desionización capacitiva se puede evaluar principalmente en función de su capacidad de electroadsorción, de la velocidad a la que puede realizar este fenómeno, de la reversibilidad del mismo y de la estabilidad química del material durante muchos ciclos. Como se ha visto en la introducción, en todos los materiales revisados, todas estas propiedades dependen a su vez de modo más o menos complejo de factores relacionados con la distribución de tamaños de poro, con el volumen de poros y la superficie específica, con la composición química y con la conductividad eléctrica del material, factores que a su vez se interrelacionan entre sí de forma también intrincada.

Como también se ha visto, en el caso de los aerogeles de carbono todos estos factores dependen completamente de parámetros que se pueden controlar en el proceso de síntesis como son las concentraciones de precursores y catalizador, la temperatura de pirólisis y el grado de activación. También se ha visto que el empleo de aditivos funcionales puede mejorar en muchas ocasiones algunas de las propiedades electroquímicas interesantes para la CDI.

Aunque se han realizado diversos trabajos en este sentido, las relaciones entre los tres conjuntos de variables definidos anteriormente (variables de síntesis, del material y electroquímicas) no están actualmente bien dilucidadas.

El aerogel de carbono constituye un modelo excelente para estudiar todas estas relaciones en profundidad ya que, a diferencia de otros materiales, permite un elevado control sobre sus propiedades finales mediante los parámetros de síntesis entre cuyos valores se pueden determinar combinaciones que permitan obtener aerogeles de carbono con propiedades electroquímicas adecuadas para ser un material de electrodo competitivo en desionización capacitiva.

Objetivos y plan de trabajo

Con el presente trabajo se pretende contribuir al esclarecimiento de las relaciones entre estructura y propiedades electroquímicas y a hallar combinaciones de parámetros de síntesis que permitan obtener aerogeles de carbono con propiedades electroquímicas adecuadas para ser un material de electrodo competitivo en desionización capacitiva.

Los objetivos específicos que se quieren alcanzar son:

I. Evaluar el efecto de un amplio rango de proporciones resorcinol-catalizador y resorcinol-agua sobre los parámetros texturales y las propiedades electroquímicas de aerogeles de carbono.

II. Determinar la aplicabilidad de aerogeles de carbono con mesoporosidad controlada a la electroadsorción de iones fosfato y nitrato.

III. Estudiar el efecto de la temperatura de pirólisis y del negro de carbono como aditivo funcional en la textura de los aerogeles de carbono y en las propiedades eléctricas (resistividad) y electroquímicas.

IV. Analizar el efecto del empleo de la tierra de diatomea como aditivo preservador de la textura porosa y la resistencia mecánica de los aerogeles de carbono.

V. Evaluar el efecto sinérgico de la funcionalización mediante dopado con nitrógeno y la combinación de varios aditivos, como negro de carbono, manganeso y/o diatomea en las propiedades texturales y electroquímicas de aerogeles de carbono.

En el plan de trabajo diseñado para el logro de estos objetivos se especifican los trabajos experimentales necesarios para llegar a resultados medibles y conclusiones válidas, reflejándose todos ellos en el compendio de publicaciones que constituyen los capítulos de la presente memoria y que se detallan a continuación

1. Síntesis y caracterización de varios aerogeles de carbono obtenidos por policondensación de resorcinol y formaldehído empleando carbonato sódico como catalizador, con proporciones de resorcinol-formaldehído (R/F= 0.5) y varias proporciones de resorcinol-agua (R/W=0.04 a 0.013) y resorcinol-catalizador

($100 \leq R/C \leq 600$). Los geles precursores se pirolizan a 800 °C en atmósfera inerte de nitrógeno y una parte de los aerogeles pirolizados se activan a la misma temperatura con CO_2 durante 2 horas.

2. Caracterización textural, mediante isotermas de adsorción–desorción de nitrógeno para determinar el área superficial, volumen de poro y la distribución de tamaño de poro empleando el modelo 2D-NLDFT-HS y mediante microscopía electrónica de transmisión.

3. Determinación de la capacidad de los aerogeles de carbono mediante voltametría cíclica con electrodos de material en polvo, en celda Swagelock de tres electrodos, a diferentes velocidades de barrido y empleando NaCl como electrólito. Evaluación de la resistencia de polarización mediante espectroscopia de impedancia electroquímica con el mismo montaje electroquímico.

4. Determinación de las capacidades másica y volumétrica de electroadsorción de los diferentes aerogeles en formato monolito, en celda simétrica de dos electrodos, midiendo la corriente capacitiva en condiciones potenciostáticas.

Los puntos del 1 a 4 del plan de trabajo se desarrollan a lo largo de la sección 2.1 del capítulo 2 de la presente memoria.

5. Síntesis de aerogeles de carbono con proporciones optimizadas R/F= 0.5, R/W=0.06 y R/C= 200 a 600. Los geles precursores se pirolizan a 800 °C en atmósfera inerte de nitrógeno y una parte de los aerogeles pirolizados se activan a la misma temperatura con CO_2 durante 2 horas.

6. Caracterización textural, mediante isotermas de adsorción–desorción de nitrógeno para determinar el área superficial, volumen de poro y la distribución de tamaño de poro mediante DFT y DR.

7. Caracterización química y estructural de los materiales mediante difracción de Rayos X, espectroscopía Raman, análisis elemental y espectroscopía fotoelectrónica de Rayos X (XPS).

8. Determinación de la capacidad de los aerogeles de carbono mediante voltametría cíclica con electrodos de material en polvo, en celda Swagelock de tres electrodos, a diferentes velocidades de barrido y empleando $NaNO_3$ y Na_2HPO_4/NaH_2PO_4 como electrólitos. Evaluación de la cinética de adsorción mediante cronoculometría. Evaluación de la resistencia de polarización mediante espectroscopia de impedancia electroquímica.

9. Determinación de las capacidad gravimétrica de electroadsorción de los diferentes aerogeles en formato monolito, en celda simétrica de dos electrodos, midiendo la variación de conductividad eléctrica, en condiciones potenciostáticas, en cada una de las soluciones de electrólito definidas en el punto 8.

Los puntos 5 a 9 del plan de trabajo se desarrollan a lo largo de la sección 2.2. del capítulo 2 de la presente memoria.

10. Síntesis de aerogeles de carbono con proporciones optimizadas R/F= 0.5, R/W=0.06 y R/C= 25 a 200. Los geles precursores se pirolizan a 500 ^{o}C y a 1000 ºC durante 2 horas. Preparación de una serie similar en las mismas condiciones pero añadiendo un 10% w/w de negro de carbono a la mezcla de resorcinol-formaldehido..

11. Caracterización textural, mediante isotermas de adsorción–desorción de nitrógeno para determinar el área superficial, volumen de poro y la distribución de tamaño de poro mediante DFT y DR. Caracterización morfológica mediante TEM y FE-SEM.

12. Caracterización química de los materiales mediante microanálisis SEM/EDX y análisis elemental CHNS.

14. Determinación de la capacidad de los materiales mediante voltametría cíclica con electrodos de material en polvo, en celda Swagelock de tres electrodos, a diferentes velocidades de barrido y empleando H_2SO_4 como electrólito. Determinación de la degradación del electrodo mediante ciclos repetidos de carga/descarga potenciostática a 1,4 V durante 500 horas.

15. Determinación de la resistividad eléctrica de los materiales mediante la técnica de Van der Pauw.

Los puntos 10 a 15 del plan de trabajo se desarrollan a lo largo de la sección 3.1. del capítulo 3 de la presente memoria.

16. Síntesis de aerogeles funcionalizados con nitrógeno a base de precursores de melamina (M), resorcinol (R) y formaldehído (F) con proporciones molares R/M = 0,5 y diferentes proporciones de (M+R)/C manteniendo (M+R)/F y (M+R)/W en 0,428 y 0,052, respectivamente. Se preparan compuestos funcionales híbridos conteniendo negro de carbono (CB) y/o diatomea (D). Se pirolizan a 800 ºC y se lixivian con HF para retirar el aditivo síliceo.

17. Caracterización textural, mediante isotermas de adsorción–desorción de nitrógeno para determinar el área superficial, volumen de poro y la distribución de tamaño de poro mediante DFT y DR.

18. Medidas de las propiedades elásticas mediante ensayos de microcompresión y obtención de curvas de presión-desplazamiento de los materiales.

19. Medidas de resistencia a la rotura mediante ensayos de microdureza.

Los puntos 16 a 19 del plan de trabajo se desarrollan a lo largo de la sección 3.2. del capítulo 3 de la presente memoria.

20. Síntesis de aerogeles funcionalizados con nitrógeno a base de precursores de melamina (M), resorcinol (R) y formaldehído (F) con proporciones molares R/M, (M+R)/C, (M+R)/F y (M+R)/W de 0,5, 135, 0,428 y 0,052 respectivamente. Se obtienen compuestos funcionales híbridos conteniendo negro de carbono (CB) y diatomea (D), seguido de pirólisis a 800 ºC durante 2 horas y lixiviado con HF de la mitad de los que llevan D.

21. Caracterización textural, mediante isotermas de adsorción–desorción de nitrógeno para determinar el área superficial, volumen de poro y la distribución de tamaño de poro mediante 2D-NLDFT-HS y del volumen de microporos mediante DR. Caracterización morfológica mediante microscopías TEM y FE-SEM.

22. Caracterización química y estructural de los materiales mediante difracción de Rayos X y espectroscopia Raman.

23. Determinación de los límites elásticos y de rotura mediante ensayos de microcompresión y obtención de curvas de presión-desplazamiento de los materiales.

24. Medidas de resistencia a la rotura mediante ensayos de microdureza.

25. Determinación de la capacidad de los aerogeles de carbono mediante voltametría cíclica con electrodos de material en polvo, en celda Swagelock de tres electrodos, a diferentes velocidades de barrido y empleando NaCl como electrólito. Evaluación de la cinética de adsorción mediante cronoculometría. Evaluación de la resistencia de polarización mediante espectroscopia de impedancia electroquímica.

26. Evaluación de la resistividad eléctrica de los materiales mediante el cálculo de la pendiente de la recta ajustada de corriente-voltaje en monolitos de dimensiones conocidas.

Los puntos 20 a 26 del plan de trabajo se desarrollan a lo largo de la sección 3.3 del capítulo 3 de la presente memoria.

27. Síntesis de aerogeles funcionalizados con nitrógeno a base de precursores de melamina (M), resorcinol (R) y formaldehído (F) con proporciones molares R/M, (M+R)/C, (M+R)/F y (M+R)/W de 0,5, 135, 0,428 y 0,052, respectivamente. Se añaden negro de carbono y/o(CB) y/o diatomea (D). Se pirolizan a 480 ºC durante 2 horas y se lixivia con HF. Se dopa el material pirolizado con Mn por inmersión en una solución de $Mn(NO_3)_2$ seguido de pirólisis a 750 ºC durante 120 minutos.

28. Caracterización textural, mediante isotermas de adsorción–desorción de nitrógeno para determinar el área superficial, volumen de poro y la distribución de tamaño de poro mediante 2D-NLDFT-HS y del volumen de microporos mediante DR y porosimetría de mercurio para determinación de la macroporosidad. Caracterización morfológica mediante TEM y SEM-STEM.

29. Caracterización química y estructural de los materiales mediante difracción de Rayos X, XPS y análisis elemental.

26. Determinación de la capacidad de los aerogeles de carbono mediante voltametría cíclica y ciclos de carga/descarga galvanostática con electrodos de material en polvo, en

celda Swagelock de tres electrodos, a diferentes velocidades de barrido y empleando NaCl como electrólito. Evaluación de la resistencia de polarización mediante espectroscopia de impedancia electroquímica.

30. Determinación de la capacidad gravimétrica de electroadsorción de los diferentes aerogeles en formato monolito, en celda simétrica de dos electrodos, midiendo la variación de conductividad eléctrica, en condiciones potenciostáticas, en soluciones de NaCl 0,025 y 0,1 M.

Los puntos 27 a 30 del plan de trabajo se desarrollan a lo largo de la sección 3.4 del capítulo 3 de la presente memoria.

1.5. REFERENCIAS

[1] Blair, J.W.; Murphy, G.W. (1960). Electrochemical demineralization of Water with Porous Carbon Electrodes of Large Surface Area, 27. Washington D.C.: U.S. Dept. of the Interior.

[2] S. Evans, W.S. Hamilton, Mechanism of Demineralization at Carbon Eelectrodes, Journal of the Electrochemical Society 113(12) (1966) 1314-&.

[3] G.W. Murphy, D.D. Caudle, Mathematical Theory of Electrochemical Demineralization in Flowing Systems, Electrochimica Acta 12(12) (1967) 1655-&.

[4] B.B. Arnold, G.W. Murphy, Studies on Electrochemistry of Carbon and chemically modified Carbon Surfaces, Journal of Physical Chemistry 65(1) (1961) 135-&.

[5] Reid, G.W. (1968). Field operation of a 20 gallons per day pilot plant unit for electrochemical desalination of brackish water, 293. Washington D.C.: U.S. Dept. of the Interior.

[6] Johnson, A.M.; Venolia, A.W.; Wilbourne, R.G.; Newman, J.; Wong, C.M.; Gilliam, W.S. (1970). "The electrosorb processes for desalting water" **516**. Washington D.C.: U.S. Dept. of the Interior.

[7] A.M. Johnson, J. Newman, DESALTING BY MEANS OF POROUS CARBON ELECTRODES, Journal of the Electrochemical Society 118(3) (1971) 510-&.

[8] Y. Oren, A. Soffer, ELECTROCHEMICAL PARAMETRIC PUMPING, Journal of the Electrochemical Society 125(6) (1978) 869-875.

[9] J.C. Farmer, D.V. Fix, G.V. Mack, R.W. Pekala, J.F. Poco, Capacitive deionization of NaCl and NaNO3 solutions with carbon aerogel electrodes, Journal of the Electrochemical Society 143(1) (1996) 159-169.

[10] J.C. Farmer, D.V. Fix, G.V. Mack, R.W. Pekala, J.F. Poco, Capacitive deionization of NH_4ClO_4 solutions with carbon aerogel electrodes, Journal of Applied Electrochemistry 26(10) (1996) 1007-1018.

[11] Tung-Yu Ying, Kun-Lin Yang, Sotira Yiacoumi, Costas Tsouris, Electrosorption of Ions from Aquaeous Solutions by Nanostructured Carbon Aerogels, Journal of Colloid and Interface Science 250, 18–27 (2002)

[12] P.R. Madaria, N. Mohan, C. Rajagopal, B.S. Garg, Application of carbon aerogel for electrolytic removal of mercury from aqueous solutions, Journal of Scientific & Industrial Research 63(11) (2004) 938-943.

[13] P. Rana, N. Mohan, C. Rajagopal, Electrochemical removal of chromium from wastewater by using carbon aerogel electrodes, Water Research 38(12) (2004) 2811-2820.

[14] C.-M. Yang, B.W. Cho, 윤경석, 최운혁, H.H. Soo, W.I. Cho, Porous Carbon Aerogel-Silica Gel Composite Electrodes for Capacitive Deionization Process, Journal of the Korean Electrochemical So 7(1) (2004) 38-43.

[15] D.K. Kohli, R. Singh, M.K. Singh, A. Singh, R.K. Khardekar, P.R. Sankar, P. Tiwari, P.K. Gupta, Study of carbon aerogel-activated carbon composite electrodes for capacitive deionization application, Desalination and Water Treatment 49(1-3) (2012) 130-135.

[16] G. Rasines, P. Lavela, C. Macias, M.C. Zafra, J.L. Tirado, C.O. Ania, On the use of carbon black loaded nitrogen-doped carbon aerogel for the electrosorption of sodium chloride from saline water, Electrochimica Acta 170 (2015) 154-163.

[17] M.C. Zafra, P. Lavela, G. Rasines, C. Macias, J.L. Tirado, C.O. Ania, A novel method for metal oxide deposition on carbon aerogels with potential application in capacitive deionization of saline water, Electrochimica Acta 135 (2014) 208-216.

[18] J. Landon, X. Gao, B. Kulengowski, J.K. Neathery, K. Liu, Impact of Pore Size Characteristics on the Electrosorption Capacity of Carbon Xerogel Electrodes for Capacitive Deionization, Journal of the Electrochemical Society 159(11) (2012) A1861-A1866.

[19] B.E. Conway, E. Ayranci, H. Al-Maznai, Use of quasi-3-dimensional porous electrodes for adsorption and electrocatalytic removal of impurities from waste-waters, Electrochimica Acta 47(5) (2001) 705-718.

[20] M.W. Ryoo, J.H. Kim, G. Seo, Role of titania incorporated on activated carbon cloth for capacitive deionization of NaCl solution, Journal of Colloid and Interface Science 264(2) (2003) 414-419.

[21] X.Z. Wang, M.G. Li, Y.W. Chen, R.M. Cheng, S.M. Huang, L.K. Pan, Z. Sun, Electrosorption of ions from aqueous solutions with carbon nanotubes and nanofibers composite film electrodes, Applied Physics Letters 89(5) (2006).

[22] X.Z. Wang, M.G. Li, Y.W. Chen, R.M. Cheng, S.M. Huang, L.K. Pan, Z. Sun, Electrosorption of NaCl solutions with carbon nanotubes and nanofibers composite film electrodes, Electrochemical and Solid State Letters 9(9) (2006) E23-E26.

[23] L. Wang, M. Wang, Z.-H. Huang, T. Cui, X. Gui, F. Kang, K. Wang, D. Wu, Capacitive deionization of NaCl solutions using carbon nanotube sponge electrodes, Journal of Materials Chemistry 21(45) (2011) 18295-18299.

[24] Y. Zhan, L. Pan, C. Nie, H. Li, Z. Sun, Carbon nanotube-chitosan composite electrodes for electrochemical removal of Cu(II) ions, Journal of Alloys and Compounds 509(18) (2011) 5667-5671.

[25] C. Nie, L. Pan, Y. Liu, H. Li, T. Chen, T. Lu, Z. Sun, Electrophoretic deposition of carbon nanotubes-polyacrylic acid composite film electrode for capacitive deionization, Electrochimica Acta 66 (2012) 106-109.

[26] Z. Peng, D. Zhang, L. Shi, T. Yan, High performance ordered mesoporous carbon/carbon nanotube composite electrodes for capacitive deionization, Journal of Materials Chemistry 22(14) (2012) 6603-6612.

[27] J. Yang, L. Zou, H. Song, Preparing MnO2/PSS/CNTs composite electrodes by layer-by-layer deposition of MnO2 in the membrane capacitive deionisation, Desalination 286 (2012) 108-114.

[28] C. Yan, L. Zou, R. Short, Single-walled carbon nanotubes and polyaniline composites for capacitive deionization, Desalination 290 (2012) 125-129.

[29] H. Li, S. Liang, J. Li, L. He, The capacitive deionization behaviour of a carbon nanotube and reduced graphene oxide composite, Journal of Materials Chemistry A 1(21) (2013) 6335-6341.

[30] Y. Liu, W. Ma, Z. Cheng, J. Xu, R. Wang, X. Gang, Preparing CNTs/Ca-Selective zeolite composite electrode to remove calcium ions by capacitive deionization, Desalination 326 (2013) 109-114.

[31] J. Yang, L. Zou, N.R. Choudhury, Ion-selective carbon nanotube electrodes in capacitive deionisation, Electrochimica Acta 91 (2013) 11-19.

[32] H. Li, L. Zou, L. Pan, Z. Sun, Novel Graphene-Like Electrodes for Capacitive Deionization, Environmental Science & Technology 44(22) (2010) 8692-8697.

[33] H. Li, L. Pan, C. Nie, Y. Liu, Z. Sun, Reduced graphene oxide and activated carbon composites for capacitive deionization, Journal of Materials Chemistry 22(31) (2012) 15556-15561.

[34] D. Zhang, X. Wen, L. Shi, T. Yan, J. Zhang, Enhanced capacitive deionization of graphene/mesoporous carbon composites, Nanoscale 4(17) (2012) 5440-5446.

[35] D. Zhang, T. Yan, L. Shi, Z. Peng, X. Wen, J. Zhang, Enhanced capacitive deionization performance of graphene/carbon nanotube composites, Journal of Materials Chemistry 22(29) (2012) 14696-14704.
[36] H. Wang, D. Zhang, T. Yan, X. Wen, J. Zhang, L. Shi, Q. Zhong, Three-dimensional macroporous graphene architectures as high performance electrodes for capacitive deionization, Journal of Materials Chemistry A 1(38) (2013) 11778-11789.
[37] H. Yin, S. Zhao, J. Wan, H. Tang, L. Chang, L. He, H. Zhao, Y. Gao, Z. Tang, Three-Dimensional Graphene/Metal Oxide Nanoparticle Hybrids for High-Performance Capacitive Deionization of Saline Water, Advanced Materials 25(43) (2013) 6270-6276.
[38] M.D. Andelman, Charge barrier flow-through capacitor, Can Patent, CA 2,444,390 (2002).
[39] T.J. Welgemoed, C.F. Schutte, Capacitive Delonization Technology (TM) : An alternative desalination solution, Desalination 183(1-3) (2005) 327-340.
[40] K. Dermentzis, K. Ouzounis, Continuous capacitive deionization-electrodialysis reversal through electrostatic shielding for desalination and deionization of water, Electrochimica Acta 53(24) (2008) 7123-7130.
[41] P. Xu, J.E. Drewes, D. Heil, G. Wang, Treatment of brackish produced water using carbon aerogel-based capacitive deionization technology, Water Research 42(10-11) (2008) 2605-2617.
[42] M. Noked, E. Avraham, A. Soffer, D. Aurbach, The Rate-Determining Step of Electroadsorption Processes into Nanoporous Carbon Electrodes Related to Water Desalination, Journal of Physical Chemistry C 113(51) (2009) 21319-21327.
[43] Y.-J. Kim, J. Hur, W. Bae, J.-H. Choi, Desalination of brackish water containing oil compound by capacitive deionization process, Desalination 253(1-3) (2010) 119-123.
[44] M.A. Anderson, A.L. Cudero, J. Palma, Capacitive deionization as an electrochemical means of saving energy and delivering clean water. Comparison to present desalination practices: Will it compete?, Electrochimica Acta 55(12) (2010) 3845-3856.
[45] J.-H. Lee, W.-S. Bae, J.-H. Choi, Electrode reactions and adsorption/desorption performance related to the applied potential in a capacitive deionization process, Desalination 258(1-3) (2010) 159-163.
[46] O. Arar, U. Yuksel, N. Kabay, M. Yuksel, Removal of Cu2+ ions by a micro-flow electrodeionization (EDI) system, Desalination 277(1-3) (2011) 296-300.

[47] Y.-h. Zhang, F.-x. Gan, M. Li, D.-h. Wang, Z.-m. Huang, Y.-p. Gao, Treatment of Reused Comprehensive Wastewater in Iron and Steel Industry With Electrosorption Technology, Journal of Iron and Steel Research International 18(6) (2011) 37-42.
[48] C. Forrestal, P. Xu, P.E. Jenkins, Z. Ren, Microbial desalination cell with capacitive adsorption for ion migration control, Bioresource Technology 120 (2012) 332-336.
[49] M.E. Suss, T.F. Baumann, W.L. Bourcier, C.M. Spadaccini, K.A. Rose, J.G. Santiago, M. Stadermann, Capacitive desalination with flow-through electrodes, Energy & Environmental Science 5(11) (2012) 9511-9519.
[50] Z. Chen, H. Zhang, C. Yang, X. Sun, H. Guo, C. Wu, F. Xue, L. Gao, Effects of ageing and incorporation of ion-exchange membrane on the electrosorption performance of activated carbon based electrodes modules, Desalination and Water Treatment 51(16-18) (2013) 3489-3496.
[51] O.N. Demirer, R.M. Naylor, C.A.R. Perez, E. Wilkes, C. Hidrovo, Energetic performance optimization of a capacitive deionization system operating with transient cycles and brackish water, Desalination 314 (2013) 130-138.
[52] S.-i. Jeon, H.-r. Park, J.-g. Yeo, S. Yang, C.H. Cho, M.H. Han, D.K. Kim, Desalination via a new membrane capacitive deionization process utilizing flow-electrodes, Energy & Environmental Science 6(5) (2013) 1471-1475.
[53] K.B. Hatzell, E. Iwama, A. Ferris, B. Daffos, K. Urita, T. Tzedakis, F. Chauvet, P.-L. Taberna, Y. Gogotsi, P. Simon, Capacitive deionization concept based on suspension electrodes without ion exchange membranes, Electrochemistry Communications 43 (2014) 18-21.
[54] S. Porada, D. Weingarth, H.V.M. Hamelers, M. Bryjak, V. Presser, P.M. Biesheuvel, Carbon flow electrodes for continuous operation of capacitive deionization and capacitive mixing energy generation, Journal of Materials Chemistry A 2(24) (2014) 9313-9321.
[55] Y. Oren, Capacitive delonization (CDI) for desalination and water treatment - past, present and future (a review), Desalination 228(1-3) (2008) 10-29.
[56] M.M. Dubinin, THE POTENTIAL THEORY OF ADSORPTION OF GASES AND VAPORS FOR ADSORBENTS WITH ENERGETICALLY NONUNIFORM SURFACES, Chemical Reviews 60(2) (1960) 235-241.
[57] N. Epstein, ON TORTUOSITY AND THE TORTUOSITY FACTOR IN FLOW AND DIFFUSION THROUGH POROUS-MEDIA, Chemical Engineering Science 44(3) (1989) 777-779.

[58] M. Polanyi, POTENTIAL THEORY OF ADSORPTION, Science 141(358) (1963) 1010-&.
[59] Siedlews.J, MECHANISM OF CATALYTIC OXIDATION ON ACTIVATED CARBON . ELECTROCHEMICAL DETERMINATION OF NUMBER OF ACTIVE CENTERS IN CHEMISORPTION OF OXYGEN ON SURFACE OF CARBON, International Chemical Engineering 5(4) (1965) 616-&.
[60] L.M. Chang, X.Y. Duan, W. Liu, Preparation and electrosorption desalination performance of activated carbon electrode with titania, Desalination 270(1-3) (2011) 285-290.
[61] K. Laxman, M.T.Z. Myint, R. Khan, T. Pervez, J. Dutta, Effect of a semiconductor dielectric coating on the salt adsorption capacity of a porous electrode in a capacitive deionization cell, Electrochimica Acta 166 (2015) 329-337.
[62] S. Porada, R. Zhao, A. van der Wal, V. Presser, P.M. Biesheuvel, Review on the science and technology of water desalination by capacitive deionization, Progress in Materials Science 58(8) (2013) 1388-1442.
[63] L. Zou, G. Morris, D. Qi, Using activated carbon electrode in electrosorptive deionisation of brackish water, Desalination 225(1-3) (2008) 329-340.
[64] C.-L. Yeh, H.-C. Hsi, K.-C. Li, C.-H. Hou, Improved performance in capacitive deionization of activated carbon electrodes with a tunable mesopore and micropore ratio, Desalination 367 (2015) 60-68.
[65] C.-H. Hou, N.-L. Liu, H.-C. Hsi, Highly porous activated carbons from resource-recovered Leucaena leucocephala wood as capacitive deionization electrodes, Chemosphere 141 (2015) 71-79.
[66] J. Liu, M. Lu, J. Yang, J. Cheng, W. Cai, Capacitive desalination of ZnO/activated carbon asymmetric capacitor and mechanism analysis, Electrochimica Acta 151 (2015) 312-318.
[67] H.-h. Li, J. Yang, C. Zhang, H.-y. Li, P.-p. Pei, The influence of the acidic scouring treatment on the wastewater treatment of TiO2 loaded activated carbon electrode, Journal of Porous Materials 22(4) (2015) 887-895.
[68] T.Y. Ying, K.L. Yang, S. Yiacoumi, C. Tsouris, Electrosorption of ions from aqueous solutions by nanostructured carbon aerogel, Journal of Colloid and Interface Science 250(1) (2002) 18-27.

[69] C.M. Yang, W.H. Choi, B.K. Na, B.W. Cho, W.I. Cho, Capacitive deionization of NaCl solution with carbon aerogel-silica gel composite electrodes, Desalination 174(2) (2005) 125-133.
[70] H.-H. Jung, S.-W. Hwang, S.-H. Hyun, L. Kang-Ho, G.-T. Kim, Capacitive deionization characteristics of nanostructured carbon aerogel electrodes synthesized via ambient drying, Desalination 216(1-3) (2007) 377-385.
[71] L. Li, L. Zou, H. Song, G. Morris, Ordered mesoporous carbons synthesized by a modified sol-gel process for electrosorptive removal of sodium chloride, Carbon 47(3) (2009) 775-781.
[72] K.C. Leonard, J.R. Genthe, J.L. Sanfilippo, W.A. Zeltner, M.A. Anderson, Synthesis and characterization of asymmetric electrochemical capacitive deionization materials using nanoporous silicon dioxide and magnesium doped aluminum oxide, Electrochimica Acta 54(22) (2009) 5286-5291.
[73] Z. Wang, B. Dou, L. Zheng, G. Zhang, Z. Liu, Z. Hao, Effective desalination by capacitive deionization with functional graphene nanocomposite as novel electrode material, Desalination 299 (2012) 96-102.
[74] C. Nie, L. Pan, H. Li, T. Chen, T. Lu, Z. Sun, Electrophoretic deposition of carbon nanotubes film electrodes for capacitive deionization, Journal of Electroanalytical Chemistry 666 (2012) 85-88.
[75] X. Gao, A. Omosebi, J. Landon, K. Liu, Enhancement of charge efficiency for a capacitive deionization cell using carbon xerogel with Modified potential of zero charge, Electrochemistry Communications 39 (2014) 22-25.
[76] W. Huang, Y. Zhang, S. Bao, R. Cruz, S. Song, Desalination by capacitive deionization process using nitric acid-modified activated carbon as the electrodes, Desalination 340 (2014) 67-72.
[77] L. Liu, L. Liao, Q. Meng, B. Cao, High performance graphene composite microsphere electrodes for capacitive deionisation, Carbon 90 (2015) 75-84.
[78] X. Xu, Y. Liu, T. Lu, Z. Sun, D.H.C. Chua, L. Pan, Rational design and fabrication of graphene/carbon nanotubes hybrid sponge for high-performance capacitive deionization, Journal of Materials Chemistry A 3(25) (2015) 13418-13425.
[79] C. Hu, F. Liu, H. Lan, H. Liu, J. Qu, Preparation of a manganese dioxide/carbon fiber electrode for electrosorptive removal of copper ions from water, Journal of Colloid and Interface Science 446 (2015) 359-365.

[80] T. Wu, G. Wang, Q. Dong, B. Qian, Y. Meng, J. Qiu, Asymmetric capacitive deionization utilizing nitric acid treated activated carbon fiber as the cathode, Electrochimica Acta 176 (2015) 426-433.
[81] Y. Wang, X. Han, R. Wang, S. Xu, J. Wang, Preparation optimization on the coating-type polypyrrole/carbon nanotube composite electrode for capacitive deionization, Electrochimica Acta 182 (2015) 81-88.
[82] Y. Liu, L. Pan, T. Chen, X. Xu, T. Lu, Z. Sun, D.H.C. Chua, Porous carbon spheres via microwave-assisted synthesis for capacitive deionization, Electrochimica Acta 151 (2015) 489-496.
[83] Y. Liu, T. Chen, T. Lu, Z. Sun, D.H.C. Chua, L. Pan, Nitrogen-doped porous carbon spheres for highly efficient capacitive deionization, Electrochimica Acta 158 (2015) 403-409.
[84] Z. Li, B. Song, Z. Wu, Z. Lin, Y. Yao, K.-S. Moon, C.P. Wong, 3D porous graphene with ultrahigh surface area for microscale capacitive deionization, Nano Energy 11 (2015) 711-718.
[85] A.G. El-Deen, J.-H. Choi, C.S. Kim, K.A. Khalil, A.A. Almajid, N.A.M. Barakat, TiO2 nanorod-intercalated reduced graphene oxide as high performance electrode material for membrane capacitive deionization, Desalination 361 (2015) 53-64.
[86] F. Duan, X. Du, Y. Li, H. Cao, Y. Zhang, Desalination stability of capacitive deionization using ordered mesoporous carbon: Effect of oxygen-containing surface groups and pore properties, Desalination 376 (2015) 17-24.
[87] Q. Dong, G. Wang, T. Wu, S. Peng, J. Qiu, Enhancing capacitive deionization performance of electrospun activated carbon nanofibers by coupling with carbon nanotubes, Journal of Colloid and Interface Science 446 (2015) 373-378.
[88] L. Chang, J. Li, X. Duan, W. Liu, Porous carbon derived from Metal-organic framework (MOF) for capacitive deionization electrode, Electrochimica Acta 176 (2015) 956-964.
[89] C.-Y. Ma, S.-C. Huang, P.-H. Chou, W. Den, C.-H. Hou, Application of a multiwalled carbon nanotube-chitosan composite as an electrode in the electrosorption process for water purification, Chemosphere 146 (2016) 113-20.
[90] D.S. Zhang, L.Y. Shi, J.H. Fang, K. Dai, X.K. Li, Preparation and desalination performance of multiwall carbon nanotubes, Materials Chemistry and Physics 97(2-3) (2006) 415-419.

[91] M.C. Zafra, P. Lavela, C. Macias, G. Rasines, J.L. Tirado, Electrosorption of environmental concerning anions on a highly porous carbon aerogel, Journal of Electroanalytical Chemistry 708 (2013) 80-86.
[92] M.C. Zafra, P. Lavela, G. Rasines, C. Macias, J.L. Tirado, Effect of the resorcinol/catalyst ratio in the capacitive performance of carbon xerogels with potential use in sodium chloride removal from saline water, Journal of Solid State Electrochemistry 18(10) (2014) 2847-2856.
[93] G. Rasines, P. Lavela, C. Macias, M.C. Zafra, J.L. Tirado, C.O. Ania, Mesoporous carbon black-aerogel composites with optimized properties for the electro-assisted removal of sodium chloride from brackish water, Journal of Electroanalytical Chemistry 741 (2015) 42-50.
[94] G. Rasines, P. Lavela, C. Macias, M.C. Zafra, J.L. Tirado, J.B. Parra, C.O. Ania, N-doped monolithic carbon aerogel electrodes with optimized features for the electrosorption of ions, Carbon 83 (2015) 262-274.
[95] R.W. Pekala, J.C. Farmer, C.T. Alviso, T.D. Tran, S.T. Mayer, J.M. Miller, B. Dunn, Carbon aerogels for electrochemical applications, Journal of Non-Crystalline Solids 225(1) (1998) 74-80.
[96] K.L. Yang, S. Yiacoumi, C. Tsouris, Electrosorption capacitance of nanostructured carbon aerogel obtained by cyclic voltammetry, Journal of Electroanalytical Chemistry 540 (2003) 159-167.
[97] S.W. Hwang, S.H. Hyun, Capacitance control of carbon aerogel electrodes, Journal of Non-Crystalline Solids 347(1-3) (2004) 238-245.
[98] C.-H. Hou, C. Liang, S. Yiacoumi, S. Dai, C. Tsouris, Electrosorption capacitance of nanostructured carbon-based materials, Journal of Colloid and Interface Science 302(1) (2006) 54-61.
[99] Kadam M K, Nadakati S M, Tendulkar M S. Electrode for capacitive deionization. WO2009077276A1.
[100] M. Seredych, D. Hulicova-Jurcakova, G.Q. Lu, T.J. Bandosz, Surface functional groups of carbons and the effects of their chemical character, density and accessibility to ions on electrochemical performance, Carbon 46(11) (2008) 1475-1488.

[101] J.-Y. Choi, J.-H. Choi, A carbon electrode fabricated using a poly(vinylidene fluoride) binder controlled the Faradaic reaction of carbon powder, Journal of Industrial and Engineering Chemistry 16(3) (2010) 401-405.
[102] B.-H. Park, J.-H. Choi, Improvement in the capacitance of a carbon electrode prepared using water-soluble polymer binder for a capacitive deionization application, Electrochimica Acta 55(8) (2010) 2888-2893.
[103] Y.J. Lee, J.C. Jung, S. Park, J.G. Seo, S.-H. Baeck, J.R. Yoon, J. Yi, I.K. Song, Effect of preparation method on electrochemical property of Mn-doped carbon aerogel for supercapacitor, Current Applied Physics 11(1) (2011) 1-5.
[104] S. Nadakatti, M. Tendulkar, M. Kadam, Use of mesoporous conductive carbon black to enhance performance of activated carbon electrodes in capacitive deionization technology, Desalination 268(1-3) (2011) 182-188.
[105] G. Rasines, P. Lavela, C. Macias, M. Haro, C.O. Ania, J.L. Tirado, Electrochemical response of carbon aerogel electrodes in saline water, Journal of Electroanalytical Chemistry 671 (2012) 92-98.
[106] N.A.M. Barakat, K.A. Khalil, A.G. El-Deen, H.Y. Kim, Development of Cd-doped Co Nanoparticles Encapsulated in Graphite Shell as Novel Electrode Material for the Capacitive Deionization Technology, Nano-Micro Letters 5(4) (2013) 303-313.
[107] Z. Lin, Z. Li, K.-s. Moon, Y. Fang, Y. Yao, L. Li, C.-p. Wong, Robust vertically aligned carbon nanotube-carbon fiber paper hybrid as versatile electrodes for supercapacitors and capacitive deionization, Carbon 63 (2013) 547-553.
[108] H. Luo, Y. Yang, X. Zhao, J. Zhang, Y. Chen, 3D sponge-like nanoporous carbons via a facile synthesis for high-performance supercapacitors: direct carbonization of tartrate salt, Electrochimica Acta 169 (2015) 13-21.
[109] C. Yang, Y. Liu, C. Ma, M. Norton, J. Qiao, Preparing Desirable Activated Carbons from Agricultural Residues for Potential Uses in Water Treatment, Waste and Biomass Valorization 6(6) (2015) 1029-1036.
[110] M. Monthioux, V.L. Kuznetsov, Who should be given the credit for the discovery of carbon nanotubes?, Carbon 44(9) (2006) 1621-1623.
[111] Y. Hanzawa, K. Kaneko, N. Yoshizawa, R.W. Pekala, M.S. Dresselhaus, The pore structure determination of carbon aerogels, Adsorption-Journal of the International Adsorption Society 4(3-4) (1998) 187-195.

[112] R.W. Pekala, C.T. Alviso, F.M. Kong, S.S. Hulsey, AEROGELS DERIVED FROM MULTIFUNCTIONAL ORGANIC MONOMERS, Journal of Non-Crystalline Solids 145(1-3) (1992) 90-98.
[113] H. Tamon, H. Ishizaka, T. Araki, M. Okazaki, Control of mesoporous structure of organic and carbon aerogels, Carbon 36(9) (1998) 1257-1262.
[114] H. Tamon, H. Ishizaka, Influence of gelation temperature and catalysts on the mesoporous structure of resorcinol-formaldehyde aerogels, Journal of Colloid and Interface Science 223(2) (2000) 305-307.
[115] S.A. Al-Muhtaseb, J.A. Ritter, Preparation and properties of resorcinol-formaldehyde organic and carbon gels, Advanced Materials 15(2) (2003) 101-+.
[116] T.F. Baumann, M.A. Worsley, T.Y.-J. Han, J.H. Satcher, Jr., High surface area carbon aerogel monoliths with hierarchical porosity, Journal of Non-Crystalline Solids 354(29) (2008) 3513-3515.
[117] H. Tamon, H. Ishizaka, M. Mikami, M. Okazaki, Porous structure of organic and carbon aerogels synthesized by sol-gel polycondensation of resorcinol with formaldehyde, Carbon 35(6) (1997) 791-796.
[118] N. Job, A. Thery, R. Pirard, J. Marien, L. Kocon, J.N. Rouzaud, F. Beguin, J.P. Pirard, Carbon aerogels, cryogels and xerogels: Influence of the drying method on the textural properties of porous carbon materials, Carbon 43(12) (2005) 2481-2494.
[119] J. Wang, S.Q. Zhang, J. Shen, Y.Z. Guo, S.M. Attia, B. Zhou, Z.Q. Lai, G.Z. Zheng, Y.S. Gui, Electrical transport properties of carbon aerogels, Journal of Porous Materials 8(2) (2001) 167-170.
[120] J. Wang, X. Yang, D. Wu, R. Fu, M.S. Dresselhaus, G. Dresselhaus, The porous structures of activated carbon aerogels and their effects on electrochemical performance, Journal of Power Sources 185(1) (2008) 589-594.
[121] S.H. Kwon, E. Lee, B.-S. Kim, S.-G. Kim, B.-J. Lee, M.-S. Kim, J.C. Jung, Preparation of activated carbon aerogel and its application to electrode material for electric double layer capacitor in organic electrolyte: Effect of activation temperature, Korean Journal of Chemical Engineering 32(2) (2015) 248-254.
[122] Q. Lei, H. Song, X. Chen, M. Li, A. Li, B. Tang, D. Zhou, Effects of graphene oxide addition on the synthesis and supercapacitor performance of carbon aerogel particles, Rsc Advances 6(47) (2016) 40683-40690.

[123] P. Hao, Z. Zhao, L. Li, C.-C. Tuan, H. Li, Y. Sang, H. Jiang, C.P. Wong, H. Liu, The hybrid nanostructure of MnCo2O4.5 nanoneedle/carbon aerogel for symmetric supercapacitors with high energy density, Nanoscale 7(34) (2015) 14401-14412.
[124] E. Isaacs Paez, M. Haro, E.J. Juarez-Perez, R.J. Carmona, J.B. Parra, R. Leyva Ramos, C.O. Ania, Fast synthesis of micro/mesoporous xerogels: Textural and energetic assessment, Microporous and Mesoporous Materials 209 (2015) 2-9.
[125] K.Y. Kang, S.J. Hong, B.I. Lee, J.S. Lee, Enhanced electrochemical capacitance of nitrogen-doped carbon gels synthesized by microwave-assisted polymerization of resorcinol and formaldehyde, Electrochemistry Communications 10(7) (2008) 1105-1108.
[126] D. Fairen-Jimenez, F. Carrasco-Marin, C. Moreno-Castilla, Inter- and intra-primary-particle structure of monolithic carbon aerogels obtained with varying solvents, Langmuir 24(6) (2008) 2820-2825.
[127] L. Zubizarreta, A. Arenillas, A. Dominguez, J.A. Menendez, J.J. Pis, Development of microporous carbon xerogels by controlling synthesis conditions, Journal of Non-Crystalline Solids 354(10-11) (2008) 817-825.

Capítulo 2

Efectos de los parámetros de síntesis sobre las propiedades texturales y capacidad de electroadsorción de aerogeles de carbono


JOURNAL OF
SOLID STATE
CHEMISTRY
JSSC

2.1.1. Introduction

Capacitive deionization (CDI) is currently considered one of the most promising technology to purify low and medium saline water streams in terms of cost and desalting efficiency. CDI is based on the electrostatic interactions of ionic species dissolved in an electrolyte with oppositely charged electrodes. Hence, high desalting capacities can only be achieved in high conductive large surface area electrodes, which pore structure would favor the adsorption of the solvated ions. Electrodes based on carbon materials are being regarded as the most suitable for CDI applications. Carbon materials such as carbon nanotubes [1,2], mesoporous carbon [3,4], hierarchically porous carbon [5], hollow carbon spheres [6], graphene [7-9] and their composites have been developed as highly efficient electrodes. Among carbon materials, carbon aerogels (CAG) could also be considered as candidates for CDI applications [10-12,].

The sol-gel processing of resorcinol-formaldehyde (RF) mixtures alongside with the supercritical drying with CO_2 are the pillars of the method proposed by Pekala and coworkers to yield nanoporous organic aerogels [3]. Since then, much research has been carried out on the carbonized products because of their interesting features as highly porous materials with good electrical and thermal conductivity, corrosion resistance, and suitable mechanical properties.All these advantageous properties, and cost effectiveness, are responsible of their numerous applications in catalysis [16], energy storage [17-19] and environmental [20-22].,

An optimal porosity in carbon aerogels requires an appropriate selection of the synthesis parameters. Ritter et al. reviewed the preparative factors, as reactants concentration, pH, solvent-exchange, drying method, influencing on the textural properties of the carbon aerogels [23] and Baumann et al. described the synthesis of hierarchical aerogel monoliths with bimodal (macroporous and microporous) pore size distributions using acid pH [24]. More recently, Suss et al applied these materials in a flow-through CDI systems, and compared the performance with other deionization technologies [25]. Also, the thermal treatment of the organic aerogel is crucial to set the porous properties of the carbonized product. Particularly, the temperature of the pyrolysis and the activation conditions (time, temperature, activation agent) are important factors to be taken into account, often yielding porosity values and surface areas exceeding, respectively, 80% and 2000 $m^2 g^{-1}$ [23,26, 27].

There are several examples in the literature on the potential application of carbon aerogels in capacitive deionization, including our own studies [25,28-34], discussing the effects of the different synthesis parameters as the precursor's molar ratio [26-28], thermal treatment [29] and porous features [32-34]. However, most of the studies focus on the electrochemical performance of powder electrodes of small dimensions at lab scale [32-36], and data are extrapolated to larger and self-supported monolithic electrodes used in the large scale applications of CDI. At converse, studies on self-supported monolith electrodes are rather scarce. In this regard, our previous work [29-30] has revealed that the monolithic morphology can provide different features, leading to superior CDI performance, lower oxidation resiliency and thus improved stability of the electrodes.

Bearing all this in mind, the objective of this work was to screen the electrochemical performance of a series of aerogel electrodes (both in monolithic and powder morphology) for their potential application in CDI processes. We have correlated the capacitive deionization performance with their physicochemical properties, linking them with the main synthesis parameters as R/C and R/W. For this purpose, we have selected a series of aerogels with different R/C (ranging from $100 \leq R/C \leq 800$), and R/W molar ratio ($0.04 \leq R/W \leq 0.13$), while trying to optimize the textural and capacitive properties towards the removal of ions from solution.

2.1.2. Experimental section

2.1.2.1. Materials preparation

The carbon aerogels were synthesized by the sol-gel polymerization of resorcinol (R) and formaldehyde (F) mixtures in water (W), using sodium carbonate as catalyst (C). Details on the experimental procedure have been reported elsewhere [26-29]. Briefly, the R/F molar ratio was set at 0.5, the R/C molar ratio was varied from 100 to 600, while R/W ranged from 0.04 to 0.13. The reactants were vigorous stirred in sealed glass moulds to ensure a homogeneous polymerization, and the obtained hydrogel was aged in an oven at 40 ºC for 24 h and then at 70 ºC for 120 h. Drying was performed using CO_2 at supercritical conditions (40ºC and 100 bar). In order to avoid the shrinkage of the gel and ensure CO_2 solubility during the drying process, a previous controlled water-acetone exchange is required. Pyrolysed aerogels were prepared at 800 ºC under nitrogen atmosphere (i.e., heating rate 2 ºC min^{-1} up to 400 ºC and hold for 60 min followed by

heating up to 800 ºC and hold for 60 min). A second batch of aerogels was prepared by activation of the carbonized ones under a CO_2 stream at 800 ºC for 2 hours. The nomenclature of the samples is (R/C)-(R/W)-(tt) where *tt* refers to the thermal treatment of the hydrogels (*py* for pyrolysed and *act* for activated samples).

2.1.2.2. Textural characterization

N_2 adsorption-desorption isotherms were recorded at -196 ºC (ASAP 2010, Micromeritics). For this purpose, the carbon aerogels were previously outgassed under primary vacuum at 120 ºC overnight (heating ramp of 2 ºC min^{-1}). The specific surface area, S_{BET}, total pore volume, V_T, and micro-/ mesopore volumes were calculated from the gas adsorption isotherms. The pore size distributions were calculated by using the new 2D-NLDFT-HS method [37]. Transmission electron microscopy was performed in a JEOL-JEM 2010.

2.1.2.3. Electrochemical characterization

Experiments were performed by assembling the electrode components in three-electrode Swagelok^{TM} type cells. The working electrode consisted of a mixture of active material (70%), Superior graphite (20%) and PVDF binder (10%). The mixture was slurried in N-methyl pyrrolidone and spread on a 13 mm titanium disk, and then the electrode was dried at 70ºC overnight. A Hg/Hg_2SO_4 and a platinum wire were respectively used as reference and counter electrode. A 0.1 M NaCl solution in deionized water was used as electrolyte. Cyclic voltammetry experiments were conducted between -0.5 and +0.5 V versus the reference electrode at 0.5 mV s^{-1} and monitored with a Biologic VMP multichannel potentiostat. The polarization resistances were determined from the electrochemical impedance spectra (EIS) recorded on freshly assembled cells by using an Autolab PGSTAT12 system. The equilibrium voltage was perturbed with an AC voltage signal of 5 mV over the frequency range 25 kHz to 10 mHz. The polarization resistance (R_{pol}) was calculated by fitting the recorded spectra according to an equivalent circuit formed by the bulk solution resistance (R_{el}) and the stance where the polarization resistance (R_{pol}) connected in series to a Warburg impedance element and in parallel to a CPE is a constant phase element. The high-frequency response was ascribed to the bulk

resistance of the solution (R_{el}). The resistance to ion migration through the pore structure (R_{pol}) was determined from the real impedance of the semicircle at intermediate frequencies [38].

2.1.2.4. Desalting capacity

A symmetrical batch-type cell was assembled to perform the capacitive deionization experiments, using two monolithic aerogel electrodes (weight ca. 150 mg and ca. 0.3 cm^3), separated by Whatman glass GF/A fiber sheets. Their surfaces were polished to ensure a good contact with the titanium current collector. The pieces were washed in deionized water for 30 minutes and then immersed into 15 mL of a 0.025 M NaCl solution (ca.1.5 g/L) magnetically stirred to favor mass transfer from the bulk solution to the electrode. The cell was charged by applying a potentiostatic pulse (0.9, 1.2 or 1.5 V for 120 min). Afterwards, the electrodes were discharged at 0 V for the same period of time. A conductivity-meter was used to monitor the changes of the ionic conductivity and hence ion concentration. The gravimetric capacitances of the aerogel series in the CDI two-electrode cell have been computed from the charge/discharge current curves using equation 1:

$$C_w = \frac{1}{w_e \, E_c} \int_{t_0}^{t_n} i \, d \qquad (1)$$

where C_W is the gravimetric capacitance in Fg^{-1}, W_e is the weight of the monolithic electrode (the one working as cathode) in g, E_{ce} is the voltage applied to the cell in volts, t_0 and t_n are the times in seconds at the beginning and the end of the third cycle of charge and i is the current in amperes. The volumetric capacitances C_V have been computed in a similar way, using equation 1 but replacing the electrode weight by the electrode volume in cm^3.

2.1.3. **Results and discussion**

2.1.3.1. Characterization of the aerogels

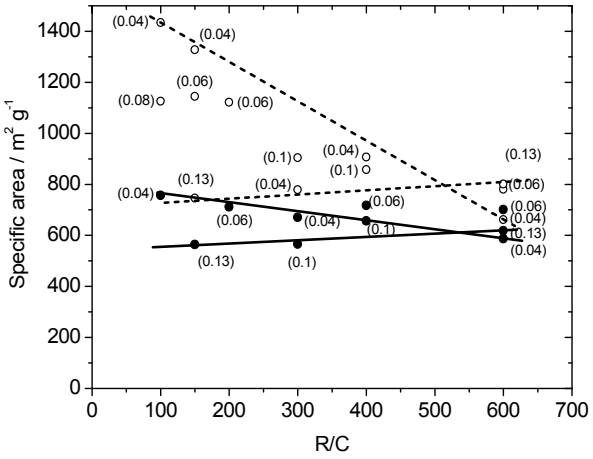
Specific area / m^2 g^{-1}
R/C
(0.04)
(0.04)
(0.06)
(0.08)
(0.06)
(0.1)
(0.04)
(0.1)
(0.13)
(0.13)
(0.04)
(0.06)
(0.04)
(0.06)
(0.06)
(0.04)
(0.1)
(0.13)
(0.1)
(0.06)
(0.06)
(0.04)
(0.13)
(0.04)

a

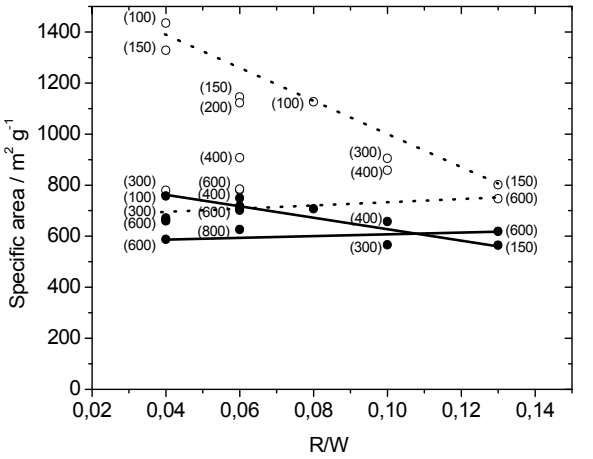
Specific area / m^2 g^{-1}
R/W
(100)
(150)
(150)
(200)
(100)
(400)
(300)
(400)
(300)
(600)
(400)
(100)
(600)
(300)
(600)
(600)
(800)
(600)
(400)
(300)
(150)
(600)
(600)
(150)

b

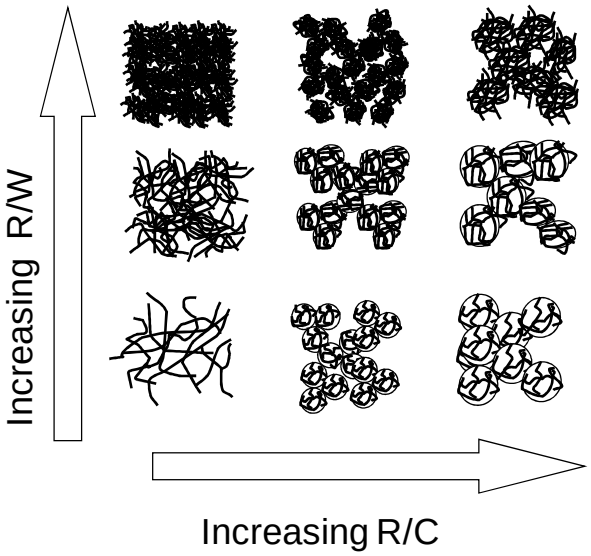
Increasing R/W
Increasing R/C

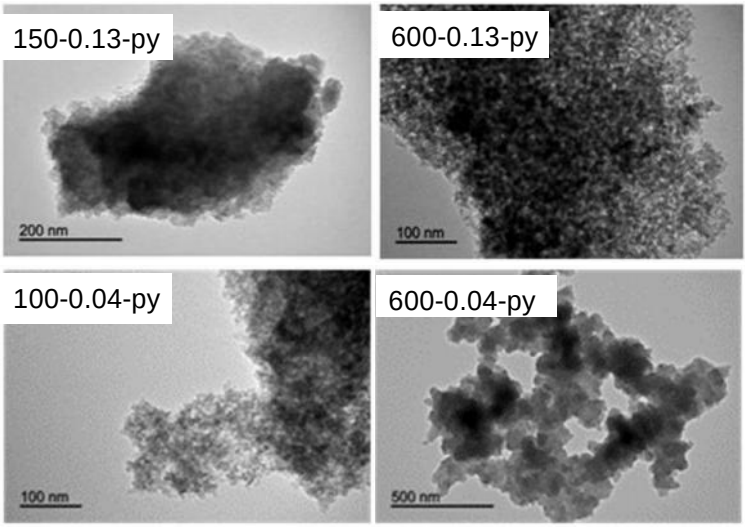
150-0.13-py
200 nm
600-0.13-py
100 nm
100-0.04-py
100 nm
600-0.04-py
500 nm

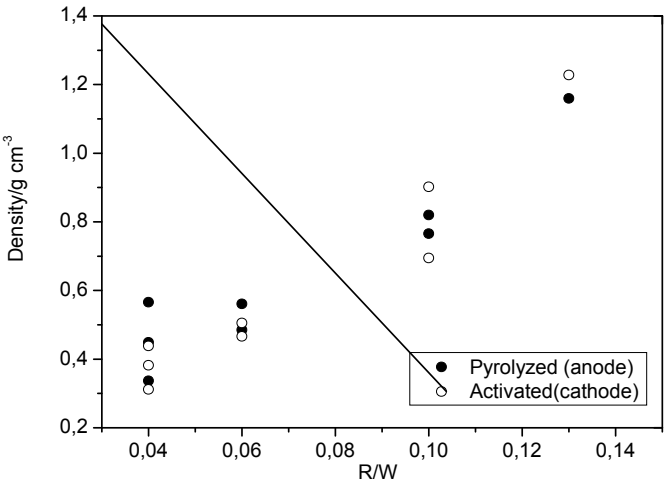
Density/g cm-3
1,4
1,2
1,0
0,8
0,6
0,4
0,2
0,04
0,06
0,08
0,10
0,12
0,14
R/W
Pyrolyzed (anode)
Activated(cathode)

effects on the R/W ratio have been reported in the literature [23,24,26,27,29]. For instance (Table S1 and Figure S2), for R/C ratio of 600, the formation of mesoporosity is higher for R/W of 0.13 as seen in the wide hysteresis loop compared to the sample with R/W of 0.06 (similar total pore volume but narrower hysteresis loop shifted towards higher relative pressures).

On the contrary, the differences in specific surface and micropore volumes become large for the activated aerogels series (Table S1, Figure S2), though the trend for the mesopore volumes is similar to that described for the pyrolyzed aerogels. For instance, surface area values are higher for the samples with lower R/C as low as 100 and 150, regardless the R/W ratio, indicating that they are more prone to be activated. Similarly, the influence of the R/W ratio depends on the R/C values. For instance, in the samples synthesized with R/C of 150, the activation treatment is more effective for low R/W values (i.e., 1328, 1145 and 746 m^2/g for 150-0.04-act, 150-0.06- act, and 150-0.13- act, respectively), whereas for R/C of 600 the effect is smaller (i.e., 662, 781 and 801 m^2/g for 600-0.04- act, 600-0.06- act, and 600-0.13- act, respectively). This is explained by the different nanostructure of the pyrolyzed aerogels and their differences in the evolution of the porosity upon CO_2 activation; the aerogels prepared using low R/C and R/W molar ratio display a low density of dense carbon clusters (Figure 2), allowing a good access of CO_2 to these clusters during the activation step, thereby widening the micropores.

In contrast, aerogels with high R/W ratios present a higher density of dense carbon clusters, somehow hindering the access of CO_2 and thus making gasification less effective. On the other hand, the aerogels synthesized using high R/C and low R/W molar ratios are characterized by the presence of low density clusters, easily accessible by CO_2 during the activation. In this case, the decrease in the surface area is due to the enlargement of the micropore structure. Hence, the lower the R/W, the higher the surface area, being the effect more pronounced for aerogels synthesized using low R/C molar ratio (Table S1). Additionally, low R/C ratios render the so -called “polymeric gels” characterized by small particle sizes and high surface areas (Figure 2) that are typically very prone to shrink upon supercritical drying. Contrarily, “colloidal aerogels” are obtained at high R/C ratios, showing the opposite behavior concerning shrinkage on drying. The R/W molar ratio also influences the texture of the aerogels, with high R/W values giving rise to aerogels with low surface areas. These differences in porosity of the

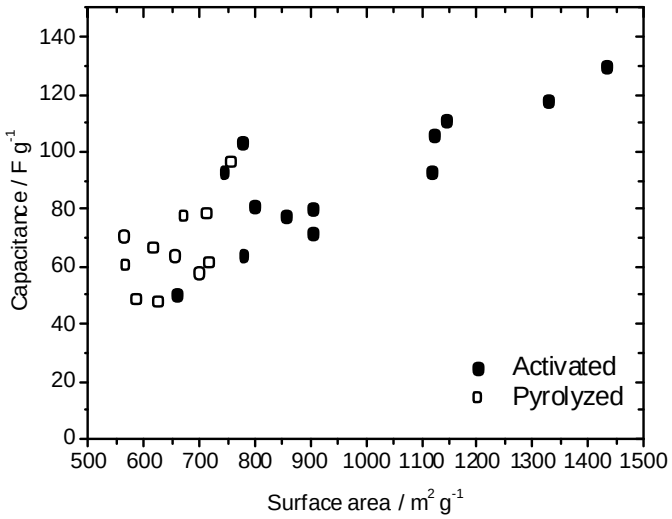
Capacitance / F g-1
Surface area / m2 g-1
Activated
Pyrolyzed
0
20
40
60
80
100
120
140
500
600
700
800
900
1000
1100
1200
1300
1400
1500

predominantly capacitive behavior when ions are effectively electrosorbed in the electric double layer formed at the electrode/electrolyte interface. In some samples, slight deviations of the rectangular shape (i.e., an anodic current increase at high potentials and/or broad humps) were observed and likely attributed to the occurrence of pseudo-faradaic reactions due to functional groups and/or electrolyte decomposition [40].

Figure 5 shows the relationship between capacitance and surface area for the pyrolyzed and activated aerogels, evidencing the progressive increase in the capacitance with the surface area of the materials. This behavior is typically observed in electrodes which electrochemical response is based on a pure capacitive phenomenon due to the electrostatic interactions between the ions of the electrolyte and the electric double layer created at electrode surface [41]. Thus, it was rather expected in the synthesized aerogels considering their chemical composition. The broad dispersion observed in the case of low surface area values, more evident in the case of pyrolyzed aerogels, can be ascribed to the non-negligible influence of the surface chemistry. Thus, pyrolyzed aerogels present low amounts of oxygen, responsible for pseudo capacitive effects. The capacitance values were also correlated to the polarization resistance. Fig. 6b shows that the R_{pol} values tend to decrease as the capacitance values increase. In addition, higher R_{pol} values were calculated for the pyrolyzed aerogels than for the activated ones. This trend can be correlated to the increased surface area of the former, which facilitates the ions migrating from the bulk electrolyte to reach the aerogel surface (Fig. 7a). Additionally, there seems to be a clear influence of the pore sizes, since low R_{pol} values were recorded for the aerogels with a large contribution of mesopores, whereas the volume of micropores does not seem to affect the R_{pol} (Fig. 7b). Similar results on the beneficial influence of a mesoporous network to provide a good kinetic

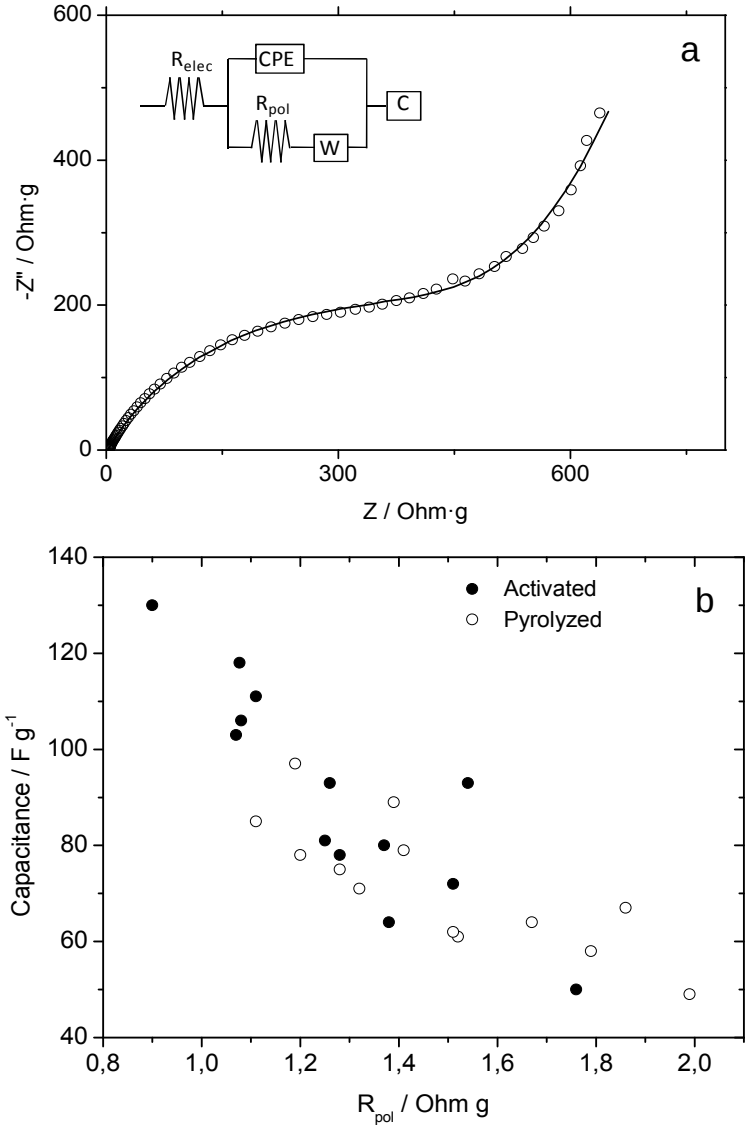
a
R_{elec}
CPE
R_{pol}
C
W
-Z'' / Ohm·g
Z / Ohm·g
0
200
400
600
0
300
600
b
Activated
Pyrolyzed
Capacitance / F g^{-1}
R_{pol} / Ohm g
40
60
80
100
120
140
0,8
1,0
1,2
1,4
1,6
1,8
2,0

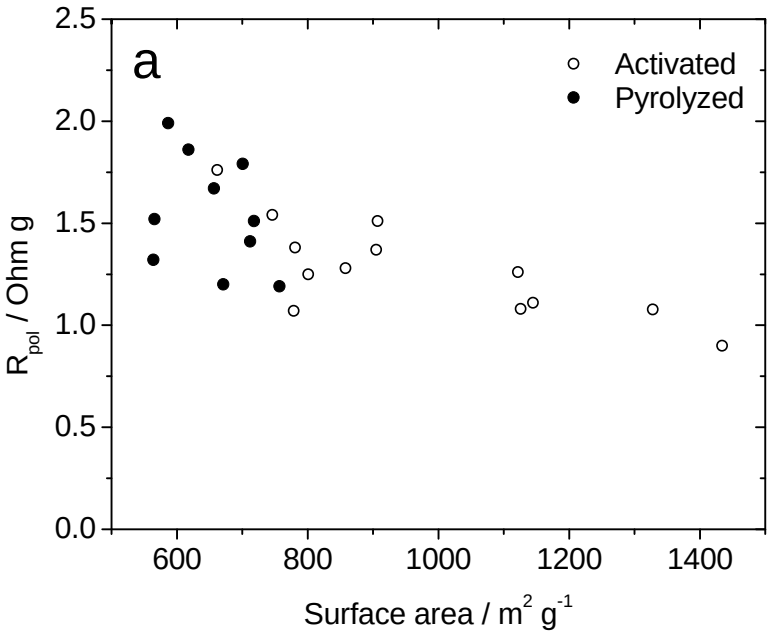
a
Activated
Pyrolyzed
R_{pol} / Ohm g
Surface area / m^2 g^{-1}
2.5
2.0
1.5
1.0
0.5
0.0
600
800
1000
1200
1400

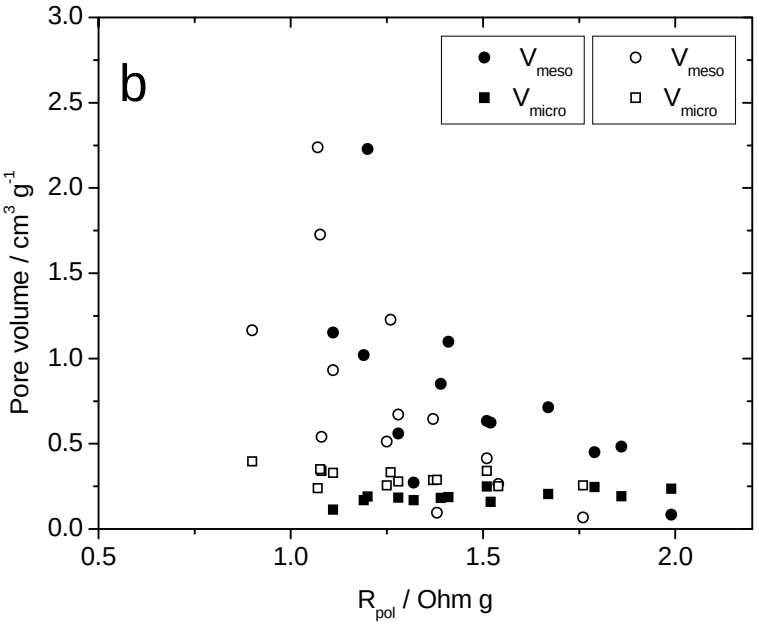
b
V_{meso}
V_{micro}
V_{meso}
V_{micro}
Pore volume / cm^3 g^{-1}
R_{pol} / Ohm g
3.0
2.5
2.0
1.5
1.0
0.5
0.0
0.5
1.0
1.5
2.0

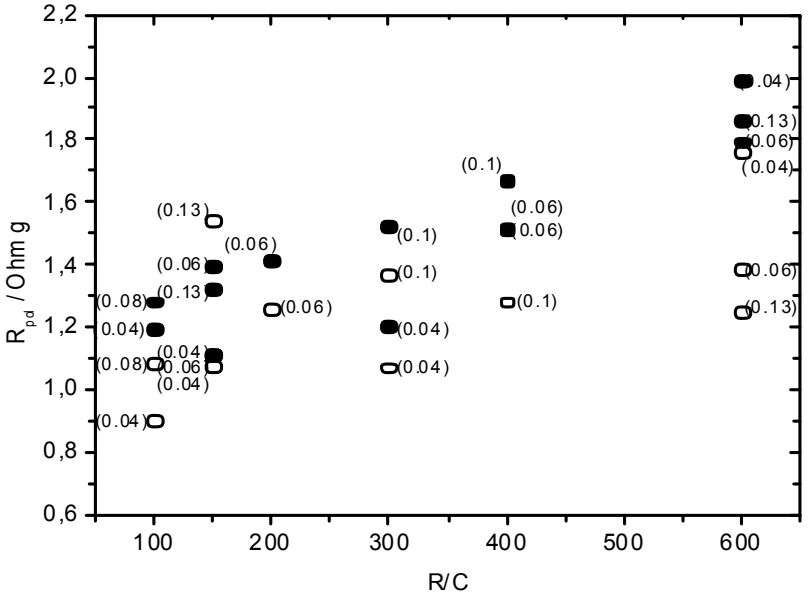
2,2
2,0
1,8
1,6
1,4
1,2
1,0
0,8
0,6
R_{pol} /Ohm g
100
200
300
400
500
600
R/C
(0.13)
(0.06)
(0.06)
(0.13)
(0.08)
0.04)
(0.04)
(0.08)
(0.06)
(0.04)
(0.04)
(0.1)
(0.06)
(0.06)
(0.1)
(0.1)
(0.06)
(0.1)
(0.04)
(0.04)
(0.04)
(0.13)
(0.06)
(0.04)
(0.06)
(0.13)

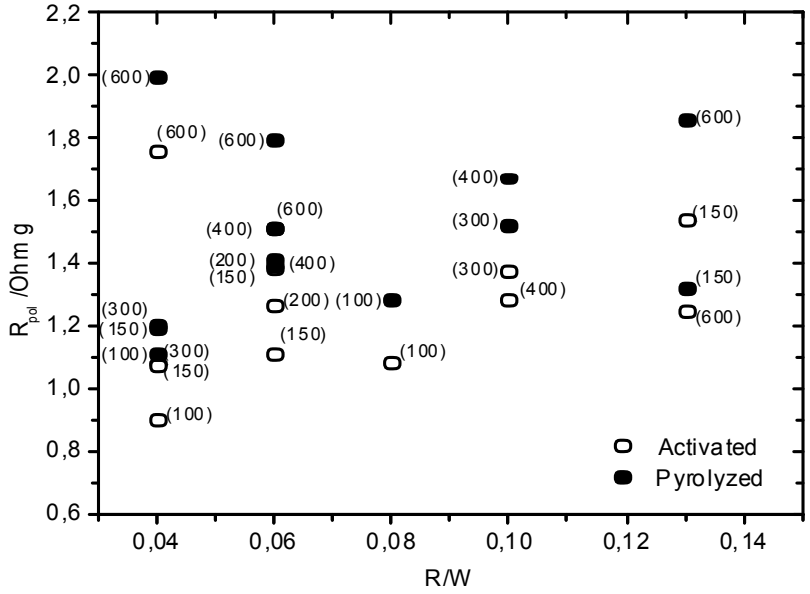
2,2
2,0
1,8
1,6
1,4
1,2
1,0
0,8
0,6
R_{pol} /Ohm g
0,04
0,06
0,08
0,10
0,12
0,14
R/W
(600)
(600)
(600)
(600)
(400)
(600)
(400)
(200)
(150)
(400)
(300)
(150)
(200)
(100)
(150)
(100)
(300)
(150)
(100)
(400)
(300)
(300)
(400)
(600)
(150)
(150)
(600)
Activated
Pyrolyzed

2.1.3.3. Desalting capacity of monolithic aerogels

Besides the electrochemical characterization of the powdered aerogels electrodes in a 3-electrode cell configuration, it is crucial to investigate the electrochemical response of the (self-supported) monolithic electrodes in symmetric cells (ca. 2-electrode cell configuration) used in desalting units. For this reason, we performed desalting studies of selected aerogels in symmetric cells using monolithic (self-supported) electrodes where the aerogel electrodes are were exposed to a bias voltage, one of them acting as anode (positive polarization) and the second one as cathode (negative polarization). Figure 8a shows the capacitance values obtained for the different aerogels in 2-electrode cell configuration and its dependence with the surface area of the electrode materials. As seen, there is not a straightforward correlation between the specific surface area and the desalting gravimetric capacity for either pyrolyzed or activated aerogels. The same trend was observed for the dependence with the polarization resistance (Figure S4). However, much of the capacitance variation of both series can be explained by analyzing the dependence of the volumetric capacitance with the combined effect exerted by both the specific surface area and the resistivity of the material. This is clearly seen in the multivariate polynomial regression analysis of both parameters using the following equations:

$$C_p = c_0 + c_1 S + c_2 R + c_3 S + c_4 S^2 + c_5 R^2 + + c_6 R^3 \qquad (2a)$$

$$C_a = c_0 + c_1 S + c_2 R \qquad (2b)$$

where C_{pyr} and C_{act} are respectively the volumetric capacitance of pyrolyzed and activated aerogels in F cm^{-3}, S is the surface area in m^2 g^{-1}, R is the electrical resistivity in Ω cm^{-1} and c_i are the polynomial coefficients of different orders.

The different polynomial fitting (c_i) and determination (r^2) coefficients for both series are compiled in Table S2. The fitting coefficient for the dependence of the capacitance with the surface area is positive for both series (pyrolyzed and activated samples), meaning that the capacity increases with the surface area; the regression coefficient for the dependence with the electric resistivity R follows the opposite trend (negative coefficient). In the case of pyrolyzed aerogels, a third order approximation was needed to

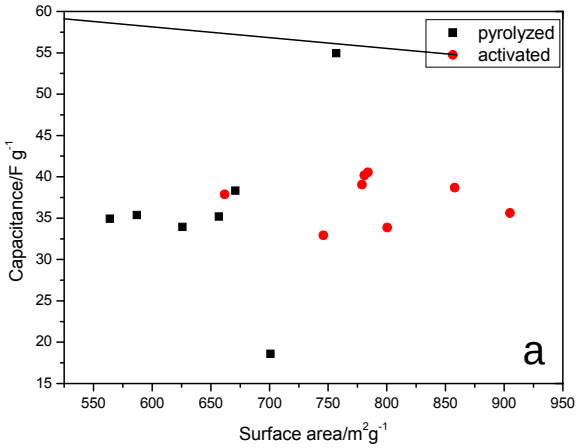
pyrolyzed
activated
a
Capacitance/F g-1
Surface area/m2g-1
60
55
50
45
40
35
30
25
20
15
550
600
650
700
750
800
850
900
950

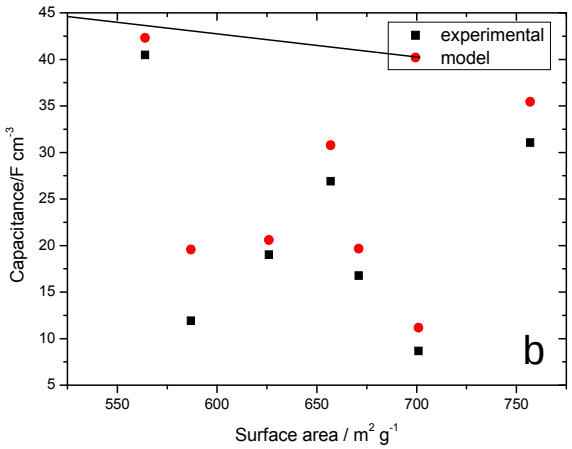
experimental
model
b
Capacitance/F cm-3
Surface area / m2 g-1
45
40
35
30
25
20
15
10
5
550
600
650
700
750

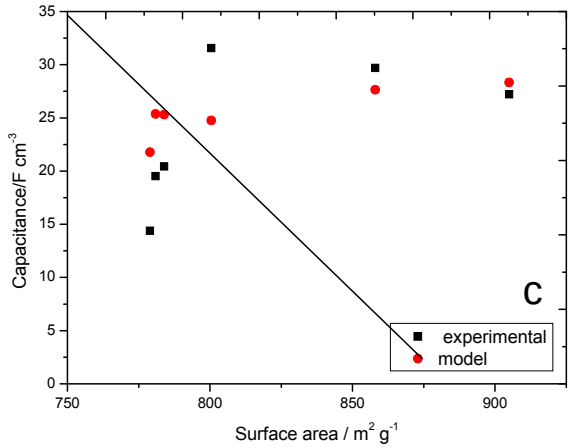
experimental
model
c
Capacitance/F cm-3
Surface area / m2 g-1
35
30
25
20
15
10
5
0
750
800
850
900

The driving terms are the first order ones, while the second and third order coefficients have much smaller impact on the capacitance. In the case of surface area, the third order term is no meaningful and has been neglected. Furthermore, more than 96% of the capacitive response can be correlated to the combined effect of R

and S following a linear dependence (since 2^{nd} and 3rd order fitting coefficients are quite small). For the activated aerogels, almost 70% of capacitive response shows a linear dependence with R and S. Such low dependence suggests that the remaining 30% of the variation of the capacitance depends on the contribution of uncontrolled resistances in the cell setup likely arising from a poor contact of the monolithic electrode with the current collector (since activated monoliths show a much lower contact surface).

2.1.4. Conclusions

A series of activated and pyrolyzed aerogels have been prepared by the sol-gel polymerization of resorcinol-formaldehyde mixtures. The influence of the different R/C ($100 \leq R/C \leq 800$) and R/W ($0.04 \leq R/W \leq 0.13$) molar ratios on the textural and electrochemical properties has been determined. Data has confirmed the strong interdependence between R/C and R/W parameters, preventing a separated evaluation. For instance, a drastic decrease in the specific surface area was observed for the activated aerogels when either R/C or R/W increased, whereas the effect was not so remarkable for the series of pyrolyzed aerogels. Along with surface area, the mesoporosity was very much conditioned by the synthesis conditions, whereas the microporosity did not follow the same trend and most samples presented quite close micropore volumes. As for the electrochemical performance, an enhanced decrease of the capacitance was observed when R/C and R/W increase, while respectively preserving low R/W and R/C ratios low capacitance values were measured in those aerogels characterized by either low R/W or R/C molar ratios. This trend is correlated to the ohmic resistance of the electrodes that strongly depends on the R/W and R/C values and the textural features of the materials. Polarization resistances are slightly higher in the pyrolyzed aerogels, compared to the activated materials. Furthermore, lower R_{pol} values are obtained for the aerogels with higher contribution of mesoporosity, regardless the microporosity. The capacitive response of the aerogel monolithic electrodes, measured in a symmetric cell

configuration, similar to those used in desalting units has been successfully correlated to the combined effect of surface area and electrical resistivity.

2.1.5. References

[1] K. Shi, M. Ren, I. Zhitomirsky, ACS Sus. Chem. Eng. 2 (2014) 1289-1298.

[2] D. Zhang, T. Yan, L. Shi, Z. Peng, X. Wen, J. Zhang, J. Mater. Chem. 22 (2012) 14696-14704.

[3] Y.-C. Tsai, R.-an Doong, Synthetic Met. 205 (2015) 48-57.

[4] Z. Peng, D. Zhang, L. Shi, T. Yan, S. Yuan, H. Li, R. Gao, J. Fang, J. Phys. Chem. C 115 (2011) 17068-17076.

[5] X. Wen, D. Zhang, L. Shi, T. Yan, H. Wang, J. Zhang, J. Mater. Chem. 22 (2012) 23835-23844.

[6] S. Zhao, T. Yan, H. Wang, G. Chen, L. Huang, J. Zhang, L. Shi, D. Zhang, Appl. Surf. Sci. 369 (2016) 460-469.

[7] Y. Wimalasiri, M. Mossad, L. Zou, Desalination 357 (2015) 178-188.

[8] H. Wang, T. Yan, P. Liu, G. Chen, L. Shi, J. Zhang, Q. Zhong, D. Zhang, J. Mater. Chem. A 5 (2016) 4908-4919

[9] P. Liu, H. Wang, T. Yan, J. Zhang, Q. L. Shi, D. Zhang, J. Mater. Chem. A 4 (2016) 5303-5313

[10] M. E. Suss, S. Porada, X. Sun, P. M. Biesheuvel, . Yoonf, V. Presser, Energy Environ. Sci. (2015) 2296-2319.

[11] Anderson MA, Cudero AL, Palma J, Electrochim. Acta 55 (2010) 3845–3856.

[12] Porada S, Zhao R, van der Wal A, Presser V, Biesheuvel P, Prog. Mater. Sci. 58 (2013) 1388-1442.

[13] R.W. Pekala, J. Mater. Sci. 24 (1989) 3221–3227.

[14] J.C. Farmer, D.V. Fix, G.V. Mack, R.W. Pekala, J.F. Poco, J. Appl. Electrochem. 26 (1996) 1007–1018.

[15] R.W. Pekala, J.C. Farmer, C.T. Alviso, T.D. Tran, S.T. Mayer, J.M. Miller, B. Dunn, J. Non-Cryst. Solids 225 (1998) 74–80.

[16] Pajonk GM, Appl. Catal. 72 (1991) 217–66.

[17] P. Lavela, F. Nacimiento, G.F. Ortiz, J.L. Tirado, J. Solid State Electrochem. 14 (2010) 139–148.

[18] Kim P-H, Kwon J-D, Kim J-S, Synth. Met. 142 (2004) 153–60.

[19] Robertson C, Mokaya R, Microporous Mesoporous Mater. 179 (2013) 151–156.

[20] Jung H-H, Hwang S-W, Hyun S-H, Lee K-H, Kim G-T, Desalination 216 (2007) 377–85.

[21] Zafra MC, Lavela P, Macías C, Rasines G, Tirado JL, J. Electroanal. Chem. 708 (2013) 80-6.

[22] Yang K-L, Yiacoumi S, Tsouris C, J. Electroanal. Chem. 540 (2003) 159–67.

[23] S.A. Al-Muhtaseb, J.A. Ritter, Adv. Mater. 15 (2003) 101–114.

[24] T.F. Baumann, M.A. Worsley, T.Y.J. Han, J.H. Satcher, J. Non-Cryst. Solids 354 (2008) 3513–3515.

[25] M.E. Suss, T.F. Baumann, W.L. Bourcier, C.M. Spadaccini, K.A. Rose, J.G. Santiago, M. Stadermann, Energy Environ. Sci., 5 (2012) 9511-9519.

[26] H. Tamon, H. Ishizaka, M. Mikami, M. Okazaki, Carbon 35 (1997) 791-796.

[27] Job N, Thery A, Pirard R, Marien J, Kocon L, Rouzaud JN, Beguin F, Pirard JP, Carbon 43 (2005) 2481–2494.

[28] C. Macías, P. Lavela, G. Rasines, M. C. Zafra, JL. Tirado, C.O. Ania, J. Appl. Electrochem. 44 (2014) 963-976.

[29] G. Rasines, P. Lavela, C. Macías, M.C. Zafra, J.L. Tirado, C.O. Ania, J. Electroanal. Chem. 741 (2015) 42-50.

[30] P. Lavela, G. Rasines, C. Macías, M. C. Zafra, J.L. Tirado, J.B. Parra, C.O. Ania, Carbon 83 (2015) 262-274.

[31] Zafra MC, Lavela P, Macías C, Rasines G, Tirado JL, J. Electroanal. Chem. 708 (2013) 80-86.

[32] Landon J, Gao X, Kulengowski B, Neathery JK, Liu K, J. Electrochem. Soc. 159, 2012, A1861–6.

[33] Jung H.H., Hwang S.W., Hyun S.H., Lee K.H., Kim G.T., Desalination, 216, 2007, 377–385.

[34] E. J. Zanto, S.A. Al-Muhtaseb, J.A. Ritter, Ind. Eng. Chem. Res. 41 (2002) 3151-3162.

[35]Gabelich C.J., Tran T.D., Suffet I.H., Environ. Sci. Technol., 36, 2002, 3010-3019.

[36] Xu P., Drewes J.E., Heil D., Wang G., Water Res., 42, 2008, 2605-2617.

[37] Jagiello J, Olivier JP, Adsorption 19 (2013) 777-783.

[38] Rasines G, Lavela P, Macıas C, Haro M, Ania CO, Tirado JL, J. Electroanal. Chem. 671 (2012) 92–8.
[39] M Thommes, K Kaneko, A.V. Neimark, J.P. Olivier, F. Rodriguez-Reinoso, J. Rouquerol, K.S.W. Sing, (IUPAC Technical Report) Pure Appl. Chem. 87 (2015) 1051–1069.
[40] Hsieh CT, Teng H, Carbon 40 (2002) 667–674.
[41] K. Kinoshita Carbon: Electrochemical and Physicochemical Properties, Wiley, New York 1988.
[42] Noked M, Avraham E, Soffer A, Aurbach D, J. Phys. Chem. C 113 (2009) 21319–21327.

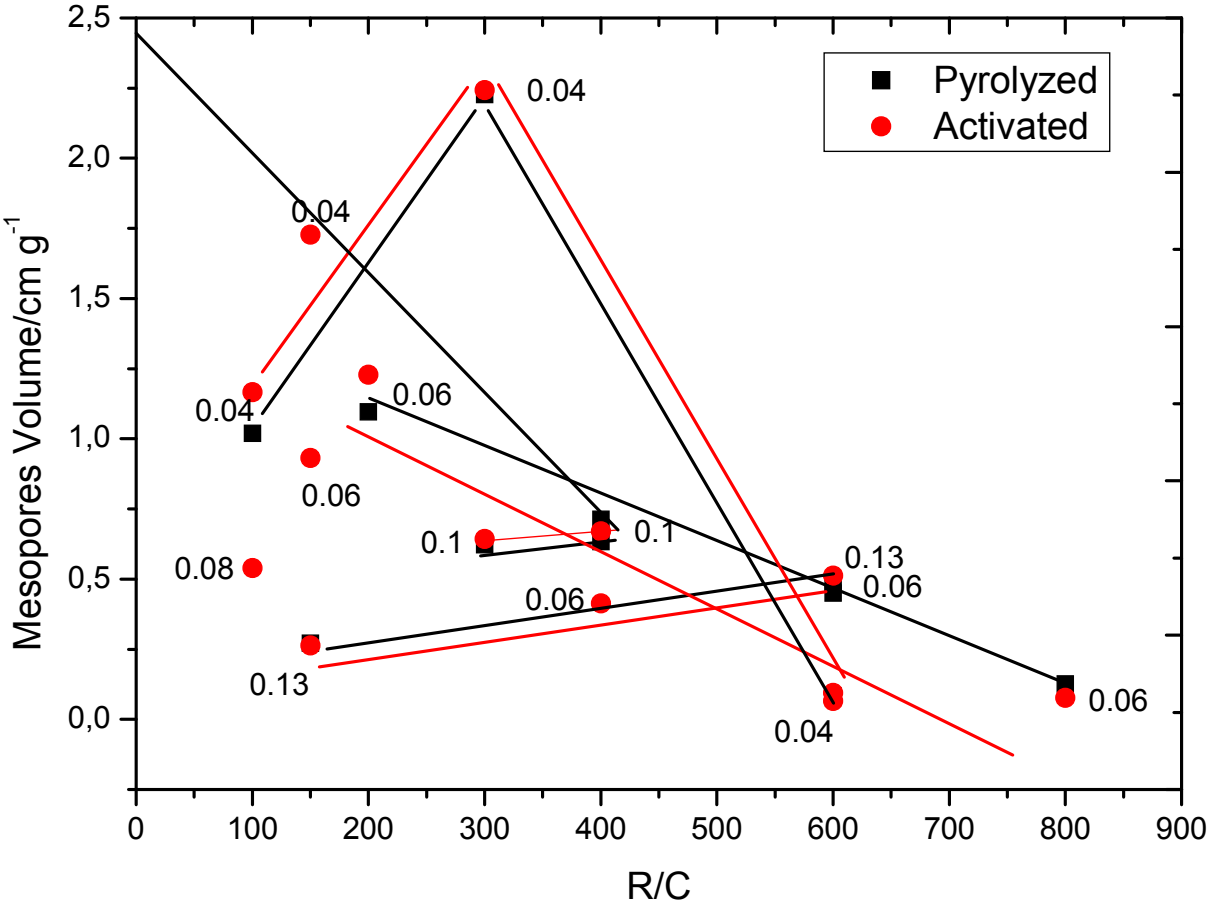
Pyrolyzed
Activated
Mesopores Volume/cm g-1
R/C
2,5
2,0
1,5
1,0
0,5
0,0
0
100
200
300
400
500
600
700
800
900
0.04
0.04
0.04
0.06
0.06
0.08
0.1
0.1
0.13
0.06
0.06
0.13
0.04
0.06

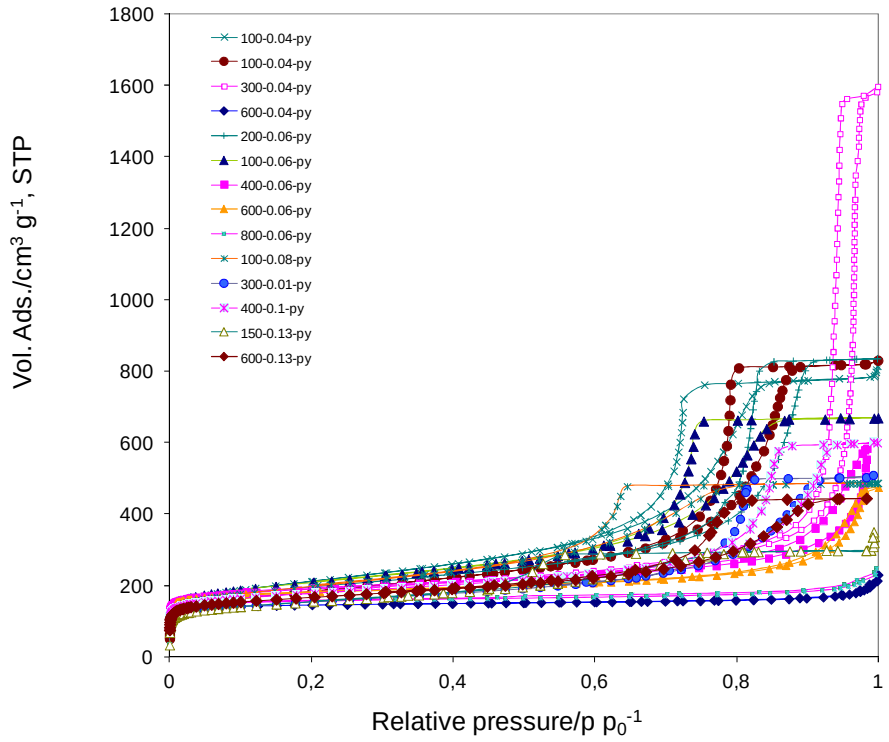
Vol. Ads./cm3 g-1, STP
Relative pressure/p p0-1
100-0.04-py
100-0.04-py
300-0.04-py
600-0.04-py
200-0.06-py
100-0.06-py
400-0.06-py
600-0.06-py
800-0.06-py
100-0.08-py
300-0.01-py
400-0.1-py
150-0.13-py
600-0.13-py

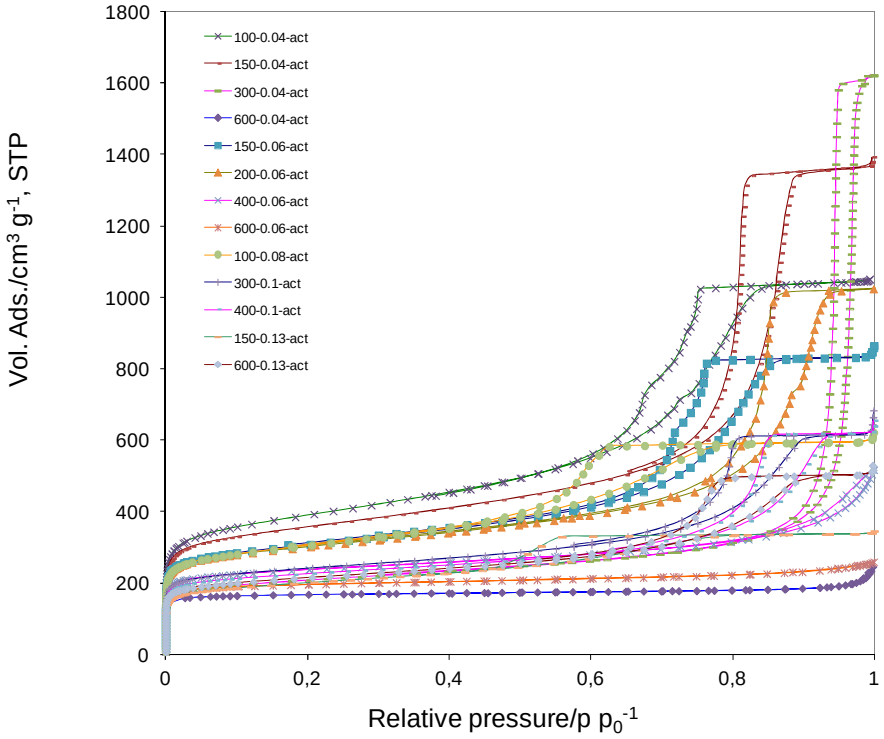
Vol. Ads./cm3 g-1, STP
Relative pressure/p p0-1
100-0.04-act
150-0.04-act
300-0.04-act
600-0.04-act
150-0.06-act
200-0.06-act
400-0.06-act
600-0.06-act
100-0.08-act
300-0.1-act
400-0.1-act
150-0.13-act
600-0.13-act

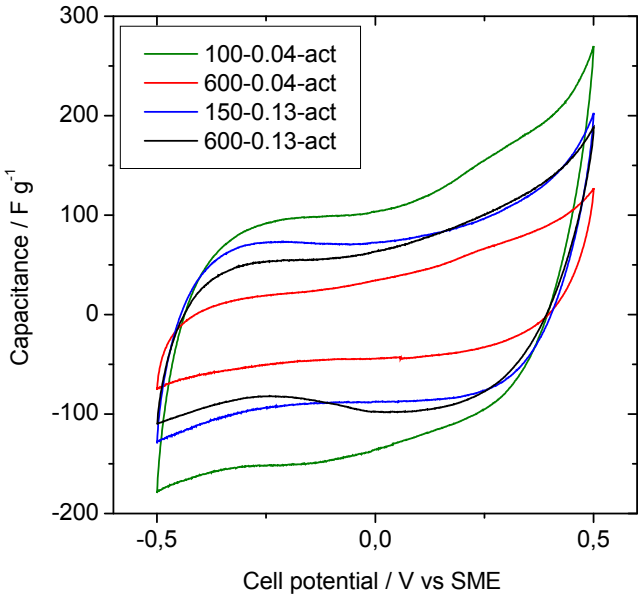
100-0.04-act
600-0.04-act
150-0.13-act
600-0.13-act
Capacitance / F g-1
Cell potential / V vs SME
300
200
100
0
-100
-200
-0,5
0,0
0,5

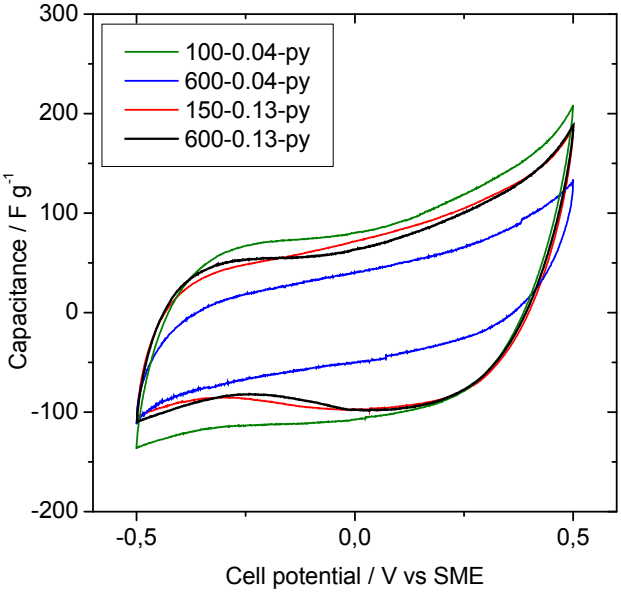
100-0.04-py
600-0.04-py
150-0.13-py
600-0.13-py
Capacitance / F g-1
Cell potential / V vs SME
300
200
100
0
-100
-200
-0,5
0,0
0,5

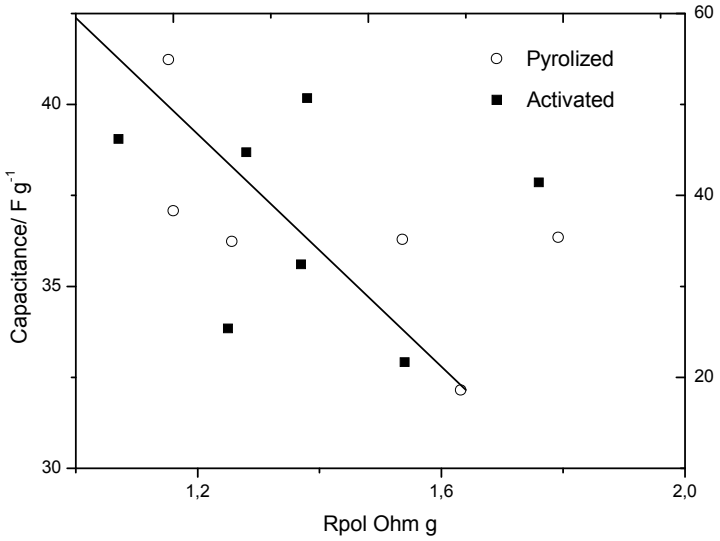
Pyrolized
Activated
Capacitance/ F g-1
Rpol Ohm g
30
35
40
60
40
20
1,2
1,6
2,0

Table S1. Summary of the main textural parameters obtained from N_2 adsorption isotherms at -196 ºC on the studied aerogels.

Sample	R/C	R/W	S_{BET}	V_{TOTAL} [A]	V_{MICRO} [B]	V_{MESO} [B]
			$m^2\ g^{-1}$	$cm^3\ g^{-1}$	$cm^3\ g^{-1}$	$cm^3\ g^{-1}$
100-0.04-py	100	0.04	757	1.2	0.17	1.02
100-0.08-py	100	0.08	707	0.75	0.20	0.55
150-0.04-py	150	0.04	659	1.27	0.14	1.09
150-0.06-py	150	0.06	749	1.03	0.20	0.82
150-0.13-py	150	0.13	564	0.46	0.17	0.27
200-0.06-py	200	0.06	712	1.29	0.17	1.10
300-0.04-py	300	0.04	671	2.44	0.19	2.23
300-0.10-py	300	0.1	566	0.78	0.16	0.62
400-0.06-py	400	0.06	718	1.17	0.25	0.63
400-0.10-py	400	0.1	657	0.93	0.20	0.71
600-0.04-py	600	0.04	587	0.26	0.24	0.08
600-0.06-py	600	0.06	701	0.72	0.25	0.45
600-0.13-py	600	0.13	618	0.67	0.19	0.48
800-0.06-py	800	0.06	626	0.35	0.24	0.13
100-0.04-act	100	0.04	1434	1.25	0.40	1.17
100-0.08-act	100	0.08	1126	0.92	0.34	0.54
150-0.04-act	150	0.04	1328	2.1	0.35	1.73
150-0.06-act	150	0.06	1145	1.30	0.33	0.93
150-0.13-act	150	0.13	746	0.52	0.25	0.26
200-0.06-act	200	0.06	1122	1.58	0.33	1.23
300-0.04-act	300	0.04	779	2.56	0.24	2.24
300-0.10-act	300	0.1	905	0.95	0.29	0.64
400-0.06-act	400	0.06	907	0.74	0.34	0.41
400-0.10-act	400	0.1	858	0.96	0.28	0.67
600-0.04-act	600	0.04	662	0.34	0.25	0.07
600-0.06-act	600	0.06	781	0.39	0.29	0.09
600-0.13-act	600	0.13	801	0.78	0.26	0.51
800-0.06-act	800	0.06	784	0.38	0.29	0.08

[A] total pore volume evaluated at $p/p_0 \sim 0.99$

[B] micro-, mesopore volumes evaluated by the 2DNLDFT-HS method

Table S2. Fitting (c_i) and determination (r^2) coefficients of the multivariate polynomial regression analysis (equations 1a and 1b) of the dependence of the surface area and capacitance values for the series of pyrolyzed and activated aerogels.

Term	Pyrolyzed	Activated
c_0	178.921	7.590
c_1	1.089	0.026
c_2	-18.797	-0.142
c_3	0.032	-
c_4	-0.004	-
c_5	0.254	-
c_6	-0.001593	-
r^2	0.966	0.688


Applied
Electrochemistry

2.2.1. Introduction

Much attention has been paid on structurally disordered carbons as materials with interesting properties for energy storage and environmental applications [1-3]. Their suitable electrical and thermal conductivity, adequate corrosion resistance, low thermal expansion coefficients, low densities and low elasticity makes them outstanding materials that can be produced at low cost and high purities for technological uses. High porosity can be achieved by selecting appropriate synthesis routes which allow controlling the microstructure at the nanometer scale. Also, activation processes can be applied to increase the pore volumes and adjust the pore size distribution, with porosity values easily exceeding 80% and surface areas as high as 2000 $m^2 g^{-1}$. Most commonly, activation processes consist of a partial burn-off of the amorphous carbon under mild oxidation conditions. For this purpose, various procedures including physical activation using CO_2 or steam and chemical activation with hydroxides and carbonates, are usually performed [4]. These highly porous carbons are especially interesting for their use as electrodes in electrosorption processes [5, 6].

When a voltage is applied between two porous carbon electrodes immersed in an inert electrolyte, an electrical double layer is formed at the interface of each electrode. The electro-assisted removal of ionic compounds is based on the separation of the charged species at the electrode/electrolyte interface due to electrostatic interactions. Thus, the charged species in the solution move to and are held on the opposite-charged electrode surface. The electroadsorption/desorption cycles are highly reversible due to the electrostatic nature of the interactions existing between the electrodes and the electrolytic solution. Based on this mechanism, large surface area electrodes are required for achieving high desalting capacities. Pore size is also important since the adsorption of large solvated ions into small pores could be considered as a limitation of the deionization process [7]. Otherwise, the concept of an electric double-layer formed by solvated ions adsorbed on sub-nanometer size pores cannot be strictly applied [8, 9].

Although studies on the electrosorption of ions were initiated several decades ago, advances on this technology have remained somewhat behind due to the lack of adequate electrode materials. For their versatility of forms and structures, a large number of carbon materials are currently being researched to optimize their electroadsorptive properties,

including carbon fibers and nanotubes [10, 11], carbon cloths [12], carbide-derived carbons[13], graphene[14], activated carbons[15], carbon aerogels[16], and templated carbon[17]. Besides, hierarchical porous carbon has also been evaluated as promising materials for capacitive deionization [18, 19]. Due to a unique combination of physicochemical and structural properties, that may be conveniently adapted during the synthesis and processing, carbon aerogels possess great potential and versatility as electrodes in electrochemical applications [20, 21]. Carbon aerogels are particularly interesting electrode materials as the supercritical drying leads to a better preservation of the pore structure of the polymerized gel, due to the lack of interfacial tensions during drying.

The objective of this work was to investigate the electrochemical behavior of micro/mesoporous activated carbon aerogels prepared using different resorcinol/catalyst ratios as electrodes for the removal of ions (i.e., phosphates and nitrates). The desalting capacity of the activated aerogels has been compared to that of the aerogels prepared from the poly-condensation of resorcinol and formaldehyde. The structural and morphological properties of the electrode materials have been characterized and the capacitive behavior has been determined by voltammetric and impedance analysis. Phosphates and nitrates are ionic species included in fertilizers, thus posing a great long-term environmental impact to groundwater pollution due to agricultural activities [22]. Although many studies report the electrosorption of ions in carbon electrodes, including aerogels, scarce studies focus on the electro-assisted removal of these anions [23].

2.2.2 **Experimental section**

2.2.2.1. Materials preparation

Three carbon aerogels were synthesized by the sol-gel polymerization method reported by Pekala et al. [24]. Resorcinol (R) and formaldehyde (F) were dissolved in water (W) and sodium carbonate was added as a catalyst (C). Three resorcinol/catalyst (R/C) ratios were fixed (i.e., 200, 400 and 600) in order to obtain aerogels with different porous structures. Otherwise, the R/F molar ratio was set at 0.5, and the R/W at 0.06. The precursors were mixed in sealed glass moulds under magnetic stirring and allowed to undergo gelation and aging in an oven at 40 ºC for 24 h and 70 ºC for 120 h. Subsequently a controlled water-acetone exchange was carried out, and then the samples

were dried under CO_2 supercritical conditions. Finally, the aerogels were pyrolysed at 800 ºC under nitrogen atmosphere with a controlled heating program (i.e., heating rate 2 ºC min^{-1} up to 400 ºC and hold for 60 min followed by heating up to 800 ºC and hold for 60 min) [25]. For the sake of clarity, the pyrolyzed samples will be named as CAGXP, where X is the corresponding R/C value. A second batch of samples was prepared by activation under a CO_2 stream at 800 ºC for 2 hours. These samples will be named as CAGXA.

2.2.2.2. *Structural and textural characterization*

X-Ray diffraction (XRD) patterns were recorded with a Siemens D500 diffractometer furnished with Cu K□ radiation and a graphite monochromator. The baseline was corrected and the Lorentz and polarization factor was applied before the determination of the line width and the position of the reflections. The pore structure of the carbon aerogels were characterized by N_2 adsorption-desorption isotherms at -196 ºC (ASAP 2010, Micromeritics). The carbon aerogels were previously outgassed under primary vacuum at 120 ºC overnight (heating ramp of 2 ºC min^{-1}). The specific surface area, S_{BET}, and total pore volume, V_T, were calculated from the isotherms. The pore size distributions were calculated by using the density functional theory (DFT) approach; the micropore volume was also evaluated by the DR method [26]. The Raman spectra were acquired with a Renishaw Raman instrument (InVia Raman Microscope), equipped with a Leica microscope. Spectra were obtained by excitation with red laser light (785 nm) in the range between 1000 and 2000 cm^{-1}. Fitting of the spectra was performed with the help of the Peakfit v. 4.11 software package. The chemical state and compositions of activated carbon aerogels were analyzed by using an X-ray Photoelectron Spectrometer (XPS, SPECS Phobios 150MCD) with Mg K source and a chamber pressure of 4×10^{-9} mbar. Powdered samples were deposited as thin film samples on a holder and subjected to high vacuum overnight. Binding energies were referenced to the C 1s line of the adventitious carbon located at 284.6 eV. The deconvolution of the spectra was performed using the Casa XPS software.

2.2.2.3. *Electrochemical response*

Electrochemical measurements were performed in three-electrode Swagelok^{TM} type cells. The working electrode consisted of a mixture of active material (70%), Superior graphite (20%) and PVDF binder (10%). The powdered samples were slurried in N-methyl pyrrolidone to yield a paste which was subsequently spread on a 13 mm titanium disk. A Hg/Hg_2SO_4 and a platinum wire were respectively used as reference and counter electrode. The electrodes were dried at 70ºC overnight. The electrode was cooled and impregnated with the electrolyte solution before being assembled into the cell. The electrolyte solutions were prepared by dissolving $NaNO_3$ and Na_2HPO_4/ NaH_2PO_4 in deionized water at 0.1 M. The use of a Na_2HPO_4/NaH_2PO_4 was intended to keep pH at the value of pH= 7. The electrochemical measurements were controlled with a Biologic VMP multichannel potentiostat. Cyclic voltammetry experiments were conducted between -0.5 and +0.5 V versus the reference electrode for several sweep rates ranging from 0.5 to 10 mV s^{-1}. The capacitance of each electrode was calculated from the voltammograms using the relationship C = I / (v*m), where I (mA) is the average current in the applied potential window, v is the applied sweep rate in mV s^{-1} and m is the mass of the electrode (normalized capacitance per unit mass of electrode). Chronocoulometric curves were performed by inducing a potentiostatic pulse of 300 mV vs Hg/Hg_2SO_4 for 120 s and recording the transient current.

Electrochemical impedance spectroscopy (EIS) was a helpful technique to analyze the kinetic response of the electro-sorption reaction. These measurements were recorded in an Autolab PGSTAT12 system, using an AC voltage signal of 5 mV vs equilibrium potential (i.e., open circuit potential, which ranged from 0.4 to 0.6 V vs reference electrode), over the frequency range 25 kHz to 10 mHz at the equilibrium potential.

Capacitive deionization experiments were developed by using two monolithic aerogel electrodes previously polished to achieve a flat surface ensuring a good contact. The monoliths were previously washed in deionized water for 30 minutes and then were vacuum impregnated with the electrolyte. They were sandwiched between titanium current collectors using two Whatman glass GF/A fiber sheets as a separator. This symmetric cell was assembled in a bath cell containing 8.5 mL of the electrolyte under continuous stirring to avoid mass transfer restrictions from the bulk solution. The deionization experiment was carried out by applying a potentiostatic pulse of 1.2 V for 150 min. Then, the discharge of the electrode was undergone at 0 V for the same period

of time. A conductivity meter was used to monitor the change in the ionic concentration. Concentration values were calculated by previously recording a conductivity-concentration plot for each salt.

2.2.3. Results and discussion

2.2.3.1. Structural characterization of the aerogels

A series of carbon aerogels prepared using different R/C ratio were prepared and subjected to pyrolysis (series P) and activation in CO_2 (series A). Information about the structural properties of the synthesized materials was by XRD and Raman spectroscopy, shown in Fig. 1 and 2, respectively. The common features of XRD patterns are two broadened bands located at ca. 22.1 and ca. 44.5º(2θ), ascribable to the (002) and (100) reflections, respectively, both characteristic of disordered carbons. However, the reflection at 44.5º was rather marked and well-defined, indicating that despite the low structural ordering of the aerogels, there is an important contribution of domains of a graphitic structure. This is an unusual characteristic of nanoporous carbon materials synthesized at low temperatures. The first-order Raman spectra of the disordered carbons exhibited two highly broadened and overlapped bands in the region between 1000 and 2000 cm^{-1}. The parameters obtained from deconvolution of the spectra are compiled in Table 1. According to literature, G band at ca. 1580 $cm^{-1}$is ascribed to a Raman-allowed E_{2g} resulting from to 'in plane' displacement of carbon atoms strongly coupled in the hexagonal sheets [27, 28]. A second maximum is observed at ca. 1350 cm^{-1} and named as 'disorder-induced' or D1 mode. It is commonly ascribed to the lack of a long range translation symmetry what breaks the k-momentum conservation rule [29]. An asymmetry of the G band is observed and resolved by adding a D2 lorentzian curve to the spectrum fitting [30]. The D2 band is usually ascribed to a lattice vibration involving graphene layers which are not directly sandwiched between two other graphene layers [31]. An additional Gaussian component was added at ca. 1495 cm^{-1}, designated as D3 band and correlated to amorphous sp^2-bonded forms of carbon. Particularly, disordered carbons located at interstitial defects [32]. The peak at ca.1310 cm^{-1} exhibits a shoulder at ca. 1160 cm^{-1}, commonly named as D4 [33], attributed to sp^2-sp^3 bonds or C–C and C=C stretching vibrations of polyene-like structures in Raman spectra of flame soot.

Table 1 Raman shift and width values for the D1 and G bands calculated from the deconvoluted spectra

	R/C	I_{D1}/I_G	D1 shift (cm^{-1})	G shift (cm^{-1})	D1 FWHM (cm^{-1})	G FWHM (cm^{-1})
Pyrolyzed	200	2.67	1309.27	1594.15	153.74	68.97
	400	2.53	1309.19	1594.00	148.18	66.64
	600	2.28	1313.15	1597.04	138.61	65.54
Activated	200	2.63	1317.53	1597.85	146.29	66.37
	400	2.38	1312.19	1592.99	136.81	66.07
	600	2.27	1312.19	1592.97	133.61	62.95

The lowest χ^2 values were achieved for the fitting of G and D2 signals to Lorentzian shapes and D1, D2 and D3 to Gaussian shapes. Table 1 clearly shows that widths of D1 and G bands are lower for the activated than for pyrolyzed aerogels. Moreover, the D1/G band intensity ratio also decreased upon activation of the samples, particularly for R/C = 400. In addition, a non negligible decrease in the I_{D1}/I_G ratio is observed when the R/C value increased in both activated and pyrolyzed aerogels. These trends indicate a dependence of the structure order with the R/C ratio, suggesting that high contents of resorcinol favor the formation of slightly more ordered carbon structures.

A semi-quantitative measurement of the functional groups attached to the aerogel surface can be determined by themogravimetric measurements in Ar atmosphere (Fig. 3). Besides the mass loss below 200ºC due to the moisture retained in the pore network or the samples, a slight loss between 200-400 ºC is observed for the pyrolyzed aerogel, indicating the presence of volatiles remaining in the sample. Above 700ºC the activated sample showed a non negligible weight loss likely due to the decomposition of surface groups incorporated during the activation.

The functionalization of the activated gels was further explored by recording the XPS spectra at the C1s and O1s levels (Fig.4). The contribution of oxygen linked to carbon was found in the C1s spectra as C-O (285.6±0.2 eV), C=O (287 eV±0.1 eV) and O=C-O (288.7±0.3 eV) (Fig. 4a, c and e) [34]. The overall contribution of the oxygenated groups increased mainly for CAG200A. This result can be correlated to the larger surface area of

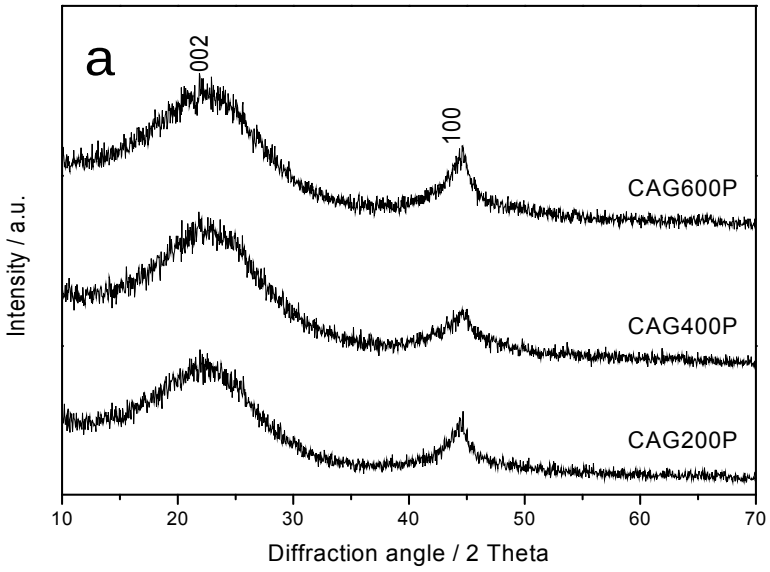
a
002
100
CAG600P
CAG400P
CAG200P
Intensity / a.u.
10
20
30
40
50
60
70
Diffraction angle / 2 Theta

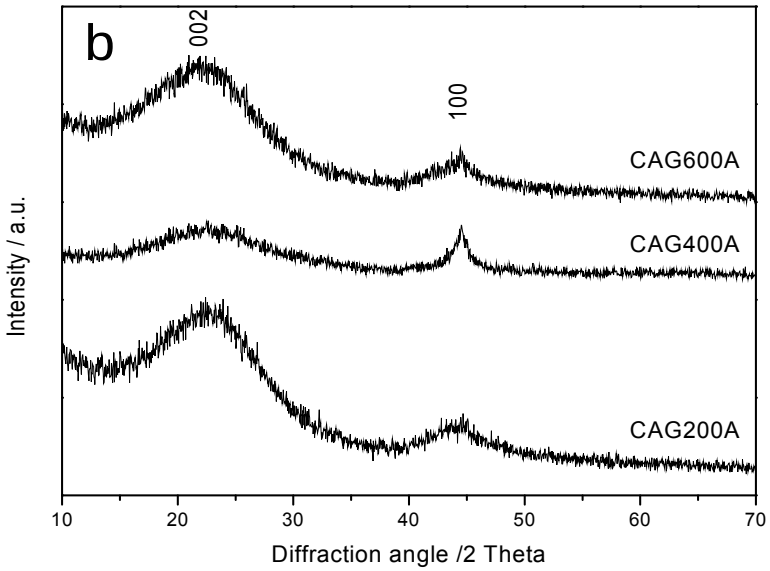
b
002
100
CAG600A
CAG400A
CAG200A
Intensity / a.u.
10
20
30
40
50
60
70
Diffraction angle /2 Theta

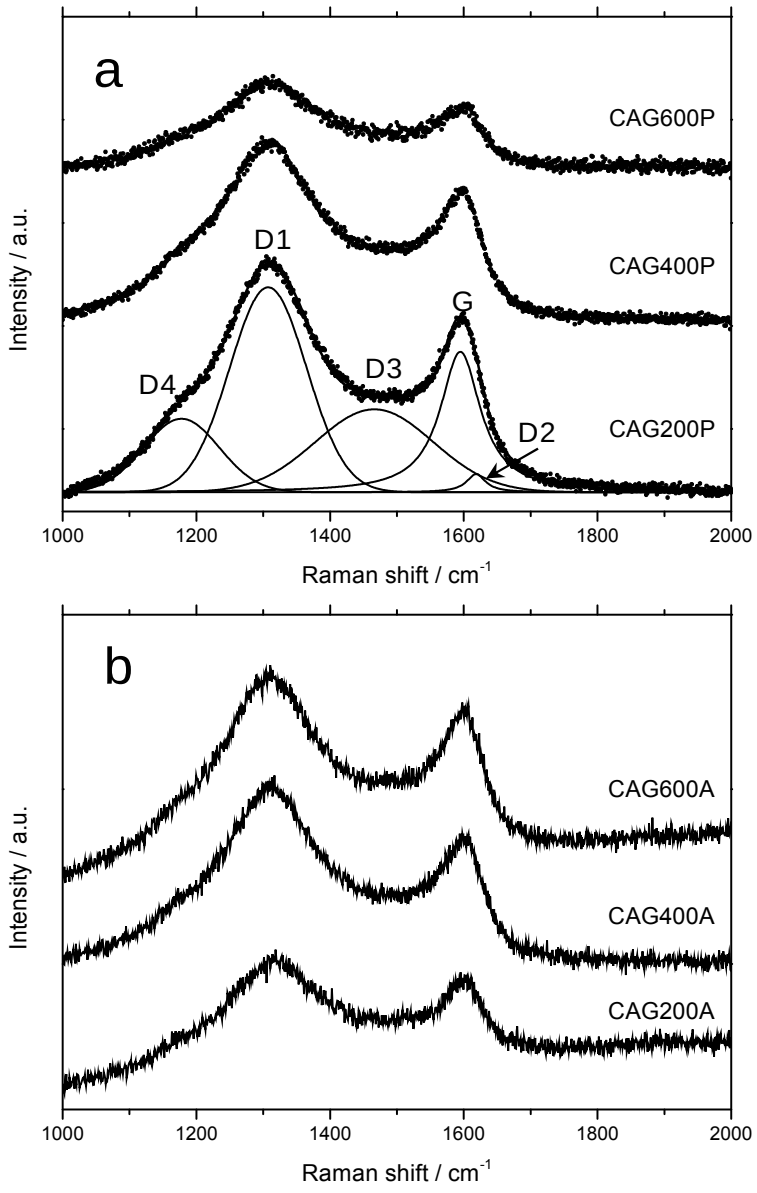
a
CAG600P
CAG400P
CAG200P
D1
D2
D3
D4
G
Intensity / a.u.
1000
1200
1400
1600
1800
2000
Raman shift / cm-1
b
CAG600A
CAG400A
CAG200A
Intensity / a.u.
1000
1200
1400
1600
1800
2000
Raman shift / cm-1

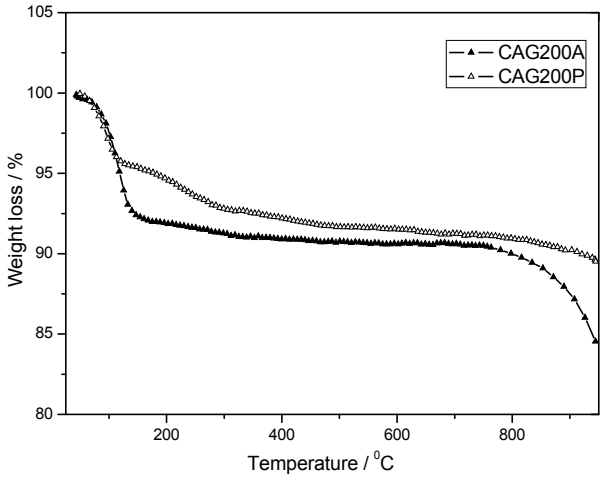

Pyrolyzed	CAG 200P	CAG 400P	CAG 600P
S_{BET} / m^2 g^{-1}	712	718	701
V_{MICRO}[a] /cm^3 g^{-1}	0.27	0.28	0.27
V_{MESO} / cm^3 g^{-1}	1.02	0.24	0.37
V_{TOTAL}[b] / cm^3 g^{-1}	1.29	0.91	0.72

Activated	CAG 200A	CAG 400A	CAG 600A
S_{BET} / m^2 g^{-1}	1123	908	781
V_{MICRO}[a] / cm^3 g^{-1}	0.41	0.34	0.30
V_{MESO} / cm^3 g^{-1}	1.15	0.34	0.04
V_{TOTAL}[b] / cm^3 g^{-1}	1.58	0.74	0.39

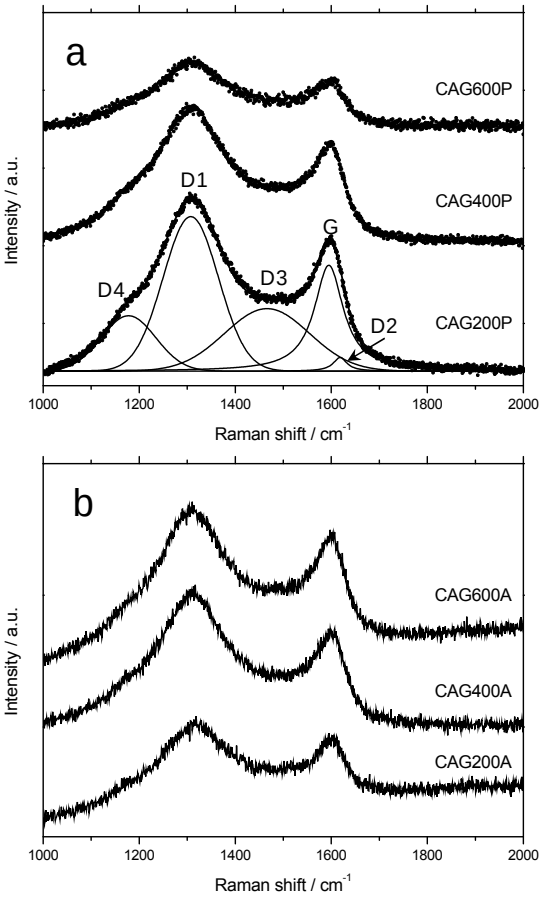
a
CAG600P
CAG400P
CAG200P
D1
D2
D3
D4
G
Intensity / a.u.
1000
1200
1400
1600
1800
2000
Raman shift / cm-1
b
CAG600A
CAG400A
CAG200A
Intensity / a.u.
1000
1200
1400
1600
1800
2000
Raman shift / cm-1

volumes corresponding to the hysteresis loop, it seems that there also occurs a slight collapse of the mesoporous structure for high R/C values.

The corresponding BET surface areas and additional porosity parameters are summarized in Table 2. For the non-activated aerogels, similar surface area values were obtained regardless the R/C ratio, with values close to 700 $m^2 g^{-1}$. This is in good agreement with the fact that their isotherms overlap at relative pressures below 0.2-0.3 and the micropore volumes calculated from DR equation for the three aerogels (Table 2). Total pore volumes monotonically increased as the R/C ratio decreased; indicating that low R/C ratio results in a fast polycondensation favoring the formation of micro and mesopores. Contrarily, high R/C values yields large macropores formed by large clusters with a highly cross-linked structure [36]. On the other hand, the activation process induced a notorious increase in the surface area and micropore volume in all the samples, with some differences depending on the R/C ratio of the aerogels. For CAG200A (lowest R/C) the activation does not seem to strongly affect the mesoporosity, since the mesopore volume increased slightly but the hysteresis loop remained unchanged in position and shape. In the case of CAG400A, the development of microporosity upon activation is accompanied with a small increase in the mesopore volume, although the hysteresis loop shifts slightly towards lower relative pressures, indicating the presence of mesopores of smaller sizes. Finally, the activation provoked a clear change in the isotherm shape (type I after activation) for the sample with the highest R/C ratio, indicating either the collapse of the large pores or the formation of larger macropores, which size cannot be determined by N_2 adsorption at -196 ºC. The pore size distribution displayed in Fig. 5 confirmed these observations, and revealed a direct relationship between the average pore size and the R/C ratio. High R/C ratios favor the formation of large pores, whereas a monodispersed pore size distribution in the mesopore range was obtained for R/C of 200, with an average pore size of ca. 14 nm. These results agree with early reports on the porosity of carbon gels prepared with various R/C ratios [37, 38]. Summarizing, we have synthesized a series of carbon aerogels that exhibit a wide variety of porous features within the micro/mesopore range, which will undoubtedly influence upon their capacitive properties for the electro-assisted removal of ions [39].

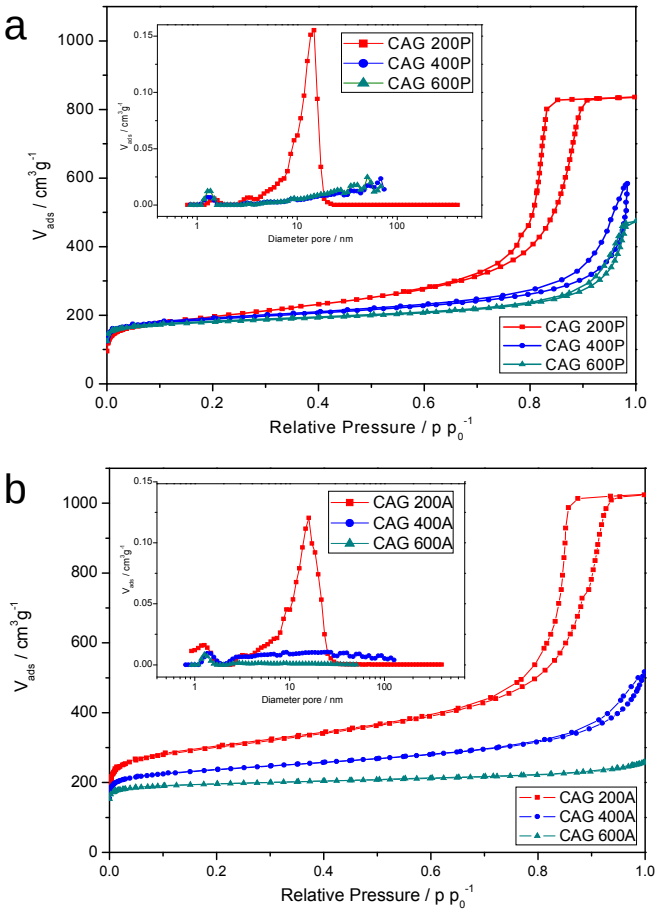
a
CAG 200P
CAG 400P
CAG 600P
Diameter pore / nm
Relative Pressure / p p0-1
b
CAG 200A
CAG 400A
CAG 600A
Diameter pore / nm
Relative Pressure / p p0-1

The capacitance values of the pyrolyzed aerogels in $NaNO_3$ electrolyte varied as follows: CAG400P (46 F g^{-1}) < CAG600P (50 F g^{-1}) << CAG200P (91 F g^{-1}). The activation induced an increase in the capacitance in all samples with the following trend: CAG600A (55 F g^{-1}) < CAG400A (71 F g^{-1}) < CAG200A (125 F g^{-1}).

Interestingly, there is no clear correlation with the surface area or micropore volume of the aerogels (Table 2); instead, the desalting capacity seems to be related to the mesoporosity, pointing out the outstanding role of the accessibility of the ions to the inner porosity of the carbon electrodes (Supplementary info). For the sake of comparison, the capacitance values recorded for the adsorption of 0.1 M solution of NaCl were 79 and 110 F g^{-1} for CAG200P and CAG200A, respectively. Recently, capacitance values of 53.50 and 73.13 F g^{-1} were respectively found for activated carbons [42]. These values are close to those recorded for CAG200A in the same rate (61.5 F g^{-1}) evidencing the validity of our approach. The highest adsorption of NO_3^- anions has also been reported for ordered mesoporous carbon and hierarchical porous carbon and attributed to the balance between hydrated radius and valence providing stronger electrostatic force [43].

Compared to nitrate salt (Fig. 6b), capacitance values were similar in phosphate electrolyte for CAG400P (50 F g^{-1}) and CAG600P (55 F g^{-1}), with a significant decrease in the value obtained for CAG200P (78 F g^{-1}). Previous reports have emphasized that the electrosorption procedure is influenced by both hydrated radius and the valence of the salt ions [44]. Therefore, we attribute this result to the large ionic size of phosphate anions [8]. Thus, it seems that the large pores in CAG400P and CAG600P would favor the adsorption of large phosphate anions, whereas the mesopores in CAG200P would not be large enough to suitably accommodate these ions. This is clearly seen also in the activated series; even though capacitance values of the activated samples are higher than those of the pyrolyzed ones -CAG400A (61 F g^{-1}), CAG600A (56 F g^{-1}) and CAG200A (82 F g^{-1})-, the effect was less pronounced than in the case of nitrates. These results point out to the lowest R/C ratio and activation as beneficial factors to provide enhanced capacitive performance for nitrate and phosphate adsorption. The high capacitance values recorded for activated samples can be correlated to the inherent decrease of density when amorphous carbon occupying inner pores is released by thermal activation. This fact is also supported by the fact that the range of size of mesopores found in CAG200P is not wide enough to accommodate the large phosphate ions, inferring

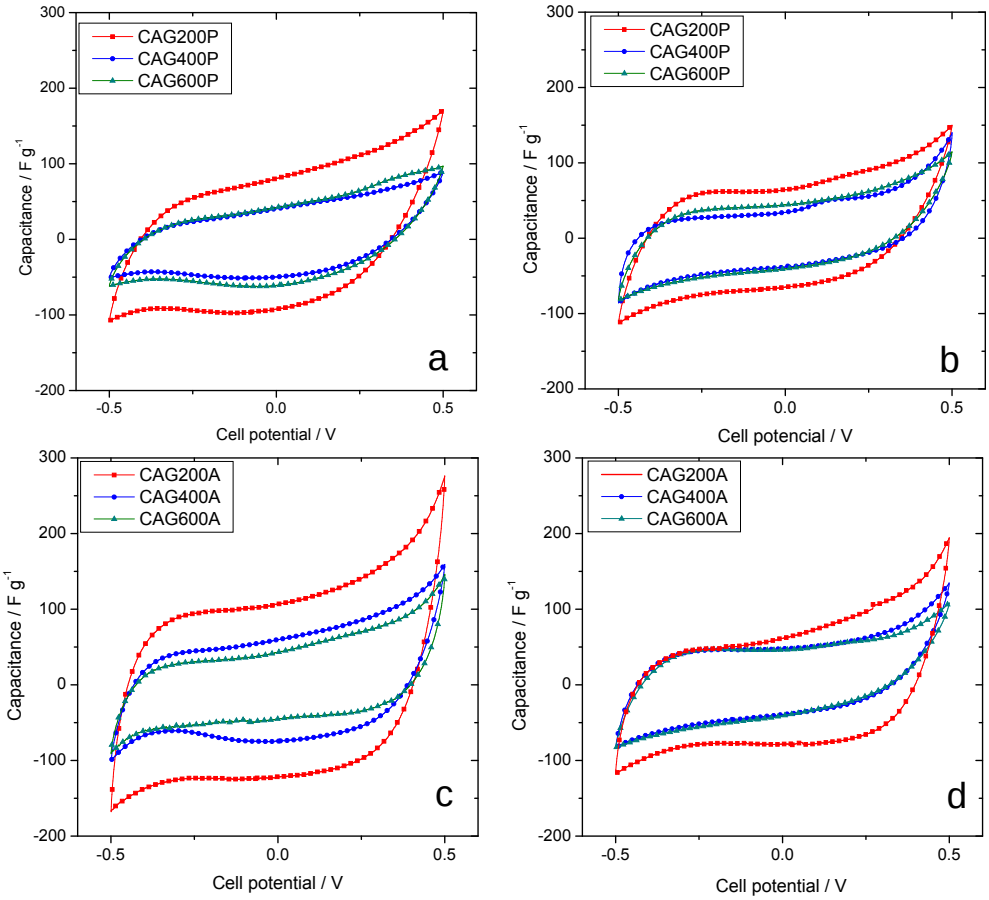
CAG200P
CAG400P
CAG600P
Capacitance / F g-1
Cell potential / V
a
CAG200P
CAG400P
CAG600P
Capacitance / F g-1
Cell potencial / V
b
CAG200A
CAG400A
CAG600A
Capacitance / F g-1
Cell potential / V
c
CAG200A
CAG400A
CAG600A
Capacitance / F g-1
Cell potential / V
d

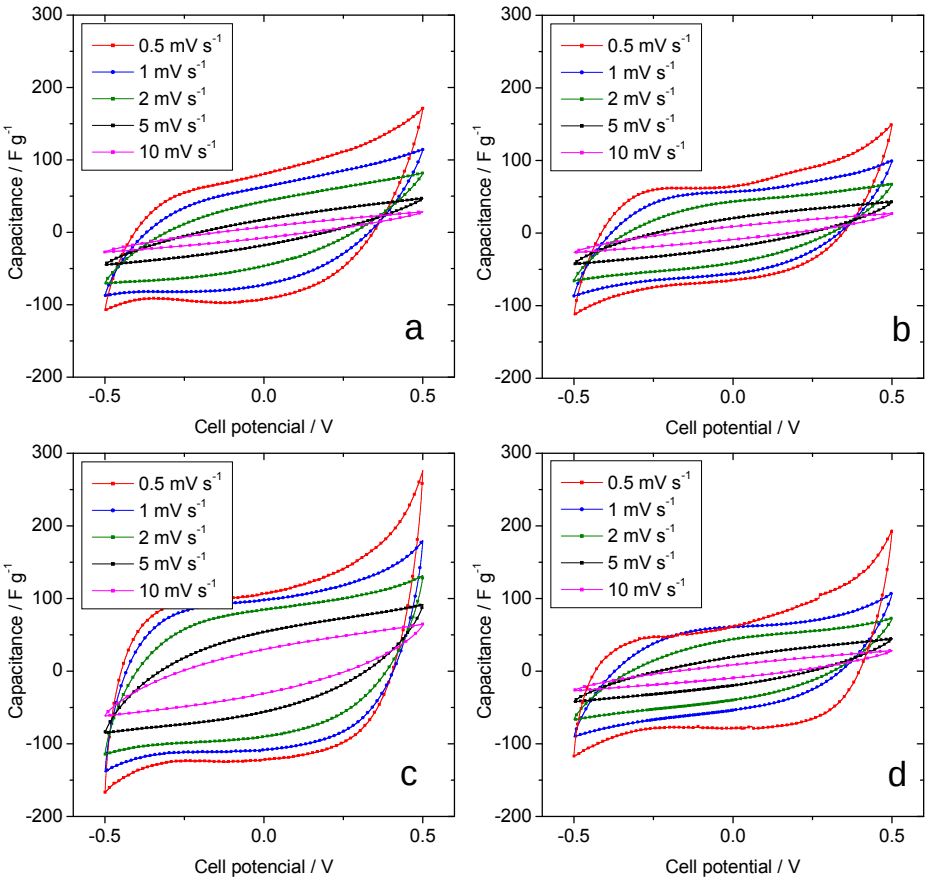

$$\tau \quad R_e C_S$$

$$\left(\quad \frac{Q}{Q_0} \right) \quad \frac{t}{R_e C_S}$$

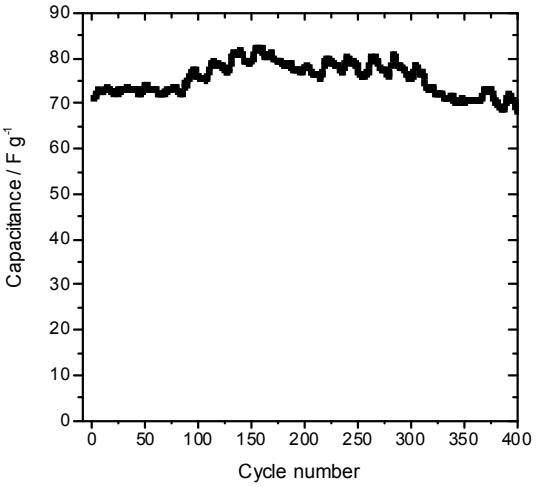
Capacitance / F g-1
Cycle number
0
10
20
30
40
50
60
70
80
90
0
50
100
150
200
250
300
350
400

resistance to ion migration through the pore structure is determined from the real impedance of the semicircle located at intermediate frequencies (R_{pol}) [45, 46]. The resistance values calculated for the aerogel electrodes (Table 4) showed a similar sequence to that observed for the time constants calculated from the chronocoulometric curves.

As seen, R_{pol} values corresponding to the electrosorption of sodium nitrate decreased with the activation of the samples, suggesting that the pore widening occurring during the activation reaction [4] facilitates the accessibility and thus the migration of ions.

Table 3 Time constants (τ) calculated from the chronocoulometric curves

Sodium nitrate	CAG 200	CAG 400	CAG 600
	τ / s	τ / s	τ / s
Pyrolyzed	61.8	66.5	64.5
Activated	54.5	57.4	61.9

Sodium phosphate	CAG 200	CAG 400	CAG 600
	τ / s	τ / s	τ / s
Pyrolyzed	63.9	67.0	64.2
Activated	63.7	62.6	61.4

Resistance values were higher for the adsorption of phosphates, as expected given the larger size of these ions. Interestingly, a high R_{pol} value was obtained for the adsorption of phosphates on activated CAG200A. Similar results were recently observed for a related aerogel prepared at R/C=100, being attributed to the higher increase of micropore volume built after the activation reaction. It exerts a sieve effect that hinders the migration of large phosphate anions [47]. This result is in good agreement with the slow relaxation observed for this aerogel (Table 3).

Comparatively, the electrochemical characterization of the series of carbon aerogel electrodes indicates the better performance of CAG200A over the rest of t he materials. It seems that the existence of a well-developed unimodal

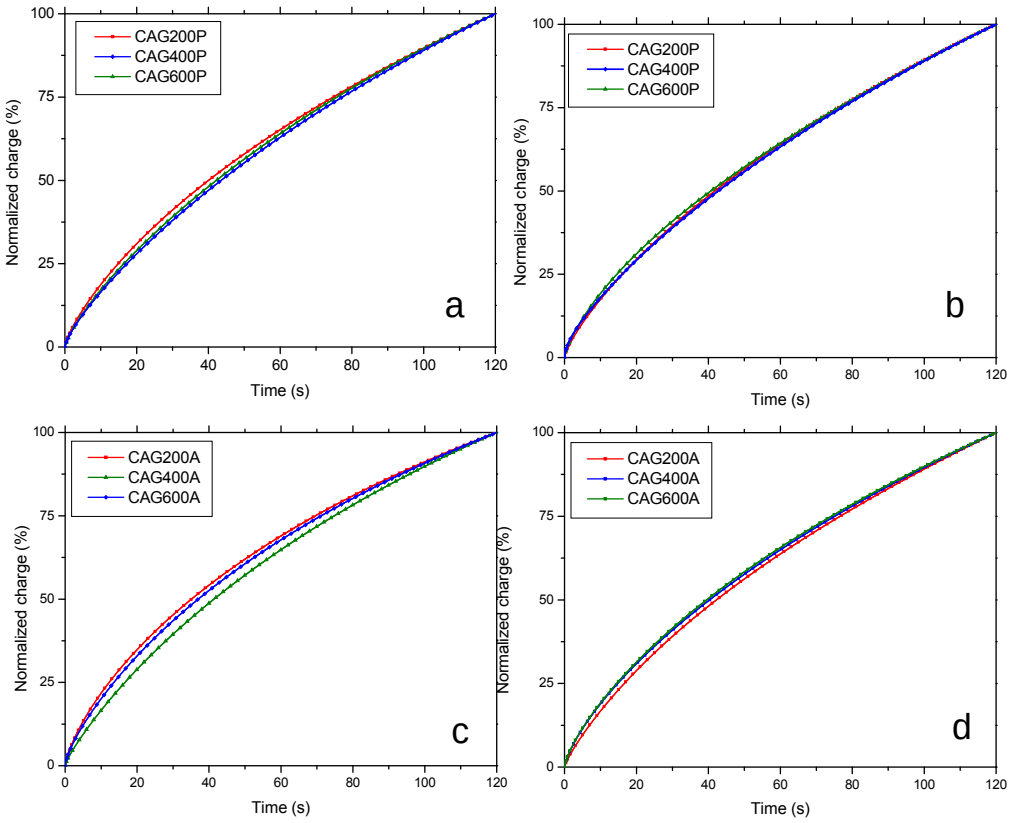
CAG200P
CAG400P
CAG600P
Normalized charge (%)
Time (s)
a
b
CAG200A
CAG400A
CAG600A
c
d

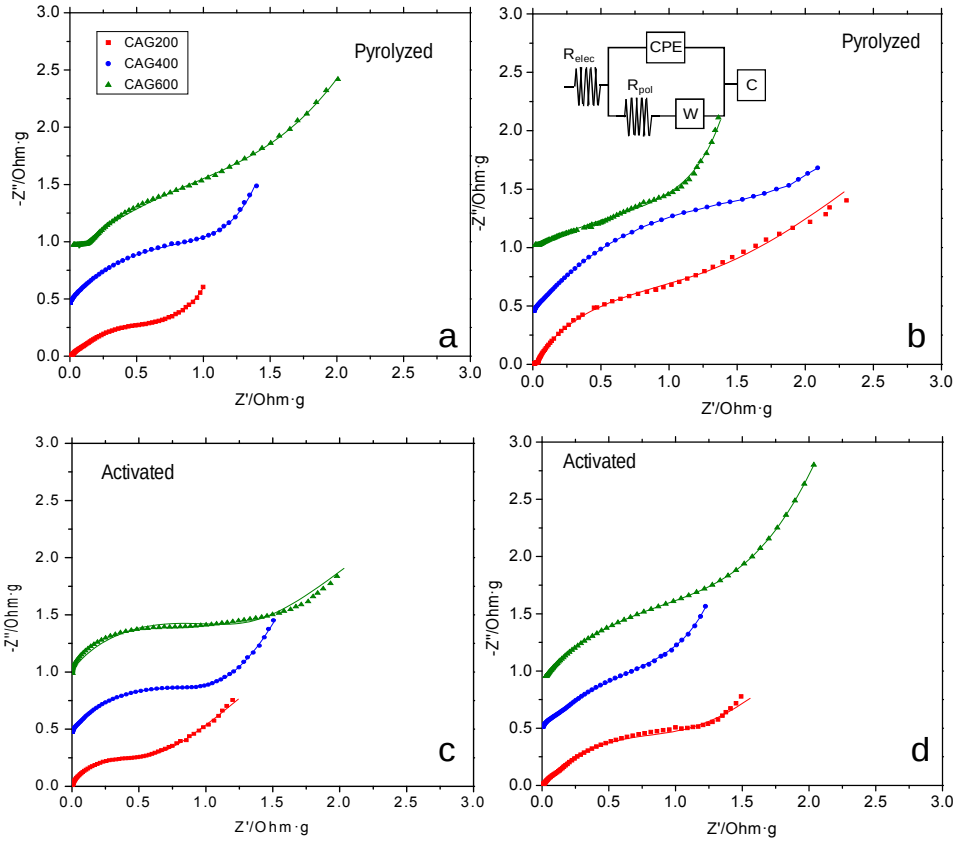

Sodium nitrate	CAG 200	CAG 400	CAG 600
	R_{pol} / Ω×g	R_{pol} / Ω×g	R_{pol} / Ω×g
Pyrolyzed	0.95	1.35	2.34
Activated	0.60	0.84	1.44

Sodium phosphate	CAG 200	CAG 400	CAG 600
	R_{pol} / Ω×g	R_{pol} / Ω×g	R_{pol} / Ω×g
Pyrolyzed	1.36	2.68	2.54
Activated	1.67	1.66	1.78

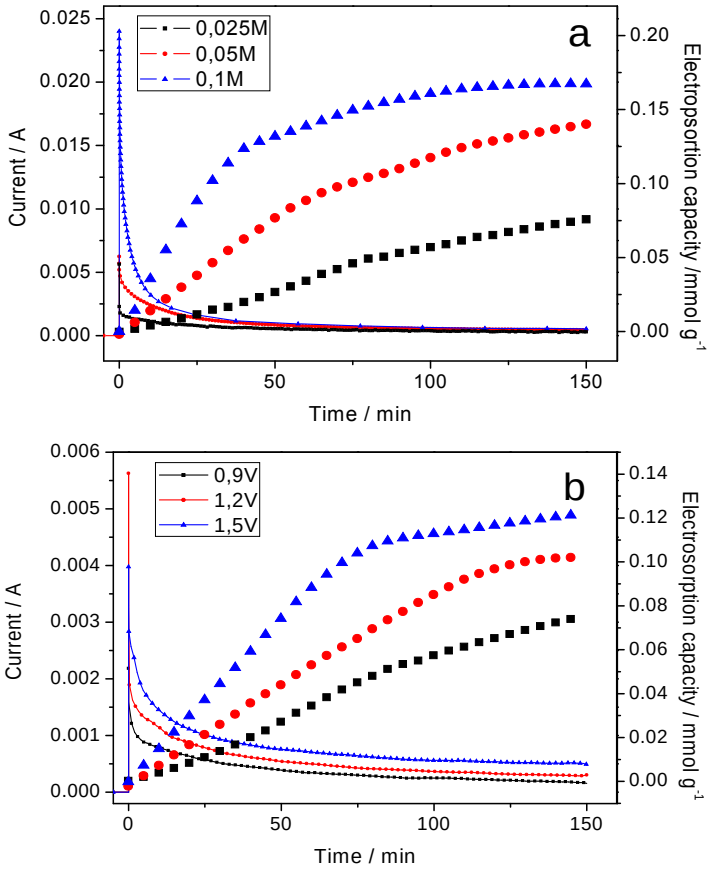
a
0,025M
0,05M
0,1M
Current / A
Electropsortion capacity /mmol g-1
Time / min
b
0,9V
1,2V
1,5V
Current / A
Electrosorption capacity / mmol g-1
Time / min

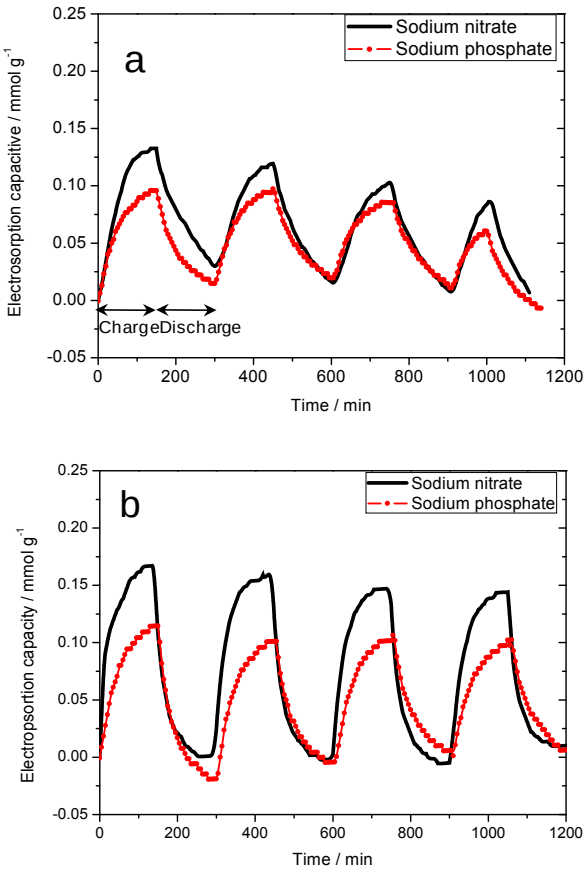
a
Sodium nitrate
Sodium phosphate
Electrosorption capacitive / mmol g-1
Charge
Discharge
Time / min
b
Sodium nitrate
Sodium phosphate
Electropsortion capacity / mmol g-1
Time / min

Three carbon aerogels with varied R/C ratio were synthesized and subsequently activated under CO_2 in order to prepare electrode materials with different micro/mesopore structure. XRD patterns and Raman spectra showed that despite the low structural ordering of the aerogels, there is an important contribution of domains of a graphitic structure, very unusual for carbon aerogels nanoporous carbons synthesized at low temperatures. Raman spectroscopy also showed a correlation between the structural ordering and the R/C ratio, with high resorcinol contents favoring the formation of more ordered carbon structures.

All the synthesized carbon aerogels presented a well developed micro/mesoporous structure. Whereas all the pyrolyzed materials presented similar microporosity, regardless the R/C ratio, the formation of mesopores with a narrow size distribution is connected to low R/C values. In contrast, high R/C values yields large macropores

resulting from large clusters with a highly cross-linked structure. Activation under CO_2 provoked an increase in the micropore volumes, accompanied by the enlargement of the mesopores, this effect being more significant for samples with R/C 400 and 600.

Cyclic voltammograms in various electrolytes showed large capacitance values for sample CAG200A, likely attributed to its enhanced surface area and pore volume, as well as an accessible pore structure that enables fast charge kinetics and ion migration for the electrosorption of both salts. The desalination experiments performed in both ionic solutions using pyrolyzed and activated CAG200A aerogel electrodes revealed an efficient electrosorption of ionic species on consecutive charge/discharge cycles, confirming the stability of the aerogel electrodes at the high applied potentials in both electrolytes.

2.2.5. References

[1] Porada S, Zhao R, van der Wal A, Presser V, Biesheuvel PM (2013) Review on the Science and Technology of Water Desalination by Capacitive Deionization. Prog Mater Sci 58:1388-1442.

[2] Candelaria SL, Shao Y, Zhou W, Li X, Xiao J, Zhang JG, Wang Y, Liu J, Li J, Cao G (2012) Nanostructured carbon for energy storage and conversion. Nano Energy 1:195-220.

[3] Oren Y (2008) Review on the Science and Technology of Water Desalination by Capacitive Deionization. Desalination 228:10-29.
[4] Marsh H, Rodríguez-Reinoso F (2006) Activated Carbon, Elsevier, Amsterdam.
[5] Anderson MA, Cudero AL, Palma J (2010) Capacitive deionization as an electrochemical means of saving energy and delivering clean water. Comparison to present desalination practices: Will it compete? Electrochim Acta 55:3845-3856.
[6] Dehkhoda AM, Ellis N, Gyenge E (2014) Electrosorption on activated biochar: effect of thermo-chemical activation treatment on the electric double layer capacitance. J Appl Electrochem 44:141–157.
[7] Peng Z, Zhang D, Shi L, Yan T, Yuan S, Li H, Gao R, Fang J (2011) Comparative Electroadsorption Study of Mesoporous Carbon Electrodes with Various Pore Structures. J Phys Chem C 115:17068-17076.
[8] Ania CO, Pernak J, Stefaniak F, Raymundo-Pinero E, Beguin F (2009) Polarization-induced distortion of ions in the pores of carbon electrodes for electrochemical capacitors. Carbon 47:3158-3166.
[9] Chmiola J, Largeot C, Taberna PL, Simon P, Gogotsi Y (2008) Desolvation of ions in subnanometer pores and its effect on capacitance and double layer theory. Angew Chem 47:1-5.
[10] Zhang D, Yan T, Shi L, Peng Z, Wen X, Zhang J (2012) Enhanced capacitive deionization performance of graphene/carbon nanotube composites J Mater Chem 22:14696-14704.
[11] Liang P, Yuan L, Yang X, Zhou S, Huang X (2013) Coupling ion-exchangers with inexpensive activated carbon fiber electrodes to enhance the performance of capacitive deionization cells for domestic wastewater desalination. Water Res 47: 2523-2530.
[12] Seo SJ, Jeon H, Lee JK, Kim GY, Park D, Nojima H, Lee J, Moon SH (2010) Investigation on removal of hardness ions by capacitive deionization (CDI) for water softening applications. Water Res 44:2267-2275.
[13] Porada S, Weinstein L, Dash R, van der Wal A, Bryjak M, Gogotsi Y, Biesheuvel PM (2012) Water Desalination Using Capacitive Deionization with Microporous Carbon Electrodes. ACS Appl Mater Interfaces 4:1194-1199.
[14] Punckt C, Pope MA, Liu J, Lin Y, Aksay I.A. (2010) Electrochemical Performance of Graphene as Effected by Electrode Porosity and Graphene Functionalization Electroanalysis. Electroanal 22:2834-2841.

[15] Ban A, Schafer A, Wendt H (1998) Fundamentals of electrosorption on activated carbon for wastewater treatment of industrial effluents. J Appl Electrochem 157:602-615.
[16] Tsouris C, Mayes R, Kiggans J, Sharma K, Yiacoumi S, DePaoli D, Dai S (2011) **Mesoporous carbon for capacitive deionization of saline water.** Environ Sci Technol, 45:10243-10249.
[17] Xu LY, Shi ZG, Feng YQ (2008) Preparation of a carbon monolith with bimodal perfusion pores. Microporous Mesoporous Mat 115:618-623.
[18] Wen X, Zhang D, Yan T, Wang H, Zhang J, Shi L (2013) Three-dimensional graphene-based hierarchically porous carbon composites prepared by a dual-template strategy for capacitive deionization. J Mater Chem A, 1:12334-12344.
[19] Wang H, Shi L, Yan T, Zhang J, Zhong Q, Zhang D (2014) Design of graphene-coated hollow mesoporous carbon spheres as high performance electrodes for capacitive deionization. J Mater Chem A, 2:4739-4750.
[20] Pekala RW, Farmer JC, Alviso CT, Tran TD, Mayer ST, Miller JM, Dunn B (1998) Carbon Aerogels for Electrochemical Applications J. Non-Cryst Solids 225:74-80.
[21] Gross J, Scherer GW, Alviso CT, Pekala RW (1997) Elastic properties of crosslinked Resorcinol-Formaldehyde gels and aerogels J. Non-Cryst Solids 211:132-142.
[22] Hadas A, Sagiv B, Haruvy N (1999) Agricultural practices, soil fertility management modes and resultant nitrogen leaching rates under semi-arid conditions. *Agricult.* Water Manag 42:81-95.
[23] Broséus R, Cigana J, Barbeau B, Daines-Martinez C, Suty H (2009) Removal of total dissolved solids, nitrates and ammonium ions from drinking water using charge-barrier capacitive deionisation. Desalination 249:217–223.
[24] Pekala RW (1989) Organic Aerogels from the Polycondensation of Resorcinol with Formaldehyde. J Mater Sci 24:3221-3227.
[25] Haro M, Rasines G, Macías C, Ania CO (2011) Stability of a carbon gel electrode when used for the electro-assisted removal of ions from brackish water. Carbon 49:3723-3730.
[26] Rouquerol F, Rouquerol J Sing K (1999) Adsorption by Powders and Porous Solids, Academic Press, London.
[27] Tuinstra F, Koenig JL (1970) Raman spectrum of graphite J Chem Phys 53:1126-1130.

[28] Cuesta A, Dhamelincourt P, Laureyns J, Martinez-Alonso A, Tascon JMD (1994) Raman microprobe studies on carbon materials. Carbon 32:1523-1532.

[29] Jawhari T, Roid A, Casado J (1995) Raman spectroscopic characterization of some commercially available carbon black materials. Carbon 33:1561-1565.

[30] Sze SK, Siddique N, Sloan JJ, Escribano R, (2001) Raman spectroscopic characterisation of carbonaceous aerosol. Atmos Environ 35:561-568.

[31] Dresselhaus MS, Dresselhaus G (1982) Light-scattering in graphite-intercalation compounds. Springer-Verlag, Berlin.

[32] Rouzaud JN, Oberlin A, Beny-Bassez C (1983) Carbon-films-structure and microtexture (optical and electron-microscopy, raman-spectroscopy). Thin Sol Films 105:75-96.

[33] Dippel B, Jander H, Heintzenberg J (1999) NIR FT Raman spectroscopic study of flame soot, Phys Chem Chem Phys 1:4707-4712.

[34] Biniak S, Szymanski G, Siedlewski J, Swiatkowski A (1997) The characterization of activated carbons with oxygen and. nitrogen surface groups. Carbon 35:1799-1810.

[35] Oh HJ, Lee JH, Ahn H-J, Jeong Y, Kim YJ, Chi CS (2006) Nanoporous activated carbon cloth for capacitive deionization of aqueous solution. Thin Solid Films 515:220-225.

[36] Tamon H, Ishizaka H, Araki T, Okazaki M (1998) Control of mesoporous structure of organic and carbon aerogels. Carbon 36:1257-1262.

[37] Job N, Thery A, Pirard R, Marien J, Kocon L, Rouzaud JN, Beguin F, Pirard JP (2005) Carbon aerogels, cryogels and xerogels: influence of the drying method on the textural properties of porous carbon materials Carbon 43:2481-2494

[38] Tamon H, Ishizaka H, Mikami M, Okazaki M (1997) Porous structure of organic and carbon aerogels synthesized by sol-gel polycondensation of resorcinol with formaldehyde. Carbon, 35:791-796.

[39] Peng Z, Zhang D, Yana T, Zhang J, Shi L (2013) Three-dimensional micro/mesoporous carbon composites with carbon nanotube networks for capacitive deionization. Appl Surf Sci 282:965-973.

[40] Hsieh CT, Teng H (2002) Influence of oxygen treatment on electric double-layer capacitance of activated carbon fabrics. Carbon 40:667-674.

[41] Pröbstle H, Wiener J, Fricke (2003) M Carbon aerogels for electrochemical double layer capacitors. J Porous Mater 10:213-222.

[42] Huang W, Zhang Y, Bao S, Cruz R, Song S (2014) Desalination by capacitive deionization process using nitric acid-modified activated carbon as the electrodes. Desalination 340:67-72.
[43] Wen X, Zhang D, Shi L, Yan T, Wang H, Zhang J (2012) Three-dimensional hierarchical porous carbon with a bimodal pore arrangement for capacitive deionization. J Mater Chem 22:23835-23844.
[44] Peng Z, Zhang D, Shi L, Yan T (2012) High performance ordered mesoporous carbon/carbon nanotube composite electrodes for capacitive deionization. J Mater Chem 22:6603-6612.
[45] Noked M, Avraham E, Soffer A, Aurbach D (2009) The rate-determining step of electroadsorption processes into nanoporous carbon electrodes related to water desalination. J Phys Chem C 113:21319-21327.
[46] Miller JM, Dunn B (1999) Morphology and electrochemistry of ruthenium/carbon aerogel nanostructures. Langmuir 15:799-806.
[47] Zafra MC, Lavela P, Macías C, Rasines G, Tirado JL (2013) Electrosorption of environmental concerning anions on a highly porous carbon aerogel. J Electroanal Chem 708:80–86.
[48] Yang J, Zou L (2014) Using recyclable calcium citrate templates to prepare mesoporous carbons as electrodes for capacitive deionization Microporous Mesoporous Mater 183:91-98.
[49] Afkhami A (2003) Adsorption and electrosorption of nitrate and nitrite on high-area carbon cloth: an approach to purification of water and waste-water samples. Carbon 41:1309-1328.

Capítulo 3

Empleo de compuestos funcionales híbridos para desionización de aguas salinas


Carbon

structure (morphology, texture, composition) of the obtained materials and consequently on their performance [4-10]. A detailed review on this matter has been published by Ritter and co-workers in 2003 [4].

Most of these works have reported the unique physical, chemical and electrochemical properties of these lightweight and high performance engineering materials, showing potential applications in sectors such as: adsorbents for gas separation [11], catalyst supports [12,13], energy storage devices[14-17], capacitive deionization for water purification [18-20], etc.

Carbon gels are mostly synthesized following the catalyzed polycondensation of resorcinol-formaldehyde mixtures in water, although some other alternative routes have been described using harmless and naturally available compounds as precursors [21, 22].

Despite carbon gels typically exhibit electrical conductivities higher than other types of aerogels (which are generally insulating materials) and most porous carbons [23, 24] (excluding carbon nanotubes, graphenes or graphitic carbons), the conductivity of resorcinol-formaldehyde derived carbon gels is still rather limited. Thus, for most electrochemical applications, the use of carbon back as conductive additive (CCA) is still recommended (or needed) in the manufacturing of the electrodes so as to limit the resistance of the system due to the conductivity limitation of the electrode materials [23-26].

The objective of this work was to synthesize carbon aerogels with controlled porosity and high electrical conductivity and to explore their potential use in electrochemical applications. The sol-gel polymerization of the gel precursors was carried out in the presence of a carbon conductive additive (i.e., carbon black); this allowed the fabrication of carbon gels with extremely high pore volumes within the micro/mesopore range, largely exceeding the porous features commonly reported for carbon gels. Although the benefits of the use of conductive carbon blacks in the manufacturing of carbon electrodes have been reported in the literature [25, 26], herein obtained results have shown that incorporating the CCA before the sol-gel reaction promotes outstanding changes in the texture of the final carbon/carbon nanocomposites, beyond the expected improved electrical conductivity.

3.1.2. Experimental

3.1.2.1. Materials Synthesis

The carbon gels were synthesized by the sol gel polymerization of resorcinol (R) and formaldehyde (F) in water (W), using sodium carbonate (C) as catalyst, carbon black (CB, Superior Graphite Co.) as conductive additive, and following an experimental procedure inspired from the method described by Pekala and co-workers [10]. Details of the conventional synthesis have been reported elsewhere [27]. Briefly, the precursors were mixed in sealed glass moulds under magnetic stirring and allowed to undergo gelation and aging in an oven at 40 º C for 24 h and 70 ºC for 120 h. Subsequently a controlled water–acetone exchange was carried out, and then the pieces were dried under CO_2 supercritical conditions. Finally, the aerogels were pyrolyzed under nitrogen atmosphere at 800 ºC (unless otherwise indicated). The resorcinol/catalyst (R/C) ratio was varied (i.e., 25, 50, 100 and 200) in order to produce samples with different porous texture, while the molar ratio R/F was fixed at 0.5, the R/W 0.06 and the CB/(R+F) was 5 and 10 wt.% (values were taken as representative of commonly used percolator mass ratio in electrochemical applications). The nomenclature of the samples was Gx-CBy, being *x* the corresponding R/C value (i.e., G25-CB) and *y* the CB/(R+F) ratio (i.e., G25-CB10). To evaluate the thermal stabilization of the organic gels upon pyrolysis, selected gel/CCA composites were also treated at 500 and 1000 ºC, obtaining series Gx-CByT, where T stands for the pyrolysis temperature. For the sake of comparison, a second series of carbon gels was prepared by the same synthetic route without the incorporation of the carbon black (series Gx).

3.1.2.2. Electrochemical characteristics

Electrodes were prepared by mixing the carbon material (90 wt.%) with a binder (10 wt.%, polyvinylidene fluoride). These mixtures were pressed into 10 -15 mg pellets. Three-electrode cells were assembled on a Teflon Swagelok system using a carbon pellet as working electrode, a high surface area activated carbon pellet (Maxsorb, S_{BET} = 2600 $m^2\ g^{-1}$) as counter electrode and saturated mercury/mercurous sulfate reference electrode. All potential values are expressed vs. the normal hydrogen electrode (NHE). Aqueous 0.5 mol L^{-1} Na_2SO_4 was used as electrolyte. The carbon pellets were dried at 60 ºC under vacuum overnight and vacuum-impregnated before assembling the cells. Several electrochemical measurements were performed on each carbon aerogel electrode, using a

computer controlled potentiostat/galvanostat (Biologic VMP-3). Aging experiments were conducted on symmetric cells –capacitors- in aqueous electrolyte- Initially the cells were galvanostatically charged/discharged between 0-1.4 V and at a specific current density of 500 mA g^{-1} over six cycles for evaluating the specific cell capacitance. Afterwards, the cells were charged up to 1.4 V followed by holding the voltage for 12 h. The cell was then cycled again and the procedure was repeated until an overall holding period of 500 h was reached. The resistivity measurements of powdered and pressed carbons were carried out at atmospheric pressure, using a home-made apparatus. Measurements were based on the van der Pauw technique [28], which involves the application of a bias current of 50 mA to the carbon pellets and measuring the voltage drop, using a four probe configuration.

3.1.2.3. Nanotextural and Chemical Characterization

The nanotexture of the prepared gels was characterized by measuring the N_2 adsorption isotherms at -196 ºC (ASAP 2010, Micromeritics). Before the experiments, the samples were outgassed under vacuum (ca. 10^{-3} torr) at 120 °C overnight. The isotherms were used to calculate the specific surface area, S_{BET}, total pore volume, V_T, and pore volumes using the DR formulism and non-local density functional theory (DFT). SEM/EDX analyses were performed with a FE-SEM apparatus (QuantaSEM, FEI). Elemental analysis was carried out in LECO CHNS-932 and LECO VTF-900 automatic analyzers.

3.1.3. Results and discussion

3.1.3.1. Synthesis of the aerogel/CCA materials

The sol-gel procedure used in this work was a simple modification of the conventional procedure reported by Pekala and co-workers [10], consisting on carrying out the sol-gel polymerization of the precursors (resorcinol and formaldehyde) in the presence of a carbon conductive additive on the mixture. As conductive additive, a carbon black (Superior Graphite, Co.) commonly used in electrochemical applications was selected; this material is characterized by low ash, moisture, sulfur and volatiles contents, as well as a high electrical conductivity provided by its ordered structure (see TEM images in Fig. 1). According to literature, the polymerization mechanism of resorcinol-

formaldehyde (RF) gels is typically controlled by the addition reaction between the precursors to form hydroxylmethyl derivatives, followed by condensation to form methylene ether bridged compounds, and cluster growth [4-7]. The initial cluster formation is followed by the spinodal decomposition of the growing clusters that promptly become unstable and thus gelation occurs. For our systems, gelation occurred regardless the amount of CCA added (i.e. 5 or 10 wt.%), indicating that the cross-linking of the clusters (that leads to the stiffing of the gel) progressed adequately upon incorporation of the CCA. It should be mentioned that the loading of the CCA was selected considering commonly percolator mass ratio reported in the literature in electrochemical applications [23-26]. Above 10 wt.%, the dispersion of the carbon black in the reactants mixture was not uniform, which impeded the homogeneous sol-gel reaction. At lower loadings (ca. 0.5-2wt.%) the effect on the electrical conductivity of the aerogel electrodes was almost negligible, thus these samples were no longer investigated.

The lack of swelling during the solvent exchange stage also indicated that cross-linking reactions were sufficiently completed in the presence of the CCA particles. The appearance of the aerogels changed with the synthesis variables; before pyrolysis, conventional RF aerogels were opaque and dark for low R/C ratios (i.e. series 25 and 50) turning translucent light red for the higher R/C ratio (Figure S1. in Supplementary File). After pyrolysis, all the materials become opaque and dark, regardless the synthesis conditions. On the other hand, all the aerogels prepared in the presence of the carbon black additive were black and opaque regardless the R/C ratio and before the pyrolysis treatment.

Scanning microscopy images also showed that the incorporation of the carbon black did not modify the gels structure compared to conventional synthesis (Fig. 2). Moreover, TEM images in Fig. 1 showed that the gel/CCA composite exhibit domains of graphitic order provided by the carbon black arranged within the amorphous carbon matrix characteristic of the materials prepared by the conventional synthesis.

Thermal annealing of the dried aerogels under inert atmosphere at 500, 800 and 1000 ºC preserved the monolithic shape of the gels, although some cracks appeared at the surface (Figure S1). This was particularly evident for the samples prepared from the highest R/C ratio, suggesting a rather uniform shrinkage for all the samples. After pyrolysis, all the gels were bright black and showed rather good mechanical strength. Moreover, the CCA

appeared to enhance the mechanical properties of the materials prepared from R/C above 100, otherwise brittle and difficult to handle without damage.

The evolution of the porous features of the synthesized materials was very dependent on the incorporation of the CCA before the sol-gel reaction. Fig. 3 and Table 1 show the main textural parameters determined by nitrogen adsorption at -196ºC.

For the carbon gels synthesized following the conventional procedure, the expected influence of the R/C ratio in the porous network connectivity and the textural parameters (micro/mesopore balance, surface area and average pore width) was observed [4-9] Briefly, a gradual shift from type I (predominant microporosity + narrow mesopores) towards type IV adsorption isotherms (low micro/mesopore ratio) was observed with the R/C ratio, accompanied by an increase in the specific surface area and pore volumes. This indicates that the development of a mesoporous structure is favored when the reactivity of the carbon precursors is lowered (reducing the amount of catalyst). Prominent hysteresis loops appearing at high relative pressures and a non-negligible microporosity contribution were also observed, which according to literature are characteristics of the so-called colloidal gels prepared using high R/C ratio [5,6].

The incorporation of the CCA allowed the preparation of ultrahigh mesoporous carbon gels as seen by the nitrogen adsorption isotherms (Fig. 3). All the samples exhibited type IV isotherms regardless the R/C ratio, along with large total pore and mesopore volumes (Table 1). It is interesting to remark that the nitrogen adsorption isotherms of the Gx-CBy composites displayed a singular shape characterized by a curvature both in the adsorption and desorption branches (marked by arrows in Fig. 3 and 4). The onset of the curvature moved upwards to higher pressures with the R/C ratio, ranging from 0.75 for G25-CB10 to 0.88 for G200-CB10.

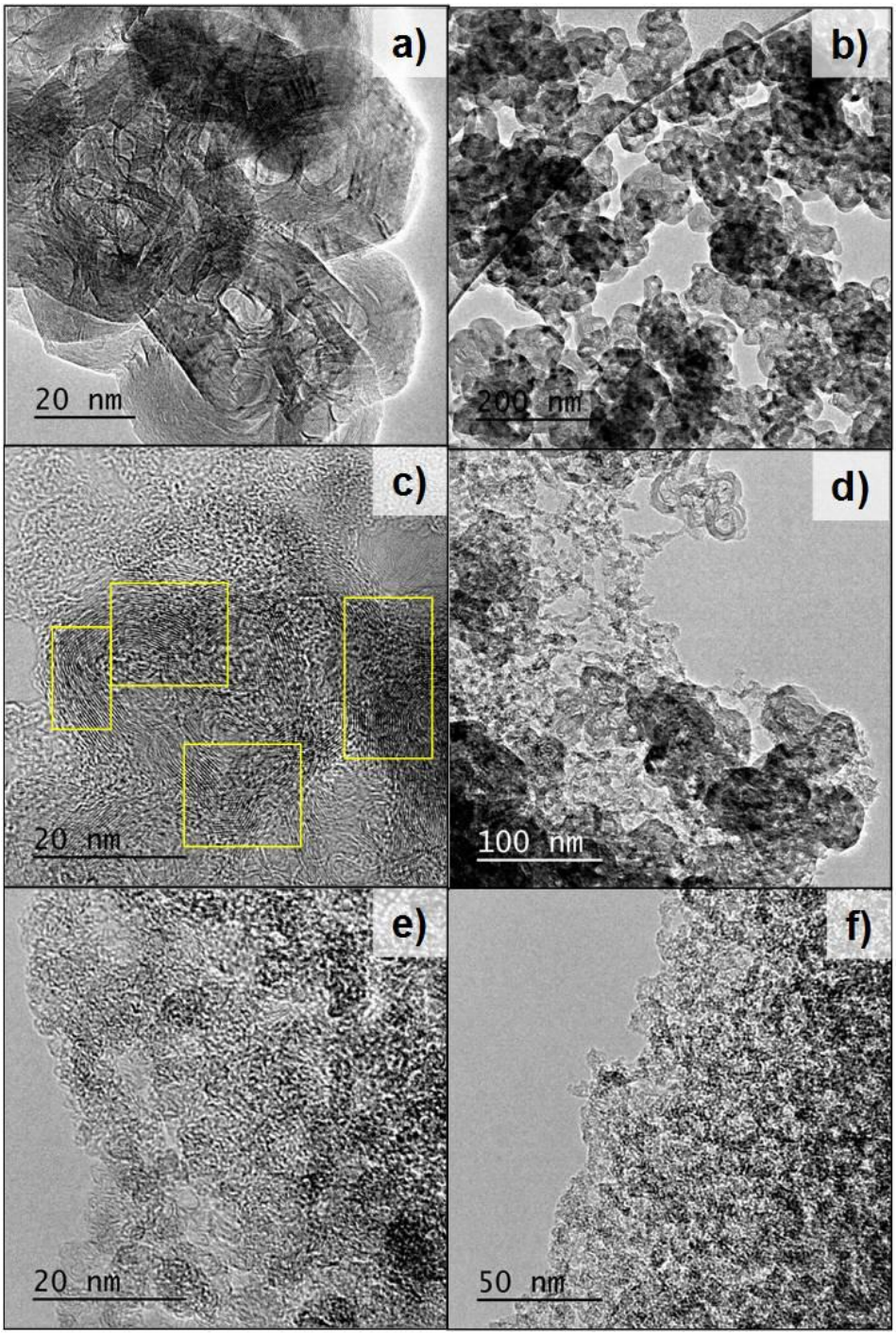
a)
20 nm
b)
200 nm
c)
20 nm
d)
100 nm
e)
20 nm
f)
50 nm

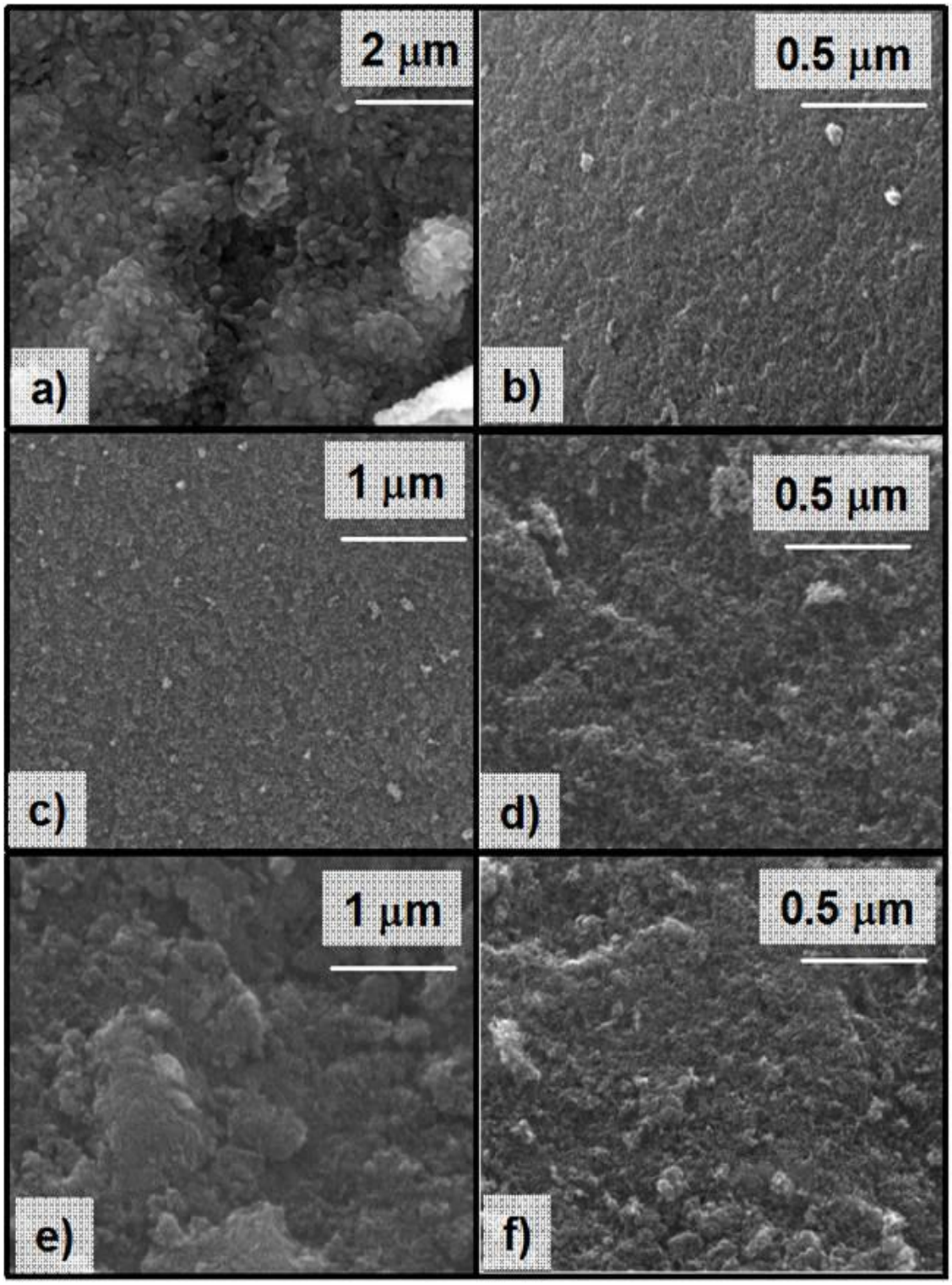
2 μm
a)
0.5 μm
b)
1 μm
c)
0.5 μm
d)
1 μm
e)
0.5 μm
f)

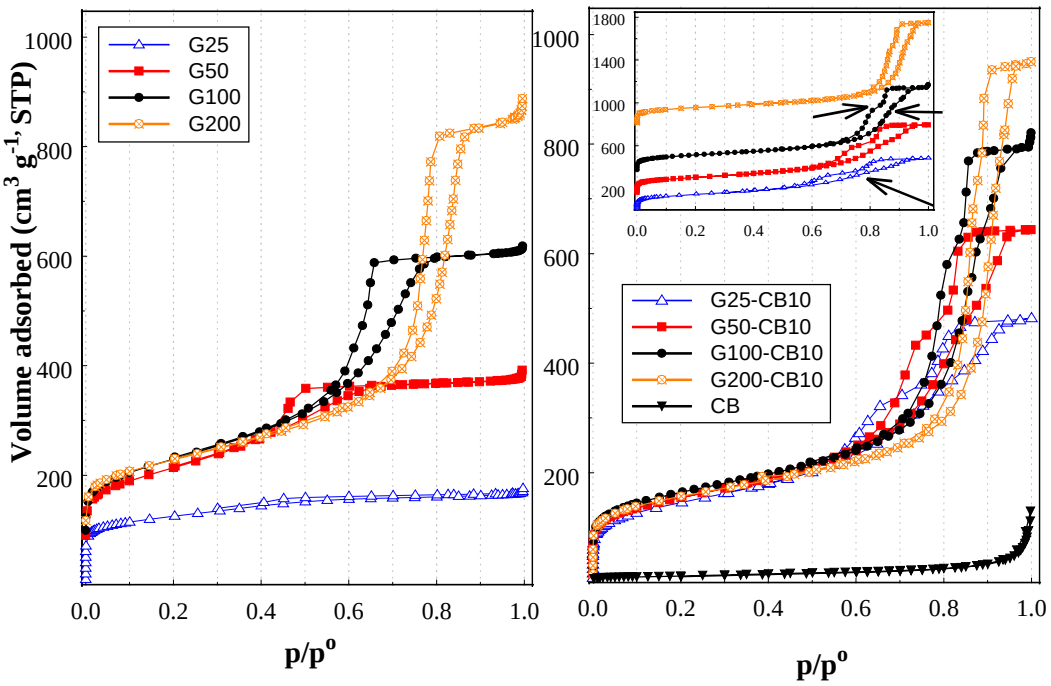
G25
G50
G100
G200
Volume adsorbed (cm3 g-1, STP)
p/po
G25-CB10
G50-CB10
G100-CB10
G200-CB10
CB
p/po

a more homogenous distribution of pore sizes compared to G25-CB10 and G50-CB10. The curvature of the adsorption/desorption branches and the position of the hysteresis loops suggest that the pore network of these materials is composed of cylindrical mesopores with uniform bodies, connected by narrower cylindrical necks of uniform widths.

Table 1. Porosity parameters obtained from the N_2 adsorption isotherms at -196 ºC for the gels prepared with and without the incorporation of the carbon conductive additive.

	S_{BET} [m^2 g^{-1}]	$V_{TOTAL\ PORES}$ [cm^3 g^{-1}]	Wo (DR) [cm^3 g^{-1}]	V_{MESO} [cm^3 g^{-1}]	Mean mesopore Size [nm]
Carbon Black	41	0.13	0.02	0.06	--
G25	455	0.26	0.17	0.09	4
G50	760	0.59	0.35	0.24	5
G100	820	0.95	0.29	0.66	8
G200	830	1.33	0.31	1.02	12
G25-CB10	535	0.74	0.18	0.56	7-13
G50-CB10	542	1.09	0.20	0.89	9-15
G100-CB10	592	1.22	0.20	1.02	13-17
G200-CB10	559	1.46	0.20	1.26	17-22
G50-CB5	633	0.88	0.21	0.67	5-8
G50-CB10-T500	569	1.02	0.21	0.81	9-15
G50-CB10-T1000	498	1.10	0.20	0.90	12-18

As for the textural parameters, pore volumes of the gel/CCA composites largely exceeded the values obtained with the conventional synthetic route (Table 1). Specific surface areas did not follow the same trend, with smaller values for the materials prepared in the presence of the CCA. Moreover, whereas surface areas discretely increase with the R/C ratio for the control Gx series (only G200 break this trend), values varied within a short range for the materials prepared in the presence of the CCA.

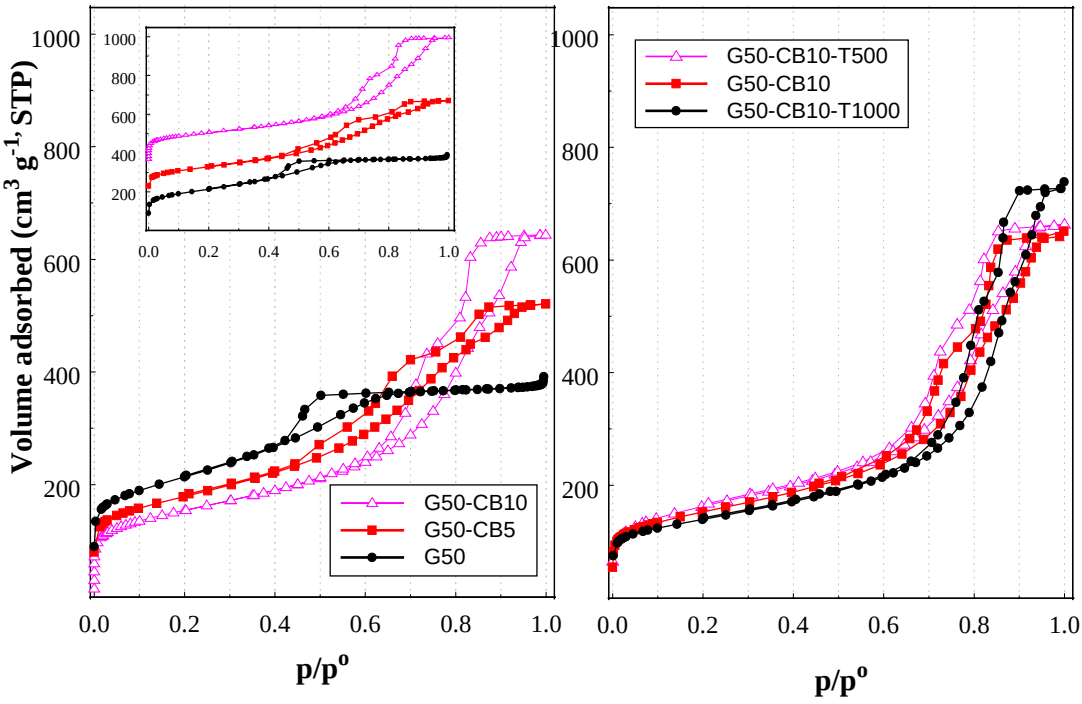
Volume adsorbed (cm3 g-1, STP)
p/po
G50-CB10
G50-CB5
G50
G50-CB10-T500
G50-CB10
G50-CB10-T1000

by narrower necks. These features allow a fine-tuning control of the micro/mesoporosity of the gels modified with a conductive additive.

To analyze the effect of the amount of carbon black incorporated during the synthesis on the porosity, two identical aerogels were prepared adding 5 and 10 wt.% of the CCA while keeping constant the rest of parameters (samples G50-CB5 and C50-CB10). The corresponding gas adsorption isotherms are shown in Fig. 3. Increasing the amount of carbon black led to higher total pore volumes and to an enlargement of the average mesopore size. This is evidenced by the shift of the hysteresis loop to higher condensation pressures in the adsorption isotherms. It may be inferred then that the pore width is not only controlled by the R/C ratio (as in conventional synthesis) but also by the amount of carbon black.

For the sample prepared with the lowest amount of CCA (carbon G50-CB5), three distinctive regions can be clearly identified as fused hysteresis loops in the nitrogen adsorption isotherm (Fig. 3). This points out the occurrence of a large pore blocking effect in the network, likely due to mesopores interconnected by narrower necks of various sizes. When the amount of carbon black increased (sample G50-CB10), only two stages (fused hysteresis loops) are distinguished, along with an upward shift in the relative pressure of the loops in the adsorption isotherms. This reveals that the size of the pore necks is enlarged with the amount of CCA. Interestingly, both samples showed a similar curvature in the adsorption isotherm appearing at relative pressures of ca. 0.8 (see inset in Fig. 3). Consequently it seems that the size of the large mesopores is mainly controlled by the R/C ratio (being similar in G50-CB5 and G50-CB10), whereas the CCA would control the size of the pore necks connecting the main cavities. Pore systems showing fused hysteresis loops have been reported for chemically modified microporous glasses [29, 30] and silica materials consisting of spherical mesopores connected through narrow openings [34].

Based on the porosity evolution of the gel/CCA composites, it can be inferred that the incorporation of the conductive additive strongly affects the polymerization mechanism of the precursors. In the conventional synthesis, highly reactive systems are favored for low R/C molar ratio, where the rate of formaldehyde consumption is accelerated leading to dense branched clusters, which easily undergo spinodal decomposition. In the presence of the aggregates of CCA, the large pore volumes and hysteresis loop suggest that the polycondensation of the monomers is slowed down. This would suppress the formation of

the hydroxymethly derivates that allow the cross-linking of the structure (in a similar way as the effect of the R/C value in the conventional synthesis [4-6, 34], generating less branched clusters that are more stable in the nucleation regime, allowing the colloidal particles to aggregate and assemble together in larger and weakly branched clusters. As a result, the carbon yields (after pyrolysis) obtained for the gel/CCA composites were larger (ca. 59-63 % for Gx-CBy) than those of the gels obtained in the conventional synthesis for all R/C values (ca. 50 % for series Gx).

During the clusters formation and growth, the carbon black aggregates (of a few nm width) would act as an ionomer finely dispersed within the primary particles of the carbon precursor monomers, creating larger and poorly cross-linked polymer particles but providing additional electrical conductivity.

The high pore volumes of the gel/CCA samples were almost unaffected by the pyrolysis temperature (Fig. 3), unlike the trend reported for carbon gels prepared by the conventional sol-gel route [4-6]. In a typical synthesis, the pyrolysis temperature may cause a structural collapse due to the surface tensions arising during gas evolution after the decomposition of the organic gels components (i.e. OH moieties, H_2O, CO_2, CO and other organic molecules). This effect is generally more remarkable in gels composed of small nodules (low R/C ratio) and narrow pores, which are less resistant to the surface tensions provoked during gas evolution. Elemental analysis confirmed the large loss of oxygen, hydrogen and other volatiles from the carbonaceous structure during pyrolysis, with carbon contents increasing from 50-75 wt.% (as-prepared gels with increasing R/C ratios) to 82-98 wt% (after pyrolysis at 550-800 and 1000 ºC). Thus, it seems that as a result of the incorporation of the carbon black, the aerogels are more resistant to surface capillary pressures, thus allowing pyrolysis with nearly no structural shrinkage/collapse. This is also supported by large carbon yield of the gel/CCA composites, compared to the conventional synthesis, as mentioned above. The enhanced resistance of the gel primary particles to collapse upon annealing would be attributed to their large porosity and the reinforcement effect of the carbon black in the matrix, in a similar way as that reported for some resins or fibers-reinforced gels [35-37].

3.1.3.2. Electrochemical characteristics in aqueous medium

To investigate the potential applications of the synthesized carbon gels as electrodes in various electrochemical systems, we have measured the electrical resistivity of the carbon

gels prepared with and without the CCA. As seen in Table 2, the resistivity values of the carbon gels prepared by the conventional sol-gel process showed a decreased trend with the R/C ratio; this has been explained in terms of the higher density of defects typically present in polymeric gels [38]. After incorporation of the carbon black additive, the resistivity decreased by an order of magnitude for all the synthesized materials, and the trend with the R/C is still subtly observed (Fig. 5). The resistivity values are also lower (i.e. higher conductivity) than those reported for amorphous carbon materials (Fig. 5) typically used in electrochemical applications [23, 24]. For a given R/C molar ratio, similar resistivity values were obtained for the aerogels prepared with 5 and 10 wt.% of the CCA (Table 2). Lower carbon black

Table 2. Resistivity values of the synthesized carbon aerogels and gel/CCA nanocomposites.

	Resistivity [Ohm sq]	**R/C**	**CCA [wt.%]**	**Pyrolysis Temp [ºC]**
Carbon Black (CCA)	2.8	n.a.	100 %	n.a.
G25	278	25	none	800
G50	247	50	none	800
G100	223	100	none	800
G200	202	200	none	800
G25-CB10	63	25	10	800
G50-CB10	58	50	10	800
G100-CB10	25	100	10	1000 (800)
G200-CB10	22	200	10	1000
G50-CB5	53	50	5	800
G50-CB10-T500	∞	50	10	500
G50-CB10-T1000	29	50	10	1000

loadings did not seem to affect the electrical conductivity of the gels, whereas higher loadings were not achievable (lack of homogenous dispersion). All this points out that the resistivity of the prepared materials does not only depend on a critical carbon black loading, but also on the interconnectivity between the CCA particles and the RF clusters during the synthesis.

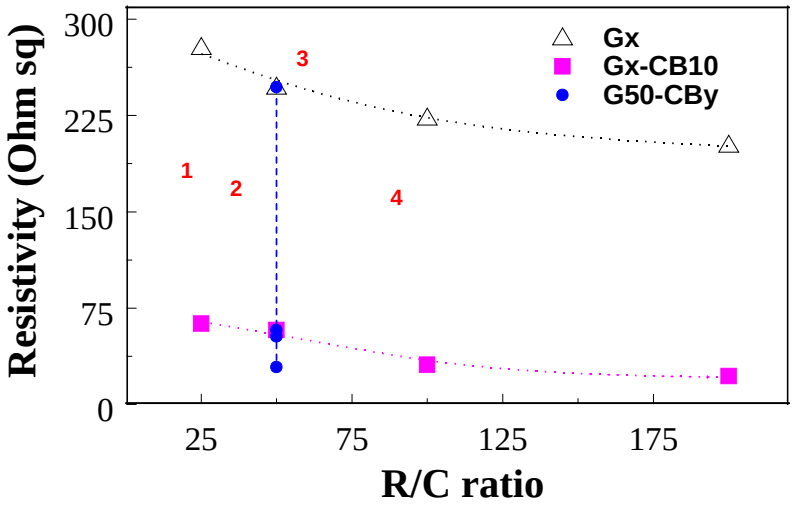
Resistivity (Ohm sq)
300
225
150
75
0
25
75
125
175
R/C ratio
Gx
Gx-CB10
G50-CBy
1
2
3
4

conductivity of the gel/CCA composites is greatly defined by the chemical composition of the carbon matrix and to a lesser extent by its texture.

The large pore volumes and low electrical resistivity of the synthesized gel/CCA nanocomposites anticipate a good performance as electrodes, further corroborated by the electrochemical response of the obtained materials analyzed in a three electrode cell configuration in neutral aqueous electrolyte. Cyclic voltammograms of selected materials (representative of the series) are shown in Fig. 6, for a potential cut-off hold between -800 and +800 mV vs NHE. Despite the thermodynamic potential for water decomposition (i.e. -380 mV vs NHE) was largely surpassed, no current leaps related with gas evolution due to the decomposition of the electrolyte were observed. This behavior is rather common for porous carbon electrodes in sodium sulfate electrolyte [40]; it has been attributed to the high overpotential for H_2 evolution of neutral electrolyte, and the ability of porous carbon electrodes to store the nascent hydrogen below -400 mV vs NHE. The wide humps observed in the anodic sweeps between +200-400 mV vs NHE (see for instance G200-CB10) confirmed the electrooxidation of the hydrogen stored on the electrodes.

Other than the humps due to electrooxidation/reduction of nascent hydrogen, the voltammograms showed the ideal rectangular shape associated to the charge/discharge of the electric double layer (pure capacitive behavior). Current peaks arising from pseudo-faradaic reactions involving redox charge transfer reactions associated to surface groups were not detected, which is in agreement with the low oxygen content of the pyrolyzed aerogels.

As mentioned above, the gels treated at 500 ºC showed a negligible electrochemical response, in accordance with the resistivity values measured for the electrodes (Table 2). This contrasts with the behavior widely reported for porous carbon electrodes where the incorporation of oxygen functionalities often leads to enhanced capacitance values due to the pseudo-capacitance contribution linked to surface functionalities [41]. Having a rich surface chemistry, it appears that the oxygen moieties decorating the carbon matrix of the gels pyrolyzed at 500 ºC are not electrochemically active. Thus, pyrolysis temperature is critical to assure the good electrochemical performance of carbon gels, even if a conductive additive is incorporated in the synthesis.

The electrodes pyrolyzed at 800 and 1000 ºC also showed a stable electrochemical response, being reversibly charged/discharged at large potential windows (ca. 1.4 V) in

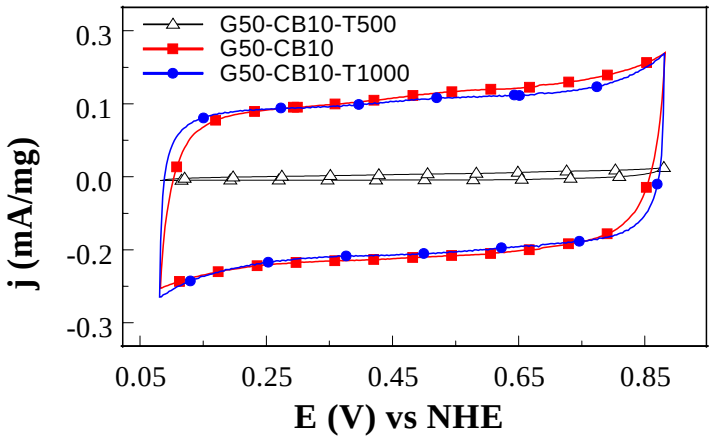
G50-CB10-T500
G50-CB10
G50-CB10-T1000
0.3
0.1
0.0
-0.2
-0.3
0.05
0.25
0.45
0.65
0.85
j (mA/mg)
E (V) vs NHE

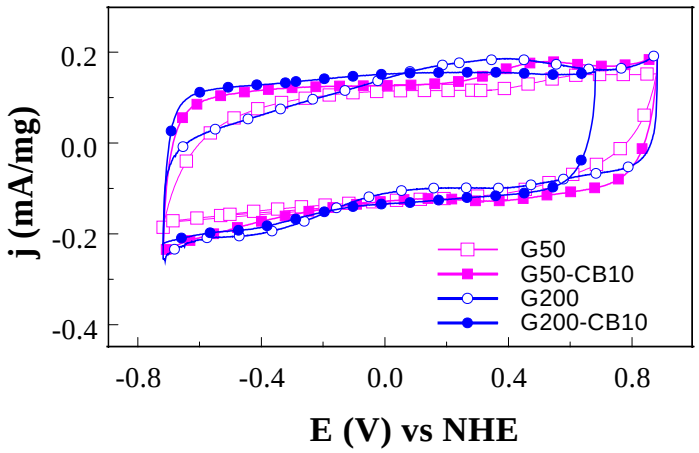
0.2
0.0
-0.2
-0.4
-0.8
-0.4
0.0
0.4
0.8
G50
G50-CB10
G200
G200-CB10
j (mA/mg)
E (V) vs NHE

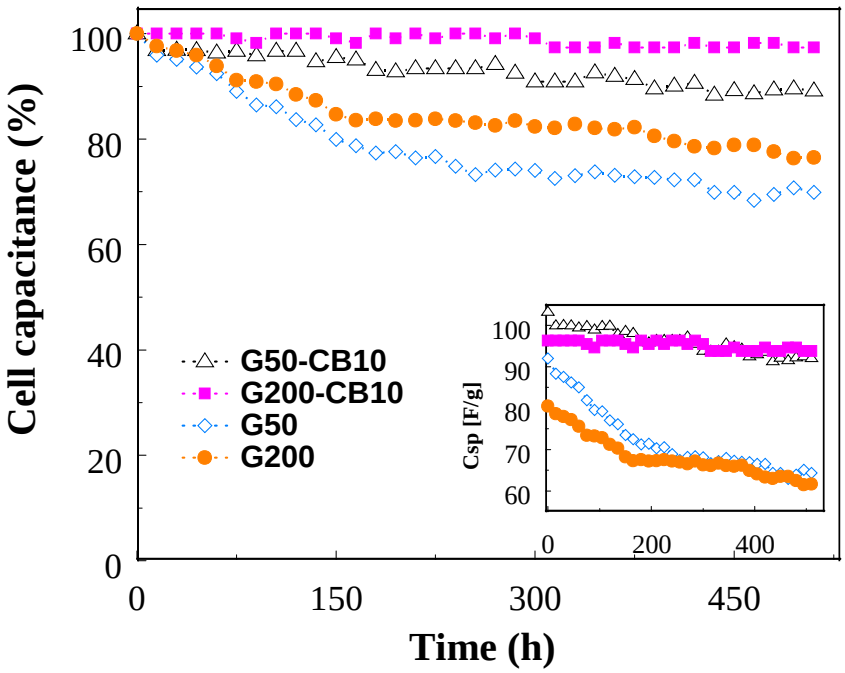
Cell capacitance (%)
Time (h)
0
20
40
60
80
100
0
150
300
450
G50-CB10
G200-CB10
G50
G200
Csp [F/g]
60
70
80
90
100
0
200
400

Moreover, the possibility to operate at a large electrochemical window coupled to the enhanced life cycles of these gel/CCA nanomaterials offers an interesting strategy for those applications where a high potential /voltage and good reversibility are desired (for instance capacitive deionization, electrochemical, energy storage, or biosensors). Additionally, the high resistance to electro-oxidation of the prepared carbon gels overcomes the limitation of most porous carbons in electrochemical applications (i.e. activated carbons), becoming an interesting feature to be further explored. Future research will focus on adjusting the micro/mesopore ratio and pore volumes in the low-nanometer scale, since this would be expected to expand the applicability of the materials.

3.1.4. Conclusions

We have synthesized electrically conductive and highly mesoporous carbon gels by a simple modification of the traditional resorcinol-formaldehyde catalyzed polycondensation route widely described in the literature for the preparation of carbon gels. The polycondensation of the reactants in the presence of a carbon conductive additive allowed a facile preparation of electrically conductive carbon aerogels with a unique combination of ultrahigh mesopore volumes and low electrical resistivity. The conductive additive had a large impact on the catalyzed sol-gel polymerization of the reactants, directing the synthesis towards the formation of less-branched clusters and of polymer particles with large sizes; this allowed a fine-tuning control over the micro/mesoporosity of the gel/CCA materials, while providing electrical conductivity within the polymer carbon gel particles.

Connectivity of the large mesopore cavities by large narrow necks assured an efficient charge/discharge rate in electrochemical applications due to the enhanced diffusion of ions in the large connected channels. The materials pyrolyzed above 500 ºC showed stable electrochemical response in neutral aqueous electrolyte, being reversibly charged/discharged at large potential windows over several hundreds of cycles, without significant losses in the current density. Another important feature related to the incorporation of the carbon black during the sol-gel step is the better life cycle of the resulting electrodes when charged/discharged at high voltage. These are interesting features for applications of carbon electrodes were a fast response is crucial.

3.1.5. References

[1] Gogotsi Y, (Ed.) in Carbon Nanomaterials, CRC Press, Boca Raton, Florida, 2006.

[2] Tascón JMD (Ed.) in Novel Carbon Adsorbents, Elsevier Ltd., Amsterdam, 2012.

[3] Lee J, Kim T, Hyeon J. Recent progress in the synthesis of porous carbon materials. Adv Mater 2006;18:2073–94.

[4] Al-Muhtaseb SA, Ritter JA. Preparation and properties of resorcinol– formaldehyde organic and carbon gels. Adv Mater 2003;15:101-14.

[5] Job N, Thery A, Pirard R, Marien R, Kocon L, Rouzaud JN, et al. Carbon aerogels, cryogels and xerogels: Influence of the drying method on the textural properties of porous carbon materials. Carbon 2005;43:2481-94

[6] Job N, Pirard R, Marien R, Pirard JP. Porous carbon xerogels with texture tailored by pH control during sol–gel process. Carbon 2004;42:619-28.

[7] Tamon H, Ishizaka H, Araki T, Okazaki M. Control of mesoporous structure of organic and carbon aerogel. Carbon 1998; 36:1257–62.

[8] Calvo EG, Ania CO, Zubizarreta L, Menendez JA, Arenillas A. new routes in the synthesis of carbon xerogels for their application in electric double layer capacitors. Energy & Fuels 2010;24:3334–9.

[9] Zubizarreta L, Arenillas A, Pirard JP, Pis JJ, Job N, Tailoring the textural properties of activated carbon xerogels by chemical activation with KOH. Microp Mesop Mater 2008;115:480–90.

[10] Pekala RW. Organic aerogels from the polycondensation of resorcinol with formaldehyde. J Mater Sci 1989;24(9):3221–7.

[11] Yamamoto T, Endo A, Ohmori T, Nakaiwa M. Porous properties of carbon gel microspheres as adsorbents for gas separation. Carbon 2004;42:1671-6.

[12] Moreno-Castilla C, Maldonado-Hodar FJ. Carbon aerogels for catalysis applications: An overview. Carbon 2005;43:455–65.

[13] Pajonk GM. Aerogel Catalysts. Appl. Catal. 1991;72:217–66.

[14] Pekala RW, Farmer JC, Alviso CT, Tran TD, Mayer ST, Miller JM, et al. Carbon aerogels for electrochemical applications. J. Non-Cryst. Solids 1998;225:74–80.

[15] Li W, Reichenauer G, Fricke J. Carbon aerogels derived from cresol-resorcinol-formaldehyde for supercapacitors. Carbon 2002;40:2955-59.

[16] Gutiérrez MC, Picó F, Rubio R, Amarilla JM, Palomares FJ, Ferrer ML, et al. PPO15-PEO22-PPO15 block copolymer assisted synthesis of monolithic macro- and

microporous carbon aerogels exhibiting high conductivity and remarkable capacitance. J Mater Chem 2009;19:1236–40.

[17] Lee YJ, Jung JC, Park S, Seo JG, Baeck SH, Yoon JR, et al. Preparation and characterization of metal-doped carbon aerogel for supercapacitor. Curr Appl Phys 2010;10:947–51.

[18] Farmer JC, Fix DV, Mack GV, Pekala RW, Poco JF. Capacitive deionization of NH_4CLO_4 solution with carbon aerogel electrodes. J Appl Electrochem 1996;26:1007–18.

[19] Haro M, Rasines G, Macias C, Ania CO. Stability of a carbon gel electrode when used for the electro-assisted removal of ions from brackish water. Carbon 2011;49:3723-30.

[20] Xu P, Drewes JE, Heil D, Wang G. Treatment of brackish produced water using carbon aerogel-based capacitive deionization technology. Water Res 2008;42:2605-17.

[21] Fellinger TP, White RJ, Titirici MM, Antonietti M. Borax-Mediated Formation of Carbon Aerogels from Glucose. Adv Funct Mater 2012;22:3254-60.

[22] Szczurek A, Amaral-Labat G, Fierro V, Pizzi A, Masson E, Celzard A. The use of tannin to prepare carbon gels. Part I: Carbon aerogels. Carbon 2011;49:2773-84.

[23] Pandolfo AG, Hollenkamp AF. Carbon properties and their role in supercapacitors. J Power Sources 2006;157:11-27.

[24] Park K, Lee J, Park P, Yoon S, Moon J, Eum H, et al. Development of a carbon sheet electrode for electrosorption desalination. Desalination 2007;206:86–91.

[25] Nadakatti S, Tendulkar M, Kadam M. Use of mesoporous conductive carbon black to enhance performance of activated carbon electrodes in capacitive deionization technology. Desalination 2011;268:182–8.

[26] Xi-miao L, Rui Z, Liang Z, Dong-hui L, Wen-ming Q, Jun-he Y, et al. Impedance of carbon aerogel/activated carbon composites as electrodes of electrochemical capacitors in aprotic electrolyte. New Carbon Materials, 2007;22:153–8.

[27] Rasines G, Lavela P, Macias C, Haro M, Ania CO, Tirado JL. Electrochemical response of carbon aerogel electrodes in saline water. J Electroanal Chem 2012;671:92-8.

[28] van der Pauw J. A Method of Measuring Specific Resistivity and Hall Effect of Discs of Arbitrary Shapes. Philips Res Repts, 1958;13:1–9.

[29] Renou J, François-Rossetti J, Imerick B. Etudes des solides poreux. Isotherms d'adsorption irregulieres. Bul. Soc. Chimique de France, 1961;91:446-50.

[30] de Boer JH. in The Structure and Properties of Porous Materials, (Eds. D. H. Everett and F. S. Stone), Butterworths, 1958 pp. 84-145.
[31] Van Der Voort P, Ravikovitch PI, De Jong KP, Neimark AV, Janssen AH, Benjelloun M, et al. Plugged hexagonal templated silica: a unique micro- and mesoporous composite material with internal silica nanocapsules, Chem Comm 2002;9:1010-1.
[32] Phuong T, Nguyen M, Do DD, Nicholson D. On The Cavitation and Pore Blocking in Cylindrical Pores with Simple Connectivity. J Phys Chem B 2011;115:12160–72.
[33] Vishnyakov A, Neimark AV. Monte Carlo Simulation Test of Pore Blocking Effects. Langmuir 2003;19:3240-7.
[34] Rasmussen CJ, Vishnyakov A, Thommes M, Smarsly BM, Kleitz F, Neimark AV. Cavitation in Metastable Liquid Nitrogen Confined to Nanoscale Pores. Langmuir 2010;26:10147–57.
[35] Petricevic R, Glora M, Fricke J. Planar fibre reinforced carbon aerogels for application in PEM fuel cells. Carbon 2001;39:857–67.
[36] Saliger R, Fischer U, Herta C, Fricke J. High surface area carbon aerogels for supercapacitors. J. Non- Cryst Solids 1998;225:81-5.
[37] Petricevic R, Reichenauer G, Bock V, Emmerling A, Fricke J. Structure of carbon aerogels near the gelation limit of the resorcinol–formaldehyde precursor. J Non- Cryst Solids 1998;225:41-5.
[38] Wang J, Zhang SQ, Shen J, Guo YZ, Attia SM, Zhou B, et al. Electrical transport properties of carbon aerogels. J Porous Mater 2001;8:167–70.
[39] Lin C, Ritter JA, Popov BN. Correlation of Double-Layer Capacitance with the Pore Structure of Sol-Gel Derived Carbon Xerogels. J Electrochem Soc 1999;146,:3639-43.
[40] Demarconnay L, Raymundo-Piñero E, Beguin F. A symmetric carbon/carbon supercapacitor operating at 1.6 V by using a neutral aqueous solution. Electrochem Comm 2010;12:1275-8.
[41] Raymundo-Piñero E, Beguin F. in Activated Carbon Surfaces in Environmental Remediation, vol 7 (T. J. Bandosz, Ed), Elsevier, Oxford, 2006, chapter 6.
[42] Bichat MP, Raymundo-Piñero E, Béguin F. High voltage supercapacitor built with seewead carbons in neutral aqueous electrolyte, Carbon 2010;48:4351-4361.
[43] Berenguer R, Marco-Lozar JP, Quijada C, Cazorla-Amoros D, Morallon E. Effect of electrochemical treatments on the surface chemistry, Carbon 2009;47:1018-1027.

3.1.6. Anexo: Supplementary Information

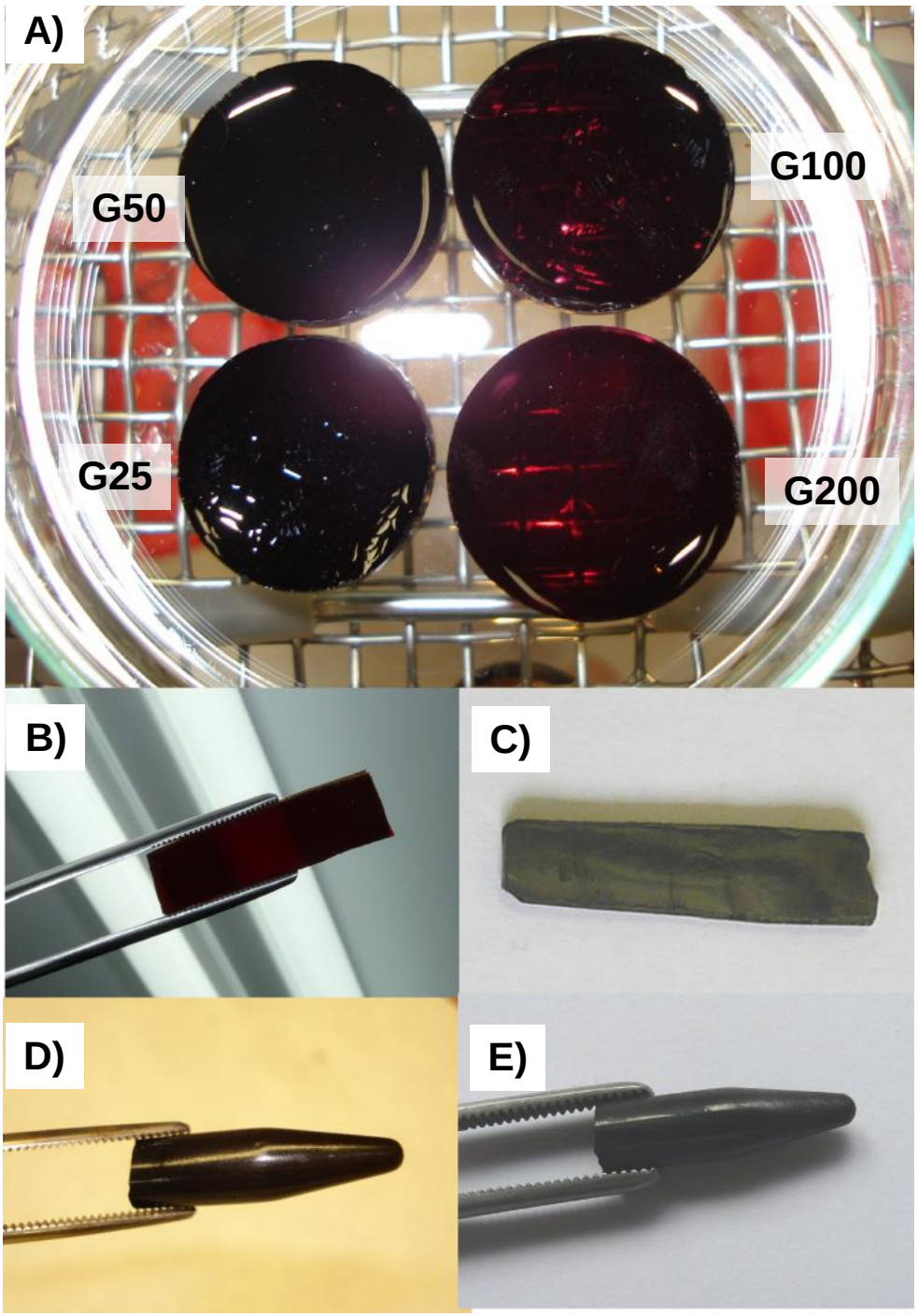

Fig. S1 Images of the prepared carbon aerogels with and without the addition of the conductive additive. (A) gels from the conventional synthesis before pyrolysis; (B) sample G200 before pyrolysis; (C) sample G200 after pyrolysis; (D) G200-CB10 before pyrolysis and (E) G200-CB10 after pyrolysis.


Carbon

the good electrochemical performance, the use of monolithic electrodes was limited due to the large shrinkage and deformation of the pieces after carbonization -leading to densification of the matrix- [5]; this is a challenge for electrochemical applications where the contact between the electrode material and the current collector is crucial to avoid efficiency losses due to resistance. Aiming at fabricating large monolithic electrodes with improved mechanical properties without adversely affecting their porosity and conductivity, we herein report the preparation of monolithic carbon aerogels with enhanced mechanical properties by using a low cost siliceous sacrificial additive (i.e. diatomite earth). The synthesis route is a simple modification of the conventional one reported elsewhere [4], and consists on allowing the sol-gel polymerization of the precursors in the presence of the additives; after the supercritical drying step, the hydrogels (series H-) were carbonized (series C-), and the siliceous additive was finally removed by HF etching (see further details in the ESI File). Selected formulations with different precursor's molar ratio (R, F and melamine, M) and additives (either diatomite (D), carbon black (B), or both) were prepared (Table 1), to show that the effect of the additive does not depend on the composition of the aerogels. From a macroscopic point of view (Fig. 1), the materials ranged from translucent (pristine) to opaque when either B or D additives were used; this was rather expected given the large amounts of additives added (ca. 10 and 50 wt.% for B and D, respectively). Fig. 1 also shows the typical shrinkage and deformation of monoliths of varied composition after carbonization to obtain carbon aerogels (series C-) due to the evolution of the volatiles. The shrinkage of the disks (Table 1) accounted for up to a 30 % reduction in volume, and it was observed regardless the composition of the aerogels; notwithstanding the deformation was more pronounced for the samples prepared using melamine and B additive. In contrast, the shrinkage and bending was not observed for the aerogels prepared in the presence of diatomite, as the carbonized disks preserved their dimensions even after the removal of the siliceous skeleton. Since we did not observe cracks between the siliceous and carbonaceous phases (Fig. 2 and 3), and we attribute this to the open pore structure of the diatomite that facilitates the evolution of volatiles upon densification by carbonization.

The aerogels ranged from brittle to sponge-like solids when D was incorporated -even after etching of the diatomite-. These differences in the consistency were also corroborated by the Crushing Strength Tests up to 30 N (Table 1) [6], a screening

technique used to evaluate the mechanical properties of the aerogels. The pristine and B-loaded materials presented a conchoidal fracture after compression above 30 N (Fig. 2). On the other hand, the aerogels synthesized in the presence of the D (either etched or not) followed a different pattern; no fracture was observed in this case, and the materials were rather gradually deformed with increasing the compressive load, suggesting a plastic character. The extent of the deformation is clearly seen by the fingerprint left by the punch in the monoliths (Fig. 2).

The mechanical properties of selected monolithic aerogels were also investigated by means of Small Punch Tests performed under quasi-statical conditions [7]. Fig. 3 shows the load-displacement curves (LDC) from biaxially stretched tests performed on selected aerogels showing the effect of both additives. The characteristic shape of the curves demonstrates the change from a stiff and brittle behavior to a compliant and plastic character of the materials when the diatomite was used as additive in the synthesis. In the case of the aerogels without D, a steep initial slope was followed by a load drop associated with pop-in cracking. The onset of the first crack corresponds to the maximum load and determines the deformation capacity of the material (inset Fig. 3). The LDC curves exhibit a much more compliant behavior when D was used as additive and no sudden crack extensions took place; this is attributed to the presence of large voids inherited from the siliceous skeleton, as it can also be seen in the SEM images. The stiffness of the samples, evaluated from the initial slope of the LDC, decreased about one order of magnitude when the D additive was used. Furthermore, the mechanical properties induced by the D are retained after carbonization and/or etching off the additive. While the maximum load up to the first pop-in crack is quite similar for all the samples, the materials prepared in the presence of D exhibit much higher displacements before cracking and larger areas under the LDC, this last value being related to toughness.

In addition to being more mechanically compliant, the aerogels prepared in the presence of the diatomite exhibited large porosity, as inferred from the N_2 adsorption data (Fig. 4, Table 1). The textural features of the aerogels were slightly altered by

Table 1. Summary of synthesis parameters, dimensions and textural characteristics of the monolithic aerogels showing the shrinkage and response to the Crushing Strength Tests. Samples before (H-) and after (C-) carbonization are compared.

Sample (*)	S_{BET} [A] [m^2g^{-1}]	V_T [B] [cm3/g]	Synthesis Parameters	Specimen dimensions[C] (mm)	Shrinkage on carbonization[D] (%)	Remarks on Crushing Strength Tests[E]
H-MRF1	458	0.99	(M+R)/C 90 (M+R)/W 0.052 (M+R)/F 0.428	4.97	--	Brittle, fracture upon load of 16 N
H-MRF1-B	450	1.55	(M+R)/C 90 (M+R)/W 0.052 (M+R)/F 0.428	4.97	--	fracture upon load of 27 N
C-MRF1	323	0.46	(M+R)/C 90 (M+R)/W 0.052 (M+R)/F 0.428	4.87/3.5	28.1	Brittle, no fracture upon load of 30N
C-MRF1-B	314	0.67	(M+R)/C 90 (M+R)/W 0.052 (M+R)/F 0.428	4.95 / 3.45	30.3	Brittle, no fracture upon load of 30N
H-RF1	592	1.32	R/C 200, R/F 0.5, R/W 0.06	5.2	--	Brittle, fracture after load of 15 N
C-RF1	862	1.48	R/C 200, R/F 0.5, R/W 0.06	5.2/3.93	24.4	Brittle, fracture after 18 N load
C-RF1-B	854	1.53	R/C 200, R/F 0.5, R/W 0.06	5.2/3.58	31.2	Brittle, fracture after 28 N load
C-RF2	894	1.17	R/C 200, R/F 0.5, R/W 0.08	5.2/3.87	25.6	Brittle, no fracture upon load of 30N
C-RF2-B	856	1.18	R/C 200, R/F 0.5, R/W 0.08	5.2/3.4	33.8	Brittle, fracture upon load of 21N
H-MRF2	212	1.44	(M+R)/C 135 (M+R)/W 0.052 (M+R)/F 0.428	5.1	--	Brittle, fracture upon load of 21N
H-MRF2-D	101	0.58	(M+R)/C 135 (M+R)/W 0.052 (M+R)/F 0.428	5.2	--	Flexible, characteristic fringerprint at loadings 5-30N
H-MRF2-BD	237	0.51	(M+R)/C 135 (M+R)/W 0.052 (M+R)/F 0.428	5.2	--	Flexible, characteristic fringerprint at loadings of 5-30N
C-MRF2	522	1.55	(M+R)/C 135 (M+R)/W 0.052 (M+R)/F 0.428	5.1/3.6	30.8	Brittle, fracture upon load of 14 N
C-MRF2-D	230	0.85	(M+R)/C 135 (M+R)/W 0.052 (M+R)/F 0.428	5.2/4.9	5.4	Flexible, characteristic fringerprint at loadings of 2-30N
C-MRF2-D (etched)	328	1.13	(M+R)/C 135 (M+R)/W 0.052 (M+R)/F 0.428	5.2/4.9	5.4	Flexible, characteristic fringerprint at loadings of 2-30N
C-MRF2-BD	118	0.41	(M+R)/C 135 (M+R)/W 0.052 (M+R)/F 0.428	5.2/5.0	4.6	Flexible, characteristic fringerprint at loadings of 5-30 N
C-MRF2-BD etched	237	0.51	(M+R)/C 135 (M+R)/W 0.052 (M+R)/F 0.428	5.2/4.9	5.2	Flexible, characteristic fringerprint at loadings of 2-30N

[*] Samples are labelled as series RF or MRF depending on the precursors; numbers indicate different formulations -for clarity- detailed in the synthesis parameters raw; “H” denotes hydrogels after supercritical drying and before carbonization; “C” denotes carbonized samples; “D” and/or “B” denote the presence of diatomite and/or carbon black

additives.

[A] Apparent surface area evaluated using BET at the N_2 adsorption isotherms at -196º C

[B] Total pore volume evaluated at relative pressure of 0.99

[C] Spherical specimens, dimensions before (samples H-) and after carbonization (samples C-) of the disks

[D] evaluated from the dimensions before/after carbonization of the spherical specimens (samples H- vs samples C-)

[E] evaluated from the Crushing Strength Tests (compression up to 30 N) of the spherical specimens

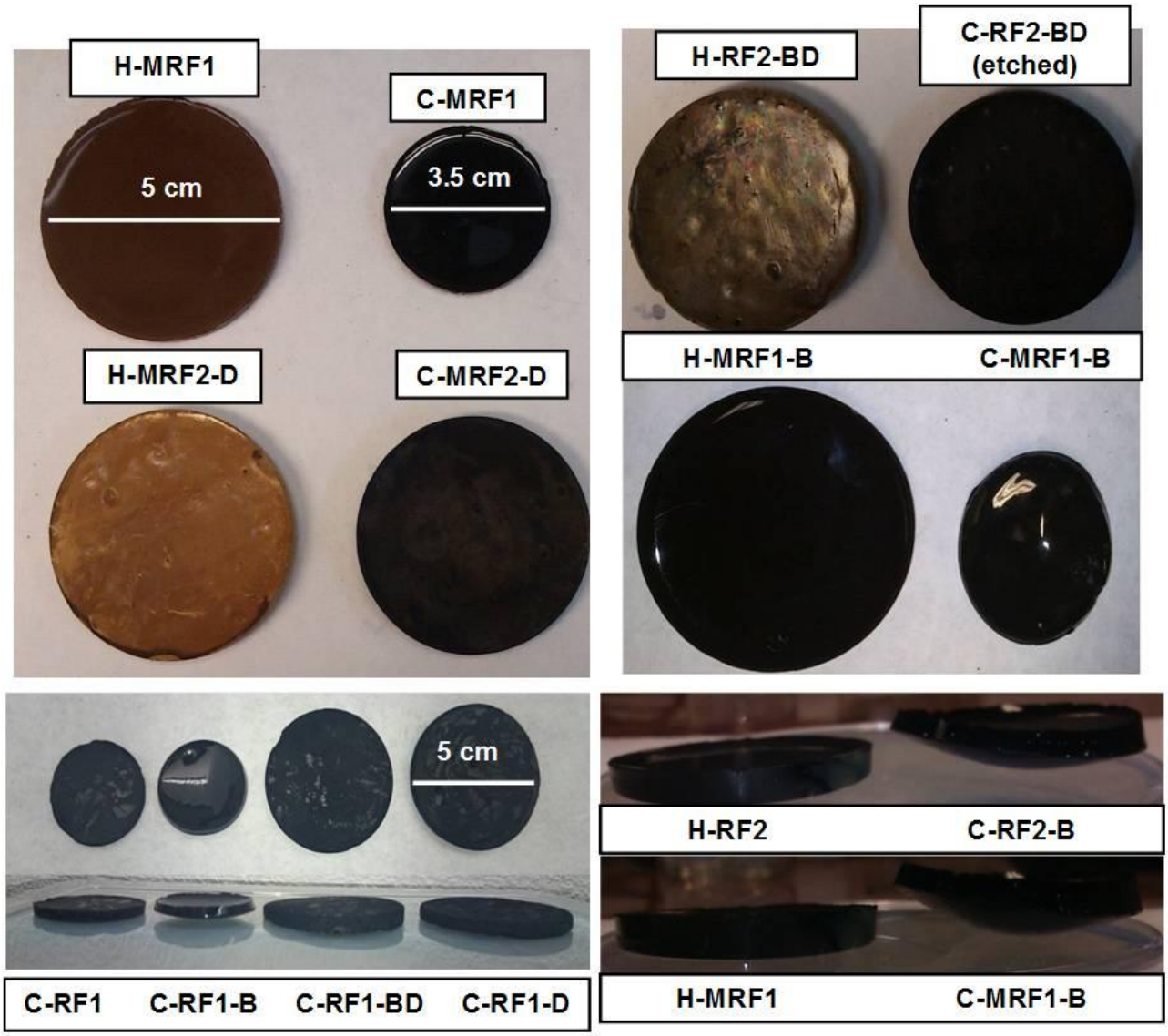

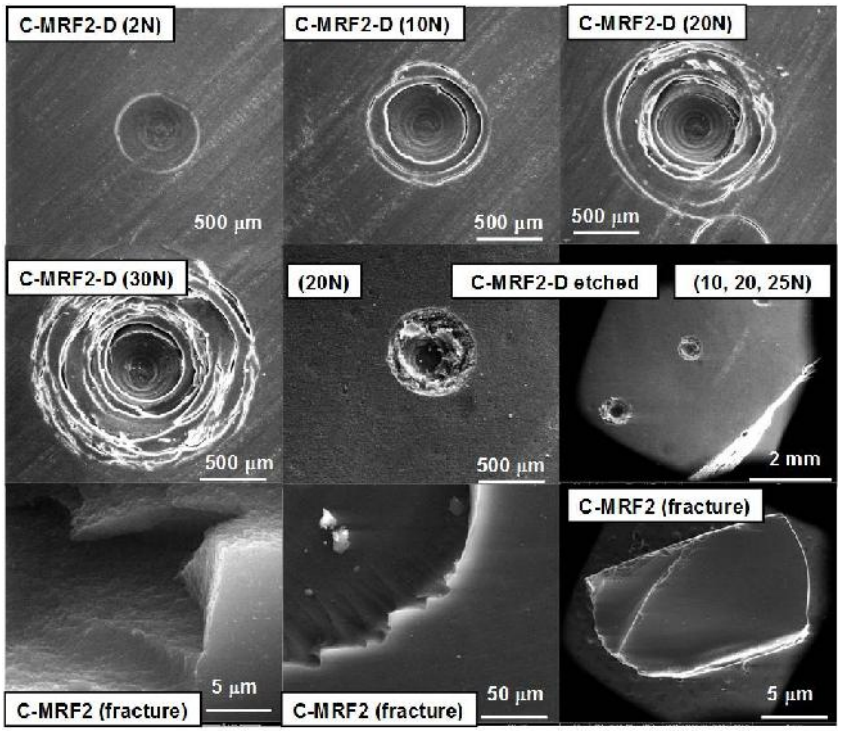
C-MRF2-D (2N)
500 μm
C-MRF2-D (10N)
500 μm
C-MRF2-D (20N)
500 μm
C-MRF2-D (30N)
500 μm
(20N)
C-MRF2-D etched
(10, 20, 25N)
500 μm
2 mm
5 μm
C-MRF2 (fracture)
C-MRF2 (fracture)
50 μm
C-MRF2 (fracture)
5 μm

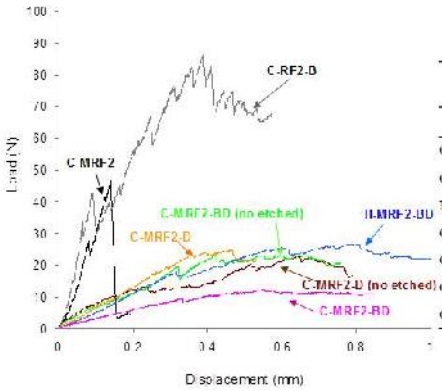

	Rigidity	Maximum Load	Toughness
	[N/mm]	[N]	[N mm]
C-MRF2	456	28	0.9
C-RF2-B	646	34	0.9
H-MRF2-BD	60	18	3.0
C-MRF2-D (no etched)	94	13	2.0
C-MRF2-D (etched)	65	23	4.3
C-MRF2-BD (no etched)	65	19	3.1
C-MRF2-BD (etched)	27	10	1.7

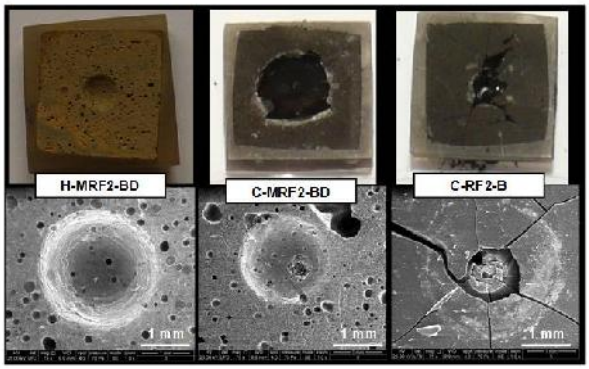

	S_{BET}	V_T [A]	V_{MIC} [B]	V_{MESO} [C]
	$m^2 g^{-1}$	$cm^3 g^{-1}$	$cm^3 g^{-1}$	$cm^3 g^{-1}$
C-MRF2	522	1.55	0.13	1.50
C-MRF2-D (etched)	409	0.79	0.12	0.81
C-MRF2-BD (etched)	470	0.75	0.16	0.54

[A] Total pore Volume evaluated at p/p_0 ~0.99
[B] Micropore volume evaluated from 2D-NLDFT method
[C] Mesopore volume evaluated from 2D-NLDFT method

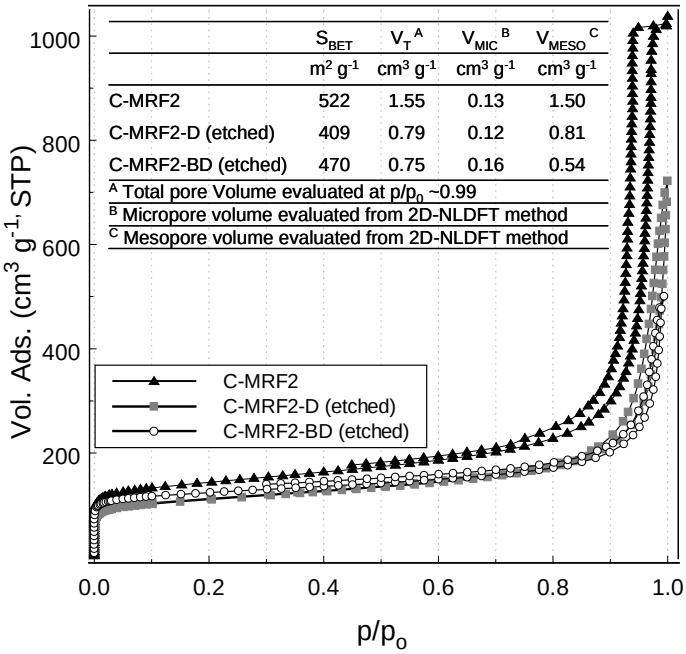

3.2.1. References

[1] Pekala RW. Organic aerogels from the polycondensation of resorcinol with formaldehyde. J Mater Sci 1989;24(9):3221–7.

[2] Pekala RW, Alviso CT, LeMay JD. Organic aerogels: Microstructural dependence of mechanical properties in compression, J. Non-Cryst. Solids 1990;125:67–75.

[3] Morales-Torres S, Maldonado-Hodar FJ, Perez-Cadenas AF, Carrasco-Marın F. Textural and mechanical characteristics of carbon aerogels synthesized by polymerization of resorcinol and formaldehyde using alkali carbonates as basification agents, Phys. Chem. Chem. Phys., 2010;12:10365-72.

[4] Macias C, Haro M, Rasines G, Parra JB, Ania CO. Carbon-black directed synthesis of mesoporous aerogels, Carbon 2013;63:487-97.

[5] Rasines G, Lavela P, Macias C, Zafra MC, Tirado JL, Ania CO. On the use of carbon black loaded N-doped carbon aerogel for the electrosorption of sodium chloride from saline water, Electrochim Acta 2015;170:154-163.

[6] Bemrose CR, Bridgewater J. A review of attrition and attrition test methods, Powder Technology 1987;49:97-126.

[7] Rodríguez C, Arencón D, Belzunce J, Maspoch M. Small punch test on the analysis of fracture behaviour of PLA-nanocomposite Films, Polymer Testing 2014;33:21-9.

3.2.2. Anexo: Supplementary Information File (ESI)

3.2.2.1. Synthesis of the MRF aerogels

Hydrogels were synthesized by the polycondensation of Melamine (M), Resorcinol (R) and Formaldehyde (F) using sodium carbonate as catalyst (C) and deionized water (W) as solvent. Carbon black (CB, Superior Graphite Co.) and diatomite (Nanolit K-6) were used as conductive and anti-shrinkage additives, respectively. Two different molar ratio of the reactants were used, as compiled in Table 1 (M+R/C of 90 and 135; M+R/W of 0.052 and 0.053, M+R/F of 0.43). The final pH of the precursors was eventually adjusted at 7.4 by adding acetic acid or sodium carbonate, respectively. For the MRF series, the samples were synthesized following a prepolymerization procedure described elsewhere [S1-S4]. Briefly, a solution containing R, F, C and W (solution A) was stirred for 1 h at 40 ºC. Separately, a solution containing M, F, W and C (solution B) was stirred for 30 min at 70 ºC. Subsequently, solutions A and B were mixed together and stirred for 20 minutes at room temperature to further allow the cross-linking of the precursors. Before gelification, diatomite (50%w/v) and/or carbon black (ca. 10%wt.) were added and magnetically stirred to ensure a homogeneous dispersion. Hydrogels were then kept in an oven at 40 ºC for 24 h and then at 70 ºC for 120 h to allow gelation and aging. After a controlled water–acetone exchange, the hydrogels were supercritically dried with CO_2 and carbonized (ca. 2 ºC/min) at 750 ºC under nitrogen atmosphere. Diatomite was removed from the samples using HF, leaving a silica free carbon monolith.

3.2.2.2. Synthesis of the RF aerogels

The resorcinol-formaldehyde carbon gels were synthesized by the sol gel polymerization of resorcinol (R) and formaldehyde (F) in water (W), using sodium carbonate (C) as catalyst, carbon black (CB, Superior Graphite Co.) as conductive additive. Different aerogels were obtained by setting the R/W ratio at 0.06 and 0.08, while the R/F molar ratio was set at 0.5, the R/C at 200 and the amount of carbon black added to the solution was ca. 0.9% w/v. In a typical synthesis, the reagents were placed into sealed glass moulds under magnetic stirring and allowed to undergo gelation and aging in an oven at 40 º C for 24 h and 70 ºC for 120 h. After the water-acetone

exchange, the samples were dried under CO_2 supercritical conditions. Finally, the aerogels were pyrolyzed at 800ºC under a N_2 stream (heating ramp of 2 ºC min^{-1}). For the sake of comparison, carbon gels prepared by the same synthetic route without the incorporation of the carbon black were also prepared.

3.2.2.3. Nomenclature of the samples

Series MRF: hydrogels synthesized by the polycondensation of melamine, resorcinol and formaldehyde.

Series RF: hydrogels synthesized by the polycondensation of resorcinol and formaldehyde.

Hydrogels are labeled as “H”, while carbonized samples are labeled as “C”.

The presence of Diatomite and Carbon Black in the samples is indicated by adding “D” or “B” to the nomenclature.

3.2.2.4. Mechanical Properties: crushing Strength Test and Small Punch Test

The Crushing Strength Tests were carried out by applying a normal force (up to 30N) to the as-prepared monoliths. This allows the evaluation of the resistance of the materials to fracture under a compressive strength limit, while measuring the characteristic fingerprint on the material upon deformation and/or fracture.

Small Punch Tests were performed under quasi-statical conditions with a low speed tensile test machine on 1x1cm square specimens of 2-3 mm thickness. The specimens were polished to control the thickness and to obtain a flat surface, and framed in a resin framework (1 x 1 mm) surrounding the material while leaving the surface of the material uncovering to allow the contact with the punch head. The test consisted on fixing the specimen between two dies (initial load of 2 N), and then deforming the specimen quasi-statically up to failure by means of a small semi-spherical punch with a head of 2 mm of diameter (biaxial expansion). The test is speed controlled with a punching speed v = 0.2 mm/min. The displacement of the punch is measured by means of an extensometer, and after correction of the flexibility of the testing device, the displacement of the central point of the specimen is calculated.

3.2.2.5. Electrical conductivity measurements

The measurement of conductivity on the previously dried as-prepared monolithic samples was carried out using an Arbin BT2000 potentiostat-galvanostat. The specimens are packed between two metallic collectors and hold under constant pressure (several values were tested to assure proper contact) and a bias voltage between 0.2-1.2 V (0.2V/s step for 120 s) was applied. The resistance is calculated from the slope of the current-voltage profiles at each voltage. The area and thickness of the monoliths, needed to evaluate the resistivity, were measured by a spring micrometer.

3.2.2.6. References

S1. Rasines G, Lavela P, Macias C, Zafra MC, Tirado JL, Ania CO, On the use of carbon black loaded N-doped carbon aerogel for the electrosorption of sodium chloride from saline water, Electrochim Acta 170 (2015) 154-163.

S2. Rasines G, Lavela P, Macias C, Zafra MC, Tirado JL, Parra JB, Ania CO, N-doped monolithic carbon aerogel electrodes with optimized features for the electrosorption of ions, Carbon 83 (2015) 262-274.

S3. Rasines G, Lavela P, Macias C, Zafra MC, Tirado JL, Ania CO, Mesoporous carbon black-aerogel composites with optimized properties for the electro-assisted removal of sodium chloride from brackish water, J Electroanal. Chem, 741 (2015) 42-50

S4. Macias C, Haro M, Rasines G, Parra JB, Ania CO, Carbon-black directed synthesis of mesoporous aerogels, Carbon 63 (2013) 487-497.

Table S1. Main characteristics of the additives used (diatomite and Carbon Black).

Sample	S_{BET} [A] $[m^2g^{-1}]$	V_{PORES} [B] [cm3/g]	Selected characteristics	Remarks
Carbon Black	22	0.17	Volatiles < 0.15 wt.% Ash < 0.05 wt.% Density 160 kg/m^3 Average particle size 6 μm	Superior Graphite Co
Diatomite	28	0.08	Average particle size 12 μm Permeability (Darcy) 0.020 Apparent density (dry) 190 g/L Apparent density (wet) 420 g/L	FN-6 / Celatom Fine-grained siliceous sediment of biogenic origin (skeletal remains of microscopic single-celled diatoms) SiO_2 (89.2 wt.%) , Al_2O_3 (4 wt.%), Fe_2O_3 (1.7 wt.%), CaO (0.5 wt.%), MgO (0.3 wt.%)

[A] Apparent surface area evaluated from N_2 adsorption isotherms at -196º C

[B] Total pore volume evaluated at relative pressure of 0.99

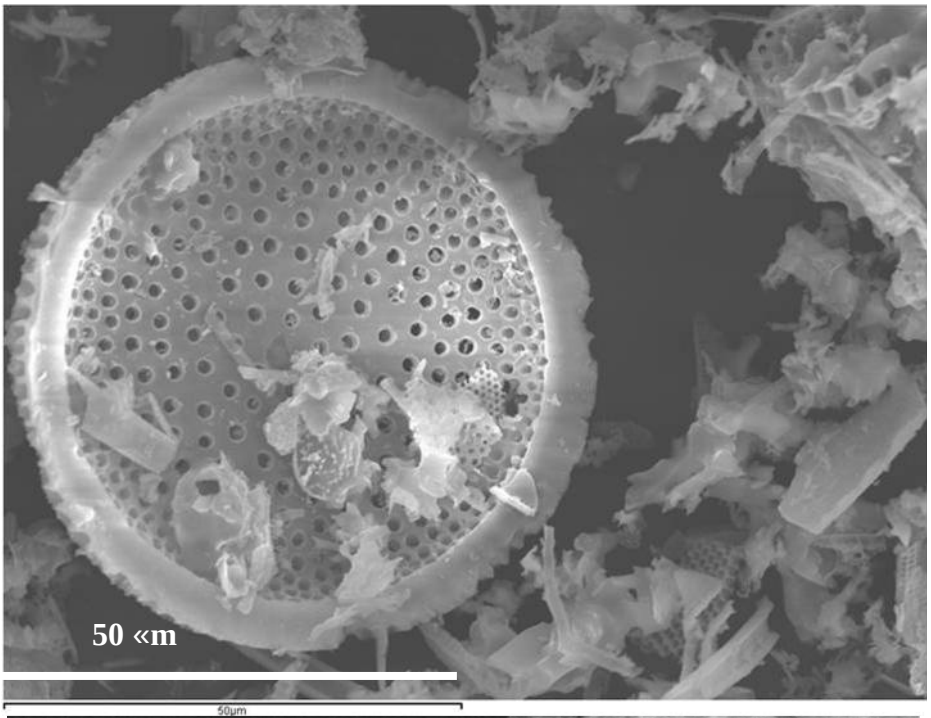
50 «m
50µm

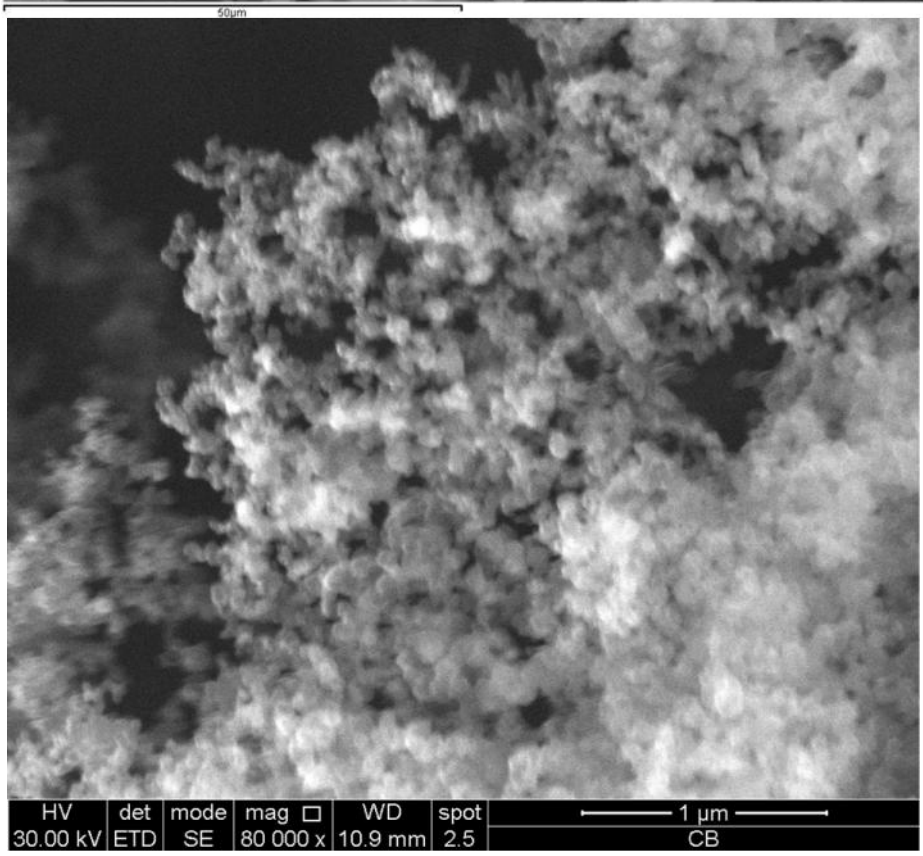
HV
30.00 kV
det
ETD
mode
SE
mag
80 000 x
WD
10.9 mm
spot
2.5
1 µm
CB

3.3. Synthesis of porous and mechanically compliant carbon aerogels using conductive and structural additives

Gels **2016**, *2*(1), 4; doi:10.3390/gels2010004

Carlos Macias[1]*, Gloria Rasines[1], Tomas E. García[2], María C. Zafra[3], Pedro Lavela[3], José L. Tirado[3] and Conchi O. Ania[4,*]

[1] I+D Department, Nanoquimia S.L., 14014 Córdoba, Spain
[2] IUTA, Universidad de Oviedo, Campus Universitario, 33203 Gijón, Spain
[3] Lab Química Inorgánica, Univ. Cordoba, Campus de Rabanales, 14071 Córdoba, Spain
[4] ADPOR Group, Instituto Nacional del Carbón (INCAR, CSIC), Oviedo, 33001 Spain

Abstract: We report the synthesis of conductive and mechanically compliant monolithic carbon aerogels prepared by the sol-gel polycondensation of the melamine-resorcinol-formaldehyde mixtures by incorporating diatomite and carbon black additives. The resulting aerogels composites displayed a well-developed porous structure, confirming that the polymerization of the precursors is not impeded in the presence of either additive. The aerogels retained the porous structure after etching off the siliceous additive, indicating the adequate cross-linking of the MRF reactants. However, the presence of diatomite caused a significant fall in the pore volumes, accompanied by the coarsening of the average pore size (predominance of large mesopores and macropores). The diatomite also prevented the structural shrinkage and deformation of the as-prepared monoliths upon densification by carbonization, even after removal of the siliceous framework. The rigid pristine aerogels became more flexible upon the incorporation of the diatomite, favoring the implementation of binderless monolithic aerogel electrodes.

3.3.1. Introduction

The flexible coordination chemistry of carbon atoms coupled to recent advances in the field of synthetic chemistry have contributed to develop highly featured carbon materials with an unforeseen control of their physicochemical and structural properties (in terms of particle size and shape, uniform porous void, and so forth), that offer unexpected opportunities in many science and engineering fields beyond traditional uses [1-3]. Creative approaches have been reported in the literature in recent years for the synthesis of carbon materials which offer specific benefits compared to traditional ones related to lower costs, greater design flexibility and high performance [1, 2]. Among different

strategies, the synthesis of carbon aerogels from the sol-gel polycondensation of resorcinol-formaldehyde mixtures (and some other precursors) has caught the attention of numerous research groups, because of the unique combination of physicochemical and structural properties of the resulting carbon materials such as controllable pore structure, high electrical conductivity, relatively low cost, and high surface area and porosity [4–8]. Indeed, after the early works of Pekala and coworkers [9,10], the interest for these solids has raised and much research efforts have been devoted to analyze the effect of the synthesis conditions on the morphological and porous structure of carbon gels and consequently on their performance [8,11-13].

Carbon aerogels seem particularly promising materials for electrochemical applications as they comply with the requirements typically needed for instance for the energy storage in electrochemical devices (i.e., supercapacitors) or the electroassisted removal of ionic species from solution (i.e., capacitive deionization), namely high surface area to form the electric double layer, resiliency to electrochemical oxidation/reduction, stability under different electrolytes, and so forth [14-16].

The technological applications in electrochemistry of carbon aerogels have often been limited by their poor mechanical properties and electrical conductivity [17-20]. Although nanoporous carbon aerogels typically exhibit higher electrical conductivity than other types of aerogels (which are mostly insulators), the conductivity of resorcinol-formaldehyde derived carbon aerogels is still a drawback [21,22]. Hence, despite their a priori favorable characteristics -in terms of porosity and resiliency to electrochemical modification-, carbon aerogels usually present low current and ionic removal efficiencies [15,16,23,24]. On the other hand, it is well known that the electrical properties of carbon materials are directly related to their structure; most carbon precursors are generally good insulators due to the high ratio of sp^3 bonded carbon atoms [3,25]. The electrical conductivity of carbon materials increases with the density of conjugated sp^2 carbon atoms (that may be raised upon thermal treatment of the precursors at temperatures above 1000ºC) and the degree of structural order of the separate conjugated systems to interconnect forming a conducting network [3,25]. However, combining high porosity and electrical conductivity is still challenging, and the lack of conductivity of nanoporous carbons is usually overcome by using small amounts of carbon black as low cost conductive additive in the manufacture of the electrodes, to lower the resistance and thus

enhancing the electrodes performance [23]. Also, the mechanical stiffness of monolithic electrodes is the main reason for the prevalence of the use of electrodes in powder form.

Resorcinol-formaldehyde aerogels are usually fragile materials, although the mechanical stiffness is largely related to the cross-linking degree of the precursors and the porosity of the aerogels [9,20,24]. Organic hydrogels are mechanically reinforced upon carbonization at high temperature to render denser carbon gels, that become more rigid (although typical Young modules are still a factor of 100-1000 lower than those of silica glass) but their deformation capacity decreases [9,20,24]. In a previous study we reported the good electrochemical performance of binderless monolithic aerogel electrodes over powdered materials due to the combination of a nanoporous structure interconnected with a macroporous network [26-28]; their technological implementation at large scale was, however, limited due to the large shrinkage and deformation of the pieces after the carbonization; the contact between the bent monolithic electrodes and the current collector was compromised, leading to important efficiency losses due to resistance.

Aiming at fabricating large monolithic electrodes with improved mechanical properties without compromising the porosity and conductivity, we herein report the preparation of carbon aerogel monoliths with enhanced mechanical properties by using low cost structure and conductive additives: diatomaceous earth and carbon black. The synthesis route is a simple modification of the conventional one [9], and consists on allowing the sol-gel polymerization of the precursors (melamine-resorcinol-formaldehyde) in the presence of the additives. Data has shown that the obtained aerogel composites displayed a highly porous structure, and improved electrical conductivity and mechanical properties provided by the additives, even after the removal of the sacrificial siliceous framework. The incorporation of the diatomite during the synthesis prevented the deformation of the electrodes upon densification by carbonization; such mechanical compliance may contribute to the implementation of binderless monolithic aerogel electrodes.

3.3.2. **Results and Discussion**

3.3.2.1. Characterization of the aerogels

In a previous study we reported the two-step synthesis of N-doped carbon aerogels based on the prepolymerization of resorcinol-formaldehyde-melamine (MRF) mixtures [26,27]. Regardless the solution pH and M/R molar ratio, the hydrogels prepared by the conventional one-step route displayed essentially a microporous character, as opposed to the meso-/macroporous network of those prepared upon the prepolymerization of the precursors. These MRF aerogels presented promising electrochemical features due to a unique pore structure dominated by large pores, and an improved wettability provided by the presence of N-surface groups. The materials still displayed poor electrical conductivity (although superior than that of RF aerogels) and limited mechanical characteristics (large deformation and bending upon carbonization), for which the use of large monolithic electrodes was still quite challenging.

We herein report a simple modification of the above-mentioned method for the synthesis of MRF aerogels consisting on carrying out the sol-gel polymerization of the precursors in the presence of two additives: diatomaceous earth as low cost sacrificial structural additive to improve the stiffness of the aerogels, and a carbon black -commonly used in electrochemical applications- to increase the conductivity of the materials. The diatomite (D) used (Nanolit, K6) is a fine-grained siliceous sediment of biogenic origin (skeletal remains of microscopic single-celled diatoms; average particle size 12 μm; chemical composition: 89.2 wt.% SiO_2, 4 wt.% Al_2O_3, 1.7 wt.% Fe_2O_3, 0.5 wt.% CaO, 0.3wt.% MgO); the carbon black (B) additive (Superior Graphite Co.; average particle size 6 μm; ash content below 0.05 wt.%, volatiles below 0.15 wt.%) is characterized by a high electrical conductivity (ca. 10 mS/cm). The presence of diatomite and carbon black in the aerogels is indicated by either “D” or “B”, respectively. The diatomite has been etched off (using HF), unless otherwise stated.

Figure 1 shows SEM images of the carbon aerogels evidencing the differences at a macroscopic scale depending on the presence the additives during the synthesis. All the aerogels prepared in the presence of diatomite (samples CG-D and CG-DB) presented similar SEM images, and are characterized by a relatively rough surface with large holes, likely inherited from the siliceous additive.

At converse, the MRF aerogels displayed a smooth compact surface formed by densely packed spherical particles. This observation is in agreement with the bulk density values of the monoliths compiled in Table 1. While CG and HG materials featured the

low density values expected for aerogels, CG-D and CG-DB displayed values close to 0.15 g cm^{-3}, likely due to the large voids created after removal of the diatomite. The presence of the nanometric particles of carbon black can be seen in the TEM images in Figure 2 at different magnifications, where the characteristic spherical aggregates of the carbon black particles (seen also as black spots in the low magnification images) appear distributed within the disordered carbon matrix of the aerogels. The aggregates have varied sizes, and are also seen in the samples before the HF etching treatment.

Table 1. Main textural characteristics of the monolithic aerogels obtained from N_2 adsorption isotherms at -196 ºC. Aerogels before (HG) and after (CG) carbonization are compared.

Sample (*)	Bulk density [g cm^{-3}]	S_{BET} [A] [m^2g^{-1}]	V_{TOTAL} [B] [cm^3g^{-1}]	$V_{MICROPORES}$ [B] [cm^3g^{-1}]	$V_{MESOPORES}$ [C] [cm^3g^{-1}]
HG	0.41	212	1.44	0.07	1.30
HG-D	0.64	101	0.58	0.04	0.51
HG-DB	0.63	237	0.51	0.05	0.45
CG	0.52	522	1.55	0.19	1.30
CG-D (non etched)	0.50	230	0.85	0.09	0.74
CG-D	0.15	409	1.23	0.16	0.99
CG-DB (non etched)	0.53	118	0.41	0.05	0.35
CG-DB	0.16	470	0.75	0.17	0.54
Diatomite	--	28	0.08	0.01	0.07
Carbon Black	--	23	0.17	0.01	0.16

[A] Apparent surface area evaluated using BET

[B] Micropore volume evaluated using the DR method

[C] Mesopore volume evaluated from 2D-NLDFT-HS method

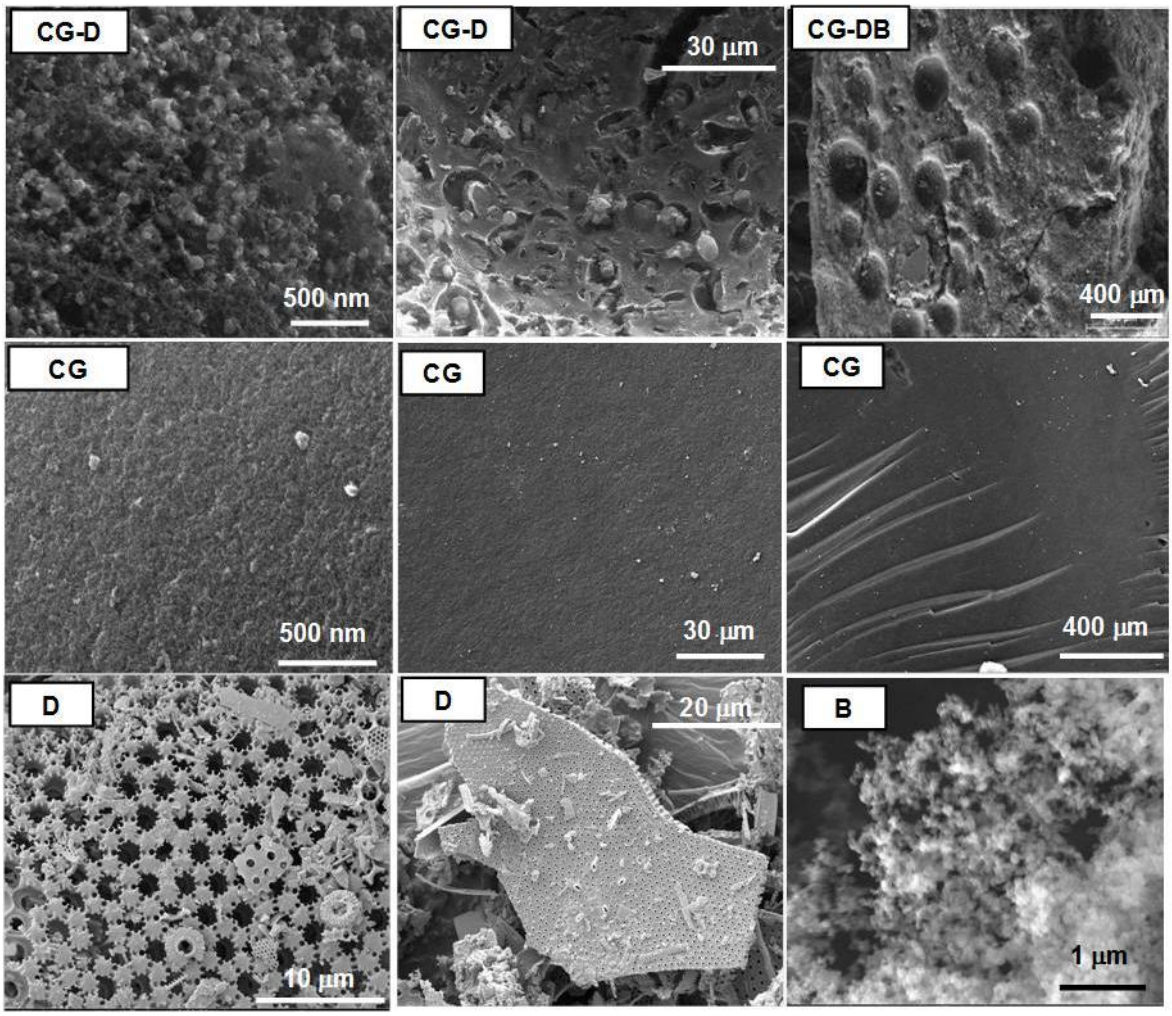
CG-D
500 nm
CG-D
30 μm
CG-DB
400 μm
CG
500 nm
CG
30 μm
CG
400 μm
D
10 μm
D
20 μm
B
1 μm

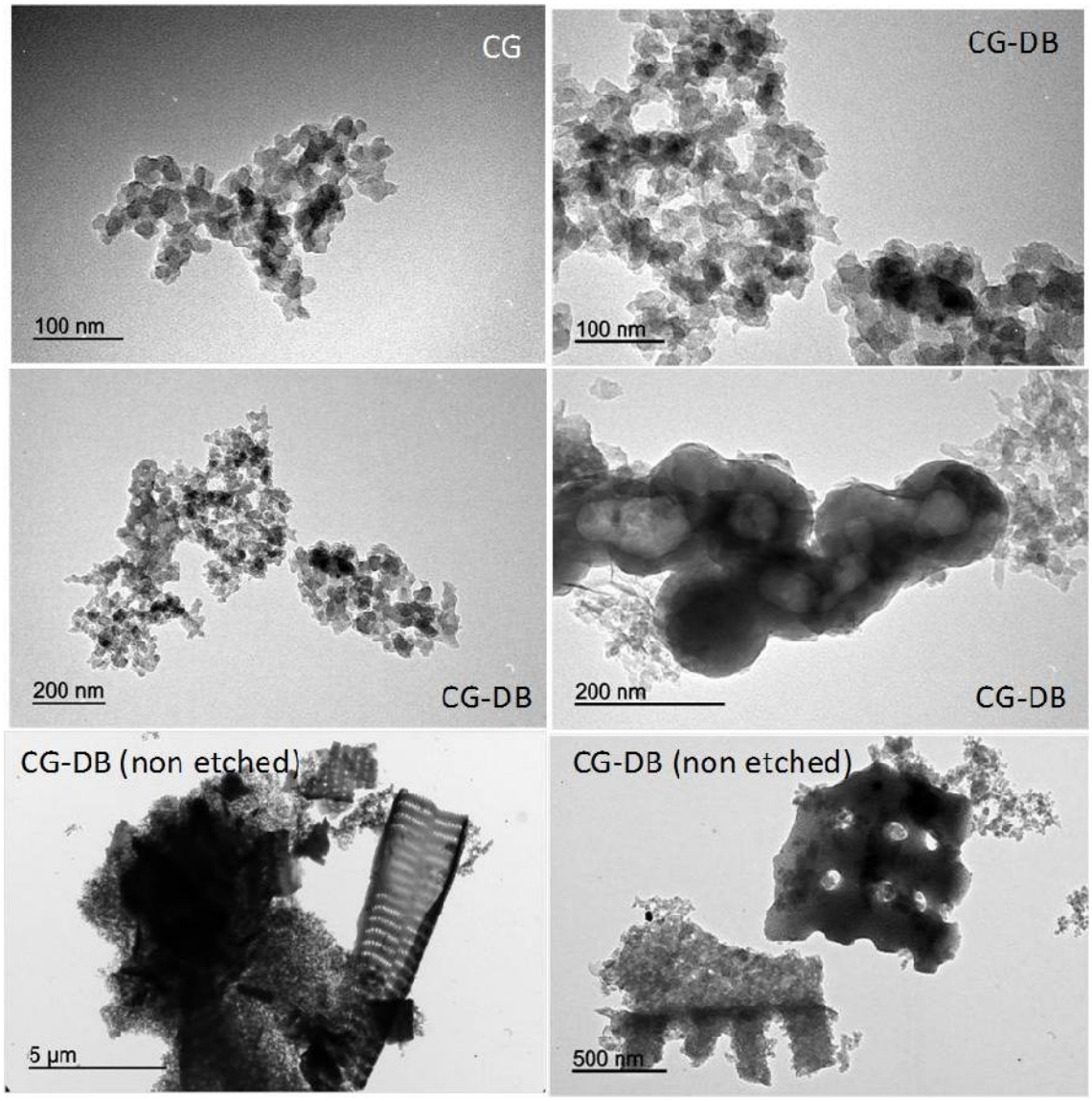
CG
100 nm
CG-DB
100 nm
200 nm
CG-DB
200 nm
CG-DB
CG-DB (non etched)
5 µm
CG-DB (non etched)
500 nm

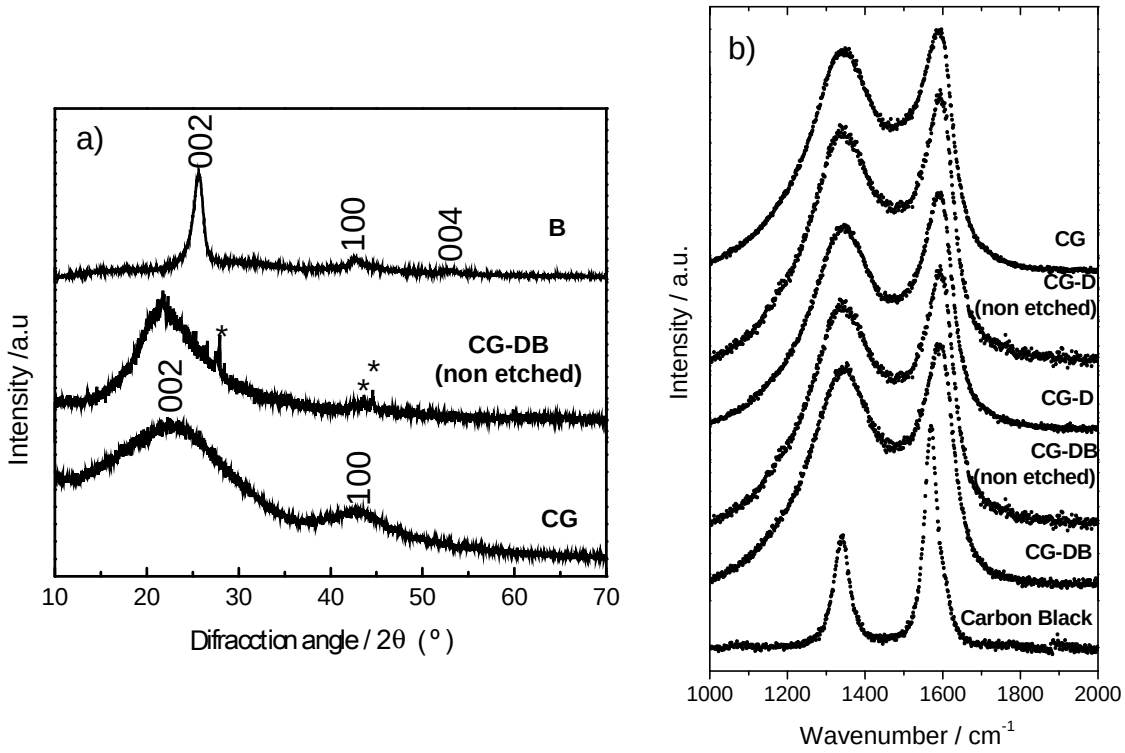

	I_D / I_G	D shift [cm^{-1}]	G shift [cm^{-1}]	D FWHM [cm^{-1}]	G FWHM [cm^{-1}]
CG	2.08	1347.14	1595.57	177.13	72.73
CG-D (non etched)	1.85	1346.80	1597.32	178.01	73.75
CG-D	1.95	1346.37	1595.64	179.68	70.96
CG-DB (non etched)	1.76	1346.34	1598.00	181.67	75.06
CG-DB	1.82	1347.56	1596.95	169.13	71.37
B	0.62	1340.23	1569.63	42.73	35.24

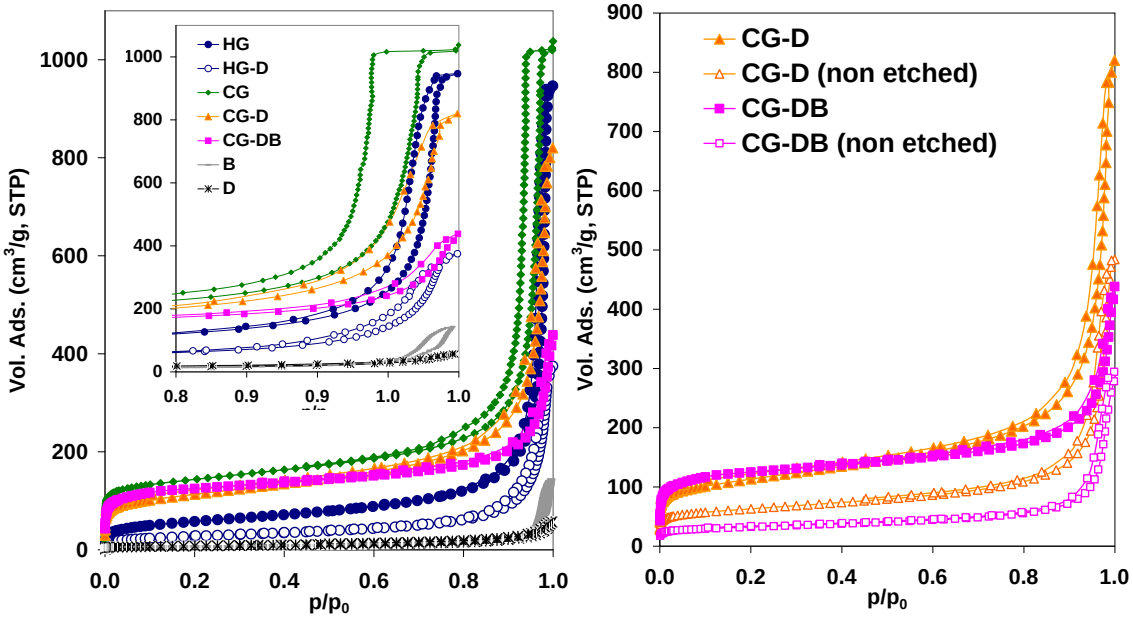
Vol. Ads. (cm3/g, STP)
p/p0
HG
HG-D
CG
CG-D
CG-DB
B
D
CG-D
CG-D (non etched)
CG-DB
CG-DB (non etched)

the aerogels retain the porous structure after etching off the siliceous additive (the porous structure does not collapse), confirming that the porosity is due to the adequate cross-linking of the MRF reactants. The large pore volumes and hysteresis loops suggest that the polycondensation of the monomers is slowed down in the presence of the additives (either B or D), as already observed in the case of carbon black alone [21,26,28]. This would lead to a lower degree of cross-linking of the monomers, generating weakly branched clusters that tend to form larger colloidal aggregates in progressively larger pores (pore coarsening) [1,4].

On the other hand, a significant fall in the pore volumes was observed for the samples synthesized in the presence of the diatomite, even after the HF etching (Table 1). This affected the whole range of relative pressures, hence D-containing aerogels displayed lower surface area values than the pristine materials. Otherwise, the addition of carbon black along with the diatomite (sample CG-DB) yielded a decrease in the mesopore volume (compared to CG-D); this contrasts with the trend observed for other composite aerogels prepared when only carbon black is used as additive, that led to an increase in the pore volume in the mesopore range [21,26,28]. When the polycondensation of the reactants is carried out in the presence of both D and B, still the formation of large pores is dominant, which is indicative of the formation of weakly branched clusters during the polymerization reaction; the low pore volumes (compared to D- or B-containing aerogels) suggest that the extent of the assembling of the clusters in large aggregates is partially hindered by the large amount of diatomite.

Further information on the nanotexture of the synthesized aerogels was obtained from the analysis of the pore size distribution. Figure 5a shows the distributions obtained by analysis of the N_2 adsorption data corresponding to the carbon aerogels after carbonization and removal of the diatomite, as these are the samples of interest for electrochemical applications. In agreement with the shape of the isotherms (i.e., position of the hysteresis loops), the effect of the additives is most remarkably noticed in the distribution of larger pores.

The pristine aerogel (sample CG) displayed the typical monodispersed distribution of pore sizes in the mesopore range, with the average mesopore size around 18 nm [21,22]. In contrast, the composite aerogels treated with diatomite and carbon black displayed a broad distribution in the mesopore range, between 5 to 40 nm. Additionally, the

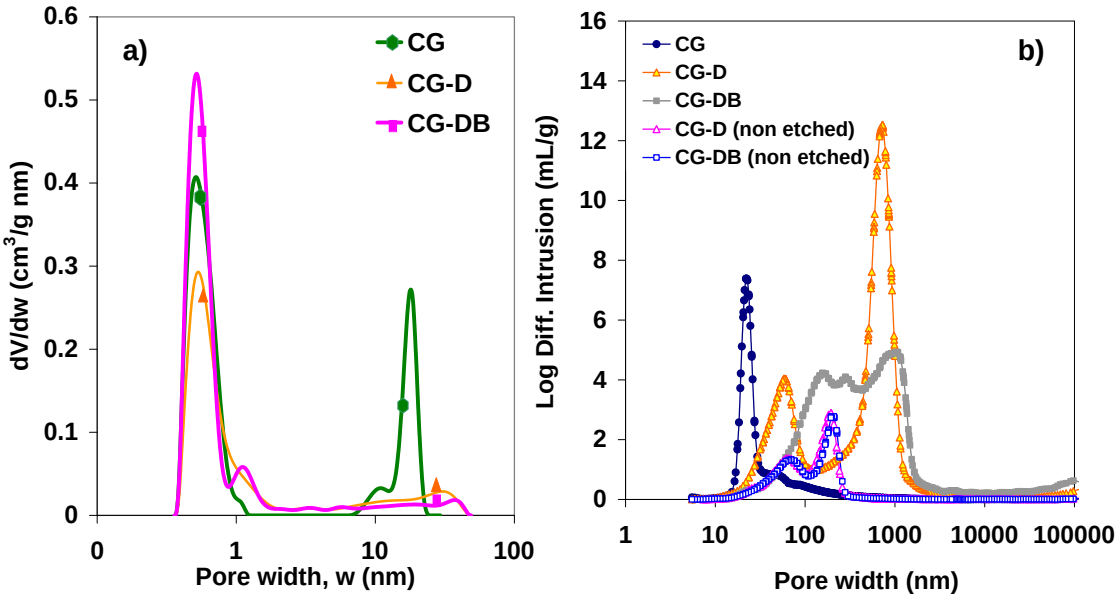
a)
CG
CG-D
CG-DB
dV/dw (cm3/g nm)
Pore width, w (nm)
0.6
0.5
0.4
0.3
0.2
0.1
0
0
1
10
100
b)
CG
CG-D
CG-DB
CG-D (non etched)
CG-DB (non etched)
Log Diff. Intrusion (mL/g)
Pore width (nm)
16
14
12
10
8
6
4
2
0
1
10
100
1000
10000
100000

pore structure of the aerogels provided by the diatomite (Figure 5b), which would facilitate the evolution of the volatiles upon carbonization.

Table 3. Shrinkage after carbonization (in C-series) of the aerogels and response to the Crushing Strength Tests. The initial dimensions of all the specimens were ca. 5 cm.

Sample	Shrinkage * (%)	Rigidity[§] [N/mm]	Maximum Load[§] [N]	Toughness[§] [N mm]	Behaviour on Crushing Strength Tests[§§]
HG	--	324	17	1.2	Brittle, fracture upon load of 21N
CG	30.8	456	28	0.8	Brittle, fracture upon load of 14 N
CG-D	5.4	65	23	3.2	Flexible, no fracture after loading at 30N
CG-DB	5.2	27	10	2.9	Flexible, no fracture after loading at 30N

[§] calculated from the Load Displacement Curves (see experimental section)

[§§] evaluated from the Crushing Strength Tests (compression up to 30 N) of the spherical specimens

These differences in the consistency of the aerogels depending on the use of additives were corroborated by the mechanical tests (performed on the samples of electrochemical interest after etching off the diatomite). First of all we applied a Crushing Strength Test as a screening tool to evaluate the resistance of the materials to fracture upon applying a force up to 30 N [31]. The pristine aerogels (HG and CG) showed the behavior of a rigid material (similar to that of non porous phenol-formaldehyde resins) with a conchoidal fracture after compression above 30 N (Figure 6, Table 2). At converse, the aerogels synthesized in the presence of the D followed a different pattern, being gradually deformed with increasing the load. The characteristic fingerprint left by the load is shown in the images in Figure 6 for CG-D (a similar behavior was obtained for all the materials prepared in the presence of the D additive); the absence of fracture after 30 N evidences the somewhat flexible character of the aerogels that undergo deformation upon the strength without fracture.

The mechanical properties were also investigated by means of Small Punch Tests [27, 32]. Figure 7 shows the effect of both additives on the load-displacement curves (LDC) from biaxially stretched tests performed on the aerogels. The change from a stiff and brittle behavior of samples HG and CG to a compliant and flexible character of the materials when the diatomite was used as additive in the synthesis is seen in the differences in the shape of the LDC curves. For the aerogels without D, a linear load-displacement behavior with a steep slope is observed, followed by an abrupt drop of load

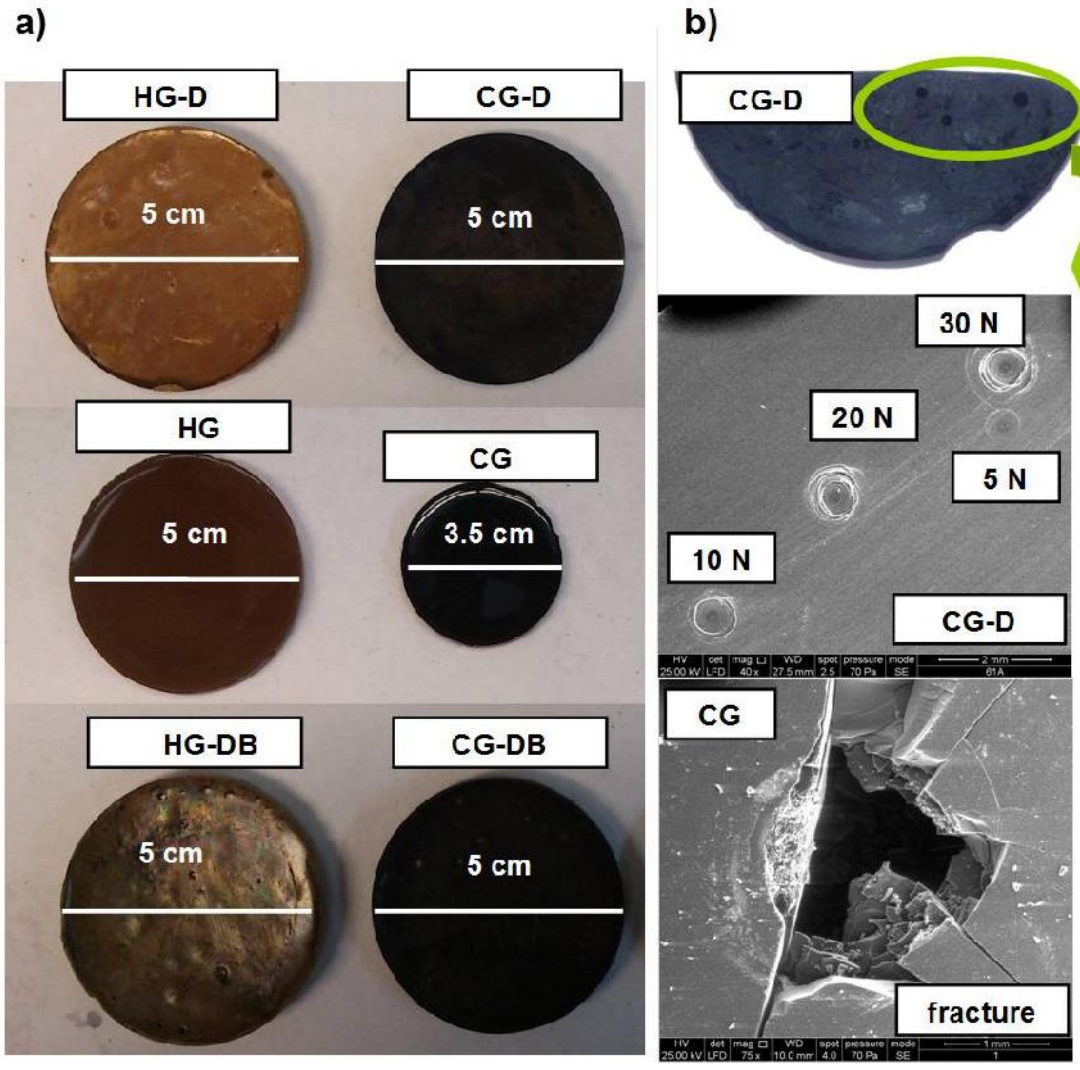
a)
HG-D
CG-D
5 cm
5 cm
HG
CG
5 cm
3.5 cm
HG-DB
CG-DB
5 cm
5 cm
b)
CG-D
30 N
20 N
5 N
10 N
CG-D
CG
fracture

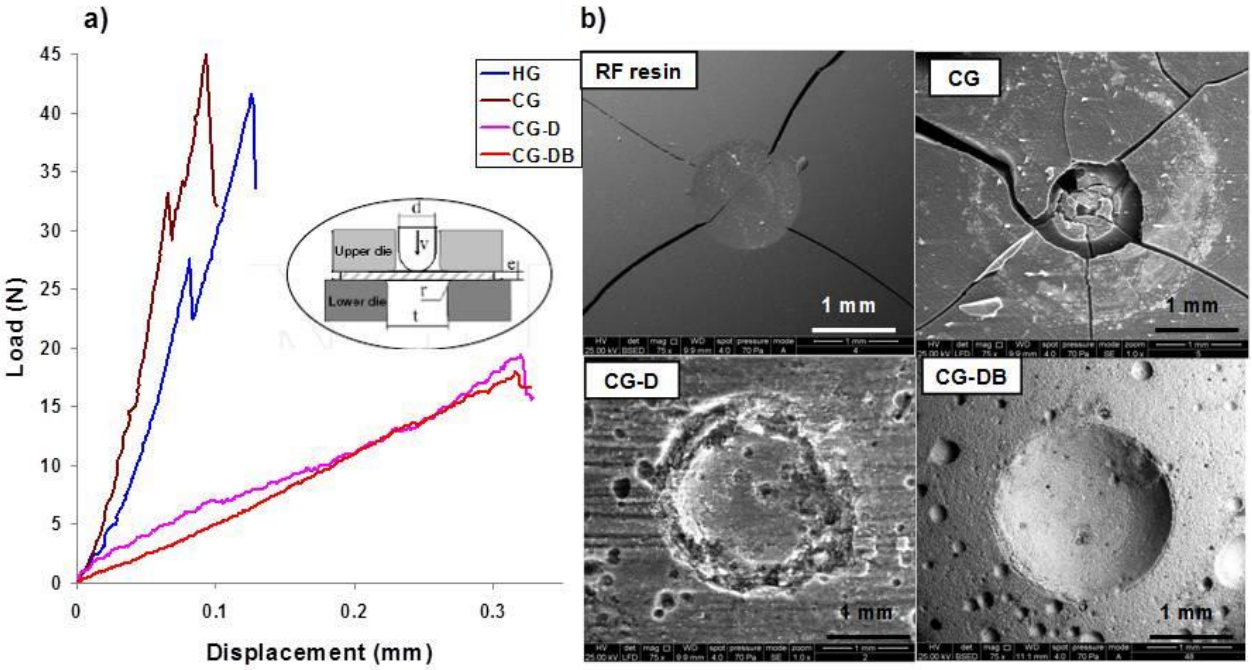
a)
b)
Load (N)
Displacement (mm)
HG
CG
CG-D
CG-DB
Upper die
Lower die
RF resin
CG
CG-D
CG-DB
1 mm

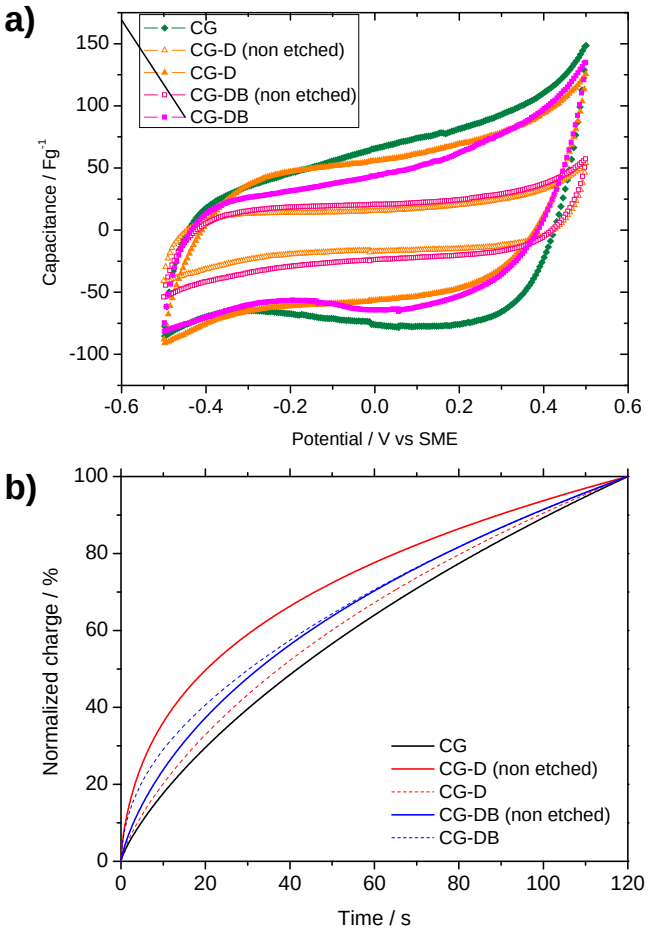
a)
CG
CG-D (non etched)
CG-D
CG-DB (non etched)
CG-DB
Capacitance / Fg-1
Potential / V vs SME
b)
Normalized charge / %
Time / s
CG
CG-D (non etched)
CG-D
CG-DB (non etched)
CG-DB

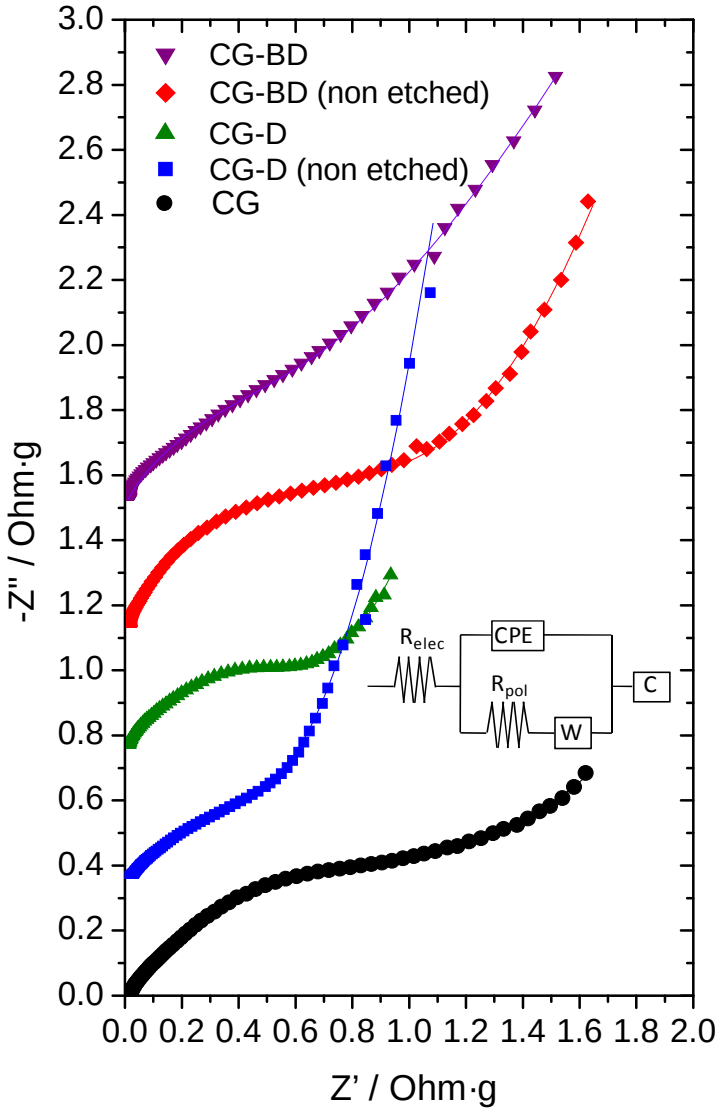
CG-BD
CG-BD (non etched)
CG-D
CG-D (non etched)
CG
-Z'' / Ohm·g
Z' / Ohm·g
0.0 0.2 0.4 0.6 0.8 1.0 1.2 1.4 1.6 1.8 2.0
0.0 0.2 0.4 0.6 0.8 1.0 1.2 1.4 1.6 1.8 2.0 2.2 2.4 2.6 2.8 3.0
R_elec
CPE
R_pol
W
C

diatomite-treated samples. This behavior can be explained in terms of the rate of EDL build up and saturation in the samples with different porosity: the seen, samples CG-D and CG-BD non etched saturate faster with ions from the electrolyte than the most porous ones.

Impedance spectra allow the determination of the internal resistance of the electrodes to the electroadsorption of ions. By assuming a mixed kinetic and charge transfer control, the kinetic response at the electrode-electrolyte interface can be correlated to both the electrical conductivity and ion accessibility to inner pores.

The Nyquist plots recorded for the aerogels are shown in Figure 9; these profiles are largely affected by the polycrystalline and highly porous texture of the electrodes; therefore, a numerical fitting to an equivalent circuit is required for a quantitative discussion (see inset in Figure 9). The different components of the equivalent circuit used are the electrolyte solution resistance (R_{el}), the Warburg impedance (W), a constant phase element (CPE), a capacitor (C) and the polarization resistance (R_{pol}). The latter parameter is mainly responsible for the resistance to the ionic migration into porous structure. The highest R_{pol} value was recorded for the CG sample (1.52 Ohm·g), while an effective decrease in the resistance was observed for the samples still containing diatomite. Thus, R_{pol} values of 0.68 and 1.1 Ohm·g were calculated before etching off the diatomite additive in samples CG-D and CG-DB, respectively. A slight increase in the resistance was observed for sample CG-D (0.74 Ohm·g) after the removal of the additive; we attribute this behavior to an improvement in the accessibility of ions to pores of small sizes (microporosity) that would remain blocked by the additive. For sample CG-DB, the R_{pol} value (0.90 Ohm·g) was slightly better than that of its corresponding non-etched counterpart, pointing out the beneficial effect of the carbon black, as a result of an enhanced conductivity and the presence of pores of wider sizes (Figure 5).

This was further supported by the electrical conductivity values measured on the monoliths, which is mainly controlled by the presence carbon black; after etching off the diatomite (insulator), the electrodes presented conductivity values close to those reported for carbon aerogels prepared without the siliceous additive, although differences also depend on the formulations (ca. N-doped aerogels display higher conductivity than RF ones) [21,26,28]. Values ranged from 2.1 mS/cm for sample CG; 2.2 mS/cm for sample CG-D and 4.3 mS/cm sample CG-DB.

3.3.3. Conclusions

We have synthesized mechanically compliant monolithic carbon aerogels with improved electrical conductivity by using diatomite and carbon black as structure and conductive additives, respectively. A simple modification of the conventional route for the preparation of melamine-resorcinol-formaldehyde aerogels by sol-gel procedures is proposed based on allowing the polymerization of the reactants in the presence of the additives. The resulting aerogel composites displayed a well-developed porous structure, confirming that the polymerization of the precursors is not impeded by the presence of large amount of additives (ca. 50 wt.% in the case of diatomite). Furthermore, the aerogels preserved a porous structure after the removal of the siliceous sacrificial additive by HF treatment, confirming that the porosity arises from the cross-linking of the reactants during polycondensation reactions.

The presence of the additives, however, caused a drop of the pore volumes along with the coarsening of the average pore size. Indeed, the aerogels prepared by allowing the polymerization in the presence of the additives are predominantly mesoporous (large mesopores), although microporosity is also developed to some extent (again confirming the adequate polymerization of the MRF monomers in the reactant's mixture). The effect is more pronounced for the case of D (compared to B), likely due to the large amount used.

Diatomite prevented the structural shrinkage of the as-prepared monoliths upon densification by carbonization, even after etching off the siliceous framework, due to the open pore structure of the additive. The as-prepared monoliths showed the characteristic rigid behavior or MRF aerogels, whereas those obtained in the presence of D displayed a flexible character, with higher maximum loading values and resiliency to fracture upon loads of 30 N. These characteristics evidence that the templating effect of diatomite as antishrinkage agent (structural additive), coupled with the presence of low amounts of carbon black as conductive additive allow the preparation of flexible monolithic carbon aerogel electrodes with a good performance for the electrochemical removal of ions from solution in terms of low polarization resistance and fast electroadsorption. As for the desalting capacity, the development of a large macroporous network of the materials prepared in the presence of the diatomite (at expenses of microporosity) resulted in lower

capacitance values. Further work is currently ongoing aiming at enhancing the capacitance values (via activation).

3.3.4. Experimental Section

3.3.4.1. Synthesis of the aerogels

Hydrogels were synthesized by the polycondensation of Melamine (M), Resorcinol (R) and Formaldehyde (F) using sodium carbonate as catalyst (C) and deionized water (W) as solvent. Carbon black (CB, Superior Graphite Co., electrical conductivity ca. 10 S/cm) and diatomite (Nanolit K-6, Nanoquimia S.L.) were used as conductive and anti-shrinkage additives, respectively. The molar ratios of the reactants used in the preparation of the gels were (M+R)/C of 135 and (M+R)/W of 0.052. The final pH of the precursors was eventually adjusted at 7.4 by adding acetic acid or sodium carbonate, respectively. For the MRF series, the samples were synthesized following a prepolymerization procedure described elsewhere [26]. Briefly, a solution containing R, F, C and W (solution A) was stirred for 1 h at 40 ºC. Separately, a solution containing M, F, W and C (solution B) was stirred for 30 min at 70 ºC. Subsequently, solutions A and B were mixed together and stirred for 20 minutes at room temperature to further allow the cross-linking of the precursors. Before gelification, diatomite (50%w/v) and/or carbon black (ca. 0.9 wt.%) were added and kneaded to ensure a homogeneous dispersion. After the gelation step, a controlled water–acetone exchange was carried out, and the hydrogels were supercritically dried with CO_2. Finally the aerogels were carbonized under nitrogen atmosphere (ca. 800ºC using a heating ramp of 2 ºC min^{-1}) to obtain denser carbon aerogels. In the case of the samples incorporating the diatomite, an additional etching off the siliceous additive was performed using HF, leaving a silica free monolithic carbon aerogel (unless otherwise stated). For the sake of comparison, carbon aerogels prepared by the same synthetic route without the incorporation of the additives were also prepared; as well as samples with the diatomaceous additive before the HF etching (labeled as “non etched”). The nomenclature of the samples is HG for hydrogels before carbonization and CG for the carbonized samples. The presence of Diatomite and Carbon Black in the samples is indicated by adding “D” or “B” to the nomenclature.

3.3.4.2. Textural and morphological characterization

The porosity of the samples was measured by N_2 adsorption isotherms at -196 ºC using a volumetric analyzer (Micromeritics ASAP 2020); the samples were previously outgassed under vacuum (ca. 10^{-3} Torr) at 120 °C overnight. For all isotherms, warm and cold free-space correction measurements were performed by using ultrahigh purity He gas (grade 5.0, 99.999% purity).Ultrahigh purity N_2 (i.e., 99.9992%) was provided by Air Products. The isotherms were used to calculate the specific surface area (S_{BET}) and pore volumes (V_{total} and micropore volume, Wo, using the Dubinin–Radushkevich equation). The pore size distributions were calculated by using the new 2D-NLDFT-HS model for carbons with energetically heterogeneous and geometrically corrugated pore walls [33,34] that gives an excellent fit to the experimental data and is free of common artifacts usually obtained in the PSD analysis when the standard NLDFT model is used. The morphology of the samples was observed by Field Emission Gun Scanning Electron Microscopy (FEG-SEM) with an X-ray Energy-Dispersive System (EDS) in a JEOL JSM-7001F, and in a FE-SEM apparatus (QuantaSEM, FEI), using an accelerating voltage of 25 kV. Transmission electron microscopy (TEM) micrographs were obtained by using a JEOL-JEM2010 instrument. Analyses were performed after the samples were dispersed in acetone. X-Ray diffraction (XRD) patterns were recorded on a Siemens D5000 diffractometer equipped with a graphite monochromator and Cu Kα radiation operating at 40 kV and 30 mA. The samples were scanned between 10º and 90º (2θ) at a 0.02◦/12 s scan rate. Raman spectra were recorded with a Renishaw Raman instrument (InVia Raman Microscope), equipped with a Leica microscope. The samples were acquired by excitation with a green laser light at 532 nm and the spectra were recorded between 1000 and 2000 cm^{-1}. The spectra were deconvoluted by using Peakfit software package.

3.3.4.3. Crushing Strength Test

The Crushing Strength Tests were carried out by applying a normal force (up to 30 N) to the as-prepared monoliths. This allows the evaluation of the resistance of the materials to fracture under a compressive strength limit, while measuring the characteristic fingerprint on the material upon deformation and/or fracture [31].

3.3.4.4. Small Punch Tests

Small Punch Tests were performed under quasi-statical conditions with a low speed tensile test machine on 1x1cm square specimens of 2-3 mm thickness [32]. The specimens were polished to control the thickness and to obtain a flat surface, and framed in a resin framework (1 x 1 mm) surrounding the material while leaving the surface of the material uncovering to allow the contact with the punch head. The test consisted on fixing the specimen between two dies (initial load of 2 N), and then deforming the specimen quasi-statically up to failure by means of a small semi-spherical punch with a head of 2 mm of diameter (biaxial expansion). The test is speed controlled with a punching speed of 0.2 mm/min. The displacement of the punch is measured by means of an extensometer, and after correction of the flexibility of the testing device, the displacement of the central point of the specimen is calculated. Thus, the characteristic load displacement curve (LDC) of each material is obtained; this curve represents the force exerted from punch against the specimen (i.e. the load reaction) versus the displacement of the punch. From the profiles, the rigidity (slope of the curve before the first crack), maximum load (onset load of the first crack) and toughness (area under the curves up to maximum load) have been evaluated.

3.3.4.5. Electrochemical characterization

Cyclic voltammetry measurements were performed in SwagelokTM type cells using a three-electrode configuration. The working electrode was manufactured by spreading on a titanium disk a homogeneous slurry containing the aerogels (70%), carbon black as percolator (20%) and polyvinylidene fluoride binder (10%) in N-methyl pyrrolidone. A platinum wire was used as a counter electrode, and Hg/Hg_2SO_4 (SME) as reference electrode. Cyclic voltammograms were recorded between -500 and +500 mV vs SME at sweep rates ranging from 0.5 to 10 mV s^{-1} in a Biologic VMP multichannel potentiostat, in 0.1 M NaCl. Chronocoulometric curves were performed by inducing a potentiostatic pulse of 300 mV versus SME for 120 s and recording the transient current. Impedance spectra (EIS) allowed analyzing the kinetic response of the electrodes to the adsorption reaction; measurements were recorded in an Autolab PGSTAT12 system, using an AC voltage signal of 5 mV vs equilibrium potential over the frequency range of 25 kHz to 10

mHz. The electrical conductivity was measured on previously dried as-prepared monolithic samples; the specimens were packed between two metallic collectors and hold under constant pressure and a bias voltage between 0.2-1.2 V was applied (0.2V/s step for 120 s) using an Arbin MSTAT (Arbin Instruments Inc.) potentiostat. The resistance is calculated from the slope of the current-voltage profiles at each voltage.

3.3.5. References and Notes

[1] Lee, J.; Kim, J.; Hyeon, T. Recent Progress in the Synthesis of Porous Carbon Materials, *Adv. Mater*., 2006, *18*, 2073-2094.

[2] Hu, B.; Wang, K.; Wu, L.; H., Yu, S.; H.; Antonietti, M.; Titirici, M.M. Engineering Carbon Materials from the Hydrothermal Carbonization Process of Biomass. *Adv Mater*., **2002**, *2*, 813-828.

[3] Novel Carbon Adsorbents, J.M.D. Tascon (Ed.), Elsevier, Amsterdam, 2012.

[4] Al-Muhtaseb, S.A.; Ritter, J.A. Preparation and properties of resorcinol-formaldehyde organic and carbon gels, *Adv. Mater*., **2003**, *15*, 101-114.

Pajonk, G.M. Aerogel Catalysts, *Appl. Catal.*, **1991**, *72*, 217-66.

[5] Lee, Y.J.; Jung, J.C.; Park, S.; Seo, J.G.; Baeck, S.H.; Yoon, J.R.; Yi, J.; Song, I.K. Preparation and characterization of metal-doped carbon aerogel for supercapacitor, *Curr. Appl. Phys.*, **2010**, 10, 947-951.

[6] Szczurek A.; Amaral-Labat, G.; Fierro, V.; Pizzi A.; Masson, E.; Celzard A. The use of tannin to prepare carbon gels. Part I: Carbon Aerogels. *Carbon*, **2011**, 49, 2773-2784.

[7] Job, N.; Thery, A.; Pirard, R.; Marien, J.; Kocon, L.; Rouzaud, J.N.; Beguin, R.; Pirard, J.P. Carbon aerogels, cryogels and xerogels: Influence of the drying method on the textural properties of porous carbon materials, *Carbon*, **2005**, *43*, 2481-2494.

[8] Pekala, R.W. Organic aerogels from the polycondensation of resorcinol with formaldehyde, *J. Mater. Sci.*, **1989**, *24*, 3221-3227.

[9] Antonietti, M.; Fechler, N.; Fellinger, T.-P. Carbon Aerogels and Monoliths: Control of Porosity and Nanoarchitecture via Sol-Gel routes. *Chem. Mater.*, **2014**, *26*, 196-210.

[10] Wu, D.C.; Fu, R.W.; Zhang, S.T.; Dresselhaus, M.S.; Dresselhaus, G. Preparation of low-density carbon aerogels by ambient pressure drying, *Carbon*, **2004**, *42*, 2033-2039.

[11] Horikawa, T.; Hayashi, J.; Muroyama, K. Size control and characterization of spherical carbon aerogel particles from resorcinol-formaldehyde resin, *Carbon*, **2004**, *42*, 169-75.

[12] Pröbstle, H.; Wiener, M.; Fricke, J. Carbon aerogels for electrochemical double layer capacitors, *J. Porous Mater.* **2003**, *10*, 213-222.

[13] Hwang, S.W.; Hyaun, S.H. Capacitance control of carbon aerogel electrodes, *J. Non-Cryst. Solids*, **2004**, *347*, 238-245.

[14] Porada, S.; Zhao, R.; van der Wal, A.; Presser, V.; Biesheuvel, PM. *Prog. Mater. Sci.*, Review on the science and technology of water desalination by capacitive deionization.**2013**, *58*, 1388-1442.

[15] Zhao, R.; Biesheuvel, P.M.; Miedema, H.; Bruning, H.; van der Wal, A. Charge Efficiency: A Functional Tool to Probe the Double-Layer Structure Inside of Porous Electrodes and Application in the Modeling of Capacitive Deionization, *J. Phys. Chem. Lett*., **2010**, *1*, 205-210.

[16] Wang, J.; Zhang, S.Q.; Shen, J.; Guo, Y.Z.; Attai, S.M.; Zhou B.; Lai, Z.Q.; Zheng, G.Z.; GUI, Y.S.; Electrical Transport Properties of Carbon Aerogels, *J. Porous Materials*, **2001**, *8*, 167–170

[17] Martın, L., Oriol Osso, J.; Ricart, S.; Roig, A.; Garcia, O.; Sastre, R. Organo-modified silica aerogels and implications for material hydrophobicity and mechanical properties, *J. Mater. Chem.*, **2008**, *18*, 207-13.

[18] Lin, C.; Ritter, J.A.; Popov, B.N. Correlation of Double-Layer Capacitance with the Pore Structure of Sol-Gel Derived Carbon Xerogels, *J. Electrochem. Soc.* **1999**, *146*, 3639-3643.

[19] Morales-Torres, S; Maldonado-Hodar, F.J.; Perez-Cadenas, A.F.; Carrasco-Marın, F. Textural and mechanical characteristics of carbon aerogels synthesized by polymerization of resorcinol and formaldehyde using alkali carbonates as basification agents, *Phys. Chem. Chem. Phys.*, **2010**, *12*, 10365-10372.

[20] Macías, C.; Haro, M.; Rasines, G.; Parra, J.B.; Ania, C.O. Carbon-black directed synthesis of mesoporous aerogels, *Carbon*, **2013**, *63*, 487-97.

[21] Haro, M.; Rasines, G.; Macias, C.; Ania, C.O. Stability of a carbon gel electrode when used for the electro-assisted removal of ions from brackish water, *Carbon*, **2011**, *49*, 3723-3730.

[22] Pandolfo, A.G.; Hollenkamp, A.F. Carbon properties and their role in supercapacitors, *J. Power Sources*, **2006**, *157*, 11-27.

[23] Pekala, R.W.; Alviso, C.T.; LeMay, J.D. Organic aerogels: Microstructural dependence of mechanical properties in compression, *J. Non-Cryst. Solids*, **1990**, *125*, 67-75.

[24] Marsh, H.; Rodriguez-Reinoso, F. in Activated Carbons, Elsevier, 2006.

[25] Rasines, G.; Lavela, P.; Macias, C.; Zafra, M.C.; Tirado, J.L.; Ania, C.O. On the use of carbon black loaded N-doped carbon aerogel for the electrosorption of sodium chloride from saline water, *Electrochim Acta* **2015**, *170*, 154-163.

[26] Macías, C.; Rasines, G.; Garcia, T.E.; Rodriguez, C.; Lavela, P.; Tirado, J.L.; Ania, C.O. On the use of diatomite as antishrinkage additive in the preparation of monolithic carbon aerogels, *Carbon*, **2016**, *98*, 280-284.

[27] Rasines, G.; Lavela, P.; Macias, C.; Zafra, M.C.; Tirado, J.L.; Ania, C.O. Mesoporous carbon black-aerogel composites with optimized properties for the electro-assisted removal of sodium chloride from brackish water, *J. Electroanal. Chem.*, **2015**, *741*, 42-50.

[28] Ferrari, A.C.; and Robertson J. Interpretation of Raman spectra of disordered and amorphous carbon, *Phys Rev B*, **2000**, *61*, 14095–14107.

[29] Thommes, M.; Kaneko, K.; Neimark, A.V.; Olivier, J.P.; Rodriguez-Reinoso, F.; Rouquerol J.; Sing, K.S.W, Physisorption of gases, with special reference to the evaluation of surface area and pore size distribution (IUPAC Technical Report), Pure Appl. Chem. **2015**, *87*, 1051–1069.

[30] Bemrose, C.R.; Bridgewater, J. A review of attrition and attrition test methods, *Powder Technology* **1987**, *49*, 97-126.

[31] Rodríguez, C.; Arencón, D.; Belzunce, J.; Maspoch, M. Small punch test on the analysis of fracture behaviour of PLA-nanocomposite Films, *Polymer Testin,g* **2014**, *33*, 21-9.

[32] Jagiello, J.; Olivier, J.P. 2D-NLDFT Adsorption Models for Carbon Slit-Shaped Pores with Surface Energetical Heterogeneity and Geometrical Corrugation, Carbon **2013**, *55*, 70-80.

[33] Jagiello, J.; Olivier, J.P. Carbon Slit Pore Model Incorporating Surface Energetical Heterogeneity and Geometrical Corrugation, Adsorpt. **2013**, *19*, 777–783.


ACS
Sustainable
Chemistry & Engineering

3.4.1. Introduction

Highly porous carbon aerogels are nowadays a matter of subject because of their use as electrodes in adsorption/energy applications. They are outstanding materials because they combine beneficial adsorption properties and structural strength with suitable chemical stability and electronic conductivity.[1-5] Carbon aerogels are a cost effective solution in applications aiming ion removal, as capacitive deionization. Their high surface area and pore volume exert a crucial role as capacitive electrodes that physically adsorb ions from the electrolytic solution. This reversible process present remarkable advantages for brackish water desalination.[6-10] New strategies point out to optimal morphologies,[11, 12] innovative preparative routes,[13, 14]–and hybrid multifunctional materials for providing both an open structure and suitable electrochemical behavior.[15-17]

It could be expected that the use of anti-shrinkage additives, that limit the contraction of the aerogel upon carbonization and create a macroporous structure, may contribute favorably to improve their electrosorption behavior.[18] Diatomaceous earth is a non-toxic and low cost material typically used as reinforcing and anti-shrinkage additive preserving macroporosity.[19, 20] We have recently reported mechanically compliant and highly porous aerogels with enhanced electrical conductivity prepared in the presence of diatomaceous earth and carbon black as additives. These materials overcome the limitations of mechanical stiffness upon densification by carbonization, while maintaining outstanding porous features and improved electrical conductivity, both desirable characteristics for the implementation of the monolithic aerogels in electrochemical applications.[21] On the other hand, the reliability of N-doped carbons as electrodes for capacitive deionization has been evidenced.[22, 23]Also, the presence of a macropore structure in the monolithic configuration was revealed as a crucial factor for a fast electrosorption of ions during the salt deionization.[23]

Unfortunately, the sole use of diatomite templating treatment in carbon aerogels has demonstrated to be insufficient to increase capacitance in the first attempts, even if the kinetic response is clearly improved due to the macroporous structure. For this reason, we propose that the combination of capacitive effect from carbon aerogels and pseudo-faradaic reactions in transition metal compounds may contribute favorably to enhance the electropsortion capacities of new electrodes for capacitive deionization.[24]

Taking all this into account, the aim of this work was the preparation of hybrid manganese-N doped carbon aerogels with enhanced macroporosity for their application as electrodes for the electrosorption of NaCl from aqueous solution. The use of a pre-polymerization route allows an efficient polymerization of the precursors yielding highly mesoporous aerogels with high N-contents, while diatomite was also used as anti-shrinkage additive.

3.4.2. Experimental

Hydrogels were synthesized by the polycondensation of Melamine (M), Resorcinol (R) and Formaldehyde (F) using sodium carbonate as catalyst (C) and deionized water (W) as solvent. Carbon black (CB, Superior Graphite Co.) and diatomite (D, Nanolit K-6) were used as conductive and anti-shrinkage additives, respectively. The molar ratios of reactants were as follows: R:M:F of 2:1:7, (M+R)/C of 135 and (M+R)/W of 0.053. The final pH of the precursors was adjusted to 7.4 by adding sodium carbonate. The samples were synthesized according to a prepolymerization procedure described elsewhere.[23] Before gelification, diatomite (50%w/v) and/or carbon black (0.75% w/v) were added to the mixture and magnetically stirred to ensure a homogeneous dispersion. Hydrogels were then kept in an oven at 40 ºC for 24 h and then at 70 ºC for 120 h to allow gelation and aging. After a controlled water–acetone exchange, the hydrogels were supercritically dried with CO_2 and carbonized (ca. 2 ºC/min) at 480 ºC under nitrogen atmosphere. Since the diatomite is electrically non-conductive and may hinder the access of ions to the mesoporous system, it was etched-off using HF and leaving a silica free carbon monolith. Then, selected samples were doped with manganese by immersing the gel in a $Mn(NO_3)_2$ solution followed by heating up to 750 ºC for 120 min in CO_2 atmosphere. Samples will be named as MRF-X-Y-Z, where X,Y and Z respectively indicates the presence of manganese (Mn), diatomite (D) and carbon black (B), respectively.

Wettability was determined by measuring the contact angle between the electrolyte and the electrode material in both powdered and monolithic forms. It is calculated from the tangent angle of the liquid drop with a solid surface at the base. High resolution nitrogen adsorption/desorption isotherms at -196 ºC were measured for the samples in a

volumetric analyzer (ASAP 2010, Micromeritics) equipped with high-vacuum system, and three pressure transducers. The samples were degassed under vacuum at 120 ºC overnight prior to the adsorption measurements. Ultrahigh purity nitrogen (i.e., 99.9992%) was supplied by Air Products. Each isotherm measurement was performed in duplicate to guarantee the reproducibility and accuracy of the measurements (error was below 0.1%). The specific surface area, S_{BET} and total pore volume, V_T were calculated from the isotherms according to the Brunauer–Emmett–Teller theory, while the full micro-meso pore size distribution was calculated using the 2D-NLDFT-HS model [25] assuming surface heterogeneity of carbon pores.[26] Mercury porosimetry was performed in a Micromeritics Autopore IV apparatus working in the pressure range 1–2000 bars was used. X-Ray diffraction (XRD) patterns were recorded on a Siemens D5000 diffractometer equipped with a graphite monochromator and Cu K□ radiation. The samples were scanned between 10º and 90º (2□) at a 0.02◦/12 s scan rate. X-ray Photoelectron spectrometry was carried out in a XPS, SPECS Phobios 150MCD equipment provided with a X-ray monochromatic Al K (1486.61 eV) power source of 300 W (anode voltage of 12 kV). The base pressure in the ultra high vacuum chamber was 4×10^{-9} mbar. Binding energy values were referenced to the C 1s peak of the adventitious carbon at 284.6 eV before the spectra processing.[27] The accurate determination of the binding energy and relative contribution of the signals was achieved by decomposing the overall profile in Gauss–Lorentz curves with a CasaXPS software package. Elemental analysis was performed in Eurovector EA 3000 equipment. Scanning electron microscopy (SEM) was performed in a Quanta FEG 650 equipment furnished with a S/TEM detector. Transmission electron microscopy (TEM) images were recorded in a JEOL JEM 2010 microscope.

The electrochemical characterization of the carbon aerogel electrodes was performed in three-electrode Swagelok™ type cells. The working electrode consisted of a homogeneous mixture composed by the carbon active material (70 wt.%), carbon black (Superior graphite, 20 wt.%) and PVDF binder (10 wt.%) dispersed in N-methyl pyrrolidone. The slurry was cast on 13 mm titanium disks and dried at 70ºC overnight. A Hg/Hg_2SO_4 (SME) and a platinum wire were respectively used as reference and counter electrodes. The electrolyte was a 0.1 M NaCl solution in deionized water. Cyclic voltammograms and galvanostatic cycles were performed between -0.5 and +0.5 V versus

the reference electrode using a Biologic VMP multichannel potentiostat to control the process. Electrochemical impedance spectroscopy (EIS) was employed to determine the internal resistance at the electrode interphases. During the experiment, the cell is perturbed by an AC voltage signal of 5 mV vs equilibrium potential over the frequency range 25 kHz to 10 mHz.

A symmetrical batch-type cell was assembled to perform the capacitive deionization experiments. The electrodes were two monolithic aerogel electrodes weighing ca. 0.15 g and ca. 0.3 cm^3. Their surfaces were polished to ensure a good contact with the current collector. Then, the pieces were washed in deionized water for 30 minutes. The electrodes were sandwiched between titanium current collectors and separate by two Whatman glass GF/A fiber sheets. Then, they were immersed into 15 mL of a 0.025 M or 0.1 M NaCl solution magnetically stirred to favor mass transfer from the bulk solution to the electrode. The cell was charged by applying a potentiostatic pulse (0.9, 1.2 or 1.5 V for 120 or 150 min) using an Arbin BT2000 multichannel potentiostat. Afterwards, the electrodes were discharged at 0 V for the same period of time. A conductivity-meter Crison EC meter BASIC 30 was used to monitor the changes of the ionic conductivity.

3.4.3. Results and discussion

Figure 1 shows images of the monolithic carbon aerogel materials prepared in the presence and absence of the various additives used. A simple visual inspection of the pieces evidences the significant shrinkage (ca. 25-35 % reduction of diameter) of the specimen prepared in the absence of the diatomaceous anti-shrinkage additive, induced by the thermal treatment at 750ºC. On the contrary, when the siliceous additive was incorporated in the synthesis, the pieces preserved their size and shape after the carbonization and further washing with HF (ca. 5% reduction in the diameter of the specimens). The anti-shrinkage effect of the diatomite is not dependent on the formulation of the aerogel or the presence of the carbon black conductive additive.[23] In addition, the aerogels ranged from translucent (pristine MRF) to opaque when either B or D additives were used, due to the relatively large amounts of additives added. The wettability of carbon aerogels can be visualized in Fig. S1. These images reveal the

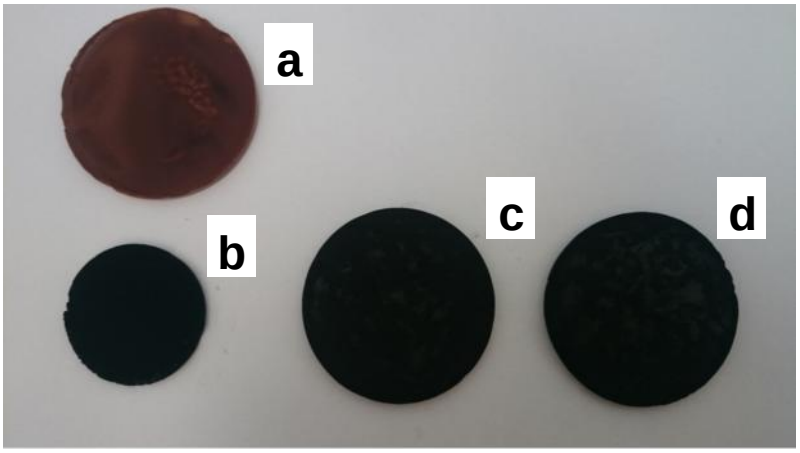
a
b
c
d

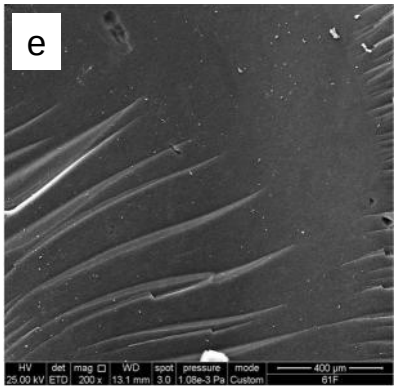
e
HV det mag WD spot pressure mode
25.00 kV ETD 200 x 13.1 mm 3.0 1.08e-3 Pa Custom
400 µm
61F

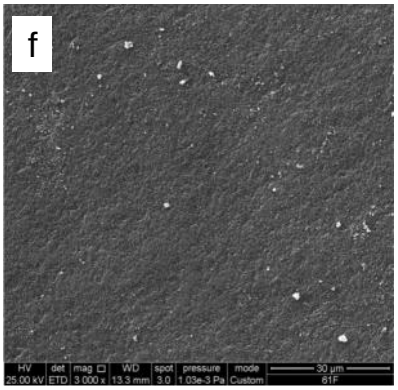
f
HV det mag WD spot pressure mode
25.00 kV ETD 3 000 x 13.3 mm 3.0 1.03e-3 Pa Custom
30 µm
61F

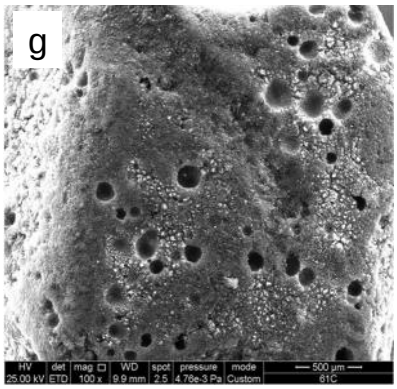
g
HV det mag WD spot pressure mode
25.00 kV ETD 100 x 9.9 mm 2.5 4.76e-3 Pa Custom
500 µm
61C

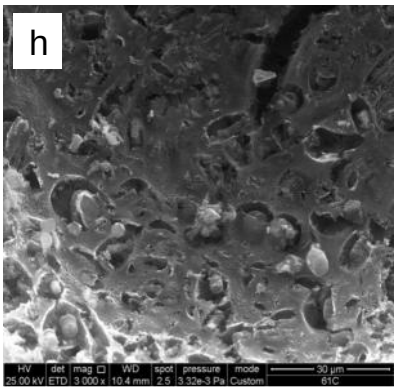
h
HV det mag WD spot pressure mode
25.00 kV ETD 3 000 x 10.4 mm 2.5 3.32e-3 Pa Custom
30 µm
61C

Table 1. Textural parameters of the composites containing N-doped carbon aerogels determined from the nitrogen isotherms at -196ºC, and monolith densities.

	S_{BET}	V_T [a]	V_{MIC} [b]	V_{MESO} [c]	Bulk density[d]
	$m^2\ g^{-1}$	$cm^3\ g^{-1}$	$cm^3\ g^{-1}$	$cm^3\ g^{-1}$	$g\ cm^{-3}$
MRF	679	1.58	0.21	1.35	0.40
MRF-Mn	844	1.96	0.25	1.76	0.40
MRF-Mn-D	862	1.17	0.29	0.86	0.15
MRF-Mn-D-CB	804	1.38	0.27	0.98	0.16

[a] total pore volume evaluated at $p/p_0 \sim 0.99$

[b, c] micro-, mesopore volume evaluated by the 2DNLDFT-HS method applied to the N_2 adsorption isotherms at 77 K

[d] Data calculated from the weight and geometrical dimensions of the monolith.

The incorporation of the diatomaceous additive created macropores, as seen in the SEM images (Figure 1). Sample MRF is characterized by a relatively smooth surface in which the carbon particles appear densely packed. At converse, MRF-Mn-D monolith displayed a rough surface with large holes, likely created during the etching off the diatomite after the acid washing. It was corroborated by the bulk density values of the monoliths (Table 1). Those samples prepared in the absence of additives -i.e., MRF and MRF-Mn-, featured a density value of 0.40 $cm^3\ g^{-1}$, similar to those reported in the literature.[28] Upon the incorporation of diatomite, there is a notorious decrease in the bulk density to values close to 0.15 $cm^3\ g^{-1}$, due to the large voids inherited from the additive. The TEM images show the dispersion of the metallic aggregates in the aerogel matrix (Figure S2, Supporting Information); MRF-Mn aerogel features typical aggregates with a

relatively compacted morphology which yield the mesoporous network. In the case of MRF-Mn-D-CB, the large voids are also observed, along to dark spots belonging to the manganese and/or carbon black particles.

Figure 2 shows the N_2 adsorption isotherms of the prepared materials; the main textural parameters are also compiled in Table 1. All the materials displayed high porous features, confirming that the incorporation of the additive (either B or D) does not hinder the polycondensation of the reactants.[29-31] All the materials displayed type IV isotherms according to IUPAC classification[32] with relatively high adsorbed volume at relative pressures below 0.2 (corresponding to micropore range) and well-defined hysteresis loop in the desorption branches at relative pressures higher than 0.7, evidencing their mesoporous character. The large pore volumes and hysteresis loops in the gas adsorption data suggest that the polycondensation of the monomers is slowed down in the presence of the additives (either B or D). This would lead to a lower degree of cross-linking of the structure, generating weakly branched clusters that tend to form larger colloidal aggregates in progressively larger pores (mesopore coarsening).[29]

The incorporation of diatomite provoked a slight fall in the pore volumes, whereas the microporosity followed a slightly increasing trend (Table 1). Consequently, the aerogels prepared in the presence of the additives displayed higher surface area values than the pristine calculated from mercury porosimetry.

MRF gel, although all the samples are highly microporous. Otherwise, the addition of carbon black (sample MRF-Mn-D-CB) yielded an increase in the mesopore volume (compared to MRF-Mn-D), as commonly observed for similar composite aerogels.[30, 31].

The impact of the additives on the texture of the carbon aerogels can also be seen in the pore size distributions (Figure 2b). In agreement with the shape of the isotherms, there is an increase in the contribution to pore widths smaller than 1 nm. Concerning mesopores, carbon aerogels treated with diatomite feature a multimodal distribution with several peaks between 5 to 25 nm. Moreover, an analysis of the pore size distribution measured by mercury porosimetry reveals an additional contribution of macropores (500 nm) in samples MRF-Mn-D and MRF-Mn-DB which is not present in the material synthesized in the absence of the diatomite (Fig. 2c).

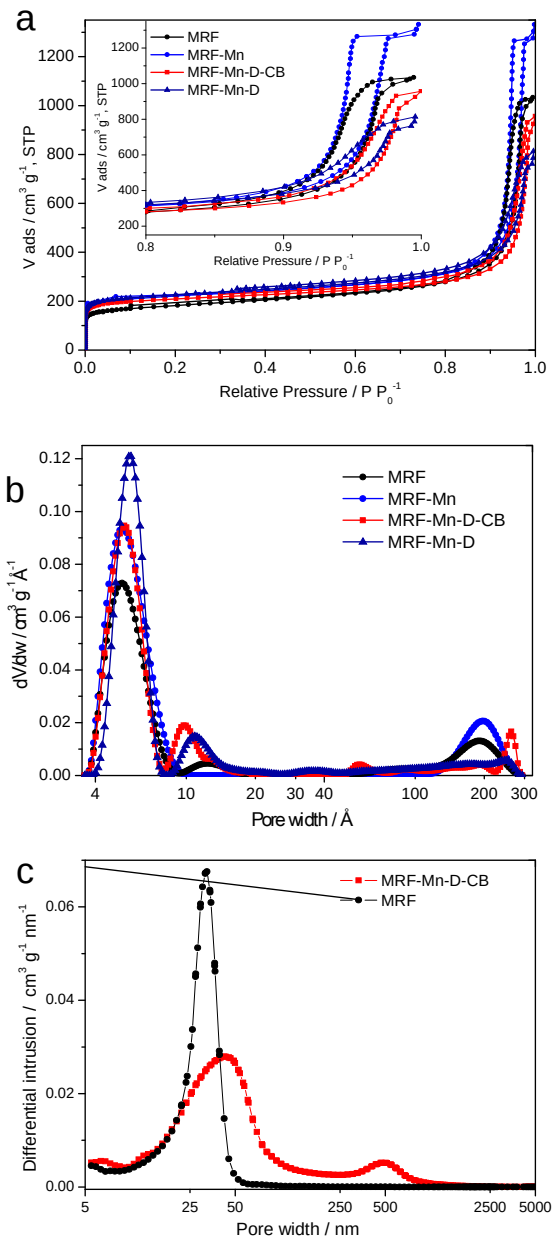
a
MRF
MRF-Mn
MRF-Mn-D-CB
MRF-Mn-D
V ads / cm3 g-1, STP
Relative Pressure / P P0-1
b
dV/dw / cm3 g-1 Å-1
Pore width / Å
c
Differential intrusion / cm3 g-1 nm-1
Pore width / nm

The chemical composition of aerogels was determined by elemental analysis and XPS (Table S1, Supporting Information). As expected, the incorporation of manganese caused a decrease in the carbon and nitrogen contents. Otherwise, XPS data revealed an increase in the overall content of oxygen in the Mn-containing aerogels, suggesting the formation of manganese oxides. No crystalline manganese phases were detected by X-ray diffraction (Fig. S3 Supporting Information), which we attribute to the low manganese content of the samples (Table S1, Supporting Information). On the other hand, the amount of nitrogen from the chemical analysis is slightly higher than that obtained from the XPS spectra. This evidences that the N-containing groups are not located at the surface of the aerogel, but also efficiently incorporated in the bulk material; hence the concentration of the doping element is lower near the surface.[33, 34] Furthermore, the amount of nitrogen groups is similar to all the samples, which confirms the efficient polymerization of the reactants in the presence of the additives.

To evaluate the influence of the additives on the nature of the different N- and O-groups, the surface chemistry of the aerogels was investigated by XPS. Five different gaussian-lorentzian components were deconvoluted from the C1s core level spectra (Figure S4, Supporting Information). The main signals were assigned to graphitic carbon in a sp^2 configuration, 284.6±0.1 eV), Csp^2–N/C–OH (285.8±0.1 eV), Csp^3–N/C=O (287.1±0.1 eV), and carboxyl (289.2±0.2 eV) groups. A shake-up satellite peak due to π-π* transitions in aromatic rings appears ca. 291.1±0.1 eV as a low intense and highly broadened band.[35] The relative contributions of the different peaks are compiled in Table 2. As seen, the contribution of the graphitic carbon prevails over other surface functionalities, regardless the carbon aerogel. The presence of the diatomite in MRF-Mn-D led to a slightly higher contribution of Csp^2–N/C–OH, while Csp^3−N/C=O significantly decreased. These tendencies were confirmed by the relative contributions of the signals ascribable to C=O in ketone/carbonyl (531.2±0.2 eV) and O-C in lactone, phenol, ether, epoxy (533.0±0.2 eV) in the O1s core level spectra (Figure S5, Supporting Information and Table 2). Three additional signals attributed to C=O in carboxylic acids (534.4±0.1 eV), adsorbed and/or occluded CO/CO_2 (536.2±0.2 eV), and trapped CO and CO_2 molecules (536.2 eV) coming

The spectra at the N1s core level were decomposed into four overlapped bands assigned to N6 pyridinic (398.3±0.2 eV), N5 pyrrolic/pyridone (400.2±0.2 eV), N-Q

Table 2. XPS parameters calculated from the deconvolution of N 1s, O1s, C1s spectra of hybrid composite containing N-doped carbon aerogels (B.E.=binding energy)..

Envelope N1s				
Assignment	**N-6**	**N-5**	**N-Q**	**N-X**
MRF	35.2	40.7	15.7	8.5
MRF-Mn	32.6	44.7	16.2	6.4
MRF-Mn-D	35.4	43.3	14.3	6.9
MRF-Mn-D-CB	32.3	49.9	12.4	5.4
Envelope O1s				
Assignment	**C=O**	**C-O-**	**COO-**	**H_2O/ Occluded CO /CO_2**
MRF	21.0	51.4	23.8	3.8
MRF-Mn	12.2	59.7	25.6	2.4
MRF-Mn-D	16.3	59.4	21.5	2.9
MRF-Mn-D-CB	18.7	56.1	23.2	2.0
Envelope C1s				
Assignment	**C-C**	**Csp^2-N/ C−OH**	**Csp^3−N/ C=O**	**O-C=O**	**π-π***
MRF	60.5	15.3	12.1	9.0	3.0
MRF-Mn	58.5	17.8	13.3	9.0	1.3
MRF-Mn-D	60.5	21.2	8.8	9.3	0.3
MRF-Mn-D-CB	63.9	16.8	9.4	8.8	1.0

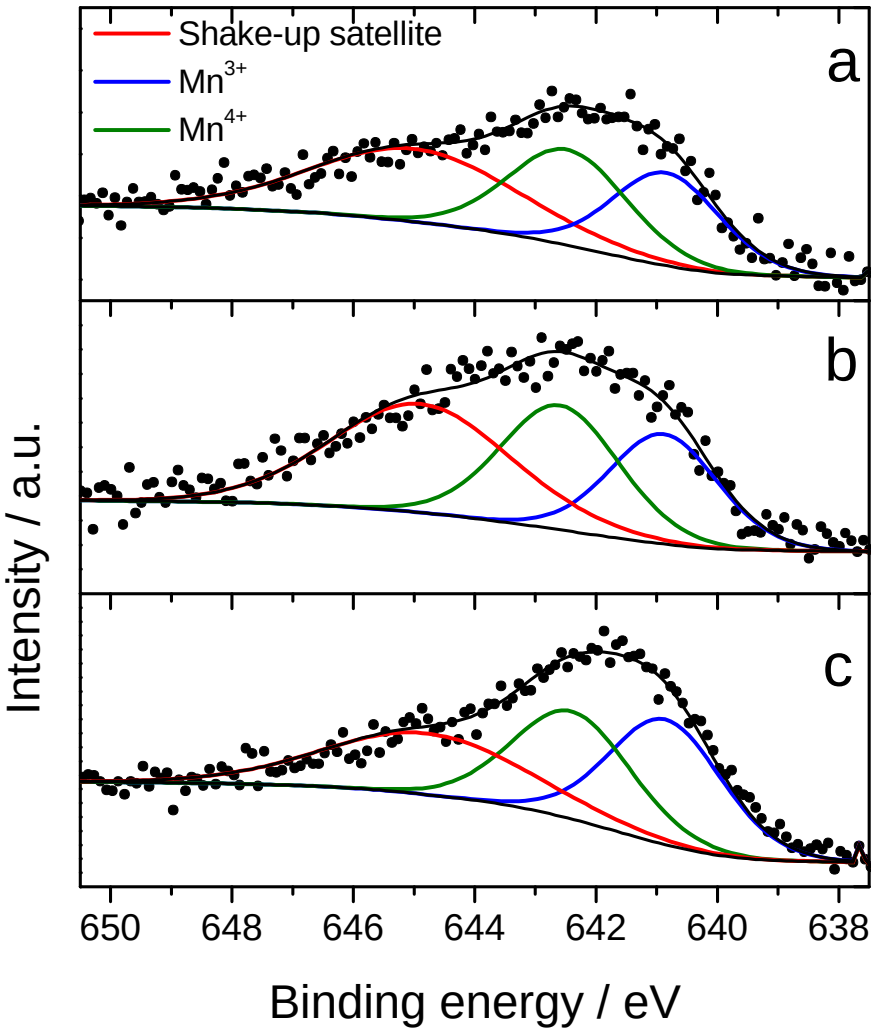
Shake-up satellite
Mn3+
Mn4+
a
b
c
Intensity / a.u.
650
648
646
644
642
640
638
Binding energy / eV

It could be envisaged that the macroporous network and the improved electrical conductivity of these composites -due to the incorporation of the carbon black additive and the occurrence of electron donating N-groups,[44-46] may lead to an enhancement of the kinetic response at the electrode–electrolyte interface.[47] To evaluate the polarization resistance of the electrodes, impedance spectroscopy was performed. The Nyquist plots are displayed in Figure 4; the profiles appeared significantly distorted due to the complex porous structure of the aerogels (Table 1), but all of them displayed a semicircle at high and intermediate frequencies prolonged by a straight line. The polarization resistance values (R_{pol}) were calculated by fitting the experimental data to the equivalent circuit depicted in Figure 4b -consisting of the electrolyte solution resistance (R_{el}), the polarization resistance (R_{pol}), the Warburg impedance (W), a constant phase element (CPE) and a capacitor (C). The resistance of the electrolyte solution is so low that its contribution to the overall resistance can be neglected. Thus the polarization resistance is mainly responsible for the internal electrode resistance, and varied upon the trend: MRF-Mn-D-CB (0.45 Ω×g), MRF-Mn-D (0.57 Ω×g), MRF (0.79 Ω×g) and MRF-Mn (1.02 Ω×g). These results clearly reveal the beneficial effect of the incorporation of the diatomite in the synthesis of the carbon aerogels, providing lower polarization resistance values than the materials prepared in the absence of the siliceous additive. This can be attributed to the macropore structure, inherited by the anti-shrinkage additive and the effect of the carbon black. Contrarily, the highest polarization resistance of MRF-Mn reveals that the single combination of the Mn phase with MRF is not an optimal solution. Likely, the less hydrophilic character of this aerogel hinders the formation of an optimal electrode electrolyte interphase that would eventually counterbalance the favorable accessibility provided by the high specific surface and pore volume.

The capacitive behavior was evaluated from the cyclic voltammograms recorded in 3-electrode cells (Figure 5). The profiles for MRF and MRF-Mn show the typical box-like shape ascribable to a capacitive behavior resulting from the electrostatic interactions between the charged electrode and opposite ions coming from the electrolyte. The positive slopes observed at extreme potential values are due to restricted ion diffusion into the micropores leading to an electrode resistivity and slight decomposition of the electrolyte.[48] In the case of the aerogels prepared in the presence of the diatomite (samples MRF-Mn-D-CB and MRF-Mn-D), slight deviations from the rectangular shape

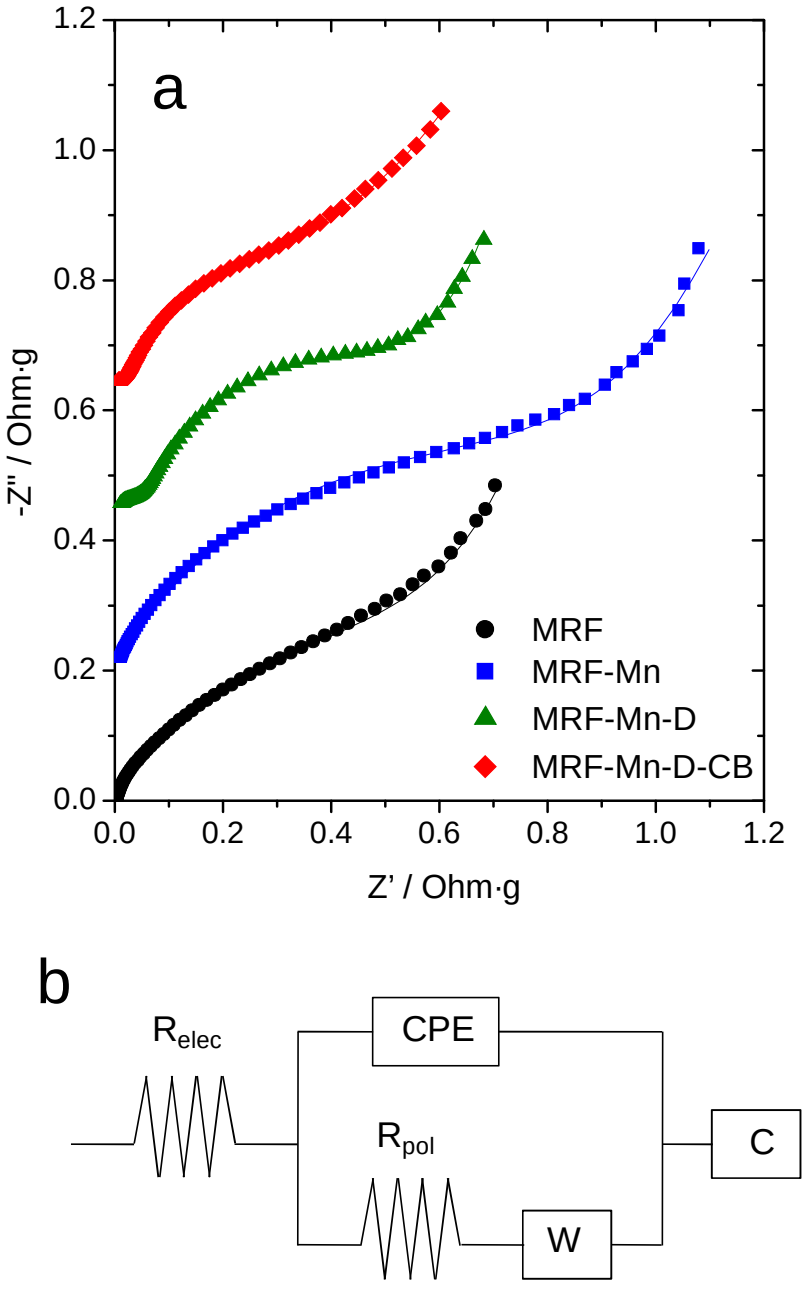
a
-Z'' / Ohm·g
Z' / Ohm·g
0.0
0.2
0.4
0.6
0.8
1.0
1.2
MRF
MRF-Mn
MRF-Mn-D
MRF-Mn-D-CB

b
R_{elec}
CPE
R_{pol}
W
C

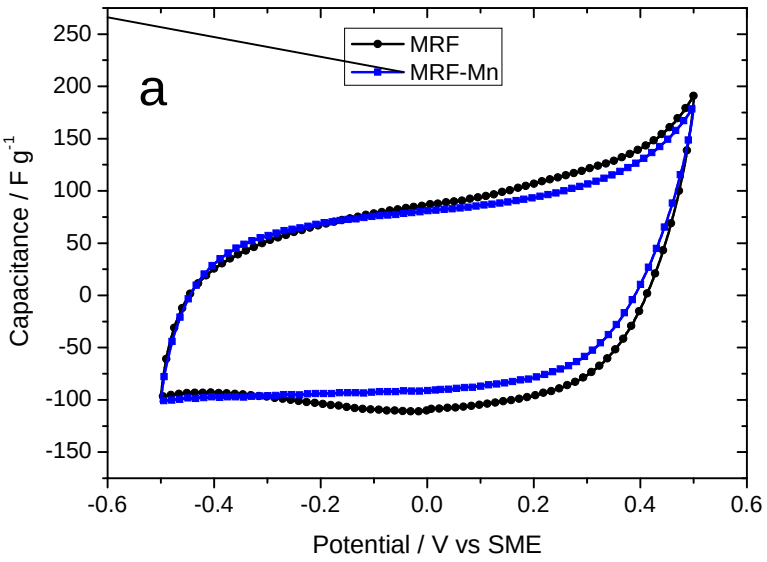
a
MRF
MRF-Mn
Capacitance / F g-1
Potential / V vs SME
250
200
150
100
50
0
-50
-100
-150
-0.6
-0.4
-0.2
0.0
0.2
0.4
0.6

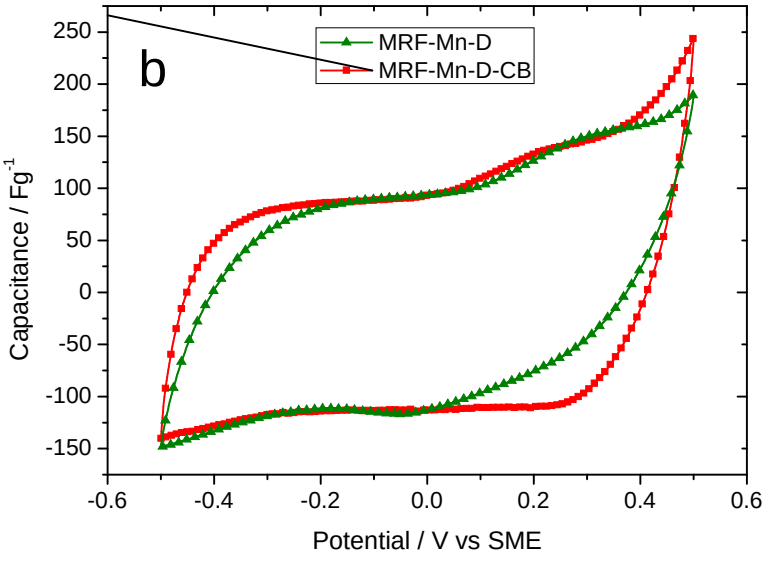
b
MRF-Mn-D
MRF-Mn-D-CB
Capacitance / Fg-1
Potential / V vs SME
250
200
150
100
50
0
-50
-100
-150
-0.6
-0.4
-0.2
0.0
0.2
0.4
0.6

error margins are considered. Thus, the mere presence of the manganese phase was not determining for a capacitance improvement despite of the larger textural features of the former sample (Table 1). Likely, the poor wettability is a crucial factor limiting the electrosorption of MRF-Mn. The highest capacitance values recorded for the MRF-Mn-D and MRF-Mn-D-CB aerogels -values of 104±2 and 113±1 F g^{-1}, respectively- are a direct consequence of the enhanced macroporosity and improved wettability of the diatomite treated aerogels. Thus, a synergic effect is exerted allowing the development of both electric double layer and pseudo-faradic effects that contribute to the achievements of high capacitance values. This behavior was confirmed by galvanostatic cycling at different current densities (Fig. S7). Thus, capacitance values of 91 and 121 F g^{-1} were respectively recorded for MRF and MRF-Mn-D-CB at 0.1 A g^{-1}, which agrees well with tendency showed by the cyclic voltammograms.

Monoliths of the aerogels were assembled in symmetric cells to determine their electrosorption capacity in 0.025 M (ca. 1.5 g/L) NaCl solutions. The electroadsorption curves at different voltages and subsequent discharges at 0 V are plotted in Figure 6. Interestingly, there does not seem to be a direct relationship between the capacitance values determined in the above- described 3-electrode cell configuration and the electrosorption capacity recorded in the 2-cell system after 120 minutes. The obtained values were quite similar for all the aerogels. For instance, a capacity of 6.7 mg of NaCl /g was observed for MRF, very close to the value measured for MRF-Mn-D-CB (ca. 6.1 mg/g), the best performing material evaluated by cyclic voltammetry (Figure 5).

This apparent disagreement can be interpreted by considering the different kinetic response of electrodes in a monolithic form, compared to powder ones.[30] The charge curve was steeper for MRF-Mn-D and MRF-Mn-D-CB, with maximum capacities being reached after 60 minutes of charge. In the case of the pristine electrodes (no additives), the profiles displayed a fast response after 60 min followed by a second process (seen as a plateau in the charge curves) up to 120 min when the material is slowly charged.The highest adsorption capacities recorded at 0.9 V corresponded to the diatomite treated MRF-Mn-D-CB, regardless the time of charge. On increasing the applied voltage to 1.2 and 1.5 V, the improved kinetic behavior of the treatment with diatomite is more clearly evidenced because of their higher adsorption capacities for short times. For instance, the

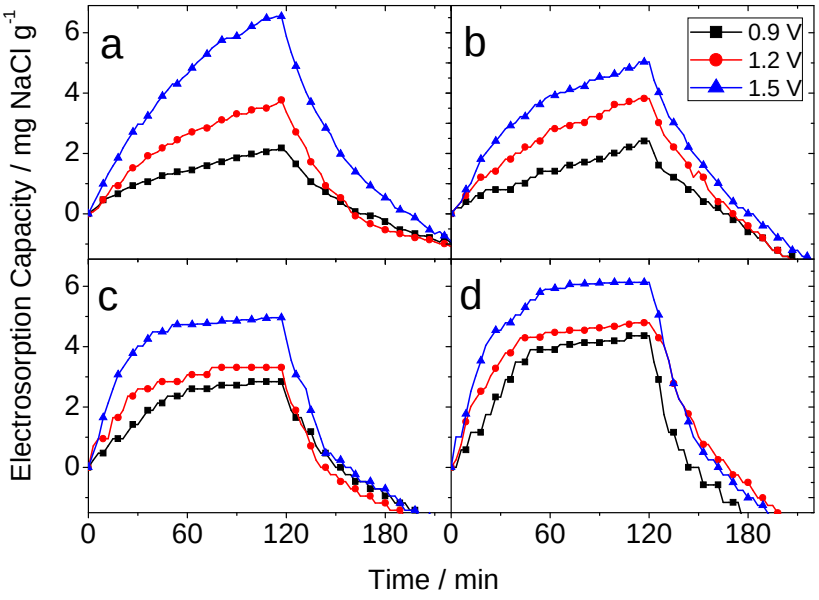
a
b
c
d
0.9 V
1.2 V
1.5 V
Electrosorption Capacity / mg NaCl g-1
Time / min
0
2
4
6
0
60
120
180

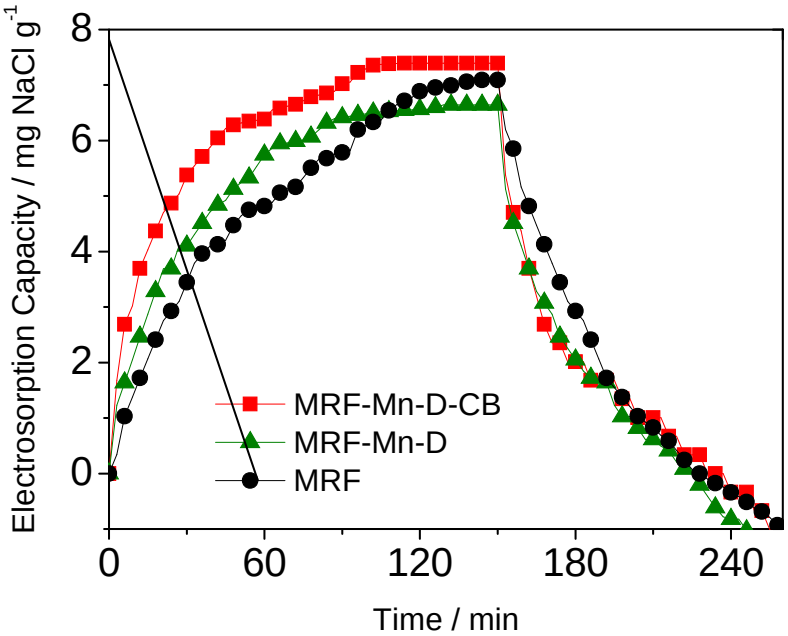
MRF-Mn-D-CB
MRF-Mn-D
MRF
Electrosorption Capacity / mg NaCl g-1
Time / min
0
2
4
6
8
0
60
120
180
240

To verify this assumption, further experiments were performed at a higher NaCl concentration (0.1 M) and longer adsorption times (150 minutes) for 1.5 V (Fig. 7 and S9). In these more demanding conditions, MRF-Mn-D-CB (7.9 mg/g) evidenced to perform better than MRF aerogel. These results reveal the synergic effect of manganese containing particles, carbon black along with the diatomite treating to reach a carbon aerogel with optimized properties for capacitive deionization.

3.4.4. Conclusions

The use of a siliceous diatomite as anti-shrinkage additive has allowed the synthesis of monolithic carbon aerogels with a well-developed micro and mesopore structure and enhanced macroporosity. The incorporation of nitrogen functionalities and carbon black as conductive additive enable to increase the electrical conductivity and wettability of the materials. The resulting carbon matrix has demonstrated to be a favorable support for manganese containing particles, which pseudofaradic effect contributes positively to the overall capacitance. These characteristics are responsible for the good electrochemical performance of the electrodes for the removal of ionic species in terms of fast kinetics and low resistance.

The morphological analysis showed the efficient anti-shrinkage effect and the sponge-like texture of the carbon aerogels after the diatomite removal. The nitrogen isotherms also revealed that the polycondensation of the reactants is not impeded by the presence of the additives (both diatomite and carbon black), leading to a multimodal distribution of pore sizes with mesopores. Concerning the deionization capacity measured in symmetric cells using monolithic electrodes, the aerogels synthesized in the presence of the diatomite showed a more advantageous response at low voltages and/or short charge time. These results demonstrate that the use of diatomite as anti-shrinkage additive can be a helpful solution to prepare highly porous carbon electrodes with optimized morphological properties for capacitive deionization.

3.4.5. References

[1] White, R. J.; Brun, N.; Budarin, V. L.; Clark, J. H.; Titirici, M. M. Always Look on the “Light” Side of Life: Sustainable Carbon Aerogels. *ChemSusChem* **2014**, *7*, 670 – 689.

[2] Pekala, R. W.; Farmer, J. C.; Alviso, C. T.; Tran, T. D.; Mayer, S. T.; Miller, J. M.; Dunn, B. Carbon aerogels for electrochemical applications. *J. Non-Cryst. Solids* **1998**, *225*, 74 – 80.

[3] Moreno-Castilla, C.; Maldonado-Hodar F. J. Carbon aerogels for catalysis applications: An overview. *Carbon* **2005**, *43*, 455 – 465.

[4] Humplik, T.; Lee, J.; O’Hern, S. C.; Fellman, B. A.; Baig, M. A.; Hassan, S. F.; Atieh, M. A.; Rahman, F.; Laoui, T.; Karnik, R.; Wang, E. N. Nanostructured materials for water desalination. *Nanotechnology* **2011**, *22*, 292001.

[5] S.A. Al-Muhtaseb, J.A. Ritter, Preparation and properties of resorcinol–formaldehyde organic and carbon gels, *Adv. Mater*. **2003**, *15*, 101-114.

[6] AlMarzooqi, F. A.; Al Ghaferi, A. A.; Saadat, I.; Hilal, N.; Application of Capacitive Deionisation in water desalination: A review. *Desalination* **2014**, *342*, 3–15.

[7] Anderson, M. A.; Cudero A. L.; Palma, J. Capacitive deionization as an electrochemical means of saving energy and delivering clean water. Comparison to present desalination practices: Will it compete? *Electrochim. Acta* **2010**, *55*, 3845–3856.

[8] Porada, S.; Zhao, R.; van der Wal, A.; Presser, V.; Biesheuvel, P. M. Review on the science and technology of water desalination by capacitive deionization. *Prog. Mater. Sci.* **2013**, *58*, 1388–1442.

[9] Oren, Y. Capacitive deionization (CDI) for desalination and water treatment—past, present and future (a review). *Desalination* **2008**, *228*, 10–29.

[10] Antonietti, M.; Fechler, N.; Fellinger, T. P. Carbon Aerogels and Monoliths: Control of Porosity and Nanoarchitecture via Sol-Gel routes. *Chem. Mater*. **2014**, *26*, 196–210.

[11] El-Deen; A. G., Barakat, N.A.M.; Khalil, K. A; Kim; H. Y. Hollow carbon nanofibers as an effective electrode for brackish water desalination using the capacitive deionization process, *New J. Chem*., **2014**, *38*, 198-205.

[12] Wen, X.; Zhang, D.; Shi, L.; Yan, T.; Wang, H.; Zhang, J., Three-dimensional hierarchical porous carbon with a bimodal pore arrangement for capacitive deionization, *J. Mater. Chem.*, **2012**, *22*, 23835- 23844.

[13] Lei, H.; Yan, T.; Wang, H.; Shi, L.; Zhang, J.; Zhang, D. Graphene-like carbon nanosheets prepared by a Fe-catalyzed glucose-blowing method for capacitive deionization, *J. Mater. Chem. A*, **2015**, *3*, 5934-5941.

[14] Kim, C.; Lee, J.; Kim, S.; Yoon J. TiO_2 sol–gel spray method for carbon electrode fabrication to enhance desalination efficiency of capacitive deionization, *Desalination* **2014**, *342*, 70–74.

[15] Wang, H.; Shi, L.; Yan, T.; Zhang, J.; Zhong Q.; Zhang, D. Design of graphene-coated hollow mesoporous carbon spheres as high performance electrodes for capacitive deionization, *J. Mater. Chem. A*, **2014**, *2*, 4739-4750.

[16] Wen, X.; Zhang, D.; Yan, T.; Zhang, J.; Shi, L. Three-dimensional graphene-based hierarchically porous carbon composites prepared by a dual-template strategy for capacitive deionization, *J. Mater. Chem. A*, **2013**, *1*, 12334–12344.

[17] Zhang, D.; Wen, X.; Shi, L. Yan, T.; Zhang, J.; Enhanced capacitive deionization of graphene/mesoporous carbon composites, *Nanoscale*, **2012**, *4*, 5440–5446.

[18] Wang, H.; Zhang, D.; Yan, T.; Wen, X; Zhang, J.; Shi, L.; Zhong Q. Three-dimensional macroporous graphene architectures as high performance electrodes for capacitive deionization. *J. Mater. Chem. A*, **2013**, *1*, 11778–11789.

[19] Yuan, P.; Liu, D.; Tan, D.-Y.; Liu, K.-K.; Yu, H.-G.; Zhong, Y.-H.; Yuan, A.-H.; Yu, W.-B.; He, H.-P. Surface silylation of mesoporous/macroporous diatomite (diatomaceous earth) and its function in Cu(II) adsorption: The effects of heating pretreatment. *Mic. Mes. Mat.* **2013**, *170*, 9–19.

[20] Yuan, W.; Yuan, P.; Liu, D.; Yu, W.; Deng, L.; Chen, F. Novel hierarchically porous nanocomposites of diatomite-based ceramic monoliths coated with silicalite-1 nanoparticles for benzene adsorption . *Mic. Mes. Mat.* **2015**, *206*, 184-193.

[21] Macías, C.; Rasines, G.; García, T.; Rodríguez, C.; Lavela, P.; Tirado, J.L.; Ania, C.O.; On the use of diatomite as antishrinkage additive in the preparation of monolithic carbon aerogels, *Carbon* **2016**, *98*, 280-284.

[22] Shi, K.; Ren, M.; Zhitomirsky, I. Activated Carbon-Coated Carbon Nanotubes for Energy Storage in Supercapacitors and Capacitive Water Purification, *ACS Sustainable Chem. Eng.* **2014**, *2*, 1289−1298.

[23] Rasines, G.; Lavela, P.; Macías, C.; Zafra, M. C.; Tirado, J. L.; Parra, J. B.; Ania C O. N-doped monolithic carbon aerogel electrodes with optimized features for the electrosorption of ions. *Carbon* **2015**, *83*, 262–274.

[24] Zafra, M.C.; Lavela, P.; Rasines, G.; Macías, C.; Tirado, J.L.; Ania, C.O. A novel method for metal oxide deposition on carbon aerogels with potential application in capacitive deionization of saline water, *Electrochimica Acta* **2014**, *135*, 208–216.

[25] Rasines, G.; Macías, C.; Haro, M.; Jagiello, J.; Ania, C.O. Effects of CO_2 activation of carbon aerogels leading to ultrahigh micro-meso porosity *Mic. Mes. Mat.* **2015**, *209*, 18–22.

[26] Jagiello, J.; Olivier, J. P. 2D-NLDFT Adsorption Models for Carbon Slit-Shaped Pores with Surface heterogeneity and geometrical corrugation. *Adsorption* **2013**, *19*, 777–783.

[27] Moulder, J. F. Stickle, W. F.; Sobol, P. E.; Bomben, K. D. *Book of Standard spectra for identification and interpretation of XPS data, Physical Electronics.* Minnesota: Eden Prairie; 1995.

[28] Job, N.; Théry, A.; Pirard, R.; Marien, J.; Kocon, L.; Rouzaud, J.N.; Béguin, F.; Pirard, J. P. Carbon aerogels, cryogels and xerogels: Influence of the drying method on the textural properties of porous carbon materials. *Carbon* **2005**, *43*, 2481–2494.

[29] Gu, X.; Yang, Y.; Hu, Y.; Hu, M.; Wang, C. Fabrication of Graphene-Based Xerogels for Removal of Heavy Metal Ions and Capacitive Deionization *ACS Sustainable Chem. Eng.* **2015**, *3*, 1056–1065.

[30] Macías, C.; Haro, M.; Parra, J.B.; Rasines, G.; Ania, C.O. Carbon-black directed synthesis of mesoporous aerogels. *Carbon* **2013**, *63*, 487–497.

[31] Rasines, G.; Lavela, P.; Macías, C.; Zafra, M.C.; Tirado, J.L.; Ania, C.O. Mesoporous carbon black-aerogel composites with optimized properties for the electro-assisted removal of sodium chloride from brackish water, *J. Electroanal. Chem.* **2015**, *741*, 42–50.

[32] Thommes, M.; Kaneko, K.; Neimark, A.V.; Olivier, J.P.; Rodriguez-Reinoso, F.; Rouquerol, J.; Sing, K.S.W. Physisorption of gases, with special reference to the evaluation of surface area and pore size distribution (IUPAC Technical Report) *Pure Appl. Chem.* **2015**, *87*, 1051–1069.

[33] Sousa, J. P. S.; Pereira, M. F. R.; Figueiredo J. L. NO oxidation over nitrogen doped carbon xerogels. *Appl. Catal. B Environ.* **2012**, *125*, 398–408.

[34] Singru, N. R.; Gurnule W. B.; Khati, V.A.; Zade, A. B.; Dontulwar, J. R. Eco-friendly application of p-cresol–melamine–formaldehyde polymer resin as an ion-exchanger and its electrical and thermal study. *Desalination* **2010**, *263*, 200–210.

[35] Li, S.-M.; Yang, S.-Y.; Wang, Y.-S.; Lien, C.-H.; Tien, H.-W.; Hsiao, S.-T.; Liao, W.-H.; Tsai,H.-P.; Chang,C.-L.; Ma, C.-C. M.; Hu C.-C. Controllable synthesis of nitrogen-doped graphene and its effect on the simultaneous electrochemical determination of ascorbic acid, dopamine, and uric acid. *Carbon* **2013**, *59*, 418–429.

[36] Yu, J.; Guo, M.; Muhammad, F.; Wang, A.; Yu, G.; Ma, H. Zhu, G. Simple fabrication of an ordered nitrogen-doped mesoporous carbon with resorcinol-melamine-formaldehyde resin. *Mic. Mes. Mat.* **2014**, *190*, 117–127.

[37] Seredych, M.; Hulicova-Jurcakova, D.; Lu, G. Q.; Bandosz, T. J. Surface functional groups of carbons and the effects of their chemical character, density and accessibility to ions on electrochemical performance. *Carbon* **2008**, *46*, 1475–1478.

[38] Terzyk, A. P. The influence of activated carbon surface chemical composition on the adsorption of acetaminophen (paracetamol) in vitro Part II. TG, FTIR, and XPS analysis of carbons and the temperature dependence of adsorption kinetics at the neutral pH. *Colloids Surf. A* **2001**, *177*, 23–45.

[39] Long, D.; Zhang, J.; Yang, J.; Hu, Z.; Cheng, G.; Liu, X.; Zhang, R.; Zhan, Li.; Qiao, W.; Ling L. Chemical state of nitrogen in carbon aerogels, issued from phenol–melamine–formaldehyde gels. *Carbon* **2008**, *46*, 1259–1262.

[40] Huang, Y.; Yang, F.; Xu, Z.; Shen, J. Nitrogen-containing mesoporous carbons prepared from melamine formaldehyde resins with $CaCl_2$ as a template. *J Colloid Interface Sci.* **2011**, *363*, 193–198.

[41] Ma, T. Y.; Dai, S.; Jaroniec, M.; Qiao, S. Z. Graphitic carbon nitride nanosheet–carbon nanotube three- dimensional porous composites as high-performance oxygen evolution electrocatalysts. *Angew. Chem. Int. Ed.* **2014**, *53*, 7281–7285.

[42] Di Castro, V.; Polzonetti, G. XPS study of MnO oxidation. *J. Electron. Spectrosc. Relat. Phenom.* **1989**, *48*, 117–123.

[43] Shi, F.; Wang, F.; Dai, H.; Dai, J.; Deng, J.; Liu, Y.; Bai, G.; Ji, K.; Au, C. T. Rod-, flower-, and dumbbell-like MnO_2: Highly active catalysts for the combustion of toluene. *Applied Catalysis A: General* **2012**, *433–434*, 206–213.

[44] Liu, E.; Shen, H.; Xiang, X.; Huang, Z.; Tian, Y.; Wu, Y.; Wu, Z.; Xie, H. A novel activated nitrogen-containing carbon anode material for lithium secondary batteries. *Materials Letters* **2012**, *67*, 390–393.

[45] Lu, Y.; Zhang, F.; Zhang, T. K.; Leng, L.; Zhang, X.; Yang , Y. M.; Huang, Y.; Zhang, M.; Chen. Y. Synthesis and supercapacitor performance studies of N-doped

graphene materials using o-phenylenediamine as the double-N precursor. *Carbon* **2013**, *63*, 508-516.

[46] Jeong, H. M.; Lee, J. W.; Shin, W. H.; Choi, Y. J.; Shin, H. J.; Kang, J. K.; Choi, J. W. Nitrogen-doped graphene for high-performance ultracapacitors and the importance of nitrogen-doped sites at basal planes. *Nano Lett* **2011**, *11*, 2472–2477.

[47] Rasines, G.; Lavela, P.; Macías, C.; Haro, M.; Ania, CO.; Tirado, J. L. Electrochemical response of carbon aerogel electrodes in saline water. *J. Electroanal. Chem.* **2012**, *671*, 92–98.

[48] Barbieri, O.; Hahn, M.; Herzog, A.; Kotz, R. Capacitance limits of high surface area activated carbons for double layer capacitors. *Carbon* **2005**, *43*, 1303–1310.

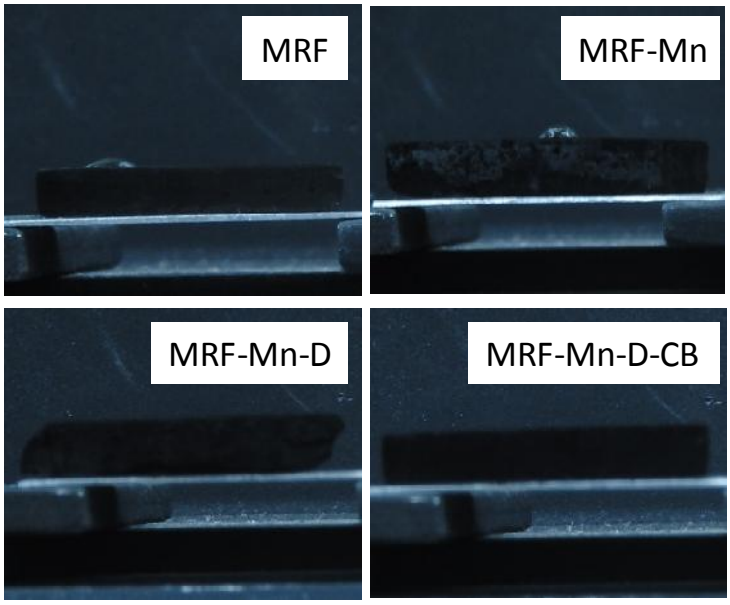
MRF
MRF-Mn
MRF-Mn-D
MRF-Mn-D-CB

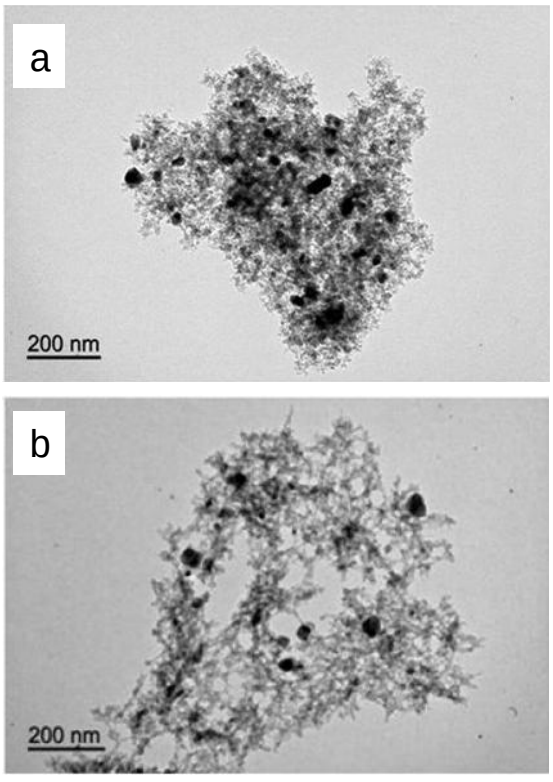
a
200 nm
b
200 nm

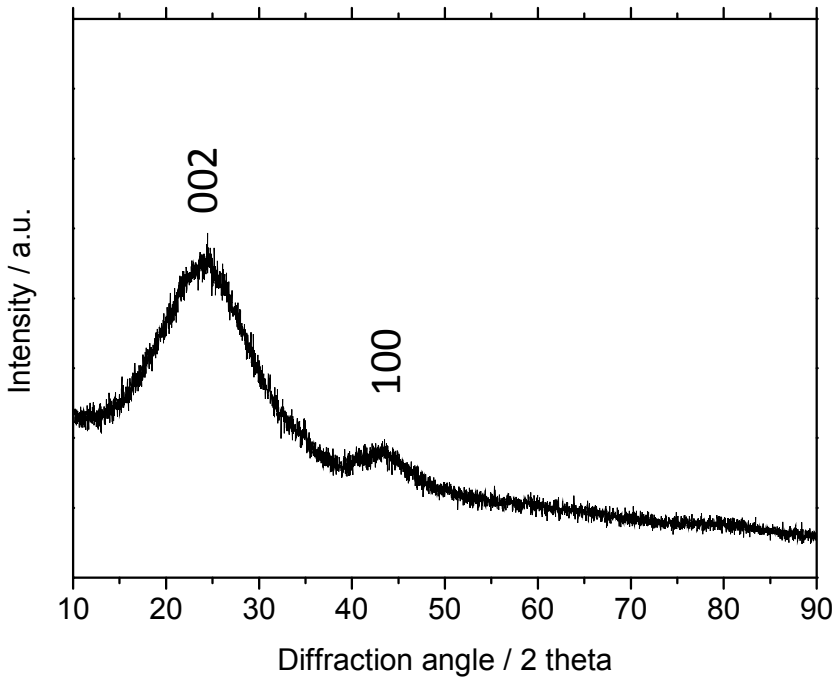
002
100
Intensity / a.u.
10
20
30
40
50
60
70
80
90
Diffraction angle / 2 theta

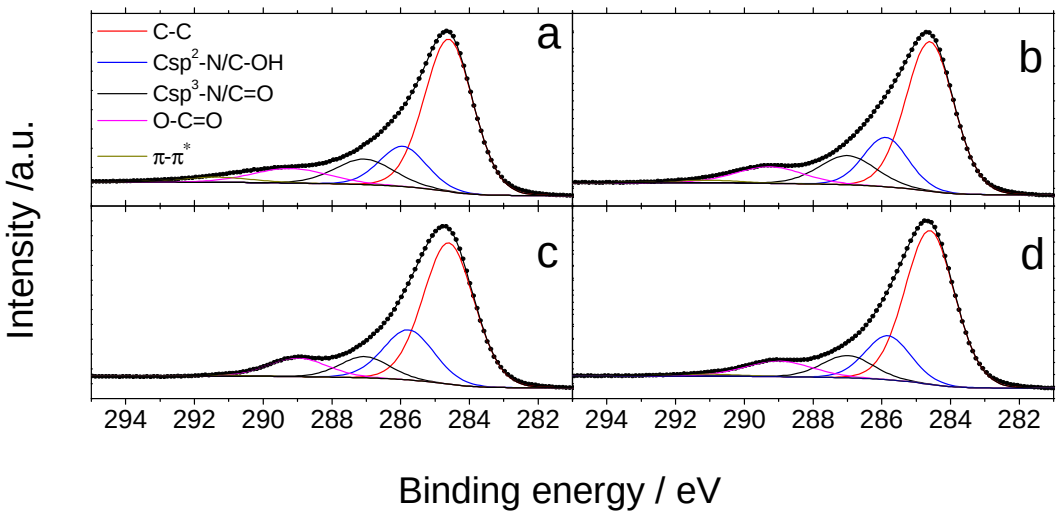
C-C
Csp2-N/C-OH
Csp3-N/C=O
O-C=O
π-π*
a
b
c
d
Intensity /a.u.
294
292
290
288
286
284
282
Binding energy / eV

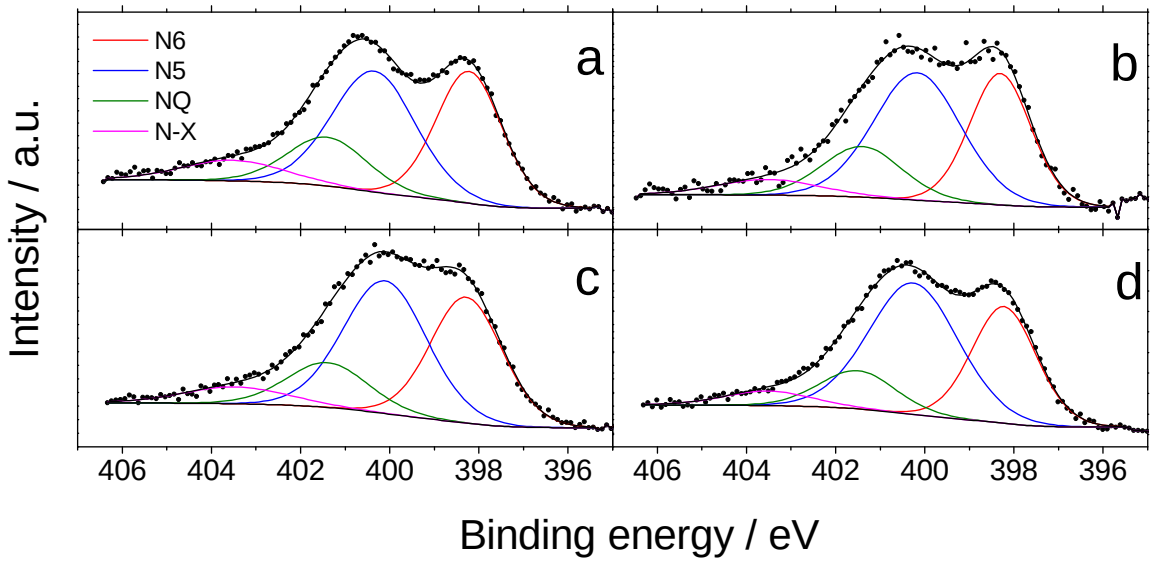
N6
N5
NQ
N-X
a
b
c
d
Intensity / a.u.
406
404
402
400
398
396
Binding energy / eV

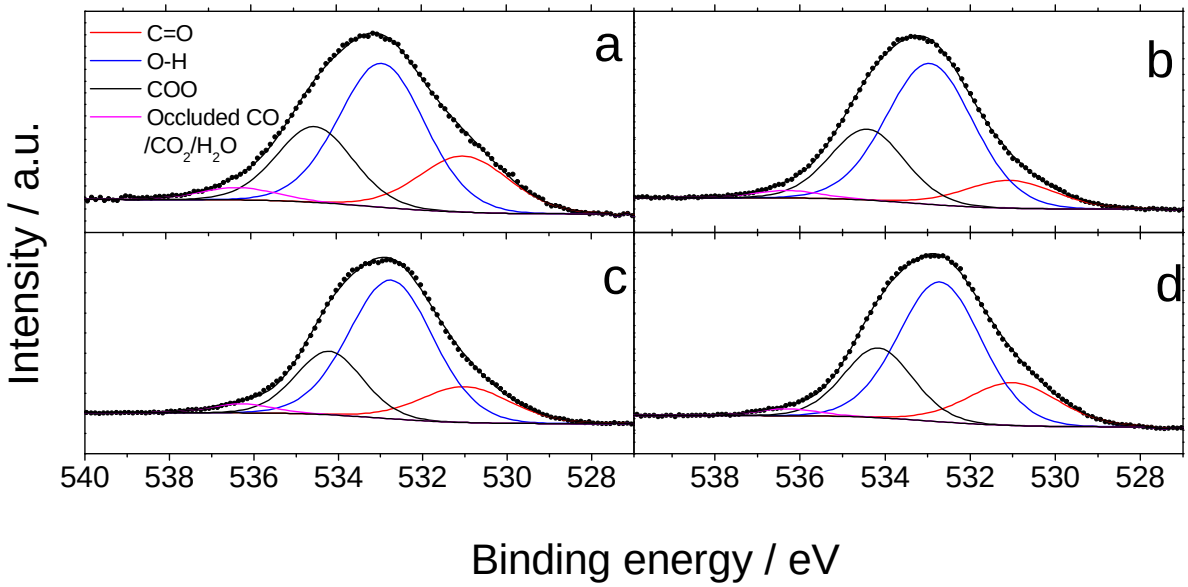
C=O
O-H
COO
Occluded CO
/CO2/H2O
a
b
c
d
Intensity / a.u.
540
538
536
534
532
530
528
Binding energy / eV

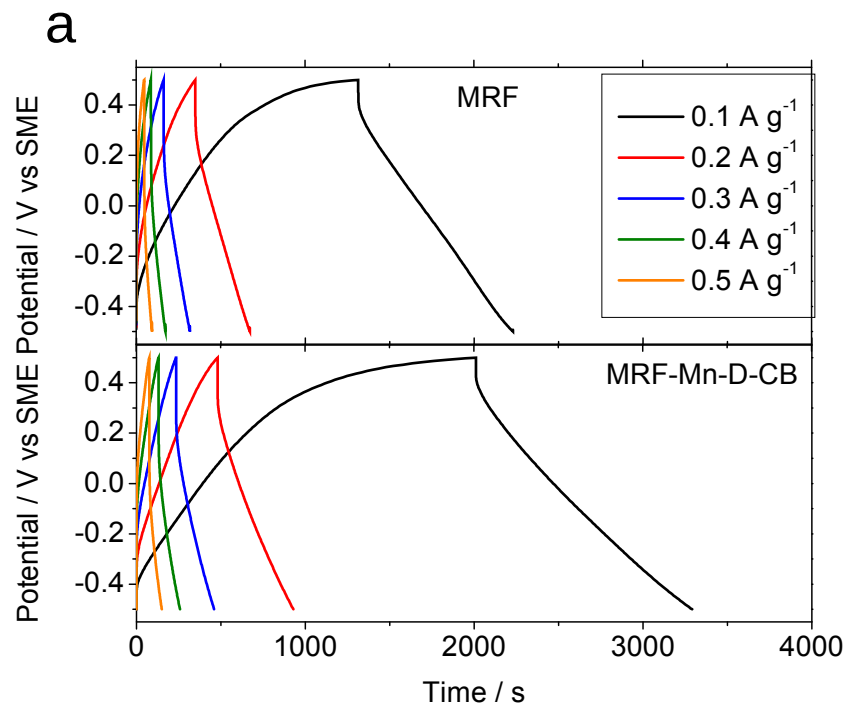
a
MRF
MRF-Mn-D-CB
0.1 A g-1
0.2 A g-1
0.3 A g-1
0.4 A g-1
0.5 A g-1
Potential / V vs SME
Potential / V vs SME
Time / s
0.4
0.2
0.0
-0.2
-0.4
0
1000
2000
3000
4000

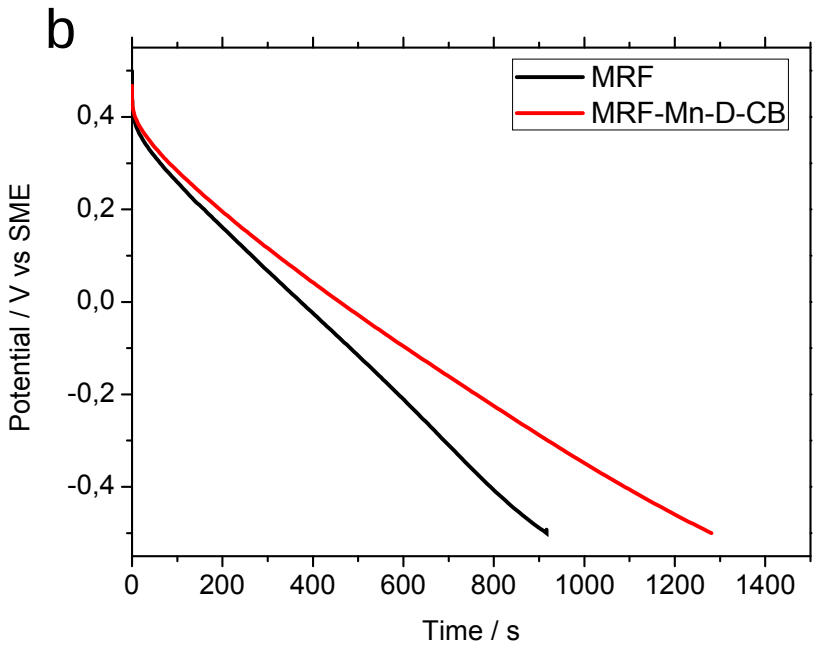
b
MRF
MRF-Mn-D-CB
Potential / V vs SME
Time / s
0,4
0,2
0,0
-0,2
-0,4
0
200
400
600
800
1000
1200
1400

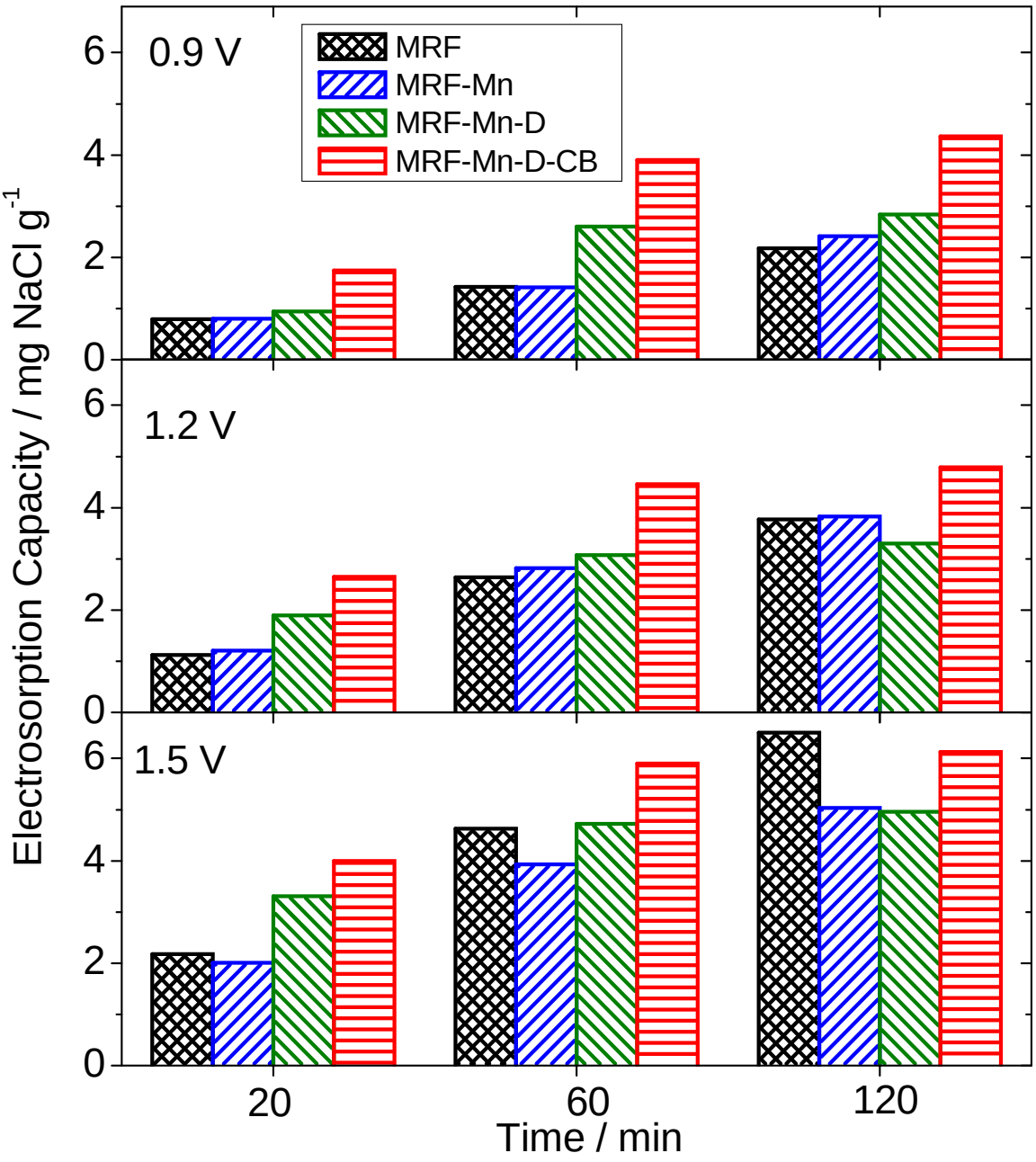
0.9 V
1.2 V
1.5 V
MRF
MRF-Mn
MRF-Mn-D
MRF-Mn-D-CB
Electrosorption Capacity / mg NaCl g-1
Time / min
0
2
4
6
20
60
120

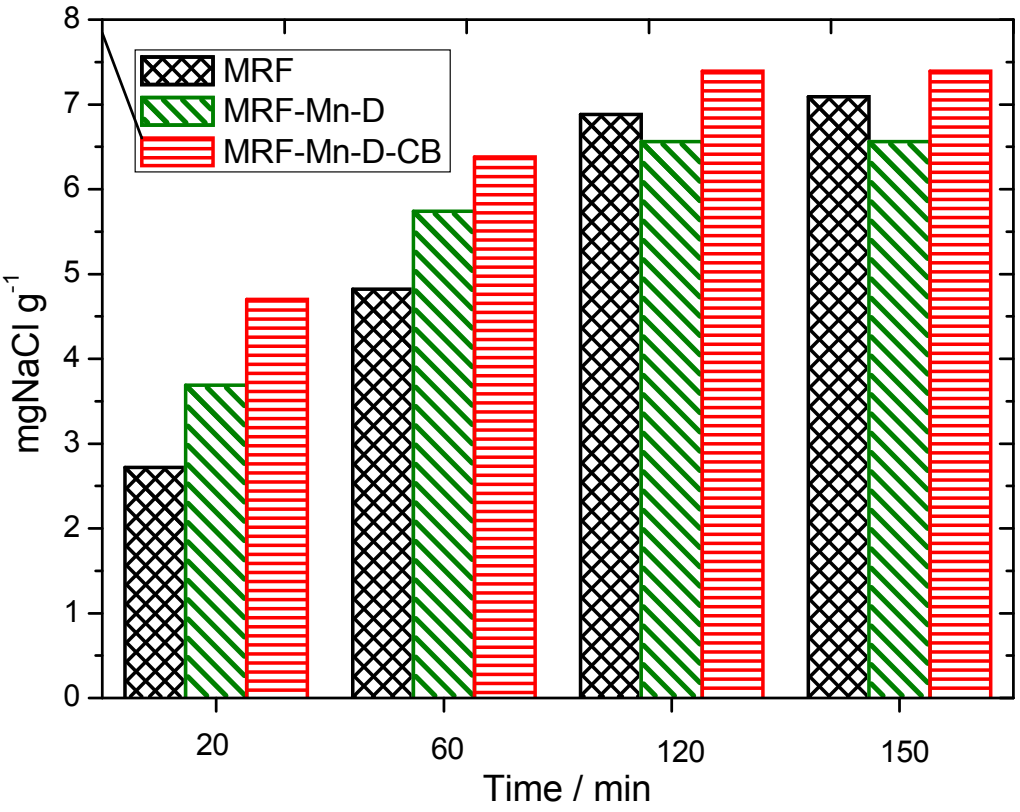
MRF
MRF-Mn-D
MRF-Mn-D-CB
mgNaCl g-1
0
1
2
3
4
5
6
7
8
20
60
120
150
Time / min

Table S1. Chemical composition (wt.%) determined by elemental analysis and XPS spectroscopy of the synthesized carbon aerogels.

		XPS			
Sample	N/C ratio	N / %	C / %	O / %	Mn / %
MRF	0.04	3.2	87.5	9.3	
MRF-Mn	0.01	1.3	85.4	12.8	0.4
MRF-Mn-D	0.03	2.2	81.1	16.2	0.4
MRF-Mn-D-CB	0.03	2.3	84.8	12.4	0.5
		Elemental analysis			
Sample	N/C ratio	N / %	C / %		
MRF	0.06	4.5	79.9	--	--
MRF-Mn	0.05	3.6	73.9	--	--
MRF-Mn-D	0.06	3.5	61.6	--	--
MRF-Mn-D-CB	0.06	3.6	59.3	--	--

Capítulo 4

Resumen y Conclusiones finales

4.1 Resumen

En la presente memoria de Tesis Doctoral se ha demostrado que el control adecuado de los parámetros de síntesis y la funcionalización de aerogeles de carbono para formar materiales híbridos son herramientas útiles para fabricar materiales de electrodo con aplicación en desionización capacitiva de aguas.

A continuación se exponen los resultados más destacables ordenados según los capítulos de esta memoria por compendio de publicaciones y que está integrada por los siguientes artículos:

1. *Sobre la correlación entre la estructura porosa y la respuesta electroquímica de aerogeles de carbono monolíticos y en polvo en desionización capacitiva.*

Se sintetizaron varios aerogeles de carbono con relaciones molares resorcinol-catalizador (R/C) que oscilaron entre 100 y 800, relación resorcinol-agua (R/W) de 0,04 a 0,13 y una relación resorcinol-formaldehído fija de 0,5, mediante polimerización y secado supercrítico con CO_2. Los aerogeles obtenidos se pirolizaron a 800 ºC y una parte se activó con CO_2 a 800 ºC durante 2 h. La caracterización textural mediante isotermas de N_2 presenta una clara influencia de las relaciones R/C y R/W en la porosidad tanto en los materiales pirolizados como en los activados. El volumen de mesoporos aumenta con R/C hasta el valor de 2,25 $cm^3\ g^{-1}$ para un R/C de 300 y a partir de este punto cae abruptamente hasta 0,08 $cm^3\ g^{-1}$. Este comportamiento se observa para un R/W de 0,04. Para R/W de 0,06 el comportamiento es algo similar aunque el máximo de mesoporos se observa a R/C 200, es menor que para R/W=0,04, y a partir de este valor la caída es menos abrupta. Para valores de R/W de 0,10 y 0,13 la tendencia es aumentar el volumen de mesoporos con el R/C en todo el rango estudiado desde 0,62 a 0,71 y de 0,27 hasta 0,48 $cm^3\ g^{-1}$ respectivamente. Un comportamiento similar se observó en los aerogeles activados indicando que la activación no afecta a la mesoporosidad, la cual estaría gobernada únicamente por las relaciones R/C y R/W. En los aerogeles pirolizados también se observa que para R/W bajos la superficie específica disminuye linealmente con R/C variando de 757 a 587 $m^2\ g^{-1}$ para R/C 100 y 600 respectivamente, mientras que para R/W altos (0,1-0,13) la tendencia es a aumentar ligeramente y de forma lineal la superficie específica con el R/C. Estas tendencias son iguales en los materiales activados

si bien las superficies específicas que presentan son sensiblemente mayores en ambos casos. La dependencia de la superficie específica con la relación R/W muestra tendencias similares: para R/C bajos la superficie disminuye con R/W de forma lineal mientras que aumenta ligeramente para R/C altos y el mismo comportamiento se observa con los activados. Este comportamiento de los parámetros texturales se explica a la luz de las diferentes estructuras poliméricas que se obtienen en los geles precursores para los diferentes valores de los parámetros de síntesis R/C y R/W.

Los aerogeles de carbono se micronizaron y se conformaron electrodos que se montaron en celdas swagelock de tres electrodos para estudiar sus propiedades electroquímicas. Las voltametrías cíclicas mostraron en todos los casos perfiles quasi-rectangulares típicos de un comportamiento capacitivo con un pequeño pico de corriente anódica en algún caso que indicaría la oxidación de grupos superficiales o descomposición de electrólito. Las capacitancias mostraron una tendencia clara a aumentar con la superficie específica oscilando de 50 a 70 F g^{-1} para los materiales de menor superficie a 120 F g^{-1} para el de mayor superficie. Se observó que en los materiales pirolizados la tendencia era menos clara lo que se atribuyó a los efectos de la química superficial; concretamente a una menor cantidad de oxígeno que en el material activado, que sería responsable de efectos pseudocapacitivos. La resistencia a la polarización (R_{pol}) medida mediante espectroscopia de impedancia electroquímica muestra una clara tendencia decreciente con la superficie específica y con la capacitancia, siendo más baja en los materiales activados que en los pirolizados. Así mismo, a medida que aumenta el volumen de mesoporos se observa una clara disminución de R_{pol} tanto en materiales pirolizados como activados, mientras que no hay relación entre este parámetro y el volumen de microporos. Este comportamiento se puede explicar por un mejor transporte de los iones en el interior del electrodo por la red porosa en los materiales con mayor volumen de mesoporos y por una mejor accesibilidad de la superficie activa. Los materiales con bajo R/W mostraron un incremento significativo de R_{pol} con la proporción R/C mientras que los R/W de 0,1 mostraron el efecto contrario.

Para determinar la capacidad desaladora se empleó una celda de dos electrodos con aerogeles monolíticos con NaCl 0,1 M como electrólito y se midió la carga total transferida durante el tercer ciclo de carga-descarga. Teniendo en cuenta únicamente la

superficie específica, no se ve una clara correlación entre este parámetro y la carga transferida, pero si se tiene en cuenta la resistividad de cada uno de los materiales, sí se observa una respuesta predecible que se puede describir mediante un polinomio de tercer grado en la resistividad y de segundo grado en la superficie la para el caso de aerogeles pirolizados y de primer grado en ambos parámetros para los aerogeles activados.

2. *Mejora en la eliminación electroasistida de iones fosfato y nitrato empleando aerogeles de carbono mesoporosos con porosidad controlada*

Se sintetizaron aerogeles de carbono mediante el método del resorcinol-formaldehído fijando la relación molar R/C= 200, 400 y 600 y R/W= 0.06. Después de un intercambio controlado agua-acetona, los materiales se secaron con CO_2 en condiciones supercríticas, se carbonizaron a 800ºC en atmósfera inerte y un lote de los aerogeles carbonizados se activó con CO_2 a 800 ºC durante 2 horas. Los materiales se caracterizaron estructuralmente mediante difracción de rayos X y espectroscopia Raman. Los difractogramas revelan la presencia de carbono mayormente desordenado, aunque con dominios grafíticos significativos. La deconvolución del espectro Raman de primer orden revela una banda G a 1580 cm^{-1} correspondiente a desplazamientos de los átomos de carbono dentro de las láminas grafénicas y una banda D1 a 1350 cm^{-1} atribuible normalmente a la falta de simetría traslacional de largo alcance. Se añade una curva lorentziana D2 para resolver la asimetría observada en la banda G que corresponde a la vibración en láminas grafénicas no apiladas. Además aparecen una curva gaussiana D3 a 1495 cm^{-1} indicativa de vibraciones de carbono sp^2 asociado a los bordes de las láminas grafénicas y una banda denominada D4 a 1160 cm^{-1} que corresponde a estiramientos de polienos sp_2-sp^3. Se muestra que la relación de intensidades D1/G disminuía tanto con la activación como cuando R/C aumentaba, indicando una dependencia del orden estructural con esta relación. Los espectros de XPS revelan la presencia de grupos C-O (285.6±0.2 eV), C=O (287 eV±0.1 eV) and O=C-O (288.7±0.3 eV) y se observa un aumento de la contribución de grupos C-O y C=O cuando disminuye R/C. El análisis textural revela que a medida que aumenta el valor de R/C en las muestras pirolizadas, el tamaño de los mesoporos aumenta transformándose parte de estos en macroporos mientras que el

volumen de microporos permanece constante. En cuanto a las superficies específicas, las muestras pirolizadas muestran valores similares entorno a 700 $m^2 g^{-1}$ y el volumen total de poros disminuye con el aumento de R/C indicando igualmente que a valores bajos se favorece la formación de meso y microporos mientras que a R/C altos se favorece la formación de macroporos. Las muestras activadas muestran una superficie específica mayor con respecto a las pirolizadas, mientras que este valor disminuía con el aumento de R/C.

Las voltametrías cíclicas a 0,5 $mV\ s^{-1}$ muestran curvas con perfiles capacitivos, cuyas capacitancias son mayores en las muestras activadas que en las pirolizadas y en ambos casos parecen mostrar una buena correlación con el volumen de mesoporos y no con el volumen de microporos o superficie específica. Este comportamiento se reproduce para el caso del fosfato sódico aunque con valores de capacitancia menores que en el caso del nitrato, lo que indica una influencia destacable del tamaño iónico sobre este parámetro.

La caracterización electroquímica por cronoculometría en nitrato sódico indica que las muestras activadas presentan una mejor cinética de transporte por los menores valores del parámetro τ en relación a las muestras pirolizadas. En cambio, la misma técnica con fosfato sódico presenta valores más similares en ambos casos lo que indica una clara dependencia de la cinética con el volumen de microporos y con el tamaño de los iones. En el caso del fosfato sódico, el tamaño del ión fosfato es un factor limitante del proceso. En cuanto a la resistencia a la polarización, tanto las muestras pirolizadas como las activadas muestran un aumento de este parámetro con el valor de R/C para ambos electrólitos, mostrando valores sensiblemente mayores para el caso del fosfato sódico en todas las muestras, lo que indica una clara dependencia de este parámetro con el tamaño iónico.

El aerogel sintetizado con un R/C de 200 y posteriormente activado fue el que mostró mejor comportamiento capacitivo en todos los casos y por tanto se seleccionó para los experimentos de electroadsorción con nitrato sódico. En este caso se observa un aumento de la capacidad y velocidad de adsorción con la concentración de electrolito y el voltaje aplicado. También se evalúa la capacidad de electroadsorción en fosfato y nitrato sódico 0,1 M con el aerogel pirolizado y obtenido con un R/C de 200, encontrándose que

la capacidad máxima es mayor en el caso del material activado que en el pirolizado y mayor para el nitrato que para el fosfato. En todos los casos la ciclabilidad fue buena, aunque mejor en el material activado, y el comportamiento fue estable durante varios ciclos.

3. *Síntesis dirigida por negro de carbono de aerogeles de carbono ultra-mesoporosos.*

Se sintetizaron varios aerogeles de carbono con diferentes relaciones molares R/C (25, 50, 100 y 200) y con las relaciones R/F y R/W fijas de 0,5 y 0,06 respectivamente, añadiendo 0%, 5% o 10% de negro de carbono durante la síntesis. Los aerogeles así preparados se sometieron a pirólisis a 500, 800 y 1000ºC. La nomenclatura empleada fue Gx-CByT siendo x la proporción R/C, y el % de negro de carbono y T la temperatura de pirólisis. Lo primero que se observa es que el empleo del aditivo carbonoso no impide el proceso de gelado ni produce hinchamiento, independientemente de la cantidad empleada. Esta observación se corrobora mediante las imágenes de TEM. La pirólisis a diferentes temperaturas preservó la integridad estructural de los monolitos aunque se observan algunas fracturas en los RC 100 y 200 pero el empleo del aditivo mejoraba sin embargo la resistencia mecánica en estos casos. Las isotermas de adsorción revelan diferencias en la estructura porosa de los materiales con aditivo y sin aditivo. La porosidad de los materiales sintetizados sin aditivo muestra el comportamiento usual en relación a la proporción R/C, es decir, un aumento gradual de la mesoporosidad, mientras que los materiales preparados en presencia del aditivo de carbono muestran un gran aumento de la mesoporosidad con respecto a los anteriores. Todas las isotermas son de tipo IV y muestran constricciones en el bucle de histéresis indicativo de mesoporos cilíndricos abiertos y bloqueados, interconectados mediante cuellos de botella. En las muestras G25-CB10 y G50-CB10, las isotermas muestran una distribución de poros heterogénea mientras que las G100/200-CB10 muestran una distribución más uniforme. Los parámetros texturales indican que la microporosidad es similar en los materiales aditivados que en los controles mientras que la mesoporosidad aumenta considerablemente en los materiales aditivados. El cálculo del tamaño de poros mediante NL-DFT revela la típica distribución monodispersa cuya media aumenta con la

proporción R/C de 5 a 12 nm, mientras que las muestras aditivadas presentan una distribución multimodal en todos los casos con tamaños medios que van de los 7 a los 22 nm. Por otra parte, la cantidad de aditivo también influye en la porosidad de los aerogeles, observándose que el aumento del 5 al 10% produce un ensanchamiento de los mesoporos que se evidencia por el desplazamiento de los bucles de histéresis de las isotermas a presiones relativas más altas por lo que esta variable junto con la proporción R/C controla el tamaño de los mesoporos. También el tamaño de los poros conectores aumenta con la cantidad de aditivo como indican el desplazamiento hacia arriba y la presencia de dos etapas en la isoterma.

La temperatura de pirólisis parece no afectar significativamente a la porosidad de los aerogeles aditivados, al contrario de lo que ocurre en los aerogeles preparados en ausencia del aditivo donde el aumento de la temperatura produce un colapso parcial de la porosidad debido a las tensiones superficiales que se ejercen en la matriz de carbono durante la desvolatilización; las partículas de negro de carbono de los materiales aditivados contrarrestan este colapso obteniéndose materiales más estables estructuralmente.

Se midió la resistitividad eléctrica de los diferentes aerogeles observándose que esta disminuye al aumentar el R/C en los aerogeles control, mientras que en los materiales aditivados decrece un orden de magnitud siguiendo la misma tendencia con R/C lo que se atribuye a una mayor densidad de defectos en los aerogeles poliméricos. Además se observa una dependencia de la resistividad con la temperatura de pirólisis en el caso de los R/C bajos, encontrándose que para $T \leq 500$ ºC el material no es conductor y para T=1000 ºC la resistividad del mismo material es casi la mitad del pirolizado a 800 ºC. Este comportamiento se atribuye a los grupos OH superficiales presentes en la matriz carbonosa, que solo se eliminan a altas temperaturas.

Los aerogeles se caracterizaron mediante voltametría cíclica observándose la forma rectangular típica del comportamiento capacitivo, a excepción de la aparición de algún hombro a potenciales anódicos debido a la electrooxidación del H_2 naciente adsorbido en los poros del material; no se observa ningún pico de corriente típico de reacciones farádicas, lo que concuerda con el bajo contenido en O_2 de los materiales pirolizados. Con esta técnica también se observa que los materiales pirolizados a 500 ºC

no presentan respuesta capacitiva. Los electrodos pirolizados a 800 y 1000 ºC mostraron un comportamiento reversible y estable durante varios ciclos. Se estudió la evolución de la capacidad a potencial constante de 1,4 V y se observó que la caída de la capacidad con el número de ciclos dependía de la relación R/C y de la presencia de aditivo, siendo los materiales más estables los preparados con un R/C 200 y aditivo.

4. *Sobre el uso de diatomeas como agente anti-encogimiento en la preparación de aerogeles de carbono monolíticos.*

Con el fin de evitar los problemas mecánicos que se encuentran durante la síntesis de un aerogel de carbono monolítico, como el encogimiento, agrietamiento, deformación o fractura, se sintetizaron varios aerogeles de carbono empleando tierra de diatomea (D) en la etapa de polimerización como aditivo estructural sacrificial. Los formulados contenían como precursores resorcinol, formaldehído y en algunos casos melamina y como aditivos diatomea y/o negro de carbono (B). Se observó que todos los aerogeles pirolizados que no contenían D se encogían en torno a un 30% con respecto a los aerogeles sin pirolizar y los que contenían B además se deformaban considerablemente, mientras que todos los que contenían D preservaban la forma y el tamaño después de pirolizar e incluso después de la eliminación de D con ácido fluorhídrico. Los ensayos de fractura a 30 N producen fractura concoidal en los materiales sin D mientras que los que llevan este aditivo, muestran deformación en lugar de fractura. Estos resultados están en concordancia con los ensayos de micropunzonado, en los que las curvas de carga-desplazamiento muestran un comportamiento inelástico y quebradizo en los materiales sin D y plástico y tenaz en los materiales con D, incluyendo los aerogeles pirolizados y con el aditivo lixiviado posteriormente con HF. Este comportamiento es atribuible a los grandes huecos que deja el aditivo después de su eliminación.

En cuanto a la caracterización textural, todas las isotermas de N_2 son de tipo IV y, mientras la microporosidad es similar en las muestras con y sin aditivo silíceo, la mesoporosidad de los materiales preparados con D disminuye. Esto se atribuye a que gran parte de la mesoporosidad pasa a macroporosidad debido a la presencia del aditivo,

ya que este produce una caída en la velocidad de polimerización produciendo partículas de polímero menos entrecruzadas y más grandes.

Por otro lado, la conductividad eléctrica está controlada principalmente por el contenido en B y los materiales con D tienen en general una conductividad menor que aumenta cuando se elimina el aditivo con HF.

5. *Síntesis de aerogeles mecánicamente conformes mediante el empleo de aditivos conductores y estructurales.*

Se sintetizaron varios aerogeles de carbono empleado tierra de diatomea (D) en la etapa de polimerización como aditivo estructural sacrificial. Los formulados contenían como precursores resorcinol, formaldehído y en algunos casos melamina (M) y como aditivos diatomea y/o negro de carbono (B). Las proporciones molares de precursores fueron (M+R)/C de 135 y (M+R)/W de 0,052. Los diferentes aerogeles obtenidos se carbonizaron a 800 ºC y parte de los que contenían D se trataron con HF para eliminar el aditivo. La caracterización por SEM muestra que todos los aerogeles con D presentan la misma superficie rugosa y con grandes cráteres mientras que los que no llevan este aditivo presentan superficies lisas y compactas. Asimismo, la densidad de los aerogeles D presentan los valores más bajos de todos después de eliminar el aditivo. En la caracterización por TEM se pueden observar las partículas de B en los materiales preparados con este aditivo. La caracterización por difracción de rayos X no revela diferencias entre los materiales con y sin B pero si aparecen picos a 27,7; 43,4 y 44,6º debidos al silicio de la diatomea en las muestras D y D+B no lixiviadas. El espectro Raman de primer orden revela las típicas bandas a 1344 cm^{-1} (banda D) y 1590 cm^{-1} (banda G) atribuibles al modo desordenado y a los desplazamientos de carbono en láminas grafénicas respectivamente. La relación I_D/I_G es algo menor en las muestras con B confirmando el mayor orden estructural que confiere este aditivo.

Las isotermas de N_2 son todas del tipo IVb con bucles de histéresis, revelando que todas las muestras son micro y mesoporosas lo que indica que los aditivos no impiden la policondensación de los precursores. El desplazamiento de los bucles de histéresis a presiones relativas mayores de las muestras con D y/o B demuestra un aumento del

tamaño de los mesoporos lo que sugiere que la policondensación se enlentece en presencia de cualquiera de los aditivos, dando lugar a clusters poco ramificados que forman grandes agregados coloidales con poros de gran tamaño. Se observa también que el volumen total de poros y la superficie específica disminuyen en los materiales con D, incluso después de lixiviados, y en los materiales con D+B cae el volumen de mesoporos contrarrestando el efecto favorable de B en su creación, lo que indicaría que la agregación de clusters se ve en parte limitada por la gran cantidad de diatomea introducida. El análisis de la distribución de poros indica que los aerogeles puros presentan una distribución bimodal con un picos principales centrados en torno a 0,5 nm y 18 nm, mientras que en los cargados con D o D+B el segundo pico se suprime apareciendo en ambos casos un pequeño montículo en torno a 50 nm. Este resultado concuerda perfectamente con la porosimetría de mercurio en la que aparece un pico a 18 nm en el aerogel puro y otro pico en torno a 50 nm en los aerogeles aditivados. Además, en los materiales lixiviados aparecen picos a 1000 nm y entre 100 y 1000 nm para los D y B+D respectivamente, correspondientes a los huecos que deja la diatomea después de eliminarse con HF.

Los ensayos de fractura a 30 N producen fractura concoidal en los materiales sin D mientras que los que llevan este aditivo muestran deformación en lugar de fractura. Estos resultados están en concordancia con los ensayos de micropunzonado en los que las curvas de carga-desplazamiento muestran un comportamiento inelástico y quebradizo en los materiales sin D y plástico y tenaz en los materiales con D, incluyendo los aerogeles pirolizados y con el aditivo eliminado posteriormente con HF. Este comportamiento es atribuible a los grandes huecos que deja el aditivo después de su eliminación.

La caracterización electroquímica se lleva a cabo mediante voltametría cíclica en NaCl 0,1 M, con una celda de tres electrodos. Los voltamogramas la forma rectangular típica de un comportamiento capacitivo de adsorción en doble capa. El aerogel puro presenta la mayor capacitancia (80 F g^{-1}) mientras que los materiales aditivados presentan una caída drástica de este valor y los materiales lixiviados presentan cierta recuperación de la capacitancia hasta valores de 50-53 F g^{-1}. Este comportamiento está en correspondencia con las variaciones en microporosidad y superficie específica obtenidas en la caracterización textural. Para ver la influencia de la porosidad en la cinética de

electroadsorción se hacen medidas cronoculométricas a 300 mV durante 120s revelando que las muestras aditivadas no lixiviadas presentan una cinética más rápida ya que se saturan antes. La resistencia de los materiales al transporte iónico, R_{pol}, se midió mediante espectroscopia de impedancia electroquímica revelando que los materiales aditivados disminuían su R_{pol} de 1,52 Ohm·g para el aerogel puro a 0,68 y 1,1 Ohm·g para las muestras D y DB respectivamente, lo que se atribuye a una mejor accesibilidad a los microporos producida por la presencia de D y a una incremento de la conductividad eléctrica del material aditivado con B, lo que a su vez se ve corroborado por las medidas de conductividad eléctrica de los monolitos.

6. *Aerogeles de carbono monolíticos dopados con nitrógeno y funcionalizados con manganeso de macroporosidad incrementada para desionización capacitiva.*

Se sintetizaron varios aerogeles de carbono empleado melamina (M), resorcinol (R) y formaldehído (F) como precursores, carbonato sódico como catalizador (C) además de diatomea (D) y negro de carbono (B) como aditivos estructurales y de conductividad respectivamente. Las proporciones molares de precursores fueron R:M:F de 2:1:7, (M+R)/C de 135 y (M+R)/W de 0,053. Las muestras se secaron en CO_2 supercrítico y se carbonizaron a 480 ºC. Los aerogeles obtenidos se lixiviaron en HF para eliminar la diatomea y se seleccionaron muestras que se doparon con Mn por inmersión y posterior activación a 750 ºC en CO_2. Los materiales aditivados con D no mostraron encogimiento después del tratamiento térmico ni después del lixiviado. Se realizó una prueba de mojabilidad que reveló que la adición de diatomea confiere un carácter hidrófilo al material asegurando una buena impregnación con el electrólito mientras que las muestras que solo contenían Mn mostraron ángulos de contacto de 71º, indicando que solamente la deposición de Mn afecta negativamente a la mojabilidad. La caracterización por SEM muestra que todos los aerogeles tratados con D presentan la misma superficie rugosa y con grandes cráteres, mientras que los que no llevan este aditivo presentan superficies lisas y compactas. Asimismo, la densidad de los aerogeles tratados con D presentan los valores más bajos de todos (0,15 $cm^3\ g^{-1}$) después de eliminar el aditivo. Las imágenes TEM muestran las nanopartículas de Mn dispersas por la matriz de carbono además de grandes huecos en caso de las muestras con D y B.

Las isotermas de adsorción de N_2 son de tipo IV en todos los casos, revelando que todos los materiales son porosos y que las reacciones de policondensación no se ven afectadas por la presencia de los aditivos D y B. Sin embargo los amplios bucles de histéresis observados en estas muestras revelan que la cinética de estas reacciones se hace más lenta dando lugar a grandes clusters poco entrecruzados y ramificados, lo que da lugar a poros de gran tamaño. Por otro lado la incorporación de D produce una ligera disminución en el volumen total de poros y un ligero incremento en la microporosidad lo que lleva a valores de superficie específica mayores que los geles sin D, mientras que todos los materiales con B presentan un incremento en el volumen de los mesoporos. El análisis de la distribución de poros indica que los aerogeles tratados con D presentan una distribución multimodal y la porosimetría de mercurio revela una contribución adicional de macroporos (500 nm) en las muestras Mn-D y Mn-DB y la muestra solo con B muestra una contribución de poros de 10 micras.

La caracterización por XPS revela que la incorporación de Mn produce una caída relativa en los contenidos de C y N, mientras produce un aumento del contenido en O lo que sugiere la formación de óxidos de manganeso. Estos no se detectaron en los diagramas de difracción probablemente debido a su bajo contenido y a su carácter amorfo. El análisis elemental, por otra parte, arroja valores de nitrógeno ligeramente superiores a los obtenidos por XPS, indicando que el N está uniformemente distribuido por toda la matriz y no solo en superficie.

Las R_{pol} de los materiales obtenidas a partir de los gráficos de Nyquist muestran la tendencia MRF-Mn-D-CB (0.45 Ω×g), MRF-Mn-D (0.57 Ω×g), MRF (0.79 Ω×g) y MRF-Mn (1.02 Ω×g) indicando que la adición tanto de D como de B disminuye la resistencia interna del material, lo que se puede atribuir a la inducción de macroporos por parte de D y al efecto conductor del B. El elevado valor obtenido para MRF-Mn puede deberse a su carácter menos hidrófilo, lo que impediría un buen contacto de la interfase electrodo-electrólito. Las voltametrías cíclicas en celda de tres electrodos revelan voltamogramas con forma rectangular típica de procesos capacitivos, que en el caso de los materiales con D presentan ciertas desviaciones en el barrido anódico que pueden ser debidas a la presencia de Mn y/o de de grupos conteniendo O y N.

Los valores de capacitancia obtenidos por voltametría cíclica, 90 F g^{-1} para MRF y 86 F g^{-1} para MRF-Mn, muestran que la baja mojabilidad de este último puede ser la causa de este valor más bajo, mientras que las capacitancias de MRF-Mn-D y MRF-Mn-D-CB de 104 y 113 F g^{-1} respectivamente pueden deberse tanto a una mayor macroporosidad como a una mejor mojabilidad.

Los ensayos de electroadsorción en monolitos en NaCl 0,025 M a 0,9, 1,2 y 1,5 V no muestran el mismo comportamiento que las capacitancias ya que los valores que presentan MRF y MRF-Mn-D-CB son muy similares, lo que puede indicar que los comportamientos del material en polvo y en monolito son diferentes. Las mayores capacidades se obtienen a 0,9 V con valores de 6,7 y 6,1 mg g^{-1} para los aerogeles MRF y MRF-Mn-D-CB, respectivamente. Los ensayos a 1,5 V y 0,1 M muestran que el material MRF-Mn-D-CB presenta una mejor cinética y una mayor capacidad de electroadsorción que MRF y MRF-Mn-D.

4.2 Summary

1. On the correlation between the porous structure and the electrochemical response of powdered and monolithic carbon aerogels as electrodes for capacitive deionization

Several carbon aerogeels were synthesized by sol-gel polymerization with different resorcinol-catalyst (R/C) and resorcinol-water molar ratios which varied between 100 and 800 and 0.04 and 0.13 respectively, while keeping a fixed resorcinol-formaldehyde molar ratio of 0.5. The obtained hydrogels were dried in supercritical CO_2, pyrolized at 800 ºC and activated with CO_2 at 800 ºC for 2 h. The N_2 adsorption isotherms show a direct influence of the R/C and R/W ratios either on the pyrolized or the activated materials. The mesopore volume increases with R/C ratio until 2,25 $cm^3\ g^{-1}$ for an R/C of 300 from which it falls abruptly till 0,08 $cm^3 g^{-1}$. This behavior is observed for an R/W of 0.04. For an R/W of 0.06 the behavior is somehow similar though the maximum of the mesopore volume is displaced to an R/C of 200, is smaller than for R/W 0.04 and the fall is less sharp. For R/W of 0.10 and 0.13 the trend is the increase of the mesopore volume with R/C for the whole range of values from 0.62 to 0.71 and from 0.27 to 0.48 0,08 $cm^3\ g^{-1}$ respectively. A similar behavior was observed in tha activated aerogels suggesting that activation does not affect the mesoporosity which is governed only by the R/C and R/W ratios. For the low R/W ratios of the pyrolized aerogels the specific surface decreases linearly with R/C from 757 to 587 $m^2\ g^{-1}$ for R/C 100 and 600 respectively, while for high R/W (0,1-0,13) the trend is a slight linear increase of the specific surface with R/C. These trends are the same in the activated materials though their specific surfaces are sensiblemente higher in both cases. The dependence of the specific surface with R/W ratio shows similar trends: for low R/C the surface decreases linearly with R/W while it increases slightly for high R/C ratios and the same is observed with the activated aerogels. This behavior of the textural parameters is explained by the different polymeric structures obtained in the precursor gels for the different R/C and R/W ratios.

The carbon aerogels were crushed and electrodes were casted and assembled in a three electrode Swagelock cells to study their electrochemical properties. The cyclic voltammetries showed in all cases the typical box-like shape of the capacitive behavior plus a small anodic peak appearing in some case suggesting oxidation of surface groups or electrolyte decomposition. Capacitances showed a clear trend to increase with the

specific surface varying from 50 to 70 F g^{-1} for lowest surface materials to 120 F g^{-1} for the highest surface material.This trend was less clear for the pyrolized materials,being attributed to the surface chemistry effects; more specifically, to a lower amount of oxygen than in the activated material, which would be responsible of the pseudo-capacitive effects. The polarization resistance (R_{pol}) measured by electrochemical impedance spectroscopy shows a clear decreasing trend with the specific surface and capacitance, being lower in the activated than in the pyrolized materials. Likewise, as the mesopore volume increases there is a clear decrease of R_{pol} either in the activated or pyrolized materials, while no correlation with the micropore volume is shown. This behavior can be explained by a better ion transport inside the porous network of the materials with the highest mesopore volume and by a better accessibility of the active surface. Este comportamiento se puede explicar por un mejor transporte de los iones en el interior del electrodo por la red porosa en los materiales con mayor volumen de mesoporos y por una mejor accesibilidad de la superficie activa. The materials with low R/W showed a meaningful increase of R_{pol} with R/C ratio while those with R/C 0.1 showed the opposite effect.

To evaluate the desalting capacity a two-electrode cell with monolithic aerogel electrodes was assembled with NaCl 0,1 M electrolyte, measuring the total charge transfer during the three charge-discharge cycle. Considering the specific surface alone no clear correlation is observed between this parameter and the total charge transfer. But considering also the electric resistivity of each material a predictable pattern is recognized that can be described by a multivaritae polynom of 3rd order in the resistivity and 2nd order in the specific surface in the case of pyrolized aerogels and of first order in both variables for the activated aerogels.

2. Improved electro-assisted removal of phosphates and nitrates using mesoporous carbon aerogels with controlled porosity

Carbon aerogels were synthesized by the resorcinol-formaldehyde method setting theresorcinol-catalyst molar ratio R/C) to 200, 400 and 600 and resorcinol-water ratio (R/W) of 0.06. After controlled water-acetone exchange the materials were dried in supercritical CO_2, carbonized at 800 ºC under nitrogen atmosphere and one batch was activated at 800 ºC during 2 h. The obtained materials were structurally characterized by

X-ray diffractionand Raman spectroscopy. The patterns reveal the presence of mainly disordered carbon, although with meaningful graphitic domains. The first order Raman spectrum deconvolution reveals a G-band at 1580 cm^{-1} assigned to the carbon atoms displacement within the graphenic sheets and a D1-band at 1350 cm^{-1} assigned usually to the lack of long range translational symmetry. A D2 lorentzian curve is added to solve the observed asymmetry in the G-band, assigned to the non-stacked graphenic sheets vibrations. Likewise a D3 gaussian curve appears at 1495 cm^{-1} assigned to vibrations of sp^2 carbon linked to graphenic sheets edges and D4-band at 1160 cm^{-1} assigned to sp^2-sp^3 polyene stretching. It is shown that the D1/G intensity ratio decreases either with activation or with R/C increase, suggesting structural order dependence with this ratio. The XPS spectra reveal the presence C-O (285.6±0.2 eV), C=O (287 eV±0.1 eV) and O=C-O (288.7±0.3 eV) groups and an increase in the contribution of the C-O and C=O groups is observed when R/C diminishes. The textural analysis reveals that as R/C increases in the pyrolized samples, the size of the mesopores increases turning part of them into macropores while the micropores volume remains constant. Regarding the specific surface, the pyrolized samples show similar values around 700 $m^2 g^{-1}$ and the total pore volume decreases with the R/C ratio increase suggesting likewise that at low values, meso and micropore formation is promoted while at high R/C ratios macropores are promoted. The activated samples show a larger surface area compared to the pyrolized ones, while this value diminishes with the increase of R/C.

Cyclic voltammetries at 0,5 mV s^{-1} showcapacitive profiles which capacitances are larger for the activated than in the pyrolized samples showing in both cases a good correlation with the mesopore volume but not with the micropore volume or the specific surface. This behavior is replicated with the sodium phosphate although with lower capacitances than the sodium nitrate, suggesting a notable influence of the ionic size on this parameter.

Electrochemical characterization by chronocoulommetry in sodium nitrate shows that activated samples have faster kinetics due to the smaller τ than in the pyrolized samples. Conversely, the same characterization in sodium phosphate shows more similar τ values suggesting a dependence on the ion size and the micropore volume of the kinetics. Sodium phosphate ionic size is a limiting factor of the process in this case. Regarding polarization resistance, either activated or pyrolized samples show an increase in this

parameter with R/C in both electrolytes, having sodium phosphate noticeably higher values in all the tested samples suggesting again a dependence of this parameter on the ionic size.

The aerogel with R/C 200 and activated was the one with best capacitive behavior and therefore was selected for the experiments of sodium nitrate electrosorption. An increase in electrosorption capacity and rate with electrolyte concentration and applied voltage is observed. The R/C 200 pyrolized aerogel was also tested for 0.1 M sodium nitrate and phosphate electrosorption, finding that the maximum capacity is higher in the activated than in the pyrolized material and higher for the nitrate than for the phosphate. Cyclability was good in all cases, though better in the activated material, and stable behavior was observed in all cycles.

3. Carbon black directed synthesis of ultra-high mesoporous carbon aerogels.

Several carbon aerogels were synthesized with different R/C molar ratios (25, 50, 100 and 200) and with R/F and R/W fixed ratios of 0,5 and 0,06 respectively with the addition of 0%, 5% o 10% of carbon black during the synthesis. So prepared aerogels were pyrolized at 500, 800 and 1000ºC and were named Gx-CByT being x the R/C ratio, y the carbon black content in % and T the pyrolysis temperature. The first observation is that carbon black additive neither impairs gelation nor produces swelling of the material, regardless of the added quantity. This observation is supported by the TEM micrographies. The structural integrity at different pyrolysis temperatures was preserved in the monolithic pieces and, although some fractures were observed in the case of R/C 100 and 200, the mechanical resistance was improved by the additive in those cases. The adsorption isotherms reveal differences in the porous structure of the materials with and without additive. The porosity of the materials synthasized without additive shows the usual behavior in what R/C ratio is concerned, a gradual increase in porosity, while the materials with carbon black additive show a high increase in the mesoporosity as compared with the former ones. All isotherms were type IV showing constrictions in the hysteresis loop suggesting open-blocked, bottle-neck interconnected, cylindrical mesopores. In G25-CB10 y G50-CB10 samples, the isotherms show a heterogeneous pore size distribution while G100/200-CB10 isotherms show a more uniform one. Textural parameters denote that microporosity in the materials with additive and in the

controls are alike while mesoporosity increases noticeably in the materials with additive. The NL-DFT pore size distribution reveals the typical unimodal distribution which peak value increases from 5 to 12 nm with R/C ratio, while the samples with additive show a multimodal distribution in all cases with average sizes varying from 7 to 22 nm. By the other hand, the amount of additive also has influence on the aerogel porosity, showing that an increase from 5 to 10% widens the mesopores which is evidenced by the hysteresis loop displacement to higher relative presures concluding that this variable, along with R/C ratio, controls the mesopore size.

Pyrolysis temperature does not seem to significantly affect the porosity of the aerogels with additive, conversely to the aerogels without additives where the increase in temperature partially collapses the porosity due to surface tensions exerted on the carbon matrix during gas evolution; carbon black particles in the materials with additive counteract the collapse obtaining more structurally stable materials.

The electrical resistivity of the different aerogels was measured and decrease of this parameter was observed when R/C was increased in the control materials, while in the materials with additive resistivity decreases an order of magnitude following the same trend with R/C which can be attributed to a higher defect density in the polymeric aerogels. A dependence of the resistivity with pyrolysis temperature is also observed in the case of low R/C, finding that for $T \leq 500$ ºC the material is non conducting and for T=1000 ºC resistivity of the same material is almost one half of the pyrolized at 800 ºC. This behavior can be attributed to the surface OH groups present in the carbon matrix which only are eliminated at high temperatures.

The aerogels were characterized by cyclic voltammetry obtaining the typical box-like shape of the capacitive behavior, excepting for a hump at anodic potentials due nascent H_2 electro-oxidation adsorbed onto the pores of the electrode. No faradaic current peak is observed which is in agreement with the low O_2 content of the pyrolized materials. With the same method is also observed that the materials pyrolized at 500 ºC do not show a capacitive response. The electrodes pyrolized at 800 y 1000 ºC showed a reversible and stable behavior during several cycles. The evolution of the capacity at 1,4 V constant potential was tested and it was observed that the capacity decrease with the number of

cycles depended on the R/C ratio and the presence of additive being the most stable materials the ones prepared with additive and an R/C of 200.

4. On the use of diatomite as anti-shrinkage additive in the preparation of monolithic aerogels.

In order to avoid those mechanical issues encountered during the synthesis of a monolithic carbon aerogel, as shrinkage, cracking, deformation or fracture, several carbon aerogels were synthesized using diatomite (D) in the polymerization stage as a sacrificial structural additive. The studied samples contained resorcinol and formaldehide, and melamine in some cases, as precursors and diatomite and/or carbon black (B) as additives. It was observed that all the pyrolized aerogels that did not contain D shrunk themselves around a 30% compared to the non pyrolized aerogels and the ones containing B, besides, noticeably deformed themselves, while all the D-containing aerogels preserved their size and shape after pyrolysis, even after D lixiviation with hydrofluoric acid. The fracture assays performed at 30 Nprovoked a conchoidal fracture in the materials without D while the ones without D show deformation instead of fracture. These results are in agreement with the small punch tests in which the strain-stress curves show an inelastic and brittle behavior in the non D-containing materials and a complaining and plastic behavior in the D-containing materials even after lixiviation with HF. This behavior can be attributed to the large pores that remain after the additive lixiviation.

Regarding the textural characterization, all N_2 isotherms are type IV and, while microporosity is similar in samples with or without diatomite, mesoporosity decreases in the materials prepared with D. This is because part of the mesoporosity turns into macroporosity due to the presence of the additive which causes a fall in the polymerization kinetics producing larger and less cross-linked polymer particles.

By the other hand, electrical conductivity is mainly controlled by B content and materials with D have in general a lower conductivity which increases on additive lixiviation with HF.

5. Synthesis of porous and mechanically compliant carbon aerogels using conductive and structural additives.

Several carbon aerogels were synthesized using diatomite (D) as sacrificial structural additive during the polymerization stage. The precusors of the formulates were resorcynol (R), formaldehyde (F) and melamine (M) in some cases and diatomite and/or carbon black (B) as additives. The molar ratios of precursors were (M+R)/C=135 and (M+R)/W=0,052. The obtained aerogels were carbonized at 800 ºC and a batch of those containing D were lixiviated with HF. SEM characterization shows that all the D-containing aerogels present the same rough surface with large craters, while theD-free onesshow a smooth compact surface. Likewise, the density of the D-aerogels shows the lowest values after additive lixiviation. Regarding TEM characterization, B particles can be observed in the materials prepared with this additive. X-ray diffraction does not reveal differences between the B-containing and not containing materials but peaks at 27,7; 43,4 y 44,6º do appear in D and D+B non lixiviated samples, due to the silica contained in the diatomite. The first order Raman spectrum reveals the typical bands at 1344 cm^{-1} (D band) and 1590 cm^{-1} (G band) assigned to the disordered mode and carbon atoms displacement in the graphenic sheets respectively. The I_D/I_G ratio is slightly lower in the B-containing samples evidencing the higher structural order conferred by this additive.

The N_2 adsorption isotherms belong to type IVb with hysteresis loops, revealing that all the samples are micro and mesoporous pointing out that the additives do not impair the polycondensation of theprecursors. The hysteresis loop displacement to highwe relative presures observed in thesamples containing D and/or B evidenced an increase in mesopore size. Suggesting that the polycondensation reaction slowed down in the presence of any of the additives giving place to weakly branched clusters whichyields large colloidal aggregates with large pore sizes. A diminution in the total pore volume and specific surface was also observed in the D-containing materials, even after etching, and mesopore volumedecreased in the materials containing D+B, counteracting the favorable effect of B on its formation.This suggested that cluster aggregation is somehow limited by the large amount of added diatomite. The pore size distribution analysis points out that pure aerogels show a bimodal distribution with peaks centered at around 0,5 nm y 18 nm, while in the samples containing D or D+B the second peak is suppressed with a small hump around 50 nm appearing in both cases. This result is in perfect agreement with mercury porosimetry in which a peak at 18 nm and another around 50 nm appears in the pure and additive-containing aerogels respectively. Likewise, peaks at 1000 nm and

between 100 and 1000 nm appear in the etched D and D+B materials respectively, corresponding to the holes left by diatomite after HF etching.

The fracture assays at 30 N produce a conchoidal fracture in the materials without D while the ones containing D show deformation instead. Those results are in agreement with small punch test results in which the load-displacement curves show a brittle and inelastic behavior of the pristine materials and plastic and compliant in the D-containing ones including the etched pyrolized aerogels. This bhavior can be explained by the large holes left by diatomite after etching.

The electrochemical characterizarion is carried out by cyclic voltammetry in 0.1 M NaCl in a three-electrode cell. All the volatmmograms show the typical box-like shape of the double layer capacitive behavior. Pristine aerogel shows the highest capacitance (80 F g^{-1}) while the naterials with additive show a drastic decrease in this parameter. However, the etched materials show some recovery of the capacitanceuntil 50-53 F g^{-1}. This behavior is in agreement with the microporosity and specific surface variationsdetermined in the textural characterization. In order to study the influence of the porosity on electrosorption kinetics, chronocoulometric measurements at 300 mV during 120 s were performed. They revealed that non etched samples with additives saturate earlier suggesting a faster kinetic. The ionic transport resistance R_{pol}, was measured by electrochemical impedance spectroscopy revealing that this parameter decreases from 1,52 Ohm·g for the pristine aerogel to 0,68 and 1,1 Ohm·g for samples D and DB respectively. This was attributed to a better micropore accesibility due to the presence of D and to an increase in electrical conductivity in the B-containing material which is at the same time corroborated by the electrical conductivity measurements carried out on the aerogel monoliths.

6. Mn containing N-doped monolithic carbon aerogels with enhanced macroporosity as electrode for capacitive deionization.

Several carbon aerogels were synthesized with melamine (M), resorcinol (R) and formaldehyde (F) as precursors, sodium carbonate as catalyst (C) and diatomite (D) and carbon black (B) as structural and conductive additives respectively. The molar ratios used were R:M:F=2:1:7, (M+R)/C= 135 and (M+R)/W= 0,053. Samples were dried in supercritical CO_2 and carbonized at 480 ºC. The obtained aerogels were etched with HF

to eliminate the diatomite and some of these samples were selected to be doped with Mn by immersion followed by CO_2 activation at 750 ºC. The materials containing D did not show shrinkage neither after thermal treatment nor after etching. A wettability test revealed that diatomite addition confers hydrophilic features to the material guaranteeing a good impregnation with the electrolyte. Otherwise, samples only containing Mn showed contact angles of 71º, suggesting that the deposition of Mn alone negatively affects to the wettability of the sample. SEM characterization shows that all the D-containing aerogels present the same rough surface with large craters, while the non D-containing ones present a smooth compact surface. Likewise, the density of the D-aerogels show the lowest values (0,15 $cm^3\ g^{-1}$) after additive lixiviation. TEM characterization shows Mn nanoparticles spreadthroughout the carbon matrixand large holes in the case of samples with D and B.

The N_2 adsorption isotherms are all type IV, revealing that all the materials are porous and the polycondensation reactions are not hindered by the presence of B and D additives. Nevertheless, the large hysteresis loops observed in these samples evidenced that the kinetic of the reactions slows down giving place to large andpoorly branched clusters. By the other hand, the incorporation of D slightly diminishes the total pore volume and slightly increases the microporosity taking to higher specific surface values than the gels without D, while all the materials with B present an increase in the mesopore volume. The pore size distribution analysis points out that aerogels treated with D present a multimodal distribution and mercury porosimetry reveals an aditional contribution of macropores (500 nm) in samples Mn-D and Mn-DB. Finally, the sample only containing B shows a contribution of 10 micron pores.

XPS characterization reveals that Mn incorporation yields a relative fall in C and N contents while the oxygen content increased, suggesting the formation of manganese oxides. These compounds were not detected in the diffraction diagrams probably due to its low content and amorphous character. By the other hand, the elemental analysisunveils a nitrogen content slightly higher than thevaluesdetermined by XPS, indicating that N is uniformly distributed in the whole carbon matrix and not only on the surface.

The R_{pol} of the materials obtained from the Nyquist plots shows the trend MRF-Mn-D-CB (0.45 Ω×g), MRF-Mn-D (0.57 Ω×g), MRF (0.79 Ω×g) y MRF-Mn (1.02 Ω×g)

suggesting that either D or B addition decreases the internal resistance of the material which can be attributed to a macropore induction by D and to a conductive effect by B. The high value obtained for MRF-Mn can be attributed to its less hydrophilic character which could impair a good electrode-electrolyte interphase contact.

Cyclic voltammetries in three-electrode cells reveal the typical box-like shape of capacitive processes, that in the case of the materials containing D show certain deviations in the anodic swept that could be due to the presence of Mn and/or groups containing O and N.

The capacitance values obtained by cyclic voltammetry, 90 F g^{-1} for MRF and 86 F g^{-1} for MRF-Mn, suggest that the poor wettability of the last could be the cause of such a low capacitance, while capacitances of MRF-Mn-D and MRF-Mn-D-CB of 104 and 113 F g^{-1} respectively can be due either to a higher macroporsity or a better wettability.

Electrosorption assays with aerogel monoliths in NaCl 0,025 M at 0,9, 1,2 and 1,5 V do not show the same behavior that capacitances ya que the values of MRF and MRF-Mn-D-CB are very similar, suggesting that the behavior of monolithic and powdered material are different. The highest capacities are obtained at 0,9 V with values of 6,7 and 6,1 mg g^{-1} for MRF and MRF-Mn-D-CB, respectively. The tests at 1,5 V and 0,1 M show that the MRF-Mn-D-CB sample shows better kinetic and electrosorption capacity than MRF y MRF-Mn-D.

4.3 Conclusiones finales

Las conclusiones generales que hemos podido obtener a la vista de los resultados presentados y discutidos en esta memoria son las siguientes:

1. La preparación de una serie de aerogeles de carbono por policondensación de resorcinol y formaldehído a diferentes proporciones molares de precursores, revela una fuerte interdependencia entre las proporciones R/C y R/W.

2. Se observa una fuerte caída de la superficie específica en los aerogeles activados cuando se incrementan las relaciones R/C o R/W, siendo este efecto más atenuado en los aerogeles pirolizados.

3. La mesoporosidad se ve afectada considerablemente por las condiciones de síntesis (e.g. relaciones R/C, R/W), mientras que la microporosidad es parecida en todos los materiales preparados.

4. La capacitancia en NaCl 0,1 M disminuye en los aerogeles preparados con altas relaciones R/C y R/W.

5. La resistencia óhmica de los aerogeles muestra una fuerte dependencia de R/C y de R/W.

6. La resistencia a la polarización es ligeramente mayor en los aerogeles pirolizados que en los activados.

7. Las resistencias de polarización más bajas se obtienen con los materiales más mesoporosos, independientemente de su microporosidad.

8. La respuesta capacitiva de aerogeles monolíticos en celdas de dos electrodos se correlaciona satisfactoriamente con el efecto combinado de la superficie específica y la resistividad del material, tanto para las muestras pirolizadas como para las activadas.

Las conclusiones de la 1 a la 8 se han obtenido de la publicación correspondiente a la sección 1 del capítulo 2.

9. Se han sintetizado aerogeles de carbono con diferentes relaciones R/C y activados con CO_2 los cuales se caracterizan con diversas técnicas y estructurales y electroquímicas y se someten a ensayos de electroadsorción en nitrato sódico y fosfato sódico.

10. Los diagramas de difracción de rayos X y los espectros Raman muestran una importante contribución de dominios grafíticos inusual en aerogeles de carbono nanoporosos sintetizados a bajas temperaturas y también se muestra una alta correlación entre la proporción R/C y el orden estructural.

11. La microporosidad fue similar para todos los materiales pirolizados, mientras que la formación de mesoporos con una distribución estrecha se produce para valores bajos de R/C. En cambio, valores elevados de este parámetro dan lugar a geles macroporosos.

12. La activación con CO_2 produce un incremento de los volúmenes de microporos acompañado de un ensanchamiento de los mesoporos siendo este efecto más significativo para valores R/C elevados.

13. Los voltamogramas cíclicos en ambos electrólitos muestran un elevado valor de capacitancia para la muestra R/C 200 activada atribuible a su mayor superficie y volumen de poros. Su mesoporosidad bien desarrollada proporciona una mejor accesibilidad, lo que facilita una mejor cinética de transporte.

14. Los experimentos de electroadsorción con el material R/C 200 activado y pirolizado mostraron un buen comportamiento con ambos electrólitos en ciclos consecutivos de carga y descarga confirmando una buena estabilidad de los electrodos de aerogel a elevados potenciales.

Las conclusiones de la 9 a la 14 se han obtenido de la publicación correspondiente a la sección 2 del capítulo 2.

15. Se han sintetizado aerogeles de carbono conductores altamente mesoporosos mediante reacción de policondensación en presencia de un aditivo conductor, negro de carbono.

16. El negro de carbono produce un gran impacto en la polimerización del gel dirigiendo la síntesis hacia partículas más grandes en clusters poco ramificados, lo que permite un

ajuste fino de la relación micro/mesoporosidad del gel aditivado y le confiere conductividad eléctrica.

17. La generación de grandes cavidades mesoporosas muy interconectadas facilita la difusión asegurando una velocidad elevada de carga y descarga de iones haciendo que sean materiales idóneos para aplicaciones capacitivas.

18. Los materiales pirolizados por encima de 500 ºC muestran una respuesta electroquímica estable en electrólito acuoso neutro para varios cientos de ciclos de carga y descarga a ventanas de potencial amplias sin pérdida significativa en densidad de corriente.

19. La incorporación del aditivo mejora la vida útil del material presentando mayor estabilidad en ciclos de carga/descarga a potencial constante de 1,4 V.

Las conclusiones de la 15 a la 19 se han obtenido de la publicación correspondiente a la sección 1 del capítulo 3.

20. Se han sintetizado aerogeles de carbono monolíticos con propiedades mecánicas y eléctricas mejoradas mediante el empleo de diatomea y negro de carbono respectivamente como aditivos funcionales, mediante modificaciones en la ruta convencional de síntesis de aerogeles.

21. Los composites resultantes presentaron unaalta porosidad confirmando que la polimerización de los precursores no se veía impedida por la presencia de altas cantidades de aditivo.

22. Los composites conservaban su estructura porosa después del lixiviado de la diatomea con HF confirmando que la porosidad surge del entrecruzamiento de los precursores durante las reacciones de policondensación.

23. La presencia de los aditivos provoca una caída en el volumen total de poros y la superficie específica junto con un agrandamiento del tamaño medio de poro.

24. Los aerogeles preparados en presencia de aditivos son principalmente mesoporosos (mesoporos anchos) aunque hay cierto desarrollo de microporosidad y el efecto es más pronunciado para la diatomea que para el negro de carbono.

25. La diatomea evita el encogimiento del monolito provocado por la densificación de la matriz de carbono durante la pirólisis, incluso después del lixiviado de la diatomea.

26. El aerogel puro presenta el comportamiento mecánico rígido típico mientras que los aditivados con diatomea presentan un carácter plástico.

27. El empleo de negro de carbono y diatomea como aditivos permite preparar electrodos mecánicamente resistentes y con baja resistencia de polarización para emplearse en desionización capacitiva aunque la disminución en microporosidad provocada por la adición de diatomea se traduzca en una caída de la capacitancia.

Las conclusiones de la 20 a la 27 se han obtenido de las publicaciones correspondientes a las secciones 2 y 3 del capítulo 3.

28. El empleo de diatomea como aditivo anti-encogimiento ha llevado a la síntesis de aerogeles de carbono monolíticos con una micro y mesoporosidad bien desarrollada y una macroporosidad remarcable.

29. La incorporación de funcionalidades de nitrógeno y de aditivo negro de carbono, incrementa la conductividad eléctrica y la mojabilidad de los monolitos de aerogel.

30. La matriz de carbono resultante es un buen soporte para nanopartículas de óxido de manganeso cuyos efectos pseudo-farádicos contribuyen positivamente a la capacitancia global.

31. Estas características son responsables del buen comportamiento en la eliminación de especies iónicas en disolución en términos de una cinética rápida y una baja resistencia.

32. El análisis morfológico demuestra un eficiente efecto anti-encogimiento y una textura esponjosa después del lixiviado de la diatomea.

33. La caracterización textural mediante isotermas de adsorción/desorción de nitrógeno revela que la policondensación de los precursores no se ve impedida por la presencia de los aditivos empleados, obteniéndose materiales con distribuciones multimodales de poros.

34. En electroadsorción en celda simétrica de dos electrodos, los aerogeles con diatomea muestran una mejor respuesta a bajos voltajes y/o tiempos cortos.

35. Estos resultados demuestran que el empleo de diatomea como aditivo anti-encogimiento puede ser una solución útil en la preparación de electrodos altamente porosos con propiedades optimizadas para desionización capacitiva.

Las conclusiones de la 28 a la 35 se han obtenido de la publicación correspondiente a la sección 4 del capítulo 3.

Capítulo 5

Otras aportaciones científicas

A continuación se exponen los resúmenes de varias publicaciones adicionales y comunicaciones a congresos. Dichos trabajos no constituyen el cuerpo de la tesis aunque han sido elaborados durante el periodo de formación del doctorado. Todas ellas están relacionadas con el trabajo de investigación de esta memoria de esta tesis y completan los estudios expuestos en los capítulos 2 y 3 descritos con anterioridad.

5.1 Publicaciones

On the use of carbon black loaded nitrogen-doped carbon aerogel for the electrosorption of sodium chloride from saline water

Electrochimica Acta, Volume 170, 10 Julio 2015, Pages 154-163

Effects of CO_2 activation of carbon aerogels leading to ultrahigh micro-meso porosity

Microporous and Mesoporous Materials, Volume 209, 15 June 2015, Pages 18-22

Mesoporous carbon black-aerogel composites with optimized properties for the electro-assisted removal of sodium chloride from brackish water

Journal of Electroanalytical Chemistry, Volume 741, 2015, Pages 42-50

N-doped monolithic carbon aerogel electrodes with optimized features for the electrosorption of ions

Carbon, Volume 83, 2015, Pages 262-274

Effect of the resorcinol/catalyst ratio in the capacitive performance of carbon xerogels with potential use in sodium chloride removal from saline water

Journal of Solid State Electrochemistry, October 2014, Volume 18, Issue 10, p 2847-2856

A novel method for metal oxide deposition on carbon aerogels with potential application in saline water removal

Electrochimica Acta, Volume 135, 20 July 2014, Pages 208-216

Electrosorption of environmental concerning anions on a

highly porous carbon aerogel

Journal of Electroanalytical Chemistry, Volume 708, 1 November 2013, Pages 80–86

Electrochemical response of carbon aerogel electrodes in saline water

Journal of Electroanalytical Chemistry, Volume 671, 15 April 2012, Pages 92-98


Electrochimica
Acta

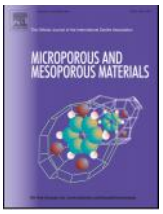
MICROPOROUS AND
MESOPOROUS MATERIALS


Journal of
Electroanalytical
Chemistry


Carbon


Journal of Solid State Electrochemistry


Electrochimica
Acta


Journal of
Electroanalytical
Chemistry


Journal of
Electroanalytical
Chemistry

5.2 Congresos

Electrochemical response of doped ultrahigh micro/mesoporous carbon aerogel electrodes in saline water. CARBON 2015, Comunicación oral, 12-15 de julio, 2015, Dresden (Alemania).

Efecto de las condiciones de prepolimerización en aerogeles nitrogenados y su influencia en desionización capacitiva. NANOUCO V Encuentro sobre Nanotecnología y Nanociencia de Investigadores y Tecnólogos Andaluces, Poster, 5 y 6 de Febrero, 2015, Córdoba (España).

Efecto de las condiciones de prepolimerización en aerogeles nitrogenados y su influencia en desionización capacitiva. RIA XXXIX-RIA, Reunion Ibérica de Adsorción, Póster, 14-17 de septiembre, 2014, Baeza (España).

Characterization of carbon aerogels with ultrahigh mesopore volume. COPS X, Póster, 11-14 de mayo, 2014, Granada (España).

Método novedoso para la deposición de óxidos metálicos en aerogeles de carbono con potencial uso desionización capacitiva de agua salina. QIES 14, 16ª Reunion Bienal del Grupo Especializado de Química Inorgánica. Póster, 15-18 de junio, 2014, Almería (España).

Carbon black directed synthesis of ultrahigh mesoporous carbon aerogels for capacitive applications. XXXIV Reunión del Grupo de Electroquímica de la Real Sociedad Española de Química y Electroquímica. Póster, 15-17 de julio, 2013, Valencia (España).

Efecto de la activación sobre la nanoporosidad de aerogeles de carbón para su uso en desionización capacitiva. NANOUCO IV. Encuentro sobre Nanotecnología y Nanociencia de Investigadores y Tecnólogos Andaluces, Poster, 7 y 8 de Febrero, 2013, Córdoba (España).

Electrochemical response of doped ultrahigh micro/mesoporous carbon aerogel electrodes in saline water

G. Rasines[1], C. Macías[1], M. C. Zafra[2], P. Lavela[2], J. L. Tirado[2], J.B. Parra[3], C.O. Ania[3*]

[1] *I+D Department, Nanoquimia S.L., PCT Rabanales 21, Ed. Aldebaran M4.7. 14014 Córdoba, Spain*
[2] *Laboratorio de Química Inorgánica, Universidad de Córdoba, Marie Curie, Campus de Rabanales, 14071 Córdoba, Spain*
[3] *Instituto Nacional del Carbón (INCAR, CSIC), 33011 Oviedo, Spain*

Introduction

Mesoporous carbon gels are interesting materials in many science and engineering fields due to their unique combination of adequate textural, morphological and structural properties that can be easily adapted during the synthesis and processing. Carbon gels are mostly synthesized following the catalyzed polycondensation of resorcinol-formaldehyde mixtures in water, although some other alternative routes have been reported using harmless and naturally available precursors. In this work we have prepared carbon gels with ultrahigh mesopore volumes and enhanced electrical conductivity by a simple modification of the conventional sol-gel method consisting on i) introducing N-doped carbon precursors (i.e., melamine) and by ii) performing the polymerization reaction in the presence of metallic and carbon conductive additives to modify the composition of the carbon aerogels [1-5].

Materials and methods

Hydrogels were synthesized by the polycondensation of Melamine (M), Resorcinol (R) and Formaldehyde (F) mixtures, using sodium carbonate as catalyst (C) and deionized water (W) as solvent. Details on the polymerization procedures and molar ratios of the reactants have been described elsewhere1-5). Briefly the precursors solutions are stirred for 20 minutes at room temperature, kept in an oven at 40 ºC for 24 h and then at 70 ºC for 120 h to allow gelation and aging. After a controlled water–acetone exchange, the hydrogels are dried under CO2 supercritical conditions and carbonized at 750 ºC under inert atmosphere. Finally, the aerogels are activated in CO2 atmosphere. For the composites, carbon black (Superior Graphite Co.) was chosen as conductive additive, incorporated to the precursor's mixture before the polymerization step.

Capacitive deionization experiments are performed in symmetric batch-type cells assembled with two monolithic carbon aerogel electrodes (cut and polished to achieve a

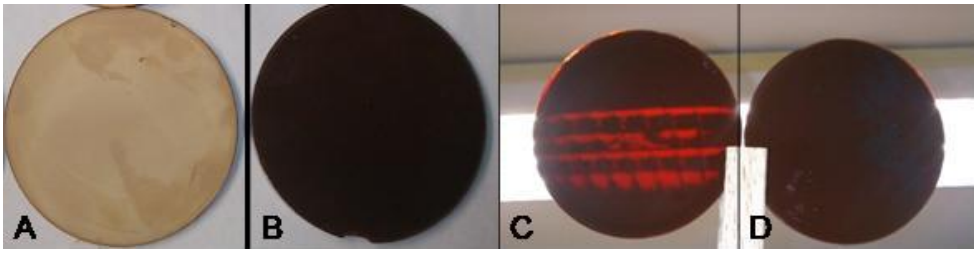
A
B
C
D

current density, chemical modifications or structural collapse. The electrodes also showed an enhanced stability upon polarization at 1.5 V.

References

[1] Rasines G, Lavela P, Macias C, Ania CO, Tirado JL. (2012). “Electrochemical response of carbon aerogel electrodes in saline water, J Electroanal Chem., Vol. 671 p. 92-98.

[2] Macias C, Haro M, Rasines G, Parra JB, Ania CO. (2013). “Carbon-black directed synthesis of mesoporous aerogels”, Carbon Vol. 63 p. 487-497.

[3] Zafra MC, Lavela P, Rasines G, Macías C, Tirado JL, Ania CO. (2014). “A novel method for metal oxide deposition on carbon aerogels with potential application in capacitive deionization of saline water”, Electrochim. Acta Vol. 135 p. 208-216.

[4] Rasines G, Lavela P, Macias C, Zafra MC, Tirado JL, Parra JB, Ania CO. (2015). “N-doped monolithic carbon aerogel electrodes with optimized features for the electrosorption of ions”, Carbon Vol. 83 p. 262-274.

[5] Rasines G, Lavela P, Macias C, Zafra MC, Tirado JL, Ania CO (2015). “Mesoporous carbon black-aerogel composites with optimized properties for the electro-assisted removal of sodium chloride from brackish water”, J. Electroanal. Chem, Vol. 741 p. 42-50

P34-CFQ Efecto de las condiciones de prepolimerización en aerogeles nitrogenados y su influencia en desionización capacitiva

G. Rasines[a*], C. Macías[a], M. C. Zafra[b], P. Lavela[b], J. L. Tirado[b], J.B. Parra[c], C.O. Ania[c]

[a] *Nanoquimia S.L., PCT Rabanales 21, Edf. Aldebarán M.4.7, 14014 Córdoba, Spain*

[b]*Laboratorio de Química Inorgánica, Universidad de Córdoba, Marie Curie, Campus de Rabanales, 14071 Córdoba, Spain.*

[c]*Instituto Nacional del Carbón (INCAR, CSIC), Apartado 73, 33080 Oviedo, Spain*

Resumen

Los aerogeles de carbono se componen de partículas nanométricas cuya agregación crea aglomerados de elevada superficie y porosidad. Los aerogeles dopados con nitrógeno han provocado recientemente gran interés para aplicaciones de electroadsorción de iones [1, 2]. La incorporación del nitrógeno a la red grafénica mejora la mojabilidad superficial, con lo que se facilita la adsorción de iones, además de aportar un efecto pseudocapacitivo beneficioso. El objetivo de este trabajo fue examinar el efecto de los parámetros de síntesis de aerogeles de carbono nitrogenados empleando melamina y resorcinol como precursores en sus propiedades nanotexturales y electroquímicas para la electroadsorción de iones en agua de baja salinidad.

Los aerogeles prepolimerizados a bajo pH poseen presentaron una estructura muy porosa, siendo determinante en la formación de mesoporos grandes (Fig.1). Se detectó un predominio de grupos piridina y pirrol en todos los aerogeles estudiados. Por otro lado, el pH alto favorece la incorporación de nitrógeno en los aerogeles. Los resultados en desionización capacitiva de monolitos mostraron un mejor rendimiento del aerogel no prepolimerizado, revelando la importancia de la macroporosidad. La muestra macroporosa MRF(0)-0.5-6 eliminó 2.73 mg h cm^{-3} en una disolución de NaCl 0.025M al aplicar un potencial de 1.5 V [3].

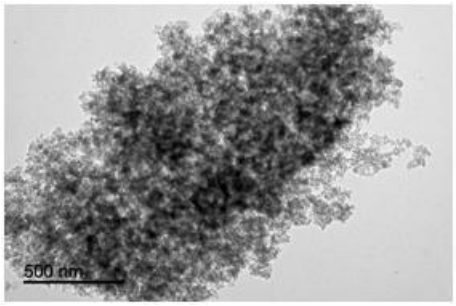

1

P27 Efecto de las condiciones de prepolimerización en aerogeles nitrogenados y su influencia en desionización capacitiva

G. Rasines[1*], C. Macías[1], M. C. Zafra[2], P. Lavela[2], J. L. Tirado[2], J.B. Parra[3], C.O. Ania[3]

[1] *Nanoquimia S.L., PCT Rabanales 21, Edf. Aldebarán M.4.7, Córdoba 14014 Córdoba, Spain*

[2] *Laboratorio de Química Inorgánica, Universidad de Córdoba, Marie Curie, Campus de Rabanales, 14071 Córdoba, Spain.*

[3] *Instituto Nacional del Carbón (INCAR, CSIC), Apartado 73, 33080 Oviedo, Spain*

Introducción

El dopado de aerogeles de carbono con heteroátomos ha atraído una gran atención en los últimos años, en especial los métodos basados en la incorporación en síntesis de precursores nitrogenados como melamina, urea, anilina o amoniaco y sales amónicas [1,2]. El aporte de nitrógeno mejora la mojabilidad superficial para facilitar la adsorción de iones y puede aportar un efecto pseudocapacitivo beneficioso [3]. El objetivo de este trabajo es examinar el efecto de los parámetros de síntesis de aerogeles de carbono nitrogenados empleando melamina y resorcinol como precursores en sus propiedades texturales y electroquímicas para la electroadsorción de iones en agua de baja salinidad. Se ha investigado el papel del pH de la disolución, la prepolimerización previa de los reactantes y por último la relación molar melamina/resorcinol.

Experimental

Los aerogeles fueron sintetizados por policondensación de melanina (M), resorcinol (R) y formaldehído (F), empleando carbonato sódico (C) y ácido acético como catalizador y regulador de pH, respectivamente. El proceso de gelado y secado está descrito en [4, 5]. La tabla 1 resume los detalles del procedimiento de síntesis. Seguidamente los aerogeles fueron pirolizados y activados a 750 ºC en atmósfera de CO_2.

Tabla 1. Concentraciones de reactantes y condiciones de síntesis de los aerogeles.

Muestras	M/R	R/F	M/F	W	Solución A	Solución B	PH A+B	Corrección PH
MRF(0)-0.5-6	0.5	0.5	7	4,16	M+F+W +C	R+ W	7,2 - 7,5	6
MRF(1)-0.5-6	0.5	0.5	7	4,16	M+F+W + C	R+F+ W + C		6
MRF(0)-0.5-8	0.5	0.5	7	4,16	M+F+W + C	R+ W		8
MRF(1)-0.5-8	0.5	0.5	7	4,16	M+F+W + C	R+F+ W + C		8
MRF(0)-2-8	2	0.5	7	5,05	M+F+W + C	R+W		8
MRF(1)-2-8	2	0.5	7	5,05	M+F+W + C	R+F+ W + C		8

Las muestras se identifican como MRF(n)-X-Y donde el valor de n es (0) para las no prepolimerizadas y (1) para las prepolimerizadas; X e Y indican la relación M/R y el pH, respectivamente.

Resultados y discusión

Las imágenes TEM mostraron diferencias texturales en función de la prepolimerización y el pH. Así, el aerogel MRF(0)-0.5-6 está constituido por partículas esféricas de tamaño superior a 100 nm. El registro de las isotermas de adsorción de nitrógeno permitió constatar que los materiales prepolimerizados a bajo pH poseen mayor área superficial que los no prepolimerizados, y a su vez el pH bajo es determinante en la formación de mesoporos grandes. En cuanto al contenido en nitrógeno, se observó mediante XPS y análisis elemental que el pH alto favorece la dispersión de grupos nitrogenados y la mayor concentración de nitrógeno. La deconvolución de los espectros de XPS indicó predominio de contribuciones de grupos nitrogenados de tipo N6 piridínico y N5 pirrólico.

Las experiencias de voltametría cíclica registraron valores de alta capacitancia con 84 F g^{-1} para los geles prepolimerizados MRF(1)-0.5-6 y MRF(1)-2-8. Los resultados revelan una correlación no lineal entre el contenido en nitrógeno, la superficie específica de los aerogeles y su comportamiento capacitivo. Por otro lado, los experimentos de desionización capacitiva de los electrodos monolíticos revelan la importancia de la meso-macroporosidad. Así, a pesar de la alta capacitancia determinada por voltametría cíclica en el aerogel prepolimerizado MRF(1)-0.5-6, esta muestra resultó no ser la más favorable en los experimentos de desionización capacitiva. La muestra macroporosa MRF(0)-0.5-6 eliminó 8,72 g/hm^2 en una solución de NaCl 0,025M al aplicar un potencial de 1,5 V.

Bibliografía

[1] Hulicova-Jurcakova, D.; Kodama, M.; Shiraishi, S.; Hator,i H.; Zhu, ZH.; Lu, GQ. Adv Funct Mater **2009**, 19, 1800–1809.
[2] Pérez-Cárdenas, M.; Moreno-Castilla, C.; Carrasco-Marín F.; Pérez-Cárdenas A.F.; Langmuir **2009**, 25, 466-470
[3] WangDW, Li.;F,YinLC.; LuX, Chen, ZG.; Gentle, IR.; Lu, GQ.; Cheng, HM. Chem Eur J **2012**, 18, 5345–535
[4] Rasines, G.; Lavela, P.; Macías, C.; Haro, M.; Ania, C.O.; Tirado, J.L. J. Electroanal Chem. **2012**, 671, 92-98
[5] Zafra, M.C.; Lavela, P.; Macías, C.; Rasines, G.; Tirado, J.L. J. Electroanal Chem. **2013**, 708, 80–86

A46 Characterization of carbon aerogels with ultrahigh mesopore volume

Ania CO [1*], Macias C [2], Rasines G [2], Jagiello J [3]

1Instituto Nacional del Carbón (INCAR, CSIC), P.O. 73, 33080 Oviedo, Spain

2 Nanoquimia S.L., Parque Científico Tecnologico Rabanales 21, c/ Astronoma Cecilia Payne s/n, Edif. Aldebaran Mod 4.7, 14014 Cordoba, Spain

3 Micromeritics Instrument Corporation, Norcross, GA, USA

Abstract

Mesoporous carbon gels are interesting materials in many science and engineering fields due to their relatively low cost and unique combination of adequate textural, morphological and structural properties that can be easily adapted during the synthesis and processing [1]. Carbon gels are mostly synthesized following the catalyzed polycondensation of resorcinol-formaldehyde mixtures in water, although some other alternative routes have been described using harmless and naturally available compounds as precursors [2].

The objective of this work was to study the properties of mesoporous carbon gels with controlled porosity and high electrical conductivity, and to explore their application as electrode materials in different electrolytes. A simple modification of the conventional sol-gel method using resorcinol-formaldehyde mixtures as precursors allowed the preparation of carbon gels with ultrahigh mesopore volume and enhanced electrical conductivity by performing the polymerization reaction in the presence of a carbon conductive additive [3,4]. A detailed textural characterization of the prepared carbon gels was carried out using 2D NLDFT [5]; the materials show heterogeneous pore systems characterized by large mesopores interconnected by necks of variable sizes, along with an enhanced electrical conductivity provided by the carbon black additive.

The electrochemical behaviour of the carbon gels resulted to be rather satisfactory, with an excellent performance in different electrolytes, which is attributed to their large porous nanotexture and enhanced electrical conductivity. The gels showed stable electrochemical response in neutral aqueous electrolyte, being reversibly charged/discharged at large potential windows, without significant losses in the current density, chemical

modifications or structural collapse. The enhanced life cycle of these electrodes makes them good candidates for their use in electrochemical applications where a fast response and high cycleability is required.

References

[1] S.A. Al-Muhtaseb, J.A. Ritter, Adv. Mater. 15 (2003) 101-14.

[2] A.G. Pandolfo, A.F. Hollenkamp, J. Power Sources 157 (2006) 11-27.

[3] M. Haro, G. Rasines, C. Macias, C.O. Ania, Carbon 49 (2011) 3723-3730.

[4] C. Macias, M. Haro, J.B. Parra, G. Rasines, C.O. Ania, Carbon 63 (2013) 487-497.

[5] J. Jagiello, J.P. Olivier, Carbon 55 (2013) 70-80.

Método novedoso para la deposición de óxidos metálicos en aerogeles de carbono con potencial uso en desionización capacitiva de agua salina

M. C. Zafra[1], P. Lavela[1*], G. Rasines[2], C. Macías[2], J. L. Tirado[1], C.O. Ania[3]

[1] *Laboratorio de Química Inorgánica, Universidad de Córdoba, Marie Curie, Campus de Rabanales, 14071 Córdoba, Spain.*

[2] *Nanoquimia S.L., PCT Rabanales 21, Edf. Aldebarán M.4.7, Córdoba 14014 Córdoba, Spain*

[3] *Instituto Nacional del Carbón (INCAR, CSIC), Apartado 73, 33080 Oviedo, Spain*

Resumen

La desionización capacitiva (CDI) es una tecnología robusta, eficiente y de bajo costo para la eleiminación de especies iónicas del agua con un bajo o moderado contenido en sal [1]. Para que se produzca la adsorción de estas especies es necesario aplicar una diferencia de potencial entre dos electrodos. Los iones son atraídos por las cargas opuestas acumuladas en los electrodos y se adsorben para ser inmovilizados según el modelode la doble capa eléctrica. Factores tales como una alta estabilidad química, una elevada área superficial y una buena conductividad eléctrica son determinantes a la hora de elegir el material adecuado. La optimización de las propiedades texturales de un aerogel de carbono debe tener en cuenta el tamaño de los iones a adsorber, su nivel de hidratación y la movilidad a lo largo de la estructura porosa [2, 3].

Para este trabajo se han sintetizado aerogeles de carbono dopados con óxido de manganeso (CAGDMnAct) o hierro (CAGDFeAct) para la desionización capacitiva de cloruro de sodio. Estos aerogeles de carbono se prepararon por el método de resorcinol-formaldehido. La incorporación de los precursores de óxidos metálicos en disolución antes del secado supercrítico es un método novedoso que garantiza la homogeneidad del material compuesto metal-carbono. Las imágenes de microscopía electrónica confirmaron el alto grado de dispersión de las partículas nanométricas de óxidos metálicos en la matriz del aerogel. Los espectros de XPS mostraron un aumento de la concentración de grupos hidroxilo y carboxilo en los aerogeles activados. El registro de las isotermas de adsorción de nitrógeno permitió constatar que los materiales poseen una elevada área superficial. No obstante, se observó una disminución del volumen de poro en las muestras dopadas

con manganeso, posiblemente atribuible al bloqueo parcial de la entrada de los poros por las partículas de óxido.

Las exeriencias de voltametría cíclica registraron valores de capacitancia de 99 F g^{-1} y 91 F g^{-1} para CAGDFeAct y CAGDMnAct, respectivamente. El estudio de la respuesta cinética de los electrodos mostró un comportamiento pobre para CAGMnAct, que se correlaciona con el bloqueo parcial de la estructura de poro por las partículas nanométricas de óxido antes aludida. A alta capacitancia del aerogel activado que contiene hierro se confirmó por experimentos de desionización capacitiva. Se registró un valor de capacidad de electroadsorción de 0.133 mmol g^{-1} para CAGDFeAct en una solución de NaCl 0.025 M cuando se aplicó 1.5V durante el período de carga.

Referencias

[1] Anderson MA., Cubero A.L., Palma J., Capacitive deionization as an electrochemical means of saving energy and delivering clean water. Comparison to prevent desalination practices: Will it compete?, Electrochim. Acta, 2010, 55, 3845-3856.

[2] Porada S., Zhao R., Van del Wal A., Presser V., Biesheuvel P.M., Review on the Science and Technology of Water Desalination by Capacitive Deionization, Prog. Mater. Sci., 2013, 58, 1388-1442.

[3] Noked M., Avraham E.A., Soffer A., Aurbach D., The electrochemistry of activated carbonaceous materials: past, present, and future, J. Solid State Electrochem., 2011, 15, 1563-1578.

PR 4 Carbon black directed synthesis of ultrahigh mesoporous carbon aerogels for capacitive applications

Carlos Macías [1], Marta Haro [2], José B. Parra [2], Gloria Rasines [1], Conchi O. Ania [2]*

[1] *Nanoquimia S.L., P.L La Minilla, La Rambla, 14540 Córdoba (Spain)*

[2] *Instituto Nacional del Carbón, INCAR-CSIC, Apdo. 73, 33080 Oviedo, Spain*

Abstract

A simple modification of the conventional sol-gel polymerization of resorcinol-formaldehyde mixtures allowed a facile preparation of ultrahigh mesoporous carbon gels. In the conventional synthesis the growth of the cluster polymer particles leading to the development of the porosity is controlled by the R/C ratio. In the presence of a carbon conductive additive, the polymerization of the reactants proceeded through the formation of less-branched polymer clusters resulting in carbon gels with large pore volumes within the micro/mesoporous range. The obtained materials displayed unusual heterogeneous pore systems characterized by large mesopores interconnected by necks of variable sizes, along with an enhanced electrical conductivity provided by the carbon black additive. The synthesized gel/CCA showed stable electrochemical response in neutral aqueous electrolyte, being reversibly charged/discharged at large potential windows, without significant losses in the current density nor chemical modification or structural collapse. All these features make these materials excellent candidates for their use as electrodes in electrochemical applications were a fast response and high cyclability is required.

P-15 Efecto de la activación sobre la nanoporosidad de aerogeles de carbón para su uso en desionización capacitiva

M. C. Zafra [a], G. Rasines [b], C. Macías [b], J. L. Tirado [a], P. Lavela [a*]

[a] *Laboratorio de Química Inorgánica, Universidad de Córdoba, Marie Curie, Campus de Rabanales, 14071 Córdoba, Spain.*

[b] *Nanoquimia S.L., PCT Rabanales 21, Edf. Aldebarán M.4.7, Córdoba 14014 Córdoba, Spain*

Resumen

Los aerogeles de carbón están constituidos por partículas uniformes con un diámetro promedio entre 5 y 10 nm e interconectadas que generan pequeños poros intersticiales de tamaño inferior a 100 nanómetros. Su elevada área superficial (600-800 m^2/g) procede del crecimiento y agregación de polímeros entrecruzados durante el proceso de polimerización sol-gel. Su elevada porosidad y área superficial puede emplearse para generar una doble capa electrizada entre el sólido y el electrólito que favorezca la adsorción reversible de iones cuando se aplica un potencial entre los electrodos de la celda simétrica [1]. Adicionalmente, los procesos de activación a alta temperatura en presencia de CO_2 o KOH permiten incrementar el volumen de poro y ajustar su tamaño y forma. Su apropiada conductividad eléctrica y termal, adecuada resistencia a la corrosión y baja densidad les convierte en materiales excepcionales para aplicaciones de electroadsorción y almacenamiento energético. Entre ellas, la desionización capacitiva es un proceso de electroadsorción de iones en la doble capa electrizada que permite retirar especies cargadas contaminantes del medio acuoso. Ventajas adicionales se obtienen cuando durante la desorción de iones, la carga aplicada puede ser recuperada. Si el proceso es eficientemente, la desionización capacitiva puede ser competitiva frente a los procesos de ósmosis inversa [2].

Los diagramas de difracción de rayos X muestran bandas anchas características de carbones altamente desordenados. Por otro lado, las medidas de área superficial revelan un aumento de la superficie en la muestra de aerogel activada que puede estar directamente relacionada con el aumento del volumen de microporos. El efecto de la activación del material también se refleja en la aparición de bandas en los espectros de infrarrojos principalmente asociadas a la funcionalización de carbonos superficiales que

han reaccionado con el agente activador. Los voltamogramas registrados sobre celdas asimétricas con contra-electrodo de platino y referencia de Hg/Hg_2SO_4 presentan el clásico perfil de caja cuadrada característico de procesos capacitivo aunque ligeramente ovalado por causa de los impedimentos cinéticos a la migración de los iones a través de la estructura nanoporosa. Comportamientos similares se han observado en carbones activados y en carbones mesoporosos [3]. El proceso de activación condujo a un aumento general de los valores de capacitancia. El menor tamaño de los iones cloruros hidratados permitió una menor disminución de la capacitancia cuando se aumentó la cinética de electroadsorción, aunque el aumento del volumen de microporos detectado tras el proceso de activación puede ser responsable de la acusada disminución de capacitancia en la muestra activada para altos valores de barrido (10 mV s^{-1}).

Referencias bibliográficas

[1] Oren Y. Desalination, **2008**, 228,10.

[2] Anderson, M. A.; Cudero, A. L.; Palma, J. Electrochim. Acta, **2010**, 55, 3845.

[3] Rasines, G.; Lavela, P.; Macías C.; Haro, M.; Ania ,C.O.; Tirado, J.L. J. Electroanal Chem., **2012**, 671, 92.